CLICK-CROSSLINKED POLYANIONIC HYDROGEL NETWORKS

SYNTHESIS AND STUDY OF CLICK-CROSSLINKED POLYANIONIC HYDROGEL NETWORKS

BY
S. ALISON STEWART, B.SC.

A Thesis Submitted to the School of Graduate Studies in Partial Fulfillment of the Requirements for the Degree of Doctor of Philosophy in Chemistry

PhD of Chemistry (2018) McMaster University
(Chemistry and Chemical Biology) Hamilton, Ontario, Canada

TITLE: Synthesis and Study of Click-Crosslinked Polyanionic Hydrogel Networks

AUTHOR: S. Alison Stewart
B.Sc. (Chemistry)
McMaster University, Hamilton, Ontario, Canada

SUPERVISOR: Professor Harald Stöver

NUMBER OF PAGES: xxvi, 173

Lay Abstract

Cell encapsulation aims to treat various hormone- and enzyme-deficiency disorders such as diabetes mellitus by encapsulating cells within a protective membrane that permits the in-diffusion of oxygen and nutrients and the outward diffusion of waste and therapeutic proteins, such as insulin. The membrane must also protect the encapsulated cells from the immune system. The primary goal of this project was to design polymeric materials for use in cell encapsulation. A series of mutually reactive polymers were developed, and the resulting polymeric hydrogels were characterized for suitability in biomedical applications by exploring properties such as swelling, stiffness, porosity and cytocompatibility. The materials were found to have tunable physical properties, and good cytocompatibility, showing promise for future use in cell encapsulation.

Abstract

Cell encapsulation aims to treat a variety of hormone- and enzyme-deficiency disorders by immobilizing therapeutic cells within a semi-permeable protective membrane. The membrane allows for in-diffusion of oxygen and nutrients and out-diffusion of waste and therapeutic proteins while simultaneously providing protection from immune cells and antibodies. Many cell therapies aim to provide long-term treatment for diseases, and designing materials that can match the longevity is critical. Synthetic polymers offer an attractive route to long-term encapsulation due to their tunable degradability and the ease of incorporating reactive moieties for covalent crosslinking.

The primary goal of the work presented in this thesis was the development of non-degradable covalently crosslinked hydrogels formed by mutually reactive polymers for use as cell immobilizing platforms. Due to research showing that polycations incite immune responses *in vivo* this project aimed to avoid the use of polycations entirely. The covalent crosslinking occurs in the presence of cells, making it essential to select reactions that do not require toxic catalysts or form offensive by-products. Diels-Alder and thiol-ene Michael Addition click reactions were chosen due to their proven cytocompatibility and modular nature.

In chapters 2 and 3, poly(methyl vinyl ether-*alt*-maleic anhydride) (PMMAn) was functionalized with furfurylamine (FFA) and *N*-2-(aminoethyl)maleimide (MAL) to form PMM-FFA and PMM-MAL, Diels-Alder reactive furan- and maleimide-bearing pendant polymers. Aqueous solutions of the polymers form bulk gels at higher concentrations (>5% w/v) and the chemical and physical properties of the gels were investigated and found to be highly tunable, with promise for use in controlled drug delivery applications. Alginate-templated matrix beads were also prepared at significantly lower polymer loading percentages (0.5 – 1.5% w/v each) and at physiological pH, and properties such as swellability and permeability were explored. This work demonstrates the first use of Diels-Alder crosslinking to reinforce alginate beads, and the matrix beads were found to have good initial cell viability post-encapsulation with 3T3 cells.

In chapter 4, PMMAn was functionalized with cysteamine vinyl sulfone (CVS) to form PMM-CVS, a vinyl sulfone-bearing pendant polymer, and aqueous solutions were

mixed with equimolar PEG-dithiol to form bulk hydrogels at concentrations between 2.5 and 7.5% w/v PMM-CVS. Thiol-ene crosslinking allowed for much more rapid gelation compared to the Diels-Alder system. Physical and chemical properties of the gels were explored, and excellent cytocompatibility of the crosslinking reaction was demonstrated. The ability to rapidly post-functionalize the gels in a step-wise fashion offers a versatile route to post-modification with various molecules. In chapter 5, PMMAn was functionalized with 2-pyridylthio cysteamine (SPy) to form PMM-SPy, a protected thiol. Alginate-templated matrix beads containing PMM-CVS and PMM-SPy were treated with TCEP to deprotect the thiol, allowing covalent crosslinking to occur in a controlled manner. Physical and chemical properties of the beads were explored in detail and the system was found to be highly tunable.

Acknowledgements

First and foremost I would like to thank my supervisor, Dr. Harald Stöver. I could not have asked for a more wonderful and supportive mentor. Dr. Stöver allowed me to choose the directions that my projects took, offered an incredible amount of guidance and understanding, and imparted his enthusiasm for research time and again. I would not have had such a positive experience, or learned nearly as much (including how to "make lemonade from lemons") without his help and support.

I would also like to thank Dr. Nicholas Burke. From the day I started in the lab as an overwhelmed fourth year thesis student, Nick was an incredible source of information, guidance and support. He was never too busy to help when I had questions or needed guidance on what to try next. His assistance with creating presentations and the way he edits papers with a fine-toothed comb are also tremendously appreciated!

I would like to thank my group members (past and present): Casey Gardner, Padraic Foley, Rachelle Kleinberger, Laurent Goujon, Samantha Ros, Jing Zhao, Christal Zhou, Sheilan Sinjari, Derrick Hastings, Yuqing Zhao, and Mitchell Johnson, for their help, support and friendship. I would also like to thank my committee members, Dr. Todd Hoare and Dr. Jose Moran-Mirabal for their helpful feedback and guidance with my projects. Thanks to Dr. Alex Adronov for giving me the opportunity to work in his lab for two summers as an undergraduate student, and helping me decide to pursue a path in chemistry. Also a big thank you to Rahima Benhabbour for being the best mentor any summer student could ask for!

Thank you to my collaborators, including Dr. Kari Dalnoki-Veress and Matilda Backholm for expertly guiding me through mechanical testing and modelling, Christal Zhou for assistance with cell viability studies, Mitchell Johnson for his expertise on cell encapsulation and live/dead assays, and Dr. Bob Berno for his invaluable assistance and knowledge of solid-state HRMAS NMR. To the wonderful and bright undergraduate thesis students that I had the opportunity to work with: Sam Ros, Caitlin Mcnamara, Michael Coulson and Rachelle Lassaline – you guys are amazing!

Finally, I would like to thank my family and friends. My parents, Jim and Sharon Stewart, have been a constant source of support and encouragement since the very beginning, and I would not be where I am today without them. Thanks to Cam and Laura

Harrington for getting me excited about chemistry when I was younger, and for all the support they've given me during grad school. Thank you to all of the amazing friends I have made during my time at McMaster University: Lucia Lee, Jen Wild, Sheilan Sinjari, Christal Zhou, Alex Nielsen, David Hurem, Monica Soos, Sumeet Sharma and Ankit Rastogi. The Phoenix nights, tacos, family dinners, coffee breaks and cottage weekends helped keep me sane(ish) over the years! And last, but not least, thanks to Mohammad Emami for supplying me with fesenjoon and emotional support when I needed it most.

List of Abbreviations

BCS	Bovine Calf Serum
BOC	Butyoxylcarbonyl
CuAAC	Cu(I) Catalyzed Azide-Alkyne Cycloaddition
CVS	Cysteamine Vinyl Sulfone
DA	Diels-Alder
DAMPs	Danger Associated Molecular Patterns
DAPI	4',6-diamidino-2-phenylindole dihydrochloride
DCM	Dichloromethane
DMEM	Dulbecco's Modified Eagle Medium
DMF	*N,N*-Dimethylformamide
DMSO	Dimethylsulfoxide
DS	Degree of Substitution
DTT	Dithiothreitol
ECM	Extracellular Matrix
EDC	1-Ethyl-3-(3-dimethylaminopropyl)carbodiimide
EHS	Engelbreth-Holm-Swarm
EthD-1	Ethidium Homodimer-1
FDA	Food and Drug Administration
FFA	furfurylamine
FTIR	Fourier Transform Infrared Spectroscopy
G	α-l-Guluronic Acid
HbA1c	Glycated Haemoglobin
HEPES	4-(2-hydroxyethyl)-1-Piperazineethanesulfonic Acid
HR-MAS	High Resolution Magic Angle Spinning
HS-PEG-SH	a,w-dithio-polyethyleneglycol
IEDDA	Inverse-Electron Demand Diels-Alder
LD50	Lethal Dose
M	β-d-Mannuronic Acid
MAS	Magic Angle Spinning

MeOH	Methanol
MES	2-(*N*-morpholino)ethanesulfonic Acid
MSC	Mesenchymal Stem Cell
NaOD	Sodium Deuteroxide
NaOH	Sodium Hydroxide
NHS	*N*-hydroxysuccinimide
p(HEMA)	Poly(hydroxyethyl methacrylate)
PAAm	Polyacylamide
PBS	Phosphate-Buffered Saline
PDA	Polydopamine
PEG	Polyethylene Glycol
PEGDA	Polyethylene Glycol Diacrylate
PEO	Polyethylene Oxide
PHT	Potassium Hydrogen Phthalate
PLL	α-Poly-L-Lysine
PMM	Poly(methyl vinyl ether-*alt*-maleic acid)
PMM-CVS	Poly(methyl vinyl ether-alt-maleic acid) Cysteamide Vinyl Sulfone
PMM-FFA	Poly(methyl vinyl ether-alt-maleic acid) Furfurylamide
PMM-MAL	Poly(methyl vinyl ether-alt-maleic acid) Maleimide
PMM-SPy	Poly(methyl vinyl ether-alt-maleic acid) Pyridylthio Cysteamide
PMMAn	Poly(methyl vinyl ether-*alt*maleic anhydride)
PNIPAM	Poly(*N*-isopropylacrylamide)
PRRs	Pattern Recognition Receptors
PS	Penicillin/Streptomycin
PVA	Polyvinyl Alcohol
RF	Radiofrequency
RGD	Arginine – Glycine – Aspartic acid
SPAAC	Strain-Promoted Azide-Alkyne Cycloaddition
SPy	2-Pyridylthio Cysteamine
TAMRA-c	Tetramethylrhodamine 5- (and 6-) Carboxamide Cadaverine
TCEP	Tris(2-carboxyethyl)phosphine

TEA	Triethylamine
TFA	Trifluoroacetic acid
TMTD	Triazolethiomorpholine Dioxide
UV-vis	Ultraviolet-Visible Spectroscopy
VEGF	Vascular Endothelial Growth Factor

Contents

List of Tables

List of Figures

List of Schemes

Chapter 1

Overview of Covalently Crosslinked Hydrogels and Their Use in Biomedical Applications

1.1. Hydrogels in Regenerative Medicine

Hydrogels are hydrophilic, water-swellable polymer networks that resist dissolution due to physical or covalent crosslinks between chains. Their ability to swell and retain water makes them interesting candidates for wound dressings,[1] drug delivery devices,[2] biosensors,[3] as well as tissue engineering scaffolds.[4,5,6,7,8]

The aim of regenerative medicine is to replace or repair damaged tissues using stem cells. These stem cells are commonly embedded in an extracellular matrix (ECM) that mimics the body's natural ECM and provides mechanical and chemical cues for cell behaviour.[9] Matrix stiffness is known to influence cellular factors such as focal-adhesion structures and cytoskeleton,[10,11] as well as play a substantial role in, e.g., mesenchymal stem cell (MSC) differentiation.[12]

Natural polymers such as gelatin,[13] agarose,[14] alginate[15] and hyaluronic acid[16] are often used as ECM mimics. Matrigel, a mixture of membrane proteins derived from Engelbreth-Holm-Swarm (EHS) mouse sarcoma cells, is another natural hydrogel that is widely used for tissue and cell transplants.[17] However, there are drawbacks to natural materials such as batch-to-batch variability,[18] poor long-term mechanical strength, and unpredictable degradability.[19] Hence, there is increased interest in using synthetic components or hydrogels designed to be anti-fouling,[20] with controlled rates of degradation,[21] and tunable mechanical properties.[22] They can also be designed to provide important cues for cell adhesion and cellular functions such as migration and differentiation.[23, 24, 25] Some examples of synthetic polymers used to prepare hydrogels include polyethylene glycol (PEG), polyethylene oxide (PEO) poly vinyl alcohol (PVA), polyacrylamide, polyethylene glycol diacrylate (PEGDA), poly(hydroxyethyl methacrylate) (pHEMA), polyacrylamide (PAAm), and poly(*N*-isopropylacrylamide) (PNIPAM).[26]

pHEMA was one of the earliest synthetic polymers used for hydrogel formation, first described in 1960 by Wichterle and Lim.[27] Since then it has found uses in various biomedical applications due to its non-toxic and anti-fouling nature, including as tissue scaffolds,[28] bone substitute,[29] and in drug delivery.[30] Recently, Cao, Zhang, Ciu, Du, & Shi (2017) prepared an artificial cornea skirt, a porous, flexible device that enables cellular integration of the host tissue through fibroblast ingrowth, using pHEMA, trimethylpropane triacrylate, and butyl acrylate. The artificial corneas were evaluated using human corneal fibroblasts, and it was found that the porosity of the gel increased the water content of the hydrogel and strengthened the cell adhesion to the gels.[31]

PEG has long been one of the most popular polymers used for hydrogel formation and has Food and Drug Administration (FDA) approval for use in humans. Additional functional groups must be incorporated to provide points for covalent attachment. PEG-based hydrogels have found applications in many areas, including drug delivery,[32] targeted cancer treatment,[33] and tissue engineering.[34] McKinnon, Domaille, Cha, & Anseth (2014) demonstrated that C2C12 mouse myoblasts encapsulated in aldehyde-hydrazine crosslinked PEG-based hydrogels developed physiologically relevant morphologies, due to the ability of the cells to remodel the hydrogel matrix.[35] Recently, Zhang, Wang, Zhang, Lin, Ge, & Zou (2016) created a macroporous hydrogel composed of PEG and gelatin. The hydrogel demonstrated good mechanical and structural properties while the macroporous scaffold enabled cell-cell interactions and tissue formation.[36] However, there has been recognition that repeated exposure to PEG can lead to anti-body formation in humans.[37] In rare cases, patients have shown severe anaphylactic reaction to PEG,[38] perhaps attributable to prior sensitization through PEG-based food-additives.

1.2. Cell Encapsulation

Current treatments for most chronic and progressive diseases include regular administration of therapeutics which may include peptide-based hormones such as insulin. Current research aims to provide long-term cell-based production of therapeutic agents within the patient, where needed with biofeedback control.[39]

Cell encapsulation, one of the most studied approaches, involves immobilization of xenogenic, allogenic or even autologous cells within a semi-permeable membrane. First described in 1933 when Bisceglie studied the effect of encapsulation on the survival of tumour cells in the pig abdominal cavity,[40] the first introduction to the idea of a bio-artificial organ came in 1964 when Chang described the encapsulation of cells for immune-protection as an alternative to creating fully artificial organs.[41] In 1980, Lim and Sun reported the first successful encapsulation of islets in an alginate capsule to function as an artificial pancreas.[42] The capsules were implanted in diabetic rats and found to respond to blood glucose levels by secreting insulin.

There is a wide variety of diseases that have been targeted for treatment by cell encapsulation, including haemophilia B,[43] anemia,[44] dwarfism,[45] kidney failure,[46] liver failure,[47] pituitary disorders,[48] central nervous system insufficiency[49] and diabetes mellitus.[50] For diabetes, encapsulation has gained favour over islet infusions due to the possibility of an immune response triggered by un-encapsulated xenogeneic islets,[51] potential exposure to zoonosis,[52] and the teratogenic and tumorigenic risk of transplanting undifferentiated pluripotent stem cells.[53]

There are a number of criteria that must be met when designing systems for cell encapsulation. Devices must be porous, allowing small molecules such as oxygen and other nutrients to readily diffuse across the membrane while simultaneously allowing for out-diffusion of therapeutic proteins. The membrane should be immuno-protective to prevent rejection of the cells upon implantation in the host, thereby eliminating the need for long-term chemical immune-suppression.[54,55,56]

It is important that both the encapsulation procedure and the polymers be non-toxic to the encapsulated cells and the host. Toxicity is cell specific and susceptibility varies widely.[57] For example, hybridoma cells have been found to have improved growth and function when encapsulated in liquefied rather than solid alginate-agarose capsules, while BHK and C2C12 were shown to retain their viability and function in solid beads.[58]

Cellular therapy is often targeted towards diseases where cells respond to external stimuli. For example, type 1 diabetes mellitus is currently treated with multiple daily insulin injections to lower blood sugar levels, aiming to avoid both hypo and hyper glycemia, and the associated diabetic complications,[59] including kidney or other organ

failure.[60] Ideally, glucose levels should be regulated on a minute-by-minute basis, with cell-based bio-feedback.[60] Therefore it is important that encapsulation does not impair cell function. For example, studies have shown that until capsule size reaches 1 mm in diameter, size does not interfere with release of insulin when challenged with glucose.[61]

Finally, there must be an accessible nutrient supply at the transplant site for encapsulated cells to survive. Limited access to oxygen results in cell hypoxia and necrosis, usually exhibiting a diffusion gradient from periphery to core.[62] Encapsulated cell death can result in the release of danger-associated molecular patterns (DAMPs) that are produced by cells undergoing necrosis.[63] The immune system of the host has special receptors called pattern recognition receptors (PRRs) that recognize DAMPs[64] and produce inflammatory cytokines in response, which can endanger encapsulated cells.[64]

Encapsulation is typically approached either through macro- or microcapsules. Macrocapsules are large, semi-permeable devices that can be found in a variety of different morphologies, including flat sheets, hollow fibres and disks.[65] These devices are usually implanted either under the skin or in the peritoneal cavity via minor surgery, allowing for easy retrieval of the device.

There have been a number of clinical trials for macroencapsulated insulin-producing cells in recent years. Sernova is in the process of conducting phase I/II clinical trials for human islets encapsulated inside their sub-cutaneous pre-vascularized Cell Pouch System™. Using a similar approach to Sernova, Shapiro et al. (2017) recently described the transplantation of β-like cells derived from human embryonic stem cells into a pre-vascularized subcutaneous site in mice.[66] Viacyte has conducted a number of phase I/II trials for their human embryonic pancreatic progenitor cells encapsulated in a macrodevice with an immunoisolating membrane called Encaptra™. Encaptra is a drug delivery device manufactured from implant-grade materials that have been selected due to its good biocompatibility and suitability for subcutaneous implantation (viacyte.com). However, macrocapsule devices do have some drawbacks, including a small surface to volume ratio, which can limit nutrient in-diffusion,[67] thereby necessitating lower cell densities.[68]

In contrast, microcapsules have large surface areas, allowing for rapid exchange of oxygen and nutrients across a semi-permeable membrane. Microcapsules have shown

promise in recent animal trials. Pham-Hua et al. (2017) recently reported restoration of normal glucose levels in mice upon implantation of islets encapsulated inside poly(*N*-vinylpyrryolidone)/tannic acid capsules.[69] Good biocompatibility and stability of ultrapure, high G-content alginate capsules implanted in non-diabetic rats was reported by Bloch, Vanichkin, Gil-Ad, Vardi, & Weizman (2017).[70] Hillberg, Oudshoorn, Lam, & Kathirgamanathan (2015) found that islets encapsulated in alginate and implanted in non-diabetic mice were biocompatible but had poor mechanical stability and easily ruptured.[71]

The first clinical trial of microencapsulated islets in patients with type 1 diabetes was carried out by Calafiore et al. (2006). Human islets encapsulated in alginate beads were transplanted into the peritoneal cavity of non-immunosuppressed patients. Although none of the patients achieved insulin independence, an improvement in glucose levels and a reduction in insulin requirement was observed.[72] In a follow-up study, patients with type 1 diabetes who received transplants of alginate-encapsulated allogenic islets were found to have stable blood glucose levels for up to 24 months post-transplant, at which point they began to steadily increase to pre-transplant levels.[73] In a recent study, two doses of 5000 or 10,000 islets/kg each of alginate-encapsulated neonatal porcine islets were transplanted in the peritoneal cavity of eight patients with type 1 diabetes for a 3-month time period. Recipients were found to have a significant improvement in their glycated haemoglobin (HbA1c) levels, a protein within red blood cells that joins with glucose in the blood and gives an indication of average blood sugar levels. A decrease in severe hypoglycaemia was also reported, although the reduction of insulin doses was minimal.[74]

Sigilon Therapeutics, a start-up company based on research conducted at the Massachusetts Institute of Technology and Harvard Medical School, is currently in pre-clinical studies for patients with diabetes, haemophilia, and lysosomal storage disorders. One of their approaches involves conjugation of non-immunogenic polymers onto the surface of alginate microspheres, creating a core-shell morphology.[75] The alginate surface is first modified with polydopamine (PDA) films, followed by conjugation of zwitterionic polymers onto the PDA layer. Coated beads were shown to have lower cellular overgrowth and fibrosis when implanted in immunocompetent mice compared with untreated alginate beads. Their other approach involves chemical modification of

the alginate to mitigate foreign body responses. They recently demonstrated that triazolethiomorpholine dioxide (TMTD)-modified alginate microspheres mitigated fibrotic response in non-human primates and mice,[76] and SC-β human embryonic stem cells encapsulated in TMTD-modified alginate beads maintained glycemic correction in diabetic mice for 174 days.[77]

Despite the large amount of research into cell encapsulation, a clinically relevant product does not currently exist. One of the key challenges that remains is the design of a system that can provide cells with a suitable microenvironment while simultaneously sustaining long-term capsule survival and function and protection from immune rejection.[78]

1.3. Alginate

Alginate is a naturally occurring anionic polymer, isolated from algae. It is a linear polysaccharide composed of 1,4′-linked β-d-mannuronic acid (M) and α-l-guluronic acid (G) residues in varying sequences. The ratio of G and M blocks depends on the alginate source. Alginate with higher G content is more rigid while M rich alginate is more soft and pliable. This is because the G units participate in ionic crosslinking with divalent ions, such as Ca^{2+}, and have a higher binding affinity than M units.[79]

Alginate has been the most widely studied biomaterial for cell encapsulation.[80] Its biocompatibility, low toxicity, ready ionic gelation and FDA approval make it an attractive choice of biomaterials. However, the suitability of alginate for cell encapsulation depends strongly on the alginate composition. Alginate systems have been found to have variability in induced inflammatory response post-transplantation.[81] Interestingly, it has also been found that as diameter of the alginate microspheres increases, fibrosis due to cellular deposition decreases.[82]

Encapsulation usually involves extrusion of an alginate-cell suspension into a gelling bath containing divalent cations such as Ca^{2+}, Ba^{2+} and Sr^{2+}. Other divalent cations such as Pb^{2+}, Cu^{2+}, Co^{2+}, Ni^{2+}, Zn^{2+} and Mn^{2+} will also crosslink alginate, but their use is generally avoided due to their toxicity to cells.[83] The binding affinity of alginate for cations has been determined to be as follows: $Pb^{2+} > Cu^{2+} > Cd^{2+} > Ba^{2+} > Sr^{2+} > Ca^{2+} >$ Co2+, $Ni^{2+} > Zn^{2+} > Mn^{2+}$.[84] A higher binding affinity is associated with a stronger gel,

therefore gels crosslinked with Ba^{2+} will be more mechanically robust than alginate crosslinked with Ca^{2+}.[85]

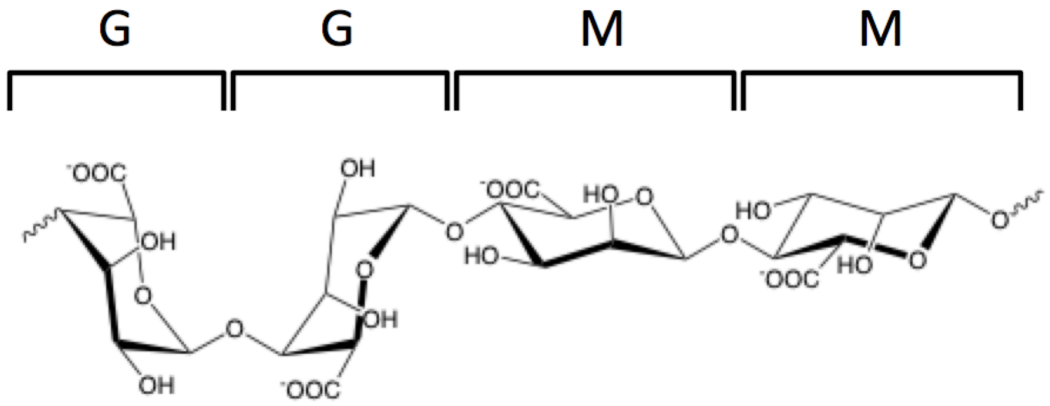

Figure 1.1. Molecular structure of alginate showing the G (guluronate) and M (mannuronate) residues.

1.4. Reinforcing Alginate Beads

Alginate gels are too porous on their own to provide adequate immune protection, allowing immune proteins to diffuse into the capsules.[86] Molecular weight cut-off for immune system exclusion has been found to be around 160 kDa.[87] While high porosity can be problematic, pore size that is too small may lead to malnutrition of cells, or accumulation of toxic waste inside the capsules due to limited in- and out-diffusion across the membrane.[88] Beads are therefore often coated with cationic polymers to control capsule porosity.[89,90,91]

The most commonly studied polycation is α-poly-L-lysine (PLL),[92] a synthetic, cationic polypeptide with well-understood toxicology.[93] However, there are some challenges associated with PLL coating of beads. PLL has been found to interfere with the ability of pancreatic islets to respond to glucose, with the PLL coating thickness having a direct correlation with cell function.[94] Positive charges on polycations such as PLL have also been shown to incite inflammatory responses upon implantation.[95,96,97] To circumvent this issue, capsules are often coated with a final layer of alginate after PLL coating in order to mask the PLL from the immune system. However, it has been demonstrated that some of the PLL is still exposed on the capsule surface.[95] Finally,

some encapsulated cells are sensitive to PLL and experience toxicity during the coating procedure.[98,99] Approaches to avoid these issues associated with PLL include coating the beads with synthetic polyanions,[100] reduction in charge density of PLL by grafting of PEG,[101,102,103] and replacement of PLL with lower charge density polycations.[104,105,106]

In addition to controlling capsule permeability, coatings are also applied to alginate beads to improve mechanical stability and durability. Covalent crosslinking is often used for mechanical stabilization of the capsules, allowing for potential use in long-term applications. Synthetic polymers offer many advantages over natural polymers for controlling capsule porosity and improving capsule longevity. They are more readily synthesized in large batches, do not suffer from batch-to-batch variation, and can be more readily engineered for various applications. Additionally, they can be more easily tailored to improve biocompatibility, or reinforce mechanical properties.[107]

It is important that the crosslinking reaction is biocompatible and can be carried out under physiological conditions. For example, photocrosslinking has been explored in depth as a way to improve capsule longevity.[108,109,110] However, photoinitator is associated with free-radical generation which can lead to cell toxicity.[111] The need for biocompatible crosslinking reactions has led to an increased interest in using "click" reactions for covalent crosslinking of alginate capsules.

1.5. "Click" Reactions and Their Applications in Biomaterials

"Click chemistry" is a term that was coined and fully defined by Kolb, Finn and Sharpless in 2001.[112] Click reactions are modular, wide in scope, give high yields, and generate only inoffensive by-products. Reaction conditions should be simple and the reaction should ideally be insensitive to water and oxygen. Starting materials should be readily available, either water should be used as a solvent, or no solvent should be used at all, product isolation should be simple and should not involve chromatographic methods, and the resulting product should be stable at physiological conditions.[112]

Click reactions proceed rapidly, and often irreversibly, to give good product yields due to their high thermodynamic driving force, usually greater than 20 kcal/mol.[112] Some examples of click reactions include: cycloadditions of unsaturated compounds, especially 1,3-dipolar cycloadditions and Diels-Alder reactions; nucleophilic substitutions,

especially ring-opening reactions of strained heterocyclic electrophiles such as epoxides; non-aldol carbonyl chemistry such as formation of ureas, thioureas, aromatic heterocyles, hydrazones and amides; and additions to carbon-carbon multiple bonds, especially epoxidation, dihydroxylation, aziridination, and Michael Addition reactions.[112]

Inspired by nature's ability to create biomolecules, click chemistry was developed to generate new compounds by joining small units together, much like modular building blocks. Initially popular in pharmaceutical research and natural product synthesis, the bio-orthogonal nature and mild reaction conditions have made click chemistry a very attractive approach for designing hydrogels for use in tissue engineering, cell encapsulation and other biomedical applications.[113,114,115]

Hydrogels have been designed for a wide variety of biomedical applications, including sustained protein release, targeted drug delivery and tissue engineering[116,117,118,119,120,121,122] and various physical and chemical crosslinkings have been explored for formation of these hydrogels.[123,124,125] Physically crosslinked hydrogels (typically formed via thermogellation, ionic crosslinking, or stereo-complexing) tend to be weak and exhibit poor long-term stability post-implantation.[126,127,128] Chemically crosslinked hydrogels generally exhibit better stability, durability and mechanical properties.[129,130] However, many chemically crosslinked hydrogels are formed via the use of initiators or enzymes that are potentially toxic to cells, and may also suffer from low specificity, leading to unwanted reactions with drugs, proteins and cells. Click chemistry has gained in popularity for preparation of hydrogels in recent years due to its high specificity, selectivity, and mild reaction conditions. Many click reactions are bioorthogonal, rendering hydrogels highly compatible with encapsulated cells.

One of the best-known click reactions is the Cu(I)-catalyzed [3+2] cycloaddition between an azide and an alkyne.[131,132] It has been widely used in protein-labelling, however it has limited use in many biomedical applications due to the toxicity of copper to cells. Mammalian cells were found to survive only low Cu(I) concentrations, resulting in very slow reaction rates.[133] A strain-promoted [3+2] azide-alkyne cycloaddition (SPAAC), developed by Agard, Prescher, & Bertozzi (2004), proceeds under physiological conditions without the need for a copper catalyst.[134] However, it is kinetically much

slower compared with the Cu(I)-catalyzed cycloaddition. Reaction kinetics have been improved via the use of novel cyclooctynes, however synthesis of these compounds is not trivial.[135,136]

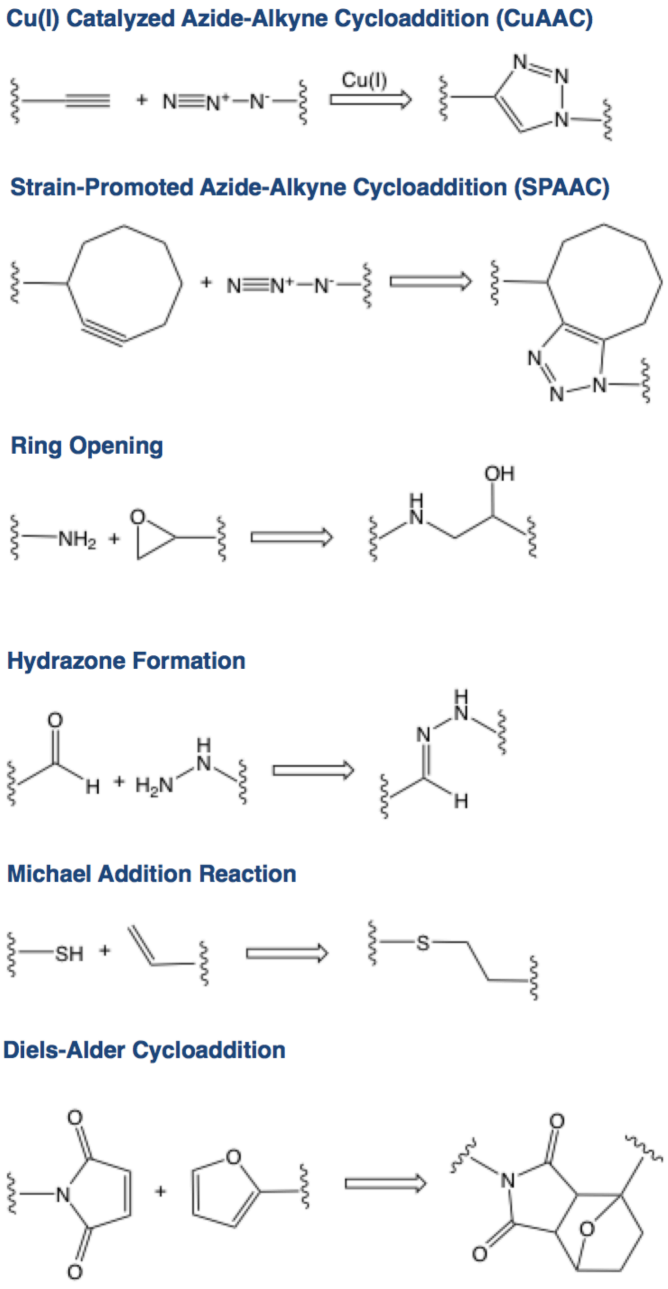

Figure 1.2. Sample click reactions.

The Diels-Alder (DA) reaction is a highly selective [4 + 2] cycloaddition between an electron-rich diene and an electron-poor dienophile. The reaction does not require a

catalyst and no by-products are formed. It is greatly accelerated in water due to increased hydrophobic effects. The DA reaction is reversible at elevated temperatures through the retro-DA reaction, which has gained interest for controlled drug release.[137] The Diels-Alder reaction has been used by Nimmo, Owen, & Shoichet (2011), to form crosslinked hydrogels composed of hyaluronic acid and PEG. The gels were formed at pH 5.5 and human epithelial cells were found to have good viability when seeded on top of the formed gels.[138] Two of the drawbacks to the Diels-Alder reaction between furan and maleimide moieties include slow reaction rates, and competing hydrolysis of maleimide. This often necessitates carrying out the reaction at pH 5.5, limiting its use in some biomedical applications. More recently, furan was replaced by methyl furan, allowing for greatly accelerated reactions times, and enabling successful 3D encapsulation of cancer cells and glioblastoma cells.[139] Alge, Azagarsamy, Donohue, & Anseth (2013) recently reported the use of the inverse-electron demand Diels-Alder reaction (IEDDA) between tetrazine-functionalized multi-arm PEG and norbornene-functional peptide as a bioorthogonal approach for biomedical applications.[140] The reaction rate was found to be rapid, with excellent compatibility with encapsulated human mesenchymal stem cells.

Another click reaction, the thiol-Michael addition reaction, consists of the addition of a thiol across a double bond in compounds such as acrylate, vinyl sulfone, maleimide or similar, resulting in a thioether linkage.[141] The thiol-Michael reaction has a high reaction rate, good coupling efficiency, tolerance for a wide variety of functional groups, and there is good access to thiol and ene functional groups.[142,143,144] Vinyl sulfone has been reported to be more reactive than acrylate in the thiol-Michael reaction due to its higher electron withdrawing capability,[142] and the resulting thioether sulfone bond is highly stable. Lutolf and Hubbell were the first to report the use of the Michael-addition reaction for formation of hydrogels.[145,146,147,] They reported the use of vinyl sulfone-terminated multi-arm PEG crosslinked with cysteine oligopeptides.[148] Later, they crosslinked the vinyl sulfone terminated PEG with dithiothreitol (DTT) for the encapsulation and sustained release of human growth hormone.[149]

1.6. Poly(methyl vinyl ether-*alt*-maleic acid)

Poly(methyl vinyl ether-*alt*-maleic anhydride)s (PMMAn) are commercially available polymers available in a variety of different molecular weights (MW). The anhydride functional groups on PMMAn offer a facile route for polymer functionalization and modification. Hydrolysis of the anhydride moieties results in a water-soluble polyanion, poly(methyl vinyl ether-*alt*-maleic acid) (PMM), sold commercially under the name Gantrez®. Gantrez® is commonly used in the pharmaceutical industry as a thickening and suspending agent, denture adhesive, and adjuvant for drug delivery systems.[150, 151, 152] PMM has also been proposed for use as a bioadhesive nanoparticles for oral drug delivery.[153]

While PMM does not gel as readily as alginate, it is known to interact strongly with calcium and other divalent cations[154] and will precipitate or gel with calcium under certain conditions.[155, 156] Highly biocompatible, the lethal dose (LD50) of Gantrez® in guinea pigs has been reported as 8-9 g/kg (data supplied by ISP Corp.). Calcium alginate capsules coated with 50/50 PMM/PMMAn, and covalently crosslinked with PLL, were shown to exhibit excellent compatibility with encapsulated C2C12 cells and showed only limited fibrotic overgrowth six weeks post-transplantation in mice.[100]

1.7. Focus of this Thesis

Alginate capsules have been shown to suffer from poor long-term mechanical stability due to the *in vivo* exchange of Ca^{2+} ions for Na^{+}, resulting in loss of ionic crosslinking and liquefaction of the capsules.[157] To improve the longevity of the capsules, as well as to provide control over the permeability, beads are often coated with polycations such as PLL. However, polycations are known to incite inflammatory responses in the host and attempts to mask the positive charges with polyanions is not entirely effective. This thesis encompasses three main goals:

1. To design covalently crosslinked, cytocompatible hydrogels to reinforce alginate beads or function independently as hydrogel supports (synthetic extracellular matrices). This requires that both the polymers and the crosslinking reaction must be cytocompatible, with no formation of toxic byproducts.

2. To replace polycations, such as PLL, which have shown cytotoxicity. This may be accomplished by pre-mixing mutually reactive polyanions with an alginate/cell suspension prior to ionic gelation of capsules with Ca^{2+}. This strategy necessitates the use of polymers that will effectively become entrapped within the alginate beads due to high molecular weight (physical entrapment) and/or interaction with Ca^{2+} (ionic immobilization).
3. To be able to either pre- or post-functionalize the synthetic hydrogels or crosslinked capsules with arginine – glycine – aspartic acid (RGD) or other peptides for cell attachment or signalling. This can be achieved either via residual reactive units on the polymer backbone (such as unhydrolysed anhydride moieties on PMMAn) or using residual reactive groups that did not participate in the crosslinking reaction.
4. Explore means of controlling hydrogel permeability through polymer loading and crosslink density

PMMAn was selected as the polymeric backbone used throughout this thesis due to the ease of functionalization with nucleophiles, allowing for simple fluorescent labelling and preparation of mutually reactive polyanions. The proven biocompatibility of PMM, as well as its ability to interact with divalent cations such as Ca^{2+}, were also attractive features. Finally, PMM is not enzymatically degradable, indicating that it should be suitable for long-term applications both in capsules and bulk hydrogel supports.

Two click reactions were studied in this thesis both for reinforcing alginate beads and for use as cellular supports. The first reaction was the Diels-Alder [4+2] cycloaddition between furan and maleimide. The reaction does not require small-molecule catalysts or additives, and occurs readily under aqueous conditions. The moderate rate of Diels-Alder coupling ensures adequate time for complete mixing and bead formation prior to gelation. PMMAn was functionalized with either furfurylamine or *N*-(2-aminoethyl maleimide) and residual anhydride groups were hydrolyzed to form PMM-FFA and PMM-MAL respectively (figure 1.3). When solutions of PMM-FFA and PMM-MAL were mixed together at concentrations of 10% w/v, bulk hydrogels formed. The properties of these hydrogels were fully explored and characterized (chapter 2). The polymers were also

mixed with sodium alginate and extruded into a $CaCl_2$ gelling bath to give calcium alginate-templated matrix beads, held together via Diels-Alder crosslinks (chapter 3).

The second reaction studied was the thiolene Michael addition between a thiol and vinyl sulfone. PMM was functionalized with either cysteamine vinyl sulfone (CVS) or 2-pyridylthio cysteamine (SPy) to give PMM-CVS and PMM-SPy, respectively (figure 1.3). In chapter 4, PMM-CVS was mixed with equimolar solutions of PEG-dithiol crosslinker to form bulk gels. The Michael addition reaction is much faster than the Diels-Alder cycloaddition, necessitating the use of a protected thiol when pre-mixing the polymers with sodium alginate in chapter 5. Treatment of PMM-SPy with a reducing agent such as tris(2-carboxyethyl)phosphine (TCEP) cleaves the disulphide linkage, resulting in a free-thiol that may participate in the thiolene Michael addition reaction.

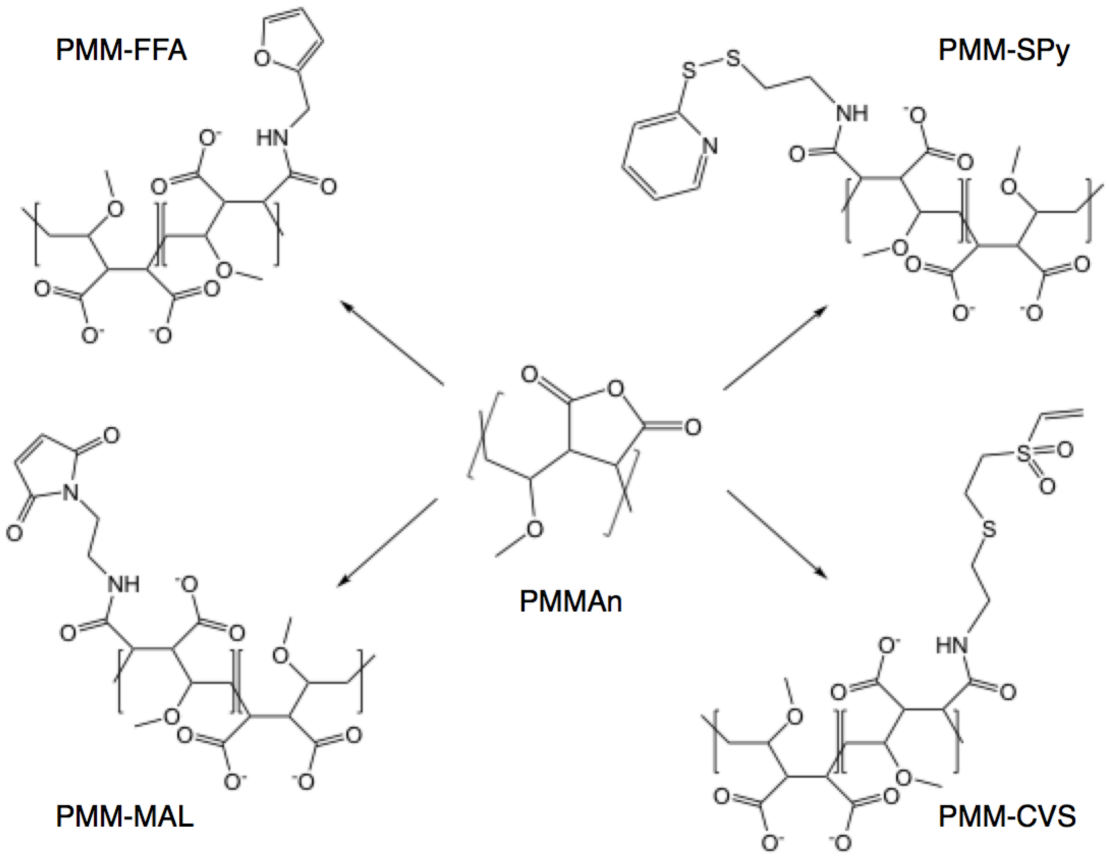

Figure 1.3. Mutually reactive polyanions (Diels-Alder: PMM-FFA/PMM-MAL; thiolene Michael Addition: PMM-SPy/PMM-CVS) prepared by functionalization of PMMAn.

Reported in this thesis are the synthesis and characterization of PMM-based Diels-Alder and thiolene reactive polymers, as well as the synthesis of a small molecule precursor. Characterization of the bulk gels formed by mixing of mutually reactive polyanions includes details on swellability, hydrolysis, post-gelation functionalization, and Young's modulus. Alginate-templated matrix beads, formed by mixing of mutually reactive polyanions with sodium alginate, followed by extrusion into $CaCl_2$ gelling bath, are fully described. Details such as polymer distribution, entrapment efficiency, permeability, swellability, and cell viability are reported.

1.8. References

(1) Zhao, X.; Wu, H.; Guo, B.; Dong, R.; Qiu, Y.; Ma, P.X. Antibacterial anti-oxidant electroactive injectable hydrogel as self-healing wound dressing with hemostasis and adhesives for cutaneous wound healing. *Biomaterials*, **2017**, *122*, 34-47.

(2) Wang, P.; Chu, W.; Zhuo, X.; Zhang, Y.; Gou, J.; Ren, T.; He, H.; Yin, T.; Tang, X. Modified PLGA-PEG-PLGA thermosensitive hydrogels with suitable thermosensitivity and properties for use in a drug delivery system. *J. Mater. Chem. B.*, **2017**, *5*, 1551-1565.

(3) Liu, S.; Su, W.; Li, Y.; Zhang, L.; Ding, X. Manufacturing of an electrochemical biosensing platform based on hybrid DNA hydrogel: Taking lung cancer-specific miR-21 as an example. *Biosens. Bioelectron.*, **2018**, *103*, 1-5.

(4) Eke, G.; Mangir, N.; Hasirci, N.; MacNeil, S.; Hasirci, V. Development of a UV crosslinked biodegradable hydrogel containing adipose derived stem cells to promote vascularization for skin wounds and tissue engineering. *Biomaterials*, **2017**, 188-198.

(5) Caló, E.; Khutoryanskiy, V.V. Biomedical applications of hydrogels: A review of patents and commercial products. *Eur. Polym. J.*, **2015**, *65*, 252-267.

(6) Wang, J.; Zhang, F.; Tsang, W.P.; Wan, C.; Wu, C. Fabrication of injectable high strength hydrogel based on 4-arm star PEG for cartilage tissue engineering. *Biomaterials*, **2017**, *120*, 11-21.

(7) Arakawa, C.; Ng, R.; Tan, S.; Kim, S.; Wu, B.; Lee, M. Photopolymerizable chitosan-collagen hydrogels for bone tissue engineering. *J. Tissue Eng. Regen. Med.*, **2017,** *11*, 164-174.

(8) Mellati, A.; Fan, C.-M.; Tamayol, A.; Annabi, N.; Dai, S.; Bi, J.; Jin, B.; Xian, C.; Khademhosseini, A.; Zhang, H. Microengineered 3D cell-laden thermoresponsive hydrogels for mimicking cell morphology and orientation in cartilage tissue engineering. *Biotechnol. Bioeng.*, **2017**, *114*, 217-231.

(9) Frantz, C.; Stewart, K. M.; Weaver, V. M. The Extracellular Matrix at a Glance. *J. Cell Sci*. **2010**, *123*, 4195−4200.

(10) Bershadsky, A.D.; Balaban, N.Q.; Geiger, B. Adhesion-dependent cell mechanosensitivity. *Annu. Rev. Cell Dev. Biol.*, **2003**, *19*, 677-695.

(11) Discher, D.E.; Janmey, P.A.; Wang, Y.-L. Tissue cells feel and respond to the stiffness of their substrate. *Science*, **2005**, *310*, 1139-1143.

(12) Engler, A.J.; Sen, S.; Sweeney, H.L.; Discher, D.E. Matrix Elasticity Directs Stem Cell Lineage Specification. *Cell*, **2006**, *126*, 677-689.

(13) Levett, P.A.; Melchels, F.P.W.; Schrobback, K.; Hutmacher, D.W.; Malda, J.; Klein, T.J. Chrondrocyte redifferentiation and construct mechanical property development in single-component photocrosslinkable hydrogels. *J. Biomed. Mater. Res.*, **2014**, *102*, 2544-2553.

(14) Tangtrongsup, S.; Kisiday, J.D. Modulating the oxidative environment during mesenchymal stem cells chondrogenesis with serum increases collagen accumulation in agarose culture. *J. Orthop. Res.*, **2018**, *36*, 506-514.

(15) Gothard, D.; Smith, E.L.; Kanczler, J.M.; Black, C.R.; Wells, J.A.; Roberts, C.A.; White, L.J.; Qutachi, O.; Peto, H.; Rashidi, H.; Rojo, L.; Stevens, M.M.; El Haj, A.J.; Rose, F.R.A.J.; Shakesheff, K.M.; Oreffo, R.O.C. In Vivo Assessment of Bone Regeneration in Alginate/Bone ECM Hydrogels with Incorporated Skeletal Stem Cells and Single Growth Factors. *PLoS ONE*, **2015,** *10*, e0145080.

(16) Ansari, S.; Diniz, I.M.; Chen, C.; Aghaloo, T.; Wu, B.M.; Shi, S.; Moshaverinia, A. Alginate/hyaluronic acid hydrogel delivery system characteristics regulate the

differentiation of periodontal ligament stem cells toward chondrogenic lineage. *J. Mater. Sci. Mater. Med.*, **2017**, *28*, https://doi.org/10.1007/s10856-017-5974-8

(17) Benton, G.; Arnaoutova, I.; George, J.; Kleinman, H.K.; Koblinski, J. Matrigel: From discovery and ECM mimicry to assays and models for cancer research. *Adv. Drug Deliv. Rev.*, **2014**, *79-80*, 3-18.

(18) Zimmermann, H.; Zimmermann, D.; Reuss, R.; Feilen, P.J.; Manz, B.; Katsen, A.; Weber, M.; Ihmig, F.R.; Ehrhart, F.; Geßner, P.; Behringer, M.; Steinbach, A.; Wegner, L.H.; Sukhoroukov, V.L.; Vásquez, J.A. Towards a medically approved technology for alginate-based microcapsules allowing long-term immunoisolated transport. *J. Mater. Sci. Mater. Med.*, **2005**, *16*, 491-501.

(19) Huang, Q.; Zou, Y.; Arno, M.C.; Chen, S.; Wang, T.; Gao, J.; Dove, A.P.; Du, J. Hydrogel scaffolds for differentiation of adipose-derived stem cells. *Chem. Soc. Rev.*, **2017**, *46*, 6255-6275.

(20) Truong, V.X.; Ablett, M.P.; Richardson, S.M.; Hoyland, J.A.; Dove, A.P. Simultaneous Orthogonal Dual-Click Approach to Tough, in-Situ-Forming Hydrogels for Cell Encapsulation. *J. Am. Chem. Soc.*, **2015**, *137*, 1618-1622.

(21) Foster, G.A.; Headen, D.M.; González-Garcia, C.; Salmerón-Sánchez, M.; Shirwan, H.; García, A.J. Protease-degradable microgels for protein delivery for vascularization. *Biomaterials*, **2017**, *113*, 170-175.

(22) Elias, P.Z.; Liu, G.W.; Wei, H.; Jensen, M.C.; Horner, P.J.; Pun, S.H. A functionalized, injectable hydrogel for localized drug delivery with tunable thermosensitivity: Synthesis and characterization of physical and toxological properties. *J. Control. Release*, **2015**, *208*, 76-84.

(23) Khetan, S.; Guvendiren, M.; Legant, W.R.; Cohen, D.M.; Chen, C.S.; Burdick, J.A. Degradation-mediated cellular traction directs stem cell fate in covalently crosslinked three-dimensional hydrogels. *Nature Materials*, **2013**, *12*, 458-465.

(24) Belair, D.G.; Schwartz, M.P.; Knusden, T.; Murphy, W.L. Human iPSC-derived endothelial cell sprouting assay in synthetic hydrogel arrays. *Acta Biomater.*, **2016**, *39*, 12-24.

(25) Lee, T.T.; García, J.R.; Paez, J.I.; Singh, A.; Phelps, E.A.; Weis, S.; Shafiq, Z.; Shekaran, A.; del Campo, A.; García, A.J.; Light-triggered in vivo activation of adhesive peptides regulates cell adhesion, inflammation, and vascularization of biomaterials. *Nature Materials*, **2015**, *14*, 352-360.

(26) Gyles, D.A.; Castro, L.D.; Silva, J.O.C. Jr.; Ribeiro-Costa, R.M. A review of the designs and prominent biomedical advances of natural and synthetic hydrogel formulations. *Eur. Polym. J.*, **2017**, *88*, 373-392.

(27) Wichterle, O.; Lim, D. Hydrophilic Gels for Biological Use. *Nature*, **1960***, 185*, 117-118.

(28) Kubinová, S.; Horák, D.; Hejčl, A.; Plichta, Z.; Kotek, J.; Proks, V.; Forosyak, S.; Syková, E. SIKVAV-modified highly superporous PHEMA scaffolds with oriented pores for spinal cord injury repair. *J. Tissue Eng. Regen. Med.*, **2015**, *9*, 1298-1309.

(29) Mabilleau, G.; Aguado, E.; Stancu, I.C.; Cinco, C.; Blasé, M.F.; Chappard, D. Effects of FGF-2 release from a hydrogel polymer on bone mass and microarchitecture. *Biomaterials*, **2008**, *29*, 1593-1600.

(30) Lee, D.; Cho, S.; Park, H.S.; Kwon, I. Ocular Drug Delivery through pHEMA-Hydrogel Contact Lenses Co-Loaded with Lipophilic Vitamins. *Scientific Reports*, **2016**, *6*, 34194.

(31) Cao, D.; Zhang, Y.; Ciu, Z.; Du, Y.; Shi, Z. New strategy for design and fabrication of polymeric hydrogel with tunable porosity as artificial corneal skirt. *Mater. Sci. Eng. C*, **2017**, *70*, 665-672.

(32) Grossen, P.; Witzigmann, D.; Sieber, S.; Huwyler, J. PEG-PCL-based nanomedicines: A biodegradable drug delivery system and its application. *J. Control. Release*, **2017**, *260*, 46-60.

(33) Arya, G.; Das, M.; Sahoo, S.K. Evaluation of curcumin loaded chitosan/PEG blended PLGA nanoparticles for effective treatment of pancreatic cancer. *Biomed. Pharmacother.*, **2018**, *102*, 555-566.

(34) Cao, L.; Cao, B.; Lu, C.; Wang, G.; Yu, L.; Ding, J. An injectable hydrogel formed by in situ cross-linking of glycol chitosan and multi-benzaldehyde

functionalized PEG analogues for cartilage tissue engineering. *J. Mater. Chem. B.*, **2015**, *3*, 1268-1280.

(35) McKinnon, D.D.; Domaille, D.W.; Cha, J.N.; Anseth, K.S. Biophysically Defined and Cytocompatible Covalently Adaptable Networks as Viscoelastic 3D Cell Culture Systems. *Adv. Mater.*, **2014**, *26*, 865-872.

(36) Zhang, J.; Wang, J.; Zhang, H.; Lin, J.; Ge, Z.; Zou, X. Macroporous interpenetrating network of polyethylene glycol (PEG) and gelatin for cartilage repair. *Biomed. Mater.*, **2016**, *11*, 035014.

(37) Garay, R.P.; El-Gewely, R.; Armstrong, J.K.; Garratty, G.; Richette, P. Antibodies against polyethylene glycol in healthy subjects and in patients treated with PEG-conjugated agents. *Expert Opin. Drug. Deliv.*, **2012**, *9*, 1319-1323.

(38) Yamasuji, Y.; Higashi, Y.; Sakanoue, M.; Katsue, H.; Kawai, K.; Arai, N.; Kanekura, T. A case of anaphylaxis caused by polyethylene glycol analogues. *Contact Dermatitis*, **2013**, *69*, 183-185.

(39) Orive, G.; Santos, E.; Pedraz, J.L.; Hernández, R.M. Application of cell encapsulation for controlled delivery of biological therapeutics. *Adv. Drug Deliv. Rev.*, **2014**, *67-68,* 3-14.

(40) Bisceglie, V.V. Über die antineoplastische Immunität. *Z. Krebsforsch*., **1933**, *40,* 141-158.

(41) Chang, T.M.S. Semipermeable Microcapsules. *Science*, **1964**, *146*, 524-525.

(42) Lim, F.; Sun, A.M. Microencapsulated islets as bioartifical endocrine pancreas. *Science*, **1980**, *210*, 908-910.

(43) Sayyar, B.; Dodd, M.; Marquez-Curtis, L.; Janowska-Wieczorek, A.; Hortelano, G. Fibronectin-Alginate microcapsules improve cell viability and protein secretion of encapsulated Factor IX-engineered human mesenchymal stromal cells. *Artif. Cells Nanomed. Biotechnol.*, **2015**, *43*, 318-327.

(44) Koo, J.; Chang. T.S.M. Secretion of erythropoietin from microencapsulated rat kidney cells. *Int. J. Artif. Organs*, **1993**, *16*, 557-560.

(45) Chang, P.L.; Shen, N.; Westcott, A.J. Delivery of recombinant gene products with microencapsulated cells in vivo. *Hum. Gene Ther*., 1993, *4*, 433-440.

(46) Manzoli, V.; Colter, D.C.; Dhanaraj, S.; Fornoni, A.; Ricordi, C.; Pileggi, A.; Tomei, A.A. Engineering human renal epithelial cells for transplantation in regenerative medicine. *Med. Eng. Phys.*, **2017**, *48*, 3-13.

(47) Selden, C.; Bundy, J.; Erro, E.; Puschmann, E.; Miller, M.; Kahn, D.; Hodgson, H.; Fuller, B.; Gonzalez-Molina, J.; Le Lay, A.; Gibbons, S.; Chalmers, S.; Modi, S.; Thomas, A.; Kilbride, P.; Isaacs, A.; Ginsburg, R.; Ilsey, H.; Thomson, D.; Chinnery, G.; Mankhala, N.; Loo, L.; Spearman, C.W. A clinical-scale BioArtifical Liver, developed for GMP, improved clinical parameters of liver function in porcine liver failure. *Sci. Rep*., **2017**, *7*, 14518.

(48) Colton, C.K. Implantable biohybrid artificial organs. *Cell Transplant*., **1995**, *4*, 415-436.

(49) Tam, R.Y.; Fuehrmann, T.; Mitrousis, N.; Shoichet, M.S. Regenerative Therapies for Central Nervous System Diseases: a Biomaterials Approach. *Neuropsychopharmacology*, **2014**, *39*, 169-188.

(50) Shapiro, A.M.J.; Pokrywczynska, M.; Ricordi, C. Clinical pancreatic islet transplantation. *Nat. Rev. Endocrinol*., **2017**, *13*, 268-277.

(51) Hamelmann, W.; Gray, D.W.; Cairns, T.D.; Ozasa, T.; Ferguson, D.J.; Cahill, A.; Welsh, K.I.; Morris, P.J. Immediate destruction of xenogenic islets in a primate model. *Transplantation*, **1994**, *58*, 1109-1114.

(52) Patience, C.; Takeuchi, Y.; Weiss, R.A. Infection of human cells by an endogenous retrovirus of pigs. *Nat Med*., **1997** *3*, 282–286.

(53) Chhabra, P.; Brayman, K. L. Stem Cell Therapy to Cure Type 1 Diabetes: From Hype to Hope. *Stem Cells Transl. Med.* **2013**, *2*, 328-336.

(54) Ferreira, D.; Westman, E.; Eyjolfsdottir, H.; Almqvist, P.; Göran, L.; Linderoth, B.; Seiger, A.; Blennow, K.; Karami, A.; Darreh-Shori, T.; Wiberg, M.; Simmons, A.; Wahlund, L.-O.; Wahlberg, L.; Eriksdotter, M. Brain changes in Alzheimer's disease patients with implanted encapsulated cells releasing nerve growth factor. *J. Alzheimers Dis*., **2015**, *43*, 1059-1072.

(55) Baimakhanov, Z.; Yamanouchi, K.; Sakai, Y.; Koike, M.; Soyama, A.; Hidaka, M.; Takatsuki, M.; Fujita, F.; Kanetaka, K.; Kuroki, T.; Eguchi, S.

Efficacy of multilayered hepatocyte sheet transplantation for radiation-induced liver damage and partial hepatectomy in a rat model. *Cell Transplant*., **2016**, *25*, 549-558.

(56) Krishnan, R.; Alexander, M.; Robles, L.; Foster; C.E. 3rd; Lakey, J.R.T. Islet and stem cell encapsulation for clinical transplantation. *Rev. Diabet. Stud*., **2014**, *11*, 84-101.

(57) Orive, G.; Hernandez, R.M.; Rodriguez-Gascon, A.; Calafiore, R.; Chang, T.M.; De Vos, P.; Hortelano, G.; Hunkeler, D.; Lacik, I.; Pedraz, J.L.; History, challenges and perspectives of cell microencapsulation. *Trends Biotechnol*., **2004**, *22*, 87-92.

(58) Orive, G.; Hernandez, R.M.; Gascon, A.R.; Igartua, M.; Pedraz, J.L. Survival of different cell lines in alginate-agarose microcapsules. *Eur. J. Pharm. Sci*., **2003**, *18*, 23-30.

(59) Fiorina, P.; Folli, F.; Maffi, P.; Placidi, C.; Venturini, M.; Finzi, G.; Bertuzzi, F.; Davalli, A.; D'Angelo, A.; Socci, C.; Gremizzi, C.; Orsenigo, E.; La Rosa, S.; Ponzoni, M.; Cardillo, M.; Scalamogna, M.; Del Maschio, A.; Capella, C.; Di Carlo, V.; Secchi, A. Islet transplantation improves vascular diabetic complications in patients with diabetes who underwent kidney transplantation: a comparison between kidney–pancreas and kidney-alone transplantation. *Transplantation*, **2003**, *75*, 1296-1301.

(60) Juang, J.H. Islet transplantation: an update. *Chang Gung Med. J*., **2004**, *27*, 1-15.

(61) De Haan, B.J.; Faas, M.M.; De Vos, P. Factors influencing insulin secretion from encapsulated islets. *Cell Transplant*., **2003**, *12*, 617-625.

(62) De Vos, P.; Van Hoogmoed, C.G.; van Zanten, J.; Netter, S.; Strubbe, J.H.; Busscher, H.J. Long-term biocompatibility, chemistry, and function of microencapsulated pancreatic islets. *Biomaterials*, **2003**, *24*, 305-312.

(63) Hirsiger, S.; Simmen, H.P.; Werner, C.M.; Wanner, G.A.; Rittirsch, D. Danger signals activating the immune response after trauma. *Mediators Inflamm*., **2012**, *2012*, 315941.

(64) Pittman, K.; Kubes, P. Damage-associated molecular patterns control neutrophil recruitment. *J. Innate Immun*., **2013**, *5*, 315-323.

(65) Scharp D.W.; Marchetti P. Encapsulated islets for diabetes therapy: history, current progress, and critical issues requiring solution. *Adv Drug Deliv Rev*., **2014**, *67-68,* 35–73.

(66) Pepper, A.R.; Pawlick, R.; Bruni, A.; Wink, J.; Rafiei, Y.; O'Gorman, D.; Yan-Do, R.; Gala-Lopez, B.; Kin, T.; MacDonald, P.E.; Shapiro, A.M.J. Transplantation of Human Pancreatic Endoderm Cells Reverses Diabetes Post Transplantation in a Prevascularized Subcutaneous Site. *Stem Cell Reports*, **2017**, *8*, 1689-1700.

(67) Orive, G.; Santos, E.; Pedraz, J.L.; Hernández, R.M. Application of cell encapsulation for controlled delivery of biological therapeutics. *Adv. Drug Deliv. Rev*. **2014**, *67-68*, 3–14.

(68) Vegas, A.J.; Veiseh, O.; Gürtler, M.; Millman, J.R.; Pagliuca, F.W.; Bader, A.R.; Doloff, J.C.; Li, J.; Chen, M.; Olejnik, K.; Tam, H.H.; Jhunjhunwala, S.; Langan, E.; Aresta-Dasilva, S.; Gandham, S.; McGarrigle, J.J.; Bochenek, M.A.; Hollister-Lock, J.; Oberholzer, J.; Greiner, D.L.; Weir, G.C.; Melton, D.A.; Langer, R.; Anderson, D.G. Long-term glycemic control using polymer-encapsulated human stem cell-derived beta cells in immune-competent mice. *Nat. Med.*, **2016**, *22*, 306-311.

(69) Pham-Hua, D.; Padgett, L.E.; Xue, B.; Anderson, B.; Zeiger, M.; Barra, J.M.; Bethea, M.; Hunter, C.S.; Kozlovskaya, V.; Kharlampieva, E.; Tse, H.M. Islet encapsulation with polyphenol coatings decreases pro-inflammatory chemokine synthesis and T cell trafficking. *Biomaterials*, **2017**, *128*, 19–32.

(70) Bloch, K.; Vanichkin, A.; Gil-Ad, I.; Vardi, P.; Weizman, A. Insulin delivery to the brain using intracranial implantation of alginate- encapsulated pancreatic islets. *J Tissue Eng Regen Med.,* **2017**, *11*, 3262-3272.

(71) Hillberg, A.L.; Oudshoorn, M.; Lam, J.B.; Kathirgamanathan, K. Encapsulation of porcine pancreatic islets within an immunoprotective capsule comprising

methacrylated glycol chi- tosan and alginate. *J Biomed Mater Res B Appl Biomater*., **2015**, *103*, 503–518.

(72) Calafiore, R.; Basta, G.; Luca, G.; Lemmi, A.; Montanucci, M.P.; Calabrese, G. Racanicchi, L.; Mancuso, F.; Brunetti, P. Microencapsulated pancreatic islet allografts into nonimmunosuppressed patients with type 1 diabetes: first two cases. *Diabetes Care*, **2006**, *29*, 137–138.

(73) Basta, G.; Montanucci, P.; Luca, G.; Boselli, C.; Noya, G.; Barbaro, B.; Qi, M.; Kinzer, K.P.; Oberholzer, J.; Calafiore, R. Long-term metabolic and immunological follow-up of nonimmunosuppressed patients with type 1 diabetes treated with microencapsulated islet allografts: four cases. *Diabetes Care*, **2011,** *34*, 2406–2409.

(74) Matsumoto, S.; Abalovich, A.; Wechsler, C.; Wynyard, S.; Elliott, R.B. Clinical benefit of islet xenotransplantation for the treatment of type 1 diabetes. *EBioMedicine*, **2016**, *12*, 255–262.

(75) Yesilyurt, V.; Veiseh, O.; Doloff, J.C.; Li, J.; Bose, S.; Xie, X.; Bader, A.R.; Chen, M.; Webber, M.J.; Vegas, A.J.; Langer, R.; Anderson, D. A Facile and Versatile Method to Endow Biomaterial Devices with Zwitterionic Surface Coatings. *Adv. Healthcare Mater.*, **2017**, *6*, 1601091.

(76) Vegas, A.J.; Veiseh, O.; Doloff, J.C.; Ma, M.; Tam, H.H.; Bratlie, K.; Li, J.; Bader, A.R.; Langan, E.; Olejnik, K.; Fenton, P.; Kang, J.W.; Hollister-Locke, J.; Bochenek, M.A.; Chiu, A.; Siebert, S.; Tang, K.; Jhunjhunwala, S.; Aresta-Dasilva, S.; Dholakia, N.; Thakrar, R.; Vietti, T.; Chen, M.; Cohen, J.; Siniakowicz, K.; Qi, M.; McGarrigle, J.; Graham, A.C.; Lyle, S.; Harlan, D.M.; Greiner, D.L.; Oberholzer, J.; Weir, G.C.; Langer, R.; Anderson, D.G. Combinatorial hydrogel library enables identification of materials that mitigate the foreign body response in primates. *Nat. Biotechnol*., **2016**, *34*, 345-352.

(77) Vegas, A.J.; Veiseh, O.; Gürtler, M.; Millman, J.R.; Pagliuca, F.W.; Bader, A.R.; Doloff, J.C.; Li, J.; Chen, M.; Olejnik, K.; Tam, H.H.; Jhunjhunwala, S.; Langan, E.; Aresta-Dasilva, S.; Gandham, S.; McGarrigle, J.J.; Bochenek, M.A.; Hollister-Locke, J.; Oberholzer, J.; Greiner, D.L.; Weir, G.C.; Melton, D.A.; Langer, R.;

Anderson, D.G. Long-term glycemic control using polymer-encapsulated human stem cell-derived beta cells in immune-competent mice. *Nat. Med.*, **2016**, *22*, 306-311.

(78) Cantarelli, E.; Citro, A.; Piemonti, L. Pancreatic Islet Transplantation Technologies: State of the Art of Micro- and Macro-Encapsulation. *Curr. Transpl. Rep.,* **2017**, *4*, 169-183.

(79) Uludag, H.; De Vos, P.; Tresco, P.A. Technology of mammalian cell encapsulation. *Adv. Drug Deliv. Rev*., **2000**, *42*, 29-64.

(80) Cantarelli, E.; Citro, A.; Piemonti, L. Pancreatic Islet Transplantation Technologies: State of the Art of Micro- and Macro-Encapsulation. *Curr. Transplant. Rep.*, **2017**, *4*, 169-183.

(81) Paredes-Juarez, G.A.; de Haan, B.J.; Faas, M.M.; De Vos, P. The role of pathogen-associated molecular patterns in inflammatory responses against alginate based microcapsules. *J. Control. Release*, **2013**, *172*, 983-992.

(82) Veiseh, O.; Doloff, J.C.; Ma, M.; Vegas, A.J.; Tam, H.H.; Bader, A.R.; Li, J.; Langan, E.; Wyckoff, J.; Loo, W.S.; Jhunjhunwala, S.; Chiu, A.; Siebert, S.; Tang, K.; Hollister-Lock, K.; Aresta-Dasilva, S.; Bochenek, M.; Mendoza-Elias, J.; Wang, Y.; Qi, M.; Lavin, D.M.; Chen, M.; Dholakia, N.; Thakrar, R.; Lacík, I.; Weir, G.C.; Oberholzer, J.; Greiner, D.L.; Langer, R.; Anderson, D.G. Size- and shape-dependent foreign body immune response to materials implanted in rodents and non-human primates. *Nat. Mater.,* **2015**, *14*, 643-651.

(83) Stokke, B.T.; Smidsroed, O.; Bruheim, P.; Skjaak-Braek, G. Distribution of uronate residues in alginate chains in relation to alginate gelling properties. *Macromolecules*, **1991**, *24*, 4637-4645.

(84) Morch, Y.A.; Donati, I.; Strand, B.L.; Skjak Braek, G. Effect of Ca2 +, Ba2 +, and Sr2 + on alginate microbeads. *Biomacromolecule*s, **2006**, *7*, 1471-1480.

(85) Teramura, Y.; Oommen, O.P.; Olerud, J.; Hilborn, J.; Nilsson, B. Microencapsulation of cells, including islets, within stable ultra-thin membranes of maleimide-conjugated PEG-lipid with multifunctional crosslinkers. *Biomaterials*, **2013**, *34*, 2683-2693.

(86) Lanza, R.P.; Ecker, D.; Kühtreiber, W.M.; Staruk, J.E.; Marsh, J.; Chick, W.L. A simple method for transplanting discordant islets into rats using alginate gel spheres. *Transplantation*, **1995**, *59*,1485-1487.

(87) De Vos, P.; Bucko, M.; Gemeiner, P.; Navratil, M.; Svitel, J.; Faas, M.; Strand, B.L.; Skjak-Braek, G.; Morch, Y.A.; Vikartovska, A.; Lacik, I.; Kollarikova, G.; Orive, G.; Poncelet, D.; Pedraz, J.L.; Ansorge-Schumacher, M.B. Multiscale requirements for bioencapsulation in medicine and biotechnology. *Biomaterials*, **2009**, *30*, 2559-2570.

(88) De Vos, P.; van Straaten, J.F.; Nieuwenhuizen, A.G.; de Groot, M.; Ploeg, R.J.; De Haan, B.J.; Van Schilfgaarde, R. Why do microencapsulated islet grafts fail in the absence of fibrotic overgrowth? *Diabetes,* **1999**, *48,* 1381-1388.

(89) Wang, T.; Lacík, I.; Brissová, M.; Anilkumar, A.V.; Prokop, A.; Hunkeler, D.; Green, R.; Shahrokhi, K.; Powers, A.C. An encapsulation system for the immunoisolation of pancreatic islets. *Nat. Biotechnol*., **1997**, *15*, 358-362.

(90) Bartkowiak, A.; Canaple, L.; Ceausoglu, I.; Nurdin, N.; Renken, A.; Rindisbacher, L.; Wandrey, C.; Desvergne, B.; Hunkeler, D. New multicomponent capsules for immunoisolation.

(91) Calafiore, R.; Pietropaolo, M.; Basta, G.; Falorni, A.; Picchio, M.L.; Brunetti, P. Pancreatic beta-cell destruction in non-obese diabetic mice. *Metabolism*, **1993**, *42*, 854-859.

(92) De Vos, P.; De Haan, B.; Van Schilfgaarde, R. Effect of the alginate composition on the biocompatibility of alginate–polylysine microcapsules. *Biomaterials*, **1997**, *18*, 273-278.

(93) Choksakulnimitr, S.; Musada, S.; Tokuda, H.; Takakura, Y.; Hashida, M. In vitro cytotoxicity of macromolecules in different cell culture systems. *J. Controlled Release,* **1995**, *34*, 233-241.

(94) De Haan, B.J.; Faas, M.M.; De Vos, P. Factors influencing insulin secretion from encapsulated islets. *Cell Transplant*., **2003**, *12*, 617-625.

(95) Tam, K.T.; Dusseault, J.; Polizu, S.; Ménard, M.; Hallé, J.P.; L'Hocine, Y. Physicochemical model of alginate–poly-l-lysine microcapsules defined at the

micrometric/nanometric scale using ATR-FTIR, XPS, and ToF-SIMS. *Biomaterials*, **2005**, *26*, 6950-6961.

(96) Bunger, C.M.; Tiefenbach, B.; Jahnke, A.; Gerlach, C.; Freier, T.; Schmitz, K.P.; Hopt, U.T.; Schareck, W.; Klar, E.; , P. Deletion of the tissue response against alginate–pll capsules by temporary release of co-encapsulated steroids. *Biomaterials*, **2005**, *26*, 2353-2360.

(97) Bunger, C.M.; Gerlach, C.; Freier, T.; Schmitz, K.P.; Pilz, M.; Werner, C.; Jonas, L.; Schareck, W.; Hopt, U.T.; De Vos, P**.** Biocompatibility and surface structure of chemically modified immunoisolating alginate–PLL capsules. *J. Biomed. Mater. Res*., **2003**, *67A*, 1219-1227.

(98) Strand, B.L.; Ryan, L.; Veld, P.I.; Kulseng, B.; Rokstad, A.M.; Skjåk-Braek, G.; Espevik, T. Poly-L-Lysine Induces Fibrosis on Alginate Microcapsules via the Induction of Cytokines. *Cell Transplant.*, **2001**, *10*, 263-275.

(99) Rokstad, A.M.; Holtan, S.; Strand, B.; Steinkjer, B.; Ryan, L.; Kulseng, B.; Skjåk-Braek, G.; Espevik, T. Microencapsulation of Cells Producing Therapeutic Proteins: Optimizing Cell Growth and Secretion. *Cell Transplant.,* **2002**, *11*, 313-324.

(100) Gardner, C.M.; Potter, M.A.; Stöver, H.D.H. Improving covalent cell encapsulation with temporarily reactive polyelectrolytes. *J. Mater. Sci.: Mater. Med.*, **2012**, *23*, 181-193.

(101) Sawhney, A.S.; Hubbell, J.A. Poly(ethylene oxide)-graft-poly(L-lysine) copolymers to enhance the biocompatibility of poly(L-lysine)-alginate microcapsule membranes. *Biomaterials*, **1992,** *13*, 863-870.

(102) Wilson, J.T.; Cui, W.; Kozlovskaya, V.; Kharlampieva, E.; Pan, D.; Qu, Z.; Krishnamurthy, V.R.; Mets, J.; Kumar, V.; Wen, J.; Song, Y.; Tsukruk, V.V.; Chaikof, E.L. Cell Surface Engineering with Polyelectrolyte Multilayer Thin Films. *J. Am. Chem. Soc.*, **2011**, *133*, 7054-7064.

(103) Spasojevic, M.; Paredes-Juarez, G.A.; Vorenkamp, J.; de Haan, B.J.; Schouten, A.J.; De Vos, P. Reduction of the Inflammatory Responses against Alginate-Poly-

L-Lysine Microcapsules by Anti-Biofouling Surfaces of PEG-b-PLL Diblock Copolymers. *PLoS ONE*, **2014**, *9*, e109837.

(104) Kleinberger, R.M.; Burke, N.A.D.; Zhou, C.; Stöver, H.D.H. Synthetic polycations with controlled charge density and molecular weight as building blocks for biomaterials. *J. Biomater. Sci. Polym. Ed.*, **2016**, *27*, 351-369.

(105) Ros, S.; Burke, N.A.D.; Stöver, H.D.H. Synthesis and Properties of Charge-Shifting Polycations: Poly[3-aminopropylmethacrylamide-*co*-2-(dimethylamino)ethyl acrylate]. *Macromolecules*, **2015**, *48*, 8958-8970.

(106) Dubey, A.; Burke, N.A.D.; Stöver, H.D.H. Preparation and characterization of narrow compositional distribution polyampholytes as potential biomaterials: Copolymers of *N*-(3-aminopropyl)methacrylamide hydrochloride (APM) and methacrylic acid (MAA). *J. Polym. Sci. A.,* **2015**, *53,* 353-365.

(107) Piskin, E. Biodegradable polymers as biomaterials. *J. Biomater. Sci. Polym. Ed*., **1995**, *6*, 775-795.

(108) Desai, N.P.; Sojomihardjo, A.; Yao, Z.; Ron, N.; Soon-Shiong, P. Interpenetrating polymer networks of alginate and polyethylene glycol for encapsulation of islets of Langerhans. *J. Microencapsul*., **2000**, *17*, 677-690.

(109) Breguet, V.; Gugerli, R.; Pernetti, M.; von Stockar, U.; Marison, I.W. Formation of microcapsules from polyelectrolyte and covalent interactions. *Langmuir*, **2005**, *21*, 9764-9772.

(110) Dusseault, J.; Leblond, F.A.; Robitaille, R.; Jourdan, G.; Tessier, J.; Menard, M.; Henley, N.; Hallé, J.P. Microencapsulation of living cells in semi-permeable membranes with covalently cross-linked layers. *Biomaterials,* **2005**, *26*, 1515-1522,

(111) Gattas-Asfura, K.M.; Stabler, C.L. Chemoselective cross-linking and functionalization of alginate via Staudinger ligation. *Biomacromolecules*, **2009**, *10*, 3122-3129.

(112) Kolb, H. C.; Finn, M. G.; Sharpless, K. B. Click chemistry: Diverse Chemical Function from a Few Good Reactions. *Angew. Chem. Int. Ed.* **2001**, *40*, 2004-2021.

(113) Kharkar, P.; Rehmann, M.S.; Skeens, K.M.; Maverakis, E.; Kloxin, A.M. Thiol-ene Click Hydrogels for Therapeutic Delivery. *ACS Biomater. Sci. Eng.*, **2016**, *2*, 165-179.

(114) Ono, R.J.; Lee, A.L.Z.; Voo, Z.X.; Venkataraman, S.; Koh, B.W.; Yang, Y.Y.; Hedrick, J.L. Biodegradable Strain-Promoted Click Hydrogels for Encapsulation of Drug-Loaded Nanoparticles and Sustained Release of Therapeutics. *Biomacromolecules*, **2017**, *18*, 2277-2285.

(115) Gao, L.; Li, X.; Wang, Y.; Zhu, W. Injectable thiol-epoxy "click" hydrogels. *J. Polym. Sci. A Polym. Chem.*, **2016**, *54*, 2651-2655.

(116) Seliktar, D. Designing cell-compatible hydrogels for biomedical applications. *Science*, **2012**, *336*, 1124-1128.

(117) Vermonden, T.; Censi, R.; Hennink, W.E. Hydrogels for protein delivery. *Chem Rev*, **2012**, *112*, 2853-2888.

(118) Lutolf, M.P.; Gilbert, P.M.; Blau, H.M. Designing materials to direct stem-cell fate. *Nature*, **2009**, *462*, 433-441.

(119) Nochi, T.; Yuki, Y.; Takahashi, H.; Sawada, S.-I.; Mejima, M.; Kohda, T.; Harada, N.; Kong, I.G.; Sato, A.; Kataoka, N.; Tokuhara, D.; Kurokawa, S.; Takahashi, Y.; Tsukada, H.; Kozaki, S.; Akiyoshi, K.; Kiyono, H. Nanogel antigenic protein-delivery system for adjuvant-free intranasal vaccines. *Nat. Mater.*, **2010**, *9*, 572-578.

(120) Lyon, L.A.; Meng, Z.; Singh, N.; Sorrell, C.D.; John, A.S. Thermoresponsive microgel-based materials. *Chem. Soc. Rev.*, **2009**, *38*, 865-874.

(121) He, C.; Kim, S.W.; Lee, D.S. In situ gelling stimuli-sensitive block copolymer hydrogels for drug delivery. *J. Control Release*, **2008**, *127*, 189-207.

(122) Yu, L.; Ding, J. Injectable hydrogels as unique biomedical materials. *Chem. Soc. Rev.*, **2008**, *37*, 1473-1481.

(123) Van Tomme, S.R.; Storm, G.; Hennink, W.E. In situ gelling hydrogels for pharmaceutical and biomedical applications. *Int J Pharm*, **2008**, *355*, 1-18.

(124) Hoare, T.R.; Kohane, D.S. Hydrogels in drug delivery: progress and challenges. *Polymer*, **2008**, *49*, 1993-2007.

(125) Oh, J.K.; Drumright, R.; Siegwart, D.J.; Matyjaszewski, K. The development of microgels/nanogels for drug delivery applications. *Prog Polym Sci*, **2008**, *33*, 448-477.

(126) Chenite, A.; Chaput, C.; Wang, D.; Combes, C.; Buschmann, M.D.; Hoemann, C.D.; Leroux, J.C.; Atkinson, B.L.; Binette, F.; Selmani, A. Novel injectable neutral solutions of chitosan form biodegradable gels in situ. *Biomaterials*, **2000**, *21*, 2155-2161.

(127) Hiemstra, C.; Zhou, W.; Zhong, Z.; Wouters, M.; Feijen, J. Rapidly in situ forming biodegradable robust hydrogels by combining stereocomplexation and photopolymerization. *J Am Chem Soc*, **2007**, *129*, 9918-9926.

(128) Lim, D.W.; Nettles, D.L.; Setton, L.A.; Chilkoti, A. Rapid cross-linking of elastin-like polypeptides with (hydroxymethyl)phosphines in aqueous solution. *Biomacromolecules*, **2007**, *8*, 1463-1470.

(129) Censi, R.; Vermonden, T.; Deschout, H.; Braeckmans, K.; Di Martino, P.; De Smedt, S.C.; van Nostrum, C.F.; Hennink, W.E. Photopolymerized thermosensitive poly(HPMAlactate)-PEG-based hydrogels: effect of network design on mechanical properties, degradation, and release behaviour. *Biomacromolecules*, **2010**, *11*, 2143-2151.

(130) Jin, R.; Hiemstra, C.; Zhong, Z.; Feijen, J. Enzyme-mediated fast in situ formation of hydrogels from dextran-tyramine conjugates. *Biomaterials*, **2007**, *28*, 2791-2800.

(131) Rostovtsev, V.V.; Green, L.G.; Fokin , V.V.; Sharpless, K.B. A stepwise huisgen cycloaddition process: copper(I)-catalyzed regioselective "ligation" of azides and terminal alkynes. *Angew. Chem., Int. Ed.*, **2002**, *41*, 2596–2599.

(132) Tornoe, C.W.; Christensen, C.; Meldal, M. Peptidotriazoles on solid phase: [1,2,3]-triazoles by regiospecific copper(i)-catalyzed 1,3-dipolar cycloadditions of terminal alkynes to azides. *J. Org. Chem.*, **2002**, *67*, 3057–3064.

(133) Sletten, E.M.; Bertozzi, C.R. Bioorthogonal chemistry: fishing for selectivity in a sea of functionality. *Angew. Chem., Int. Ed.*, **2009**, *48*, 6974–6998.

(134) Agard, N.J.; Prescher, J.A.; Bertozzi, C.R. A strain-promoted [3+2] azide-alkyne cycloaddition for covalent modification of biomolecules in living systems. *J. Am. Chem. Soc.*, **2004**, *126*, 15046–15047.

(135) Dommerholt, J.; Rutjes, F.P.; van Delft, F.L. Strain-Promoted 1,3-Dipolar Cycloaddition of Cycloalkynes and Organic Azides. *Top. Curr. Chem.*, **2016**, *374*, 16.

(136) Hodgson, S.M.; Bakaic, E.; Stewart, S.A.; Hoare, T.; Adronov, A. Properties of Poly(ethylene glycol) Hydrogels Cross-Linked via Strain-Promoted Alkyne-Azide Cycloaddition (SPAAC). *Biomacromolecules*, **2016**, *17*, 1093-1100.

(137) Gandini, A. The furan/maleimide Diels–Alder reaction: a versatile click–unclick tool in macromolecular synthesis. *Prog Polym Sci*, **2013**, *38*, 1-29.

(138) Nimmo, C.M.; Owen, S.C.; Shoichet, M.S. Diels-Alder Click Cross-Linked Hyaluronic Acid Hydrogels for Tissue Engineering. *Biomacromolecules*, **2011**, *12*, 824-830.

(139) Smith, L.J.; Taimoory, S.M.; Tam, R.Y.; Baker, A.E.G.; Mohammad, N.B.; Trant, J.F.; Shoichet, M.S. Diels-Alder Click-Cross-Linked Hydrogels with Increased Reactivity Enable 3D Cell Encapsulation. *Biomacromolecules*, **2018**, *19*, 926-935.

(140) Alge, D.L.; Azagarsamy, M. A.; Donohue, D.F.; Anseth, K.S. Synthetically Tractable Click Hydrogels for Three-Dimensional Cell Culture Formed Using Tetrazine-Norbornene Chemistry. *Biomacromolecules*, **2013**, *14*, 949-953.

(141) Mather, B.D.; Viswanathan, K.; Miller, K.M.; Long, T.E. Michael addition reactions in macromolecular design for emerging technologies. *Prog Polym Sci*, **2006**, *31*, 487-531.

(142) Chatani, S.; Nair, D.P.; Bowman, C.N. Relative reactivity and selectivity of vinyl sulfones and acrylates towards the thiol-Michael addition reaction and polymerization. *Polym Chem*, **2013**, *4*, 1048-1055.

(143) Hoyle, C.E.; Lowe, A.B.; Bowman, C.N. Thiol-click chemistry: a multifaceted toolbox for small molecule and polymer synthesis. *Chem Soc Rev*, **2010**, *39*, 1355-1387.

(144) Li, G.-Z.; Randev, R.K.; Soeriyadi, A.H.; Rees, G.; Boyer, C.; Tong, Z.; Davis, T.P.; Becer, C.R.; Haddleton, D.M. Investigation into thiol-(meth)acrylate

michael addition reactions using amine and phosphine catalysts. *Polym Chem*, **2010**, *1*, 1196-1204.

(145) Elbert, D.L.; Pratt, A.B.; Lutolf, M.P.; Halstenberg, S.; Hubbell, J.A. Protein delivery from materials formed by self-selective conjugate addition reactions. *J Control Release*, **2001**, *76*, 11-25.

(146) Lutolf, M.P.; Tirelli, N.; Cerritelli, S.; Cavalli, L.; Hubbell, J.A. Systematic modulation of Michael-type reactivity of thiols through the use of charged amino acids. *Bioconjug Chem*, **2001**, *12*, 1051-1056.

(147) Metters, A.; Hubbell, J. Network formation and degradation behavior of hydrogels formed by Michael-type addition reactions. *Biomacromolecules*, **2005**, *6*, 290-301.

(148) Lutolf, M.P.; Hubbell, J.A. Synthesis and physicochemical characterization of end-linked poly(ethylene glycol)-co-peptide hydrogels formed by Michael-type addition. *Biomacromolecules*, **2003**, *4*, 713-722.

(149) van de Wetering, P.; Metters, A.T.; Shoenmakers, R.G.; Hubbell, J.A. Poly(ethylene glycol) hydrogels formed by conjugate addition with controllable swelling, degradation, and release of pharmaceutically active proteins. *J. Control. Release,* **2005**, *102*, 619-627.

(150) Li, Y.; Lee, P.I. A new bioerodible system for sustained local drug delivery based on hydrolytically activated in situ macromolecular association. *Int. J. Pharm.* **2010**, *383*, 45-52.

(151) Caló, E.; Barros, J.; Ballamy, L.; Khutoryanskiy, V.V. Poly(vinyl alcohol)-Gantrez® AN cryogels for wound care applications. *RSC Adv.*, **2016**, *6*, 105487-105494.

(152) Gómez, S.; Gamazo, C.; San Roman, B.; Ferrer, M.; Sanz, M.L.; Irache, J.M. Gantrez® AN nanoparticles as an adjuvant for oral immunotherapy with allergens. *Vaccine*, **2007**, *25*, 5263-5271.

(153) Arbos, P.; Wirth, M.; Arangoa, M.A.; Gabor, F.; Irache, J.M. Gantrez® AN as a new polymer for the preparation of ligand-nanoparticle conjugates. *J. Control. Release,* **2002**, *83*, 321–330.

(154) Shimizu, T.; Minakata, A. Effect of divalent cations on the volume of a maleic acid copolymer gel examined by incorporating lysozyme. *Eur. Polym. J.* **2002**, *38*, 1113-1120.

(155) Gardner, C.M.; Burke, N.A.D.; Stöver, H.D.H. Cross-linked microcapsules formed from self-deactivating reactive polyelectrolytes. *Langmuir*, **2010**, *26*, 4916-4924.

(156) Gardner, C.M; Burke, N.A.D.; Chu, T.; Shen, F.; Potter, M.A.; Stöver, H.D.H. Cross-Linked Microcapsules Formed From Self-Deactivating Reactive Polyelectrolytes. *J. Biomater. Sci., Polym. Ed.* **2011**, *22*, 2127-2145.

(157) Bajpai, S.K.; Sharma, S. Investigation of swelling/degradation behaviour of alginate beads crosslinked with Ca2+ and Ba2+ ions. *React. Funct. Polym.*, **2004**, *59*, 129-140.

Chapter 2

Crosslinked hydrogels formed through Diels-Alder coupling of Furan- and Maleimide-modified Poly(methyl vinyl ether-*alt*-maleic acid)

This chapter has been reprinted with permission from Langmuir; S. Alison Stewart, Matilda Backholm, Nicholas A.D. Burke, Harald D.H. Stöver, **2016**, *32*, 1863-1870. DOI: 10.1021/acs.langmuir.5b04450.

Alison Stewart primarily planned this study. Alison Stewart synthesized all polymers and hydrogels and carried out physical characterization tests. Matilda Backholm wrote the software for measuring Young's modulus, designed the experimental set-up, assisted with data interpretation and contributed to writing of Young's modulus section. Nicholas Burke and Harald Stöver provided experimental guidance and editing feedback of the manuscript.

2.1 Abstract

The Diels-Alder [4 + 2] cycloaddition between furan- and maleimide-functional polyanions was used to form crosslinked synthetic polymer hydrogels. Poly(methyl vinyl ether-*alt*-maleic anhydride) was reacted with furfurylamine or *N*-(2-aminoethyl)maleimide in acetonitrile to form pairs of furan- and maleimide-functionalized poly(methyl vinyl ether-*alt*-maleic acid)s. Mixtures of these mutually reactive polyanions in water gelled within 15 minutes to 18 hours, depending on degree of functionalization and polymer concentrations. Solution and magic-angle spinning ^{1}H-NMR were used to confirm the formation of the Diels-Alder adduct, to analyze competing hydrolytic side reactions, and demonstrate post-gelation functionalization. The effect of the degree of furan and maleimide functionalization, polymer concentration, pH, and calcium ion concentration, on gelation time, gel mechanical properties and equilibrium swelling, are described. Release of dextran as a model drug was studied using fluorescence spectroscopy, as a function of gel composition and calcium treatment.

2.2 Introduction

Regenerative medicine aims to replace or repair damaged cells, tissue or organs through the use of stem cells. In tissue, stem cells are embedded in an extracellular matrix (ECM) comprising proteins and polysaccharides,[1] that contribute mechanical and chemical cues for cell behaviour.[2]

In recent years, synthetic polymer scaffolds have been explored as mimics for natural ECM.[3,4,5,6] These synthetic ECM mimics typically consist of crosslinked polymers[7] with high water content[8] that are formed under mild conditions and may be modified for proper cell adhesion and elasticity.[9]

Synthetic gels offer several advantages, including defined composition, scalability, and absence of biological impurities and possible pathogens.[10] In particular, the formation of crosslinked hydrogels by bio-orthogonal "click reactions" has shown promising results.[11] One approach involves Diels-Alder coupling between furan and maleimide-modified polymers. This crosslinking reaction does not require small-molecule catalysts or additives, and is accelerated in water *cf*. organic solvents.[12] Shoichet's group recently described hydrogels formed from furan-functionalized hyaluronic acid, crosslinked with bismaleimido-PEG.[13,14] The resulting gels served as temporary cell support for tissue engineering, with enzymatic breakdown of the hyaluronic acid backbone driving the degradation. These crosslinked hydrogels were found to be cytocompatible, with no adverse effects from residual furan or maleimide moieties.

This chapter describes analogous Diels-Alder crosslinked hydrogels formed from fully synthetic polymers. Specifically, poly(methyl vinyl ether-*alt*-maleic anhydride) (PMMAn) was reacted with furfurylamine and *N*-(2-aminoethyl)maleimide before residual anhydride groups were hydrolyzed to produce the corresponding functionalized poly(methyl vinyl ether-*alt*-maleic acid)s (PMM), called PMM-FFA and PMM-MAL, respectively. These reactive polymers are water-soluble as a result of their high anionic charge density, and covalently crosslink by Diels-Alder coupling when mixed together in aqueous solution (scheme 2.1).

Various PMM-based polymers have already found use as pharmaceutical thickening and suspending agents, as denture adhesives, and as adjuvants for drug delivery systems, and offer several advantages to naturally derived systems, such as ease of functionalization and minimal batch-to-batch variation.[15-18] Gardner *et al*. have shown that PMMAn can be functionalized with amino-terminal PEG and aminofluorescein, and that calcium alginate capsules bearing PMM as an outer coating showed excellent compatibility both with encapsulated cells and with the host, upon implantation in immuno-competent mice. [19-21]

PMM-FFA and PMM-MAL were further functionalized with rhodamine and fluorescein to allow tracking of both polymers by fluorescence microscopy. Solution state and magic angle spinning (MAS) ^{1}H NMR were used to characterize the soluble and crosslinked polymers, and, importantly, to investigate several hydrolysis side reactions that can compete with crosslinking. The effects of degrees of functionalization, polymer concentrations, and solution conditions such as pH and presence of Ca^{2+}, on the gelation rate and on gel properties such as swelling and elasticity, are described. The use of Ca^{2+} ions to control pore-size of the hydrogels for controlled release is also described.

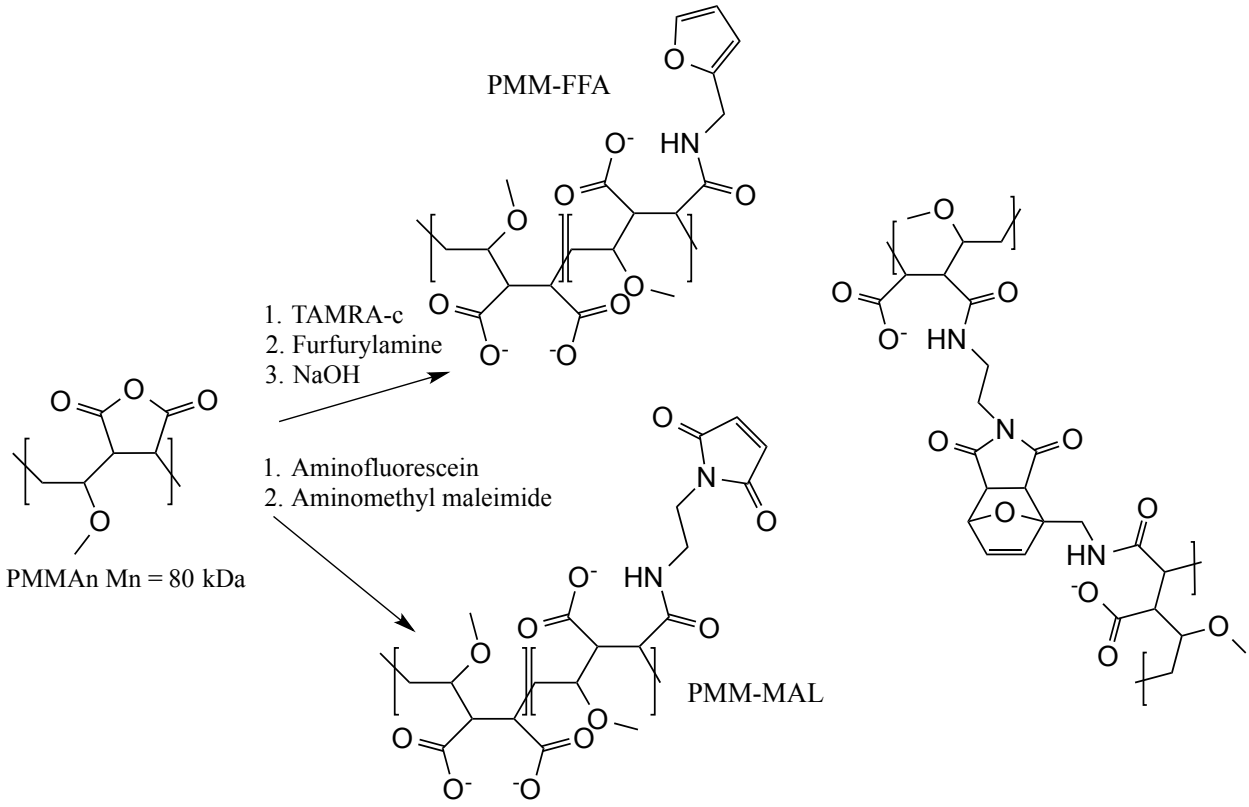

Scheme 2.1. Furan- and maleimide-functionalization of PMMAn, and the Diels-Alder crosslinked PMM-FFA/MAL hydrogel. Fluorescent labels are omitted in structures, for simplicity.

2.3 Experimental Section

2.3.1 Materials

Poly(methyl vinyl ether-*alt*-maleic anhydride) (PMMAn, M_n = 80kDa, Sigma-Aldrich, Oakville, ON) was heated in a vacuum oven at 140°C for 5 days to ensure that it was completely in the anhydride form.[19] Triethylamine, 4-(2-hydroxyethyl)-1-piperazineethanesulfonic acid (HEPES) sodium salt, N,N-dimethylformamide, fluoresceinamine, furfurylamine (FFA), 2-(*N*-morpholino)ethanesulfonic acid (MES) hemisodium salt, sodium acetate, potassium phosphate (monobasic) and tetramethylrhodamine 5- (and 6-) carboxamide cadaverine (TAMRA-cadaverine) were purchased from Sigma Aldrich (Oakville, ON) and used as received. Sodium chloride,

calcium chloride dihydrate, acetonitrile, sodium phosphate, dibasic (Reagent grade, Caledon Laboratories, Caledon, ON) and deuterium oxide (99.99 atom% D, Cambridge Isotope Laboratories, Andover, MA) were used as received. Sodium hydroxide (1.0 N) was purchased from LabChem Inc. N-(2-aminoethyl)maleimide trifluoroacetic acid was purchased from Santa Cruz Biotechnology Inc. (Santa Cruz, CA).

2.3.2. Synthesis of PMM-FFA*r* with 10 – 25 mol% FFA

PMMAn (0.500 g, 3.2 mmol anhydride) was dissolved in 10 mL acetonitrile. TAMRA-cadaverine (3.3 mg, 0.0065 mmol, 0.2 mol% relative to anhydride groups in PMMAn) was dissolved in 0.33 mL DMF, added to the PMMAn solution and allowed to stir at room temperature overnight. FFA (99 μL, 1.1 mmol, 35 mol% relative to anhydride groups in PMMAn) diluted in 2 mL acetonitrile was then added dropwise over a few minutes. After 24 h at room temperature, the mixture was diluted into 40 mL of distilled water, 1 mL of 1.0 N NaOH was added, and the resulting solution was dialyzed against 3.5 L of distilled water (adjusted to pH 7 and changed daily) for 4 days using cellulose dialysis tubing (molecular weight (MW) cut-off 3500 Da, Spectrapor). The dialyzed solution was freeze-dried to give PMM-FFA25*r* as a pink powder. The degree of substitution (DS) was determined to be 25 mol% by ^{1}H-NMR in D_2O on a Bruker AV-600 NMR spectrometer, comparing the signals for furan protons at 6.25, 6.35 and 7.40 ppm to the signal for two PMM methylene backbone protons at 1.85 ppm. The degree of TAMRA-cadaverine labelling was determined to be 0.15 mol% by UV-vis absorbance. Other PMM-FFA*r* derivatives were prepared analogously.

2.3.3. Synthesis of PMM-MAL*f* with 9 – 24 mol% MAL

The maleimide-modified PMM derivative was prepared in a similar fashion. PMMAn (0.500 g, 3.2 mmol anhydride) was dissolved in 10 mL acetonitrile. Triethylamine (150 μL, 1.1 mmol) and aminofluorescein (5.6 mg, 0.016 mmol, 0.5 mol%) in 0.5 mL DMF was added to the PMMAn and allowed to react overnight at room temperature. *N*-(2-aminoethyl)maleimide trifluoroacetate (285 mg, 1.12 mmol, 35 mol% relative to anhydride groups in PMMAn) was dissolved in a mixture of 1 mL of acetonitrile and 0.1 mL of DMF, and added dropwise to the PMMAn solution over a few

minutes. After reaction for 24 h at room temperature, the mixture was diluted into 40 mL distilled water, and dialyzed against 3.5 L of distilled water adjusted to a pH of 5.5 and changed daily for 3 days (MW cut-off 3500 Da). The solution was freeze-dried to give PMM-MAL24*f* as a yellow powder. The DS was determined to be 24 mol% by ^{1}H-NMR spectroscopy in D_2O, comparing the signal for the two maleimide vinyl protons at 6.75 ppm with that for the methylene backbone protons at 1.85 ppm. The degree of fluorescein labelling was determined to be about 0.6 mol%, by UV-vis absorbance. Other PMM-MAL*f* derivatives were prepared analogously, as described in table 2.1.

2.3.4. MAS-NMR Investigation of Crosslinking

10 mg of PMM-FFA25*r* and PMM-MAL24*f* were each dissolved in 100 μL of 0.5 M NaOD in D_2O. The two solutions were combined to give 200 μL with a total polymer concentration of 10% w/v and a pH of 5.3. The mixture was immediately used to fill a 45 μL teflon MAS insert fitted into a 7 mm diameter sapphire rotor. Spectra were recorded using MAS at a frequency of ~3500 Hz on a Bruker AV-500 spectrometer. A low power RF pulse sequence was selectively applied at a frequency of 2325 Hz, corresponding to 4.7 ppm, to saturate the residual HDO signal prior to each acquisition cycle.

2.3.5. Hydrolytic Stability of PMM-MAL24*f* and PMM-FFA25*r*

Acetate buffer (100 mM, pH 5.0), MES buffer (100 mM, pH 6.0), and phosphate buffer (100 mM, pH 7.0) were prepared in D_2O. 1% w/v solutions of PMM-FFA25*r* and PMM-MAL24*f* were prepared using the three different buffers. The samples were maintained at 37 °C and hydrolysis was monitored using ^{1}H-NMR.

Succinamic linkage hydrolysis of PMM-FFA25*r* was measured by the decrease in the broad signals at 6.30 and 7.40 ppm due to polymer-bound furan, and the accompanying increase in sharp signals at 6.45 and 7.50 ppm, corresponding to furfurylamine that had been hydrolytically cleaved from the polymer backbone. Hydrolysis of PMM-MAL24*f*, which resulted in several hydrolysis products, was monitored by the decrease in the broad polymer-bound maleimide signal at 6.83 ppm.

2.3.6. Preparation of Bulk Gels

Separate solutions of PMM-FFA*r* (12, 18 and 25% functionalized) and of PMM-MAL*f* (9, 17 and 24% functionalized) were prepared by dissolving 50 mg of each polymer in 500 μL of 0.25 M NaOH. The pH of each solution was adjusted to 5.6 ± 0.2 using <10 μL of 1.0 M NaOH. Equal aliquots of 100 μL PMM-FFA*r* and PMM-MAL*f* solutions were mixed by pipetting the two polymer solutions back and forth between the two vials four times, followed by vortexing for 10 s. 100 μL of the mixture was pipetted into a silicone rubber mold (7 mm diameter, 5 mm deep, n = 2) on a glass microscope slide. The mold was sealed with a sheet of silicone rubber and Parafilm, and the mixture allowed to gel for 24 h at 37 °C. Mixtures containing PMM-MAL and PMM-FFA with the same, and differing, degrees of functionalization were prepared.

2.3.7. Swelling of the Bulk Gels in PBS

The gels were removed from the molds, and cut in half either vertically to form semi-circles, or horizontally to form thinner disks. In either case, the pieces were quickly weighed, placed individually in separate petri dishes containing 3 mL of PBS buffer (10 mM phosphate, 154 mM NaCl, pH 7.4), and incubated at 37 °C. After 24 h and 48 h, the gel pieces were removed from the buffer, quickly dried with tissue paper and weighed again. They were then placed in fresh buffer and returned to the incubator. Equilibrium swelling was reached after 48 h and the measured pH of the gel/buffer solution was 7.4.

To examine the effect of pH on gel stability, PMM-FFA12*r*/MAL9*f* gels made as described above were placed in PBS (pH 7.5, n = 3) or saline (pH 5.5, n = 12) and incubated at 37 °C and gels were visually inspected daily over a period of 7 days.

2.3.8. Effect of Ca^{2+} on Gel Swelling

Gels composed of PMM-MAL*f* (9% functionalized) and PMM-FFA*r* (12% functionalized) were prepared at pH 5.6 as described above. The gels were cut horizontally to form thinner disks, which were weighed and then placed in separate petri dishes containing 3 mL of $CaCl_2$ (0 mM, 4.17 mM, 8.33 mM, 16.7 mM and 50 mM). The disks were incubated at 37 °C for 24 h, then quickly dried with tissue paper

and weighed. Equilibrium pH was found to be 5.7 ± 0.3 for the disks incubated with the $CaCl_2$ solutions, and about 7 for the disks incubated with water.

2.3.9. Mechanical Properties of Gels

Gels formed at pH 5.6 as described above were uncovered, coated with 1-2 drops of silicone oil to prevent water evaporation, and placed on an inverted microscope, still within their silicone rubber mold. Mechanical measurements were made with an indenter consisting of a glass melting point tube (VWR) with a hemispherical end (r = 0.83 mm) attached to a force transducer (Transducer Techniques, GSO series, 10 g full scale). The vertical position of the glass indenter was controlled with a servo motor programmed to move the rounded end of the indenter to a depth of 0.3 mm (6% of gel thickness) after contacting the gel at a constant speed of 0.1 mm/s, while the transducer measured the force as function of time and vertical position of the indenter. Three measurements at different positions of each gel were carried out, and averaged.

The gels were then individually placed in a 24-well multiwell plate and covered with 3 mL of PBS at pH 7.4 and incubated at 37 °C for 48 h, with one buffer change at 24 h and another at 48 h. The swollen gels were placed inside 8.45 mm diameter silicone molds on a glass microscope slide, covered with silicone oil, and mechanical measurements were carried out again, as described above.

2.3.10. Determination of Pore-Size – Dextran In-diffusion

5 mg each of PMM-FFA*r* (12, 18 and 25) and PMM-MAL (8, 14 and 24) were dissolved in 50 µL of water and the pH adjusted to 6.5 ± 0.2 using NaOH(aq). Solutions of equivalently functionalized PMM-FFA*r* and PMM-MAL were mixed together as described above. A 10 cm length of 0.8 mm id Tygon tubing was attached to a 1 mL syringe fitted with an 18-gauge needle. A small amount of silicone oil (Dow Corning 550 fluid) was drawn through the tubing into the syringe to lubricate the Tygon tubing. The PMM-FFA*r*/MAL polymer solutions were then drawn up into three separate pieces of tubing. The open end of the tubing was sealed with Parafilm™, and the syringe, needle and tubing assembly was placed into an incubator at 37 °C for 24 h to allow for

gelation. The Parafilm™ was removed from the end of the tubing, and the gel was expelled and cut into short cylinders using a razor blade.

PMM-FFA/MAL gel permeability was evaluated using fluorescently labelled dextran (dextran-*f*, Sigma-Aldrich) with MWs of 10, 70, 250 and 500 kDa. For each measurement, approximately 20 cylindrical gel sections were placed within a 1 mL conical vial and covered with 1 mL of 0.1% dextran-*f* in HEPES-buffered saline (pH 7.8). After 24 h exposure to the dextran-*f* with gentle agitation, about 10 gel sections were randomly selected and transferred into a single well in a glass bottomed 96-well plate, along with some of the supernatant dextran-*f* solution. The gel sections were examined by confocal fluorescence microscopy, and the fluorescence intensities from an area representing the central 20% of the gels as well as from the supernatant dextran-*f* solution were compared using NIS Elements (Nikon) software. The ratio of the intensities of the gel centre and surrounding solution are reported. Measurements were conducted for n = 8 for each dextran-*f* MW.

2.3.11. Post-Functionalization of Gels Monitored via ^{1}H NMR

20 mg each of PMM-FFA25*r* and PMM-MAL24 was dissolved in 200 μL of 0.5 M and 0.25 M NaOD, respectively. After mixing the two solutions, the pH was adjusted to 6.5 using 1 M NaOD. The polymer mixture was pipetted into a silicone rubber mold, as described above, and placed in the incubator at 37 °C. After 24 h, the gel discs were removed from the mold and ground up in a mortar and pestle, along with 2 mL of D_2O containing 50 mM formic acid as an internal standard. The resulting slurry was placed into a 15 mL conical vial and centrifuged at 1200 rpm for four minutes. The concentrated gel slurry at the bottom of the vial was pipetted into two NMR tubes. Into the first tube, 2 mg (0.016 mmol, approx. 2 x molar excess) of *N*-ethyl maleimide dissolved in 100 μL of D_2O was added via a long syringe and mixed with the slurry by drawing the solution in and out of the syringe several times. The second NMR tube was used as a control, with no ethyl maleimide added. ^{1}H NMR spectra were obtained using water suppression, both before addition of ethyl maleimide, and at regular intervals after, for 3 days. The NMR tubes were kept at 37 °C.

2.3.12. Tests for Controlled Release

15 mg of PMM-FFA18*r* and PMM-MAL14 were dissolved separately, each in 150 uL of HEPES-buffered saline (pH 7.8) containing 1.0 wt% 10 kDa dextran-*f*, and the pH values were adjusted to 6.4 ± 0.1 using 1.0 M NaOH. The solutions of PMM-FFA*r* and PMM-MAL were mixed, and gelled inside silicon molds, as described above. The resulting gels (n = 3) were weighed and placed into 8 mL cylindrical black-capped vials with 5 mL of HEPES-buffered 1.1% $CaCl_2$ and 0.45% NaCl (pH 7.8) for 4 days.

An identical mixture was used to prepare gel sections (prepared in Tygon tubing, as described above), which were placed into a 96-well plate under the HEPES-buffered $CaCl_2$/NaCl solution for analysis by confocal microscopy.

After 4 days, the solution was replaced with 5 mL of HEPES-buffered saline (pH 7.8). To monitor release, the amount of dextran-*f* in the supernatant was measured via fluorescence spectroscopy (Fluorolog) over the course of several days. The amount of dextran-*f* in the gels at t = 0 was corrected for dextran-*f* extruded from the hydrogels during the initial shrinking of gel in Ca^{2+}-containing solution, as measured by fluorescence spectroscopy. Dextran-*f* release was calculated as follows:

$$\% \text{ Released} = \frac{m_r}{m_i - m_s}$$

Where m_r corresponds to the mass of dextran-*f* released, m_i is the mass of dextran-*f* loaded into the hydrogels, and m_s is the weight of dextran-*f* that was released into the initial HEPES Ca^{2+} supernatant during shrinkage.

To replicate this process on a shorter time scale, the HEPES Ca^{2+} supernatant was removed from the gels in the multiwell plate and replaced with sodium citrate (100 mM), a calcium chelator, and the subsequent hydrogel swelling and release of dextran-*f* (4 and 10 kDa) was imaged via confocal microscopy.

Additionally, gels composed of PMM-FFA18*r*/MAL14 were prepared as described above and placed directly into HEPES-buffered saline (pH 7.8) with no exposure to Ca^{2+} ions. The fluorescence in the supernatant was measured over time.

2.3. Results and Discussion

2.3.1. Synthesis of Furan- and Maleimide-Functionalized PMM

A series of furan- and maleimide-functionalized PMMs with degrees of functionalization of 9 – 25 mol% were prepared by reacting PMMAn with 15 – 35 mol% of the corresponding amines in acetonitrile at room temperature. Fluorescent analogs PMM-FFA*r* and PMM-MAL*f*, were prepared by prior reaction with TAMRA-cadaverine or fluoresceinamine, respectively. Residual anhydride groups were hydrolyzed and the resulting polymers purified by dialysis and isolated by freeze-drying. The DS of the modified polymers was determined to be 60 – 80 % by ^{1}H NMR in D_2O (table 2.1). The ^{1}H-NMR spectra for PMM-FFA12*r* and PMM-MAL24*f* are shown in the Supplemental Information, as figures A2.1 and A2.2, respectively.

Table 2.1. DS of PMM-FFA*r* and PMM-MAL*f*

Modified PMM	DS Actual (Target)	DS Fluorophore Actual (Target)
FFA12*r*	12 (15)	0.13 (0.2)
FFA18*r*	18 (25)	0.14 (0.2)
FFA25*r*	25 (35)	0.15 (0.2)
MAL9*f*	9 (15)	0.39 (0.5)
MAL17*f*	17 (25)	0.18 (0.5)
MAL24*f*	24 (30)	0.59 (0.5)
MAL9	9 (15)	N/A
MAL14	14 (25)	N/A
MAL24	24 (30)	N/A

'*r*': rhodamine cadaverine-labelled; '*f*': fluorescein-labelled

2.3.2. Hydrolytic Stability of PMM-FFA25*r* and PMM-MAL24*f*

It was of interest to study the hydrolytic stability of the reactive polymers as hydrolysis may lead to loss of reactive groups and/or degradation of the crosslinked network. Additionally, an understanding of potential side reactions may allow the crosslinking conditions to be optimized for increased reproducibility.

While simple amides are fairly stable at room temperature in aqueous environments near neutral pH,[22] the presence of a neighbouring carboxylic acid group in maleamic or succinamic acids,[23] is known to increase the rate of amide hydrolysis, especially at pH < 7 where at least some of the carboxylic acid is in the acid form. Succinamic acid groups are present in both PMM-MAL and PMM-FFA backbones.

^{1}H NMR studies were conducted on PMM-FFA25*r* at 37 °C in solutions buffered at pH 5, 6 and 7 to assess the susceptibility of the succinamic linkages to hydrolysis at these pH values.

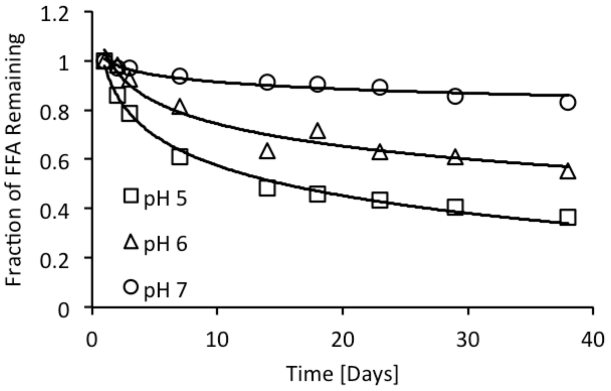

Figure 2.1. Hydrolysis of the amide linkage in PMM-FFA25*r* at 37 °C with pH buffered at 5, 6 and 7, as determined from the increase over time of the ^{1}H NMR vinyl signal for free FFA.

As expected based on small molecule work,[22,23] hydrolysis of the amide in PMM-FFA is significantly slower at pH 7 than at pH 5, showing less than 20% hydrolysis after 38 days compared to about 50% hydrolysis after 2 weeks at pH 5. As a result, the pH was maintained at 7 during dialysis and work-up of PMM-FFA to minimize hydrolysis of the succinamic acid linkages.

The hydrolysis of PMM-MAL is more complex than that of PMM-FFA, since, in addition to the hydrolysis of the analogous succinamic linkage at the backbone, PMM-MAL can also undergo hydrolysis of the maleimide group to form maleamic acid, a reaction known to be quite fast under alkaline conditions.[24,25] Maleamic acids can further hydrolyze to maleic acid and the corresponding amine. An NMR spectrum taken during

the hydrolysis of PMM-MAL24*f* and possible hydrolysis products are shown in figure A2.3. The hydrolysis of PMM-MAL24*f* at 37 °C, buffered at pH 5, 6 and 7, appears to be base-catalyzed as described previously for small molecule maleimides,[24] and at 37 °C reached approximately 50% after about 4 days at pH 5, or 2 days at pH 7, (figure 2.2) which is comparable to previously reported small molecule studies.[25]

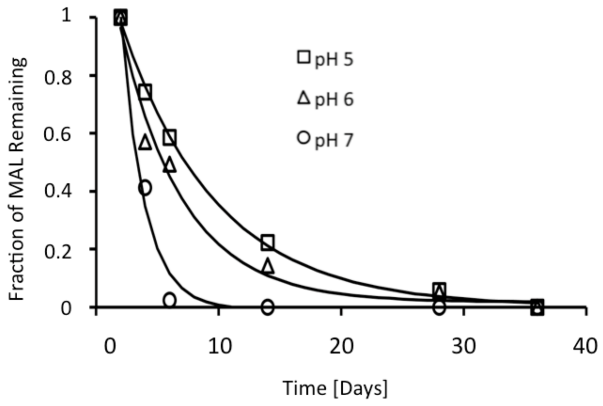

Figure 2.2. Fraction of maleimide remaining, as determined by ^{1}H NMR spectroscopy, for PMM-MAL24*f* maintained at 37°C and pH 5, 6 and 7.

In the case of PMM-MAL, it was more important to limit hydrolysis of the maleimide groups since their hydrolysis is much faster than that of the succinamic acid units. Hence, PMM-MAL solutions were maintained below pH 7, typically pH 5.5 - 6.5, before (e.g., dialysis) and during gelation. The sections below describe formation and properties of the corresponding Diels-Alder hydrogels under a range of conditions.

3.3.3. Formation of Hydrogels

The formation of Diels-Alder crosslinked hydrogels from PMM-FFA/PMM-MAL (scheme 2.1) was investigated by mixing aliquots of 5 and 10% w/v aqueous solutions of the two polymers and determining the gelation times at 37 °C. Although gelation is possible at physiological pH, the gels described in this paper were formed between pH 5 and 6 in order to limit the amount of maleimide hydrolysis during crosslinking and increase reproducibility between samples. Gelation time is defined as the time when a vial containing the polymer mixtures can be turned over without its content flowing. The

moderate rate of Diels-Alder coupling ensures adequate time for complete mixing of polymer solutions prior to gelation.[26,27]

PMM-FFA25*r*/MAL24*f* mixtures gelled after 15 minutes at 10% polymer loading, and after 18 h at 5% polymer loading. PMM-FFA12*r*/MAL9*f* and PMM-FFA18*r*/MAL17*f* mixtures both gelled within 2 h at 10% polymer loading, but did not form gels at 5% polymer loading. This significant effect of polymer loading is attributed to a combination of several factors: the bimolecular nature of the Diels-Alder coupling reaction, and onset of competition from maleimide hydrolysis.

^{1}H NMR was used to monitor the disappearance of furan and maleimide groups, as well as the formation of the Diels-Alder adduct during crosslinking. The crosslink points in such hydrogels were not expected to have sufficient rotational and translational mobility to average out the local dipolar magnetic field interactions, and thus would likely show severe peak broadening.[28] High resolution-MAS (HR-MAS) ^{1}H NMR with spin-rates of 2 - 5 kHz was hence used to generate narrow, solution-like ^{1}H NMR signals of the crosslinked gels swollen in D_2O, as described previously for crosslinked polystyrene gels swollen in organic solvents,[29,30] and amide-based hydrogel networks.[31]

3.3.4. HR-MAS NMR Investigation of Crosslinking

Both UV-vis and, more commonly, FTIR[13,32] have been used to characterize crosslinking in hydrogels. In this work, MAS NMR was used, as it allows monitoring of both crosslinking and hydrolysis side reactions during gelation. Specifically, HR-MAS ^{1}H NMR (figures A2.4 and A2.5) was found to be useful for following the reaction between PMM-FFA25*r* and PMM-MAL24*f* via the disappearance of the polymer-bound maleimide and furan signals at 6.7 and 7.3 ppm, respectively (figure 2.3). Although small-molecule Diels-Alder reactions follow second-order kinetics, the kinetics of the analogous polymeric reaction is more complicated as electrostatic repulsion between the anionic chains, as well as steric and mobility issues upon crosslinking may affect the rate of Diels-Alder coupling. It is known that crosslinking reactions between polymers generally do not go to completion, due to spatial isolation of some of the reactive groups at higher crosslink densities.[33] Accordingly, it was found that the polymeric Diels-Alder

coupling reaction goes to approximately 50% completion, based on consumption of the furan groups of PMM-FFA. The maleimide groups of PMM-MAL were consumed at a faster rate, which is attributed to partial hydrolysis.

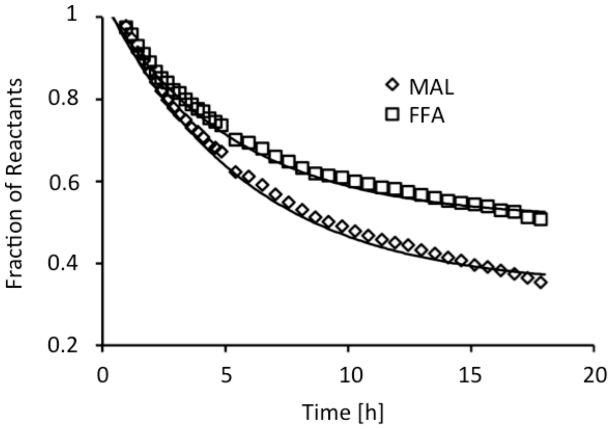

Figure 2.3. Decrease of the maleimide (MAL) and furan (FFA) HR-MAS ^{1}H NMR vinyl signals during the Diels-Alder reaction of PMM-FFA25*r*/MAL24*f* at pH 5.2.

Recent work by Shoichet suggests that the presence of residual furan and maleimide groups do not pose significant issues to embedded cells.[13] Furthermore, the residual groups provide an opportunity to post-functionalize the hydrogel through Diels-Alder reactions or thiol-maleimide coupling.

To demonstrate the ability to post-functionalize the PMM-FFA/MAL hydrogels, a PMM-FFA25*r*/MAL24 gel was exposed to a two-fold excess of *N*-ethyl maleimide, and the consumption of residual furan groups within the gel was monitored by solution-state ^{1}H NMR over three days. Figure 2.4b shows that the residual FFA pendant groups were fully consumed by the Diels-Alder reaction with *N*-ethyl maleimide within 16 h at 37 °C, while the control sample shows no apparent change even after 30 h (figure 2.4a). These results demonstrate that the hydrogels can be successfully post-functionalized, using residual furan moieties on the polymeric backbone. This could prove useful for attaching biomarkers or cell-signalling ligands to the hydrogels post-gelation.

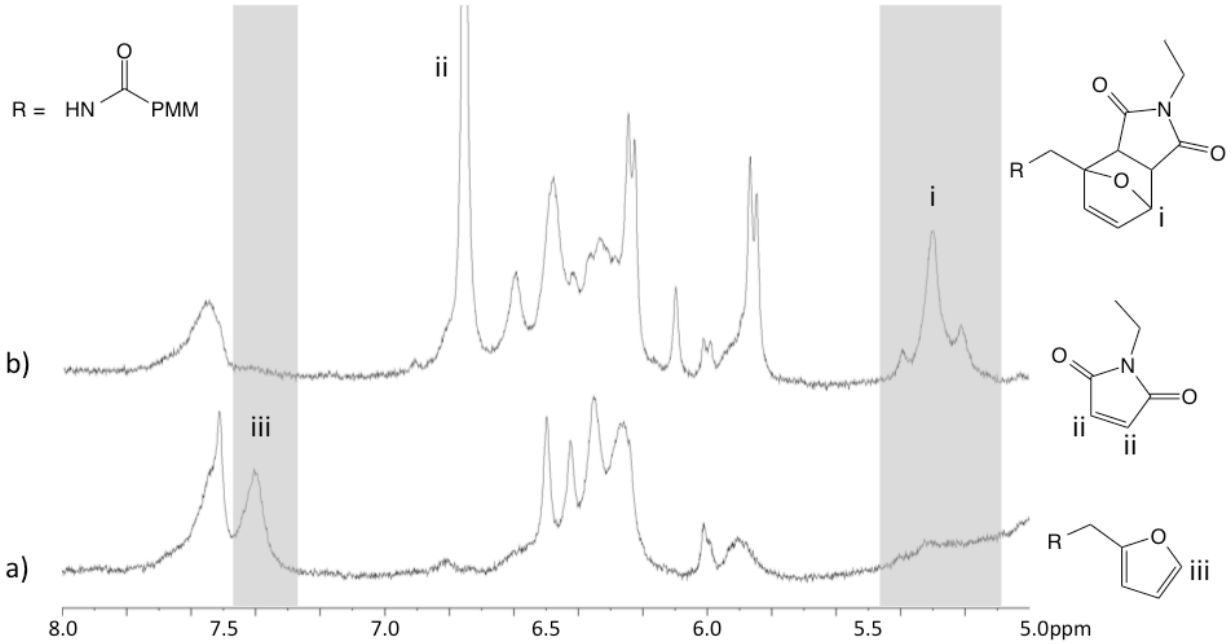

Figure 2.4. ^{1}H NMR spectra of PMM-FFA25*r*/MAL24 hydrogel suspended in D_2O a) after 30 h at 37 °C with no addition of ethyl maleimide and b) after 16 h at 37 °C following the addition of 2x molar excess of *N*-ethyl maleimide. The signals appearing in spectrum b) at 5.85 and 6.20 ppm correspond to unbound maleamic acid, and signals at 6.45 and 6.60 ppm are due to the vinyl protons in the new Diels-Alder adduct. The signals at 6.40 and 6.50 ppm and 7.55ppm in spectrum a) belong to unbound furfurylamine and consequently disappear in spectrum b) as they are consumed in the Diels-Alder reaction with ethyl maleimide.

3.3.5. Swelling Studies in PBS

To examine swelling properties, PMM-FFA/PMM-MAL crosslinked hydrogels (10% total polymer) that had been allowed to gel at pH 5.6 for 24 h were incubated in PBS (10 mM, pH 7.4) at 37 °C. The buffer was replaced after 24 and 48 h, at which point the gels had reached equilibrium weights. All hydrogels swelled to some extent, due to the high charge-density polyanionic PMM backbone (figure 2.5). PMM-FFA12*r*/MAL9*f* gels showed the highest swelling ratio, more than tripling in weight from the as-formed gel, as expected given their low degrees of functionalization and hence crosslinking. The degree of swelling generally decreased with increasing degrees of functionalization. This

effect is attributed to a combination of three factors: decrease in charge density, increase in hydrophobic content, and an increase in crosslink density.

As described earlier, hydrolysis of succinamic acid groups can cleave the pendant FFA and MAL groups from the polymer backbone, especially under acidic conditions. This process should also be active in the gels leading to a gradual loss of crosslinking. To assess hydrolysis and gel integrity over time, PMM-FFA12*r*/MAL9 gel samples were stored at pH 5.8 and at pH 7.4 in water. On the first day, these lightly crosslinked gels swelled more than had been seen in PBS, and within 5 days the gels stored at pH 5.8 had dissolved, while the gels at pH 7.4 exhibited no further change for at least seven days. In separate experiments, more highly crosslinked gels were found to remain intact for at least one year under neutral conditions. This acid-mediated hydrolysis offers an interesting route for degradation of the hydrogels.

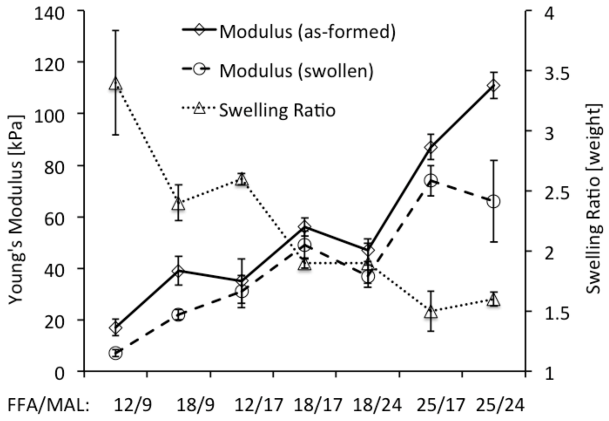

Figure 2.5. Swelling ratios (triangles, wt. swollen in PBS/wt. as formed) and Young's moduli (diamonds, as formed gels; circles, PBS-swollen gels) for 10% w/v PMM-FFA/MAL hydrogels with different degrees of functionalization.

3.3.6. Mechanical Properties of Hydrogels

The PMM-FFA/MAL hydrogels were compressed with a small hemispherical indenter to determine their elasticity as a function of gel composition and solution conditions. The force F upon deforming an elastic material with a hemisphere is described by Hertzian theory as

$$F = \frac{4ER^{1/2}}{3(1-\nu^2)}d^{3/2}$$

(1)

where d is the deformation, R (= 0.83 mm) is the radius of the hemispherical indenter, and v and E are the Poisson's ratio and Young's modulus, respectively, of the elastic substrate. The forces F for different hydrogels can be plotted as a function of strain, $d^{3/2}$ (figure A2.6). As PMM-FFA/MAL hydrogels behave like elastomers, their Poisson's ratio v is assumed to be 0.5, and the Young's modulus E can be obtained from the initial slopes ($d \leq 0.3$ mm) of the linear fits in the force versus strain plots, where the linear Hertzian theory is considered reliable.[34] Figure 2.5 shows the increase in Young's moduli for as-formed and PBS-swollen gels with increasing degrees of functionalization: The moduli for as-formed gels range from about 17 to 111 kPa, and from 7 to 74 kPa for equilibrium-swollen gels. These elastic moduli compare to those of muscle (8 - 14 kPa),[35] cartilage peri-cellular matrix (20 - 26 kPa),[35] pre-calcified bone (28 - 45 kPa)[36] and even collagenous bone (>100 kPa).[37] Figure 2.5 also shows the expected inverse relationship between elastic moduli and equilibrium swelling ratio in PBS:[35] the elastic moduli increase with nominal crosslink density, and the equilibrium swelling ratio decreases with increasing crosslink density.

3.3.7. Effect of Ca^{2+} on Gel Swelling

It is often desirable to limit swelling to help a hydrogel maintain its original shape and volume. It is known that PMM-based hydrogels will de-swell significantly in the presence of as little as 5 mM [Ca^{2+}].[38] We hence examined the effect of various [Ca^{2+}] (0, 4.17, 8.33, 16.7 and 50 mM $CaCl_2$) on PMM-FFA12*r*/MAL9*f* hydrogels. Figure 2.6 shows the progressive de-swelling of this hydrogel from a swelling ratio of 18 (cf. the as-formed gel) for distilled water, to a swelling ratio just below 1 for 50 mM $CaCl_2$. While some of the contraction may be due to shielding of electrostatic repulsion between PMM chains, the gel was less swollen in the presence of 8.33 mM $CaCl_2$ (ionic strength = 25 mM) than it was in PBS (I = 176 mM), indicating significant association of PMM chains by calcium ion bridging. In one case, the modulus of a Ca^{2+}-treated PMM-FFA12*r*/MAL17*f* gel was determined and found to have increased to 126 ± 21 kPa

compared to the untreated PBS-swollen gel (35 ± 8.6 kPa), as expected for the additional Ca^{2+}-crosslinking. These results indicate that the presence of low, cytocompatible levels of calcium can significantly reduce the swelling ratio for PMM-FFA/MAL hydrogels.

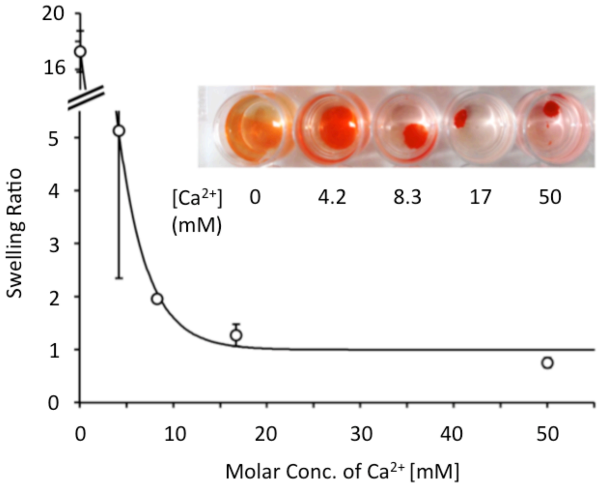

Figure 2.6. Effect of $CaCl_2$ concentration on the equilibrium swelling ratio of PMM-FFA12*r*/MAL9*f* hydrogels. Inset image shows PMM-FFA12*r*/MAL9*f* hydrogels with same initial size that have been incubated (from left to right) in 0, 4.2, 8.3, 17 and 50 mM $CaCl_2$ respectively. The trendline is intended as a visual guide only.

3.3.8. Measurement of Gel Permeability using Fluorescently-Labelled Dextran

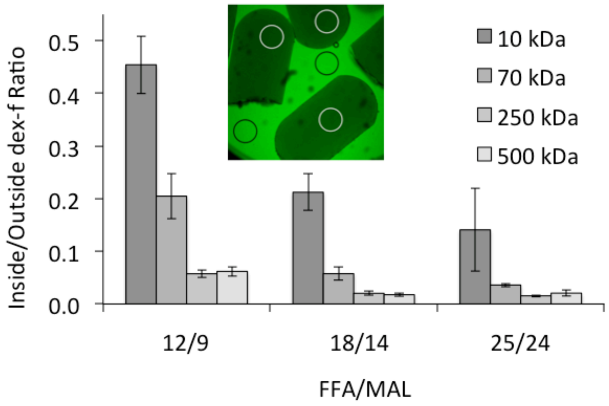

Figure 2.7. In-diffusion of dextran-*f* into different gels as function of dextran MW. The ratio of fluorescence intensities within (white circles on inset image), and outside the gels (black circles on the inset image) was obtained by confocal fluorescence microscopy. Inset shows the in-diffusion of 10 kDa dextran-*f* into PMM-FFA12*r*/MAL9 hydrogels.

It is important to know the pore size of hydrogels for various applications such as scaffolds or release devices. Gels for permeability and release studies were prepared using unlabelled PMM-MALs to allow for quantification of the fluorescein-labelled dextrans. The non-fluorescent PMM-MAL samples had maleimide contents similar to their fluorescent analogs, and the gels made with them would have swelling and mechanical properties similar to the analogous gels described above. Figure 2.7 shows that diffusion of dextran-*f* into gels decreases with higher degrees of functionalization, and with higher dextran-*f* MW. The most significant discrimination by dextran-*f* MW is between PMM-FFA12*r*/MAL9 and PMM-FFA18*r*/MAL14. Dextran-*f* MWs of 10, 70, 250, and 500 kDa correspond to hydrodynamic radii of 2.3,[39] 6.0,[39] 10.9[40] and 15.7 nm,[41] respectively. This suggests that the hydrogels made of PMM-FFA12*r*/MAL9 have a pore-size between 6.0 and 10.9 nm, as a significant amount of 70 kDa dextran-*f* diffused into the gels. However, gels composed of PMM-FFA18*r*/MAL14 and PMM-FFA25*r*/MAL24 have a smaller pore-size, between 2.3 and 6.0 nm as only the 10 kDa dextran-*f* is able to diffuse through the hydrogel pores. These results indicate that permeability can be controlled via functional group loading for PMM-FFA/MAL hydrogels.

3.3.9. Encapsulation/Controlled Release Tests

For release studies, 10 kDa dextran-*f* was used as a model drug. It was selected as it is of similar size with therapeutics such as siRNA, nanoparticles, and small proteins.[42] Dextran-*f* was incorporated into the hydrogels during gelation and it was found that exposure to Ca^{2+} and the subsequent shrinkage of the hydrogels resulted in loss of 41 ± 7% of the pre-encapsulated dextran-*f*. Figure 2.8 shows the release of dextran-*f* from the Ca^{2+}-treated gels as well as untreated gels when placed into HEPES-buffered saline. The release profile for the Ca^{2+}-treated gels shows a slow but persistent release of dextran-*f* over the course of a week. Conversely, the gels that were placed directly into saline exhibited a rapid "burst" release of the dextran-*f* before a substantial decrease in rate of out-diffusion with almost no additional release occurring over the next three days. The tunable, calcium-responsive nature of the PMM-FFA/MAL hydrogels offers an interesting approach for controlled release.

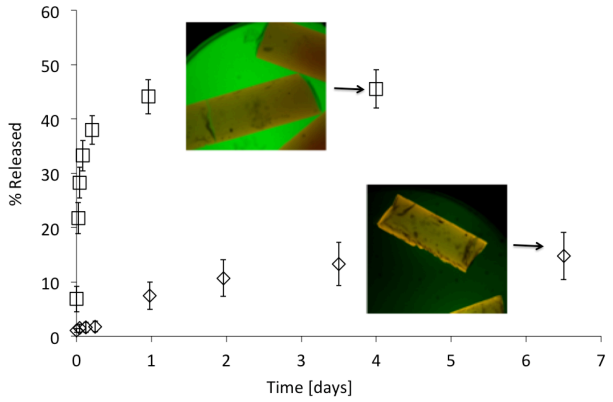

Figure 2.8. Release profile of 10 kDa dextran-*f* over time for PMM-FFA18*r*/MAL14 gels that were placed directly into HEPES-buffered saline (square markers) or first incubated in $CaCl_2$ (diamond markers).

2.4. Conclusions

Diels-Alder coupling between fully synthetic diene and dienophile-modified polyanions was used to form covalently crosslinked hydrogels under physiological conditions. The gel-forming polymers PMM-FFA and PMM-MAL were prepared and fluorescently labelled in a single step from an inexpensive, common commercial precursor. The properties of the resulting hydrogels can be tuned through degree of functionalization to have elastic moduli similar to those of fat, muscle and cartilage and pre-calcified bone. Additionally, the resulting hydrogels are highly responsive to Ca^{2+} ions, and pore-size and swelling can be readily tuned via Ca^{2+} concentration. PMM-FFA/MAL hydrogels show promise for use as synthetic ECM scaffolds, and as controlled-release delivery vectors.

2.5 Acknowledgements

We would like to thank the Natural Sciences and Engineering Research Council (NSERC) of Canada for supporting this work through Discovery and CREATE grants. We would also like to acknowledge Dr. Bob Berno in the McMaster NMR Spectroscopy

facility for his assistance with the HR-MAS experiments, and Samantha Ros for helpful discussions.

2.6 References

(1) Alberts, B.; Johnson, A.; Lewis, J., Molecular Biology of the Cell, 4th edition; Garland Science: New York, 2002.

(2) Frantz, C.; Stewart, K.M.; Weaver, V.M. The Extracellular Matrix at a Glance. *J. Cell Sci.* **2010**, *123*, 4195-4200. Patterson, J.; Martino, M.M.; Hubbell, J.A. *Materials Today* **2010**, *13*, 14-22.

(3) Patterson, J.; Martino, M.M.; Hubbell, J.A. Biomimetic materials in tissue engineering. *Materials Today* **2010**, *13*, 14-22.

(4) Freed, L.E.; Vunjak-Novakovic, G.; Biron, R.J.; Eagles, D.B.; Lesnoy, D.C.; Barlow, S.K.; Langer, R. Biodegradable Polymer Scaffolds for Tissue Engineering. *Nat. Biotechnol*. **1994**, *12*, 689-693.

(5) Li, Z.; Leung, M.; Hopper, R.; Ellenbogen, R.; Zhang, M. Feeder-free Self-renewal of Human Embryonic Stem Cells in 3D Porous Natural Polymer Scaffolds. *Biomaterials* **2010**, *31*, 404-412.

(6) Hosseinkhani, H.; Hosseinkhani, M.; Hattori, S.; Matsuoka, R.; Kawaguchi, N. Micro and Nano-scale in vitro 3D Culture System for Cardiac Stem Cells. *J. Biomed. Mater. Res., Part A* **2010**, *94A*, 1-8.

(7) Seliktar, D. Designing Cell Compatible Hydrogels for Biomedical Applications. *Science* **2012**, *336*, 1124-1128.

(8) Tibbitt, M.W.; Anseth, K.S. Hydrogels as Extracellular Matrix Mimics for 3D Cell Culture. *Biotechnol. Bioeng.* **2009**, *103*, 655-663.

(9) Lutolf, M.P.; Hubbell, J.A. Synthetic Biomaterials as Instructive Extracellular Microenvironments for Morphogenesis in Tissue Engineering. *Nat. Biotechnol*. **2005**, *23*, 47-55.

(10) Liu, X.; Ma, P.X. Polymeric Scaffolds for Bone Tissue Engineering. *Ann. Biomed. Eng.* **2004**, *32*, 477-486.

(11) Malkoch, M.; Vestberg, R.; Gupta, N.; Mespouille, L.; Dubois, P.; Mason, A.F.; Hedrick, J.L.; Liao, Q.; Frank, C.W.; Kingsbury, K.; Hawker, C.J. Synthesis of

Well-Defined Hydrogel Networks using Click Chemistry. *Chem. Commun.* **2006**, *26*, 2774-2776.

(12) Otto, S.; Engberts, J. B. Hydrophobic Interactions and Chemical Reactivity. *Org. Biomol. Chem.* **2003**, *1*, 2809-2820.

(13) Nimmo, C. M.; Owen, S. C.; Shoichet, M. S. Diels-Alder Click Cross-Linked Hyaluronic Acid Hydrogels for Tissue Engineering. *Biomacromolecules* **2011**, *12*, 824-830.

(14) Owen, S. C.; Fisher, S.A.; Tam, R.Y.: Nimmo, C. M.; Shoichet, M. S. Hyaluronic Acid Click Hydrogels Emulate the Extracellular Matrix. *Langmuir* **2013**, *29*, 7393-7400.

(15) Vandamme, K.; Melkebeek, V.; Cox, E.; Deforce, D.; Lenoir, J.; Adriaens, E.; Vervaet, C.; Remon, J.P. Influence of Reaction Medium During Synthesis of Gantrez® AN 119 Nanoparticles for Oral Vaccination. *Eur. J. Pharm. Biopharm*. **2010**, *74*, 202-208.

(16) Wong, T.W.; Wahab, S.; Anthony, Y. Effects of Microwave on Drug Release Property of Poly(Methyl Vinyl Ether-co-Maleic Acid) Matrix. *Drug Dev. Ind. Pharm.* **2007**, *33*, 737-746.

(17) Arbós, P.; Wirth, M.; Arangoa, M.; Gabor, F.; Irache, J.M. Gantrez® AN as a New Polymer for the Preparation of Ligand-Nanoparticle Conjugates. *J. Control. Rel.* **2002**, *83*, 321-330.

(18) Li, Y.; Lee, P.I. A New Bioerodible System for Sustained Local Drug Delivery Based on Hydrolytically Activated *in situ* Macromolecular Association. *Int. J. Pharm.* **2010**, *383*, 45-52.

(19) Gardner, C.M; Burke, N.A.D.; Chu, T.; Shen, F.; Potter, M.A.; Stöver, H.D.H. Poly(methyl vinyl ether-alt-maleic acid) Polymers for Cell Encapsulation. *J. Biomater. Sci., Polym. Ed.* **2011**, *22*, 2127-2145.

(20) Gardner, C.M.; Burke, N.A.D.; Stöver, H.D.H. Cross-Linked Microcapsules Formed From Self-Deactivating Reactive Polyelectrolytes. *Langmuir*, **2010**, *26*, 4916-4924.

(21) Gardner, C.M.; Potter, M.A.; Stöver, H.D.H. Improving Covalent Cell Encapsulation with Temporarily Reactive Polyelectrolytes. *J. Mater. Sci. Mater. Med.* **2012**, *23*, 181-193.

(22) Higuchi, T.; Eberson, L.; Herd, A.K. The Intramolecular Facilitated Hydrolytic Rates of Methyl-Substituted Succinanilic Acids. *J. Am. Chem. Soc.* **1966**, *88*, 3805-3808.

(23) Bender, M.L.; Chow, Y.-L.; Chloupek, F. Intramolecular Catalysis of Hydrolytic Reactions. II. The Hydrolysis of Phthalamic Acid. *J. Am. Chem. Soc.* **1958**, *80*, 5380-5384.

(24) Khan, M.N. Kinetics and Mechanism of the Alkaline Hydrolysis of Maleimide. *J. Pharm. Sci.*, **1984**, *73*, 1767-1771.

(25) Matsui, S.; Aida, H. Hydrolysis of some *N*-alkylmaleimides. *J. Chem. Soc., Perkin Trans. 2,* **1978**, 1277-1280.

(26) Rideout, D.C.; Breslow, R. Hydrophobic Acceleration of Diels-Alder Reactions. *J. Am. Chem. Soc.*, **1980**, *102*, 7816-7817.

(27) Breslow, R.; Maitra, U.; Rideout, D. Selective Diels-Alder Reactions in Aqueous Solutions and Suspensions. *Tetrahedron Lett.*, **1983**, *24*, 1901-1904.

(28) Thakur, K.A.M.; Newmark, R.A.; Kuehn, N.T.; Gregar, T.Q. High-Temperature MAS 1D and 2D NMR for Molecular Structure Characterization of Insoluble Polymers. *Macromolecules*, **2003**, *36*, 719-723.

(29) Stöver, H.D.H.; Fréchet, J.M.J. Direct Polarization Carbon-13 and Proton Magic Angle Spinning NMR in the Characterization of Solvent-Swollen Gels. *Macromolecules*, **1989**, *22*, 1574-1576.

(30) Stöver, H.D.H.; Fréchet, J.M.J. NMR Characterization of Crosslinked Polystyrene Gels. *Macromolecules*, **1991**, *24*, 883-888.

(31) Shestakova, P.; Willem, R.; Vassileva, E. Elucidation of the Chemical and Morphological Structure of Double-Network (DN) Hydrogels by High-Resolution Magic Angle Spinning HRMAS) NMR Spectroscopy. *Chem. Eur. J.* **2011**, *17*, 14867-14877.

(32) Spruell, J.M.; Wolffs, M.; Leibfarth, F.A.; Stahl, B.C.; Heo, J.; Connal, L.A.; Hu, J.; Hawker, C.J. Reactive, Multifunctional Polymer Films through Thermal

Cross-linking of Orthogonal Click Groups. *J. Am. Chem. Soc.* **2011**, *133*, 16698-16706.

(33) Gheneim, R.; Perez-Berumen, C.; Gandini, A. Diels-Alder Reactions with Novel Polymeric Dienes and Dienophiles: Synthesis of Reversibly Cross-Linked Elastomers. *Macromolecules*. **2002**, *35*, 7246-7253.Long, R.; Hall, M.S.; Wu, M.; Hui, C.-Y. Effects of Gel Thickness on Microscope Indentation Measurements of Gel Modulus. *Biophys. J*. **2011**, *101*, 643-650.

(34) Anseth, K.S.; Bowman, C.N.; Brannon-Peppas, L. Mechanical Properties of Hydrogels and their Experimental Determination. *Biomaterials*, **1996**, *17*, 1647-1657.

(35) Buxboim, A.; Ivanovska, I.L.; Discher, D.E. Matrix Elasticity, Cytoskeletal Forces and Physics of the Nucleus: How Deeply Do Cells 'Feel' Outside and In? *J. Cell Sci.*, **2010**, *123*, 297-308.

(36) Engler, A.J.; Sen, S.; Sweeney, H.L.; Discher, D.E. Matrix Elasticity Directs Stem Cell Lineage Specification. *Cell*, **2006**, *126*, 677-689.

(37) Shimizu, T.; Minakata, A. Effect of Divalent Cations on the Volume of a Maleic Acid Copolymer Gel Examined by Incorporating Lysozyme. *Eur. Polym. J.*, **2002**, *38*, 1113-1120.

(38) Watson, P.M.D.; Paterson, J.C.; Thom, G.; Ginman, U.; Lundquist, S.; Webster, C.I. Modelling the endothelial blood-CNS barriers: a method for the production of robust *in vitro* models of the rat blood-brain barrier and blood-spinal cord barrier. *BMC Neurosci.* **2013**, *14,* 1-21.

(39) Danysh, B.P.; Patel, T.P.; Czymmek, K.J.; Edwards, D.A.; Wang, L.; Pande, J.; Duncan, M.K.; Characterizing molecular diffusion in the lens capsule. *Matrix Biol.* **2010**, *29*, 228-236.

(40) Antoniou, E.; Buitrago, C.F.; Tsaniou, M.; Alexandridis, P. Solvent effects on polysaccharide conformation. *Carbohydr. Polym.* **2010**, *79*, 380-390.

(41) Watkins, K.A.; Chen, R. pH-responsive, lysine based hydrogels for the oral delivery of a wide size range of molecules. *Int. J. Pharm.* **2015**, *478*, 496-503.

2.7 Appendix

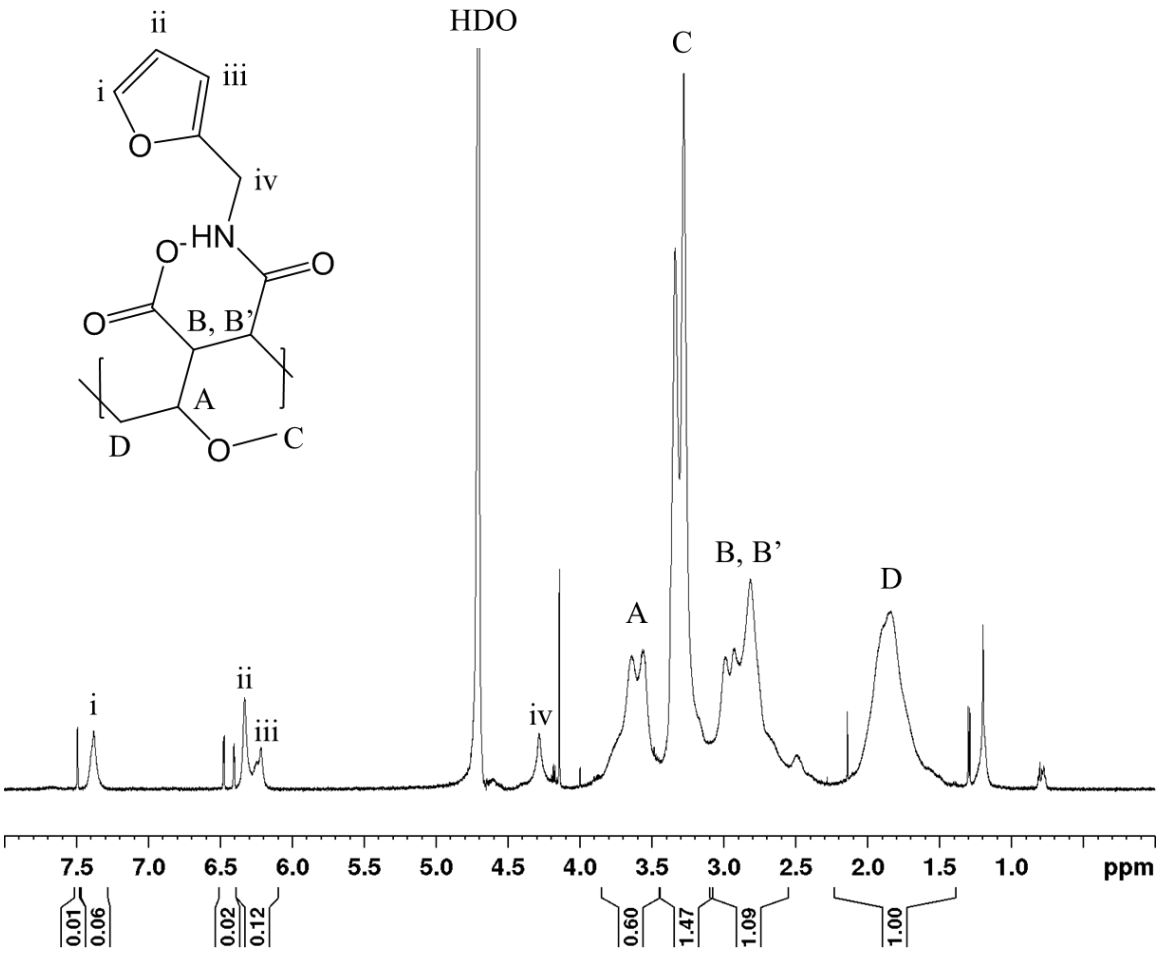

Figure A2.1. ^{1}H-NMR of PMM-FFA12 in D_2O. The ratio of the furan vinyl signals (at 6.25 (iii), 6.35 (ii), and 7.40 (i) ppm) to the backbone methylene signal (D), was used to determine the percent functionalization with FFA.

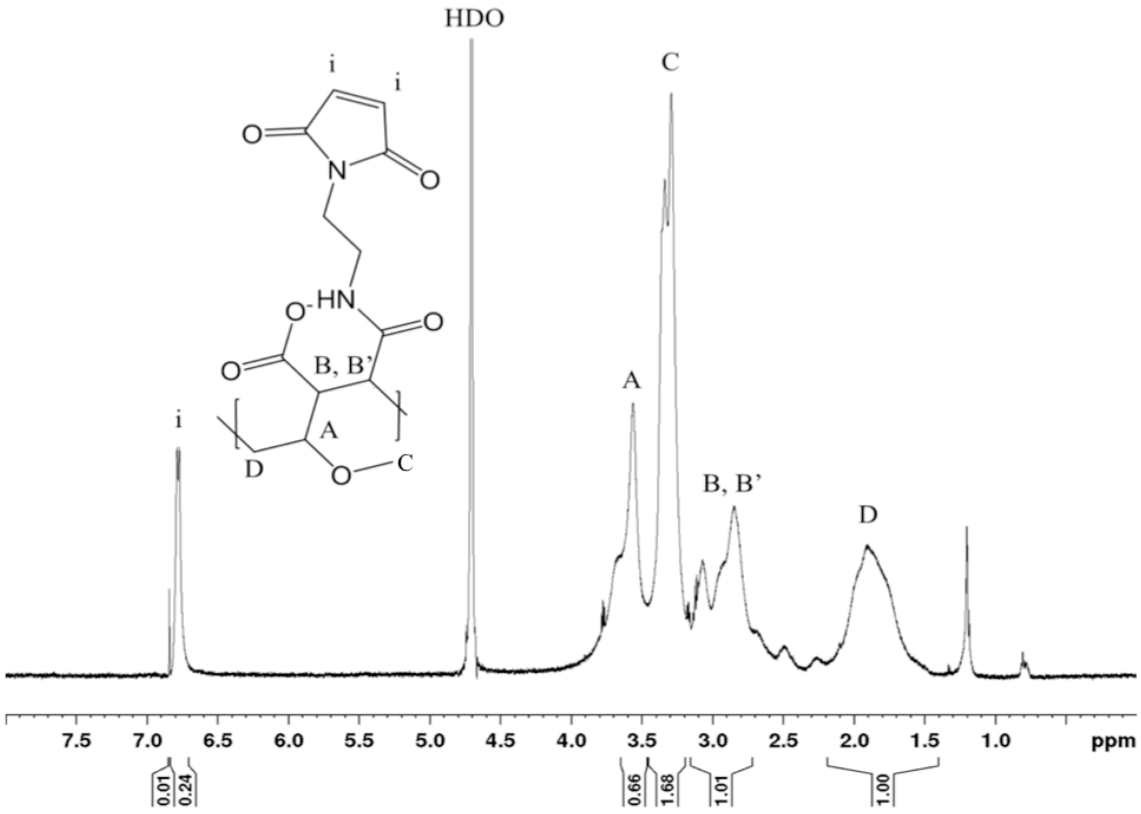

Figure A2.2. ^{1}H-NMR of PMM-MAL24 in D_2O. The ratio of the maleimide vinyl signal at 6.75 ppm (i) to the backbone methylene signal (D) was used to determine the percent functionalization with MAL.

About 1-5% of the furfurylamine and aminoethyl maleimide in the final samples are present as free small molecules, as indicated by small sharp peaks in the corresponding NMR spectra, just downfield from the corresponding signals for the polymer-bound FFA and MAL. This is attributed to electrostatic retention of some of the protonated amines by the polyanionic PMM backbone, even after dialysis. Future experiments will explore the use of added salts during dialysis to facilitate removal of these low molecular weight amines. Amide hydrolysis, occurring either during polymer dialysis or NMR sample preparation, may also be responsible for a small portion of the free FFA and MAL.

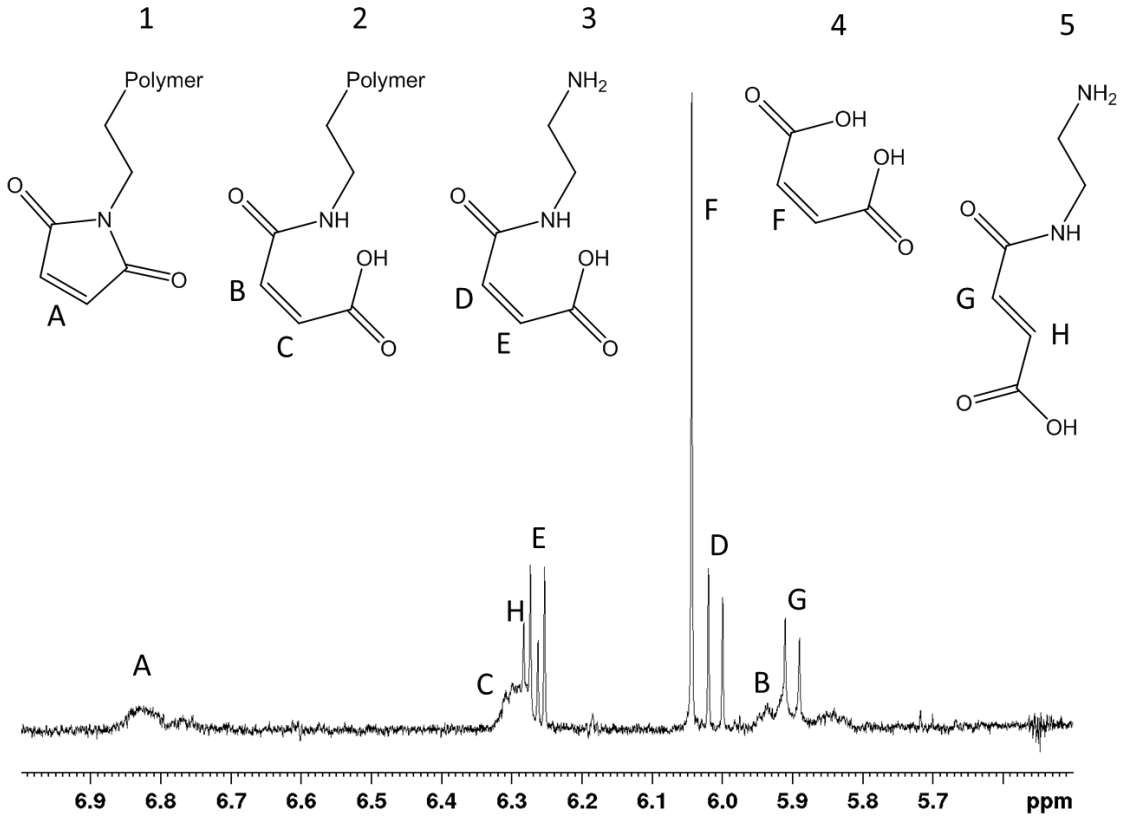

Figure A2.3. ^{1}H-NMR spectrum of a solution of PMM-MAL24 kept at pH 6 in MES buffer for 7 days at 37 °C.

Figure A2.3 shows a representative ^{1}H-NMR spectrum after 7 days of hydrolysis at 37 °C and pH 6. At this point about 80% of the initial maleimide has hydrolyzed to a mixture comprising polymer-bound maleamic acid 2 (broad signals B and C), aminoethyl maleamic acid 3 (two sharp doublets: D, E), aminoethyl fumaric acid [1,2] 5 (two sharp doublets: G, H) and maleic acid 4 (sharp singlet, F).

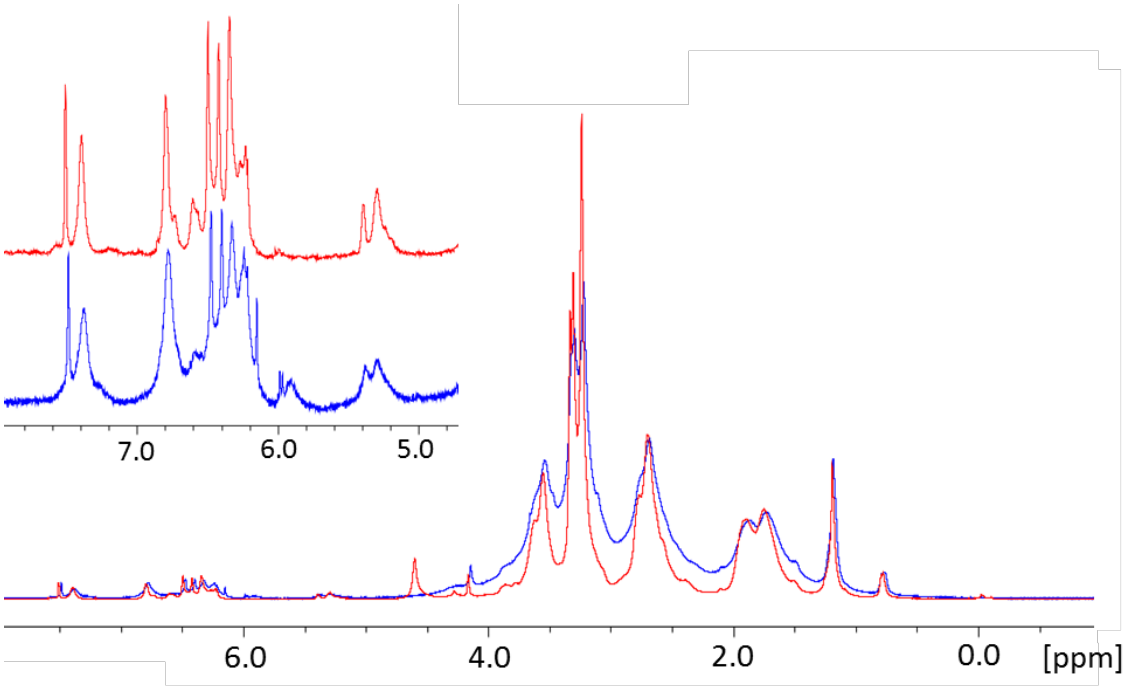

Figure A2.4. Comparison between solution-state (blue) and HR-MAS (red) spectra of crosslinked PMM-FFA25/MAL24 gels cured at pH 5.1 ± 1 at 37 °C for 18 h. MAS rate = 3500 Hz.

Figure A2.4 compares the HR-MAS spectrum (red, top trace in insert) with the broader solution-state ^{1}H-NMR spectrum (blue, bottom trace in insert), for a PMM-FFA25/PMM-MAL24 mixture with a total polymer concentration of 10% w/v (5% w/v of each polymer) at pH 5.1 in D_2O, cured for 18 h at 37 °C.

The MAS spectrum shows significantly narrower signals compared to the conventionally acquired spectrum. The inset shows the vinyl protons for polymer-bound furan at 7.4 ppm (1H) and at 6.1-6.3 ppm (2H), and for polymer-bound maleimide at 6.8 ppm (2H). The Diels-Alder adduct shows a vinyl signal at 6.6 ppm, and a bridgehead proton signal at 5.2-5.3 ppm. There are also sharper vinyl signals for free furfurylamine at 7.5, 6.5 and 6.4 ppm (1H each), and a sharper peak attributed to the bridgehead proton of the free FFA / PMM-MAL Diels-Alder adduct at 5.4 ppm. The solution-state sample also shows small amounts of free and polymer-bound maleamic acid at 5.9-6.0 ppm.

Figure A2.5 compares in detail the above PMM-FFA25/MAL24 MAS spectrum taken at 18 hours after mixing (red, top spectrum), with the corresponding MAS spectrum of the same sample taken 36 minutes after mixing (blue, bottom spectrum).

The lower spectrum (36 minutes) shows very little evidence of the Diels-Alder adduct. The upper spectrum (18 h) shows the appearance of Diels-Alder adduct signals at 5.1-5.2 (bridgehead) and 6.5 (vinyl), as well as decreases in furan (6.1, 6.2 and 7.3 ppm) and maleimide (6.7 ppm) intensity.

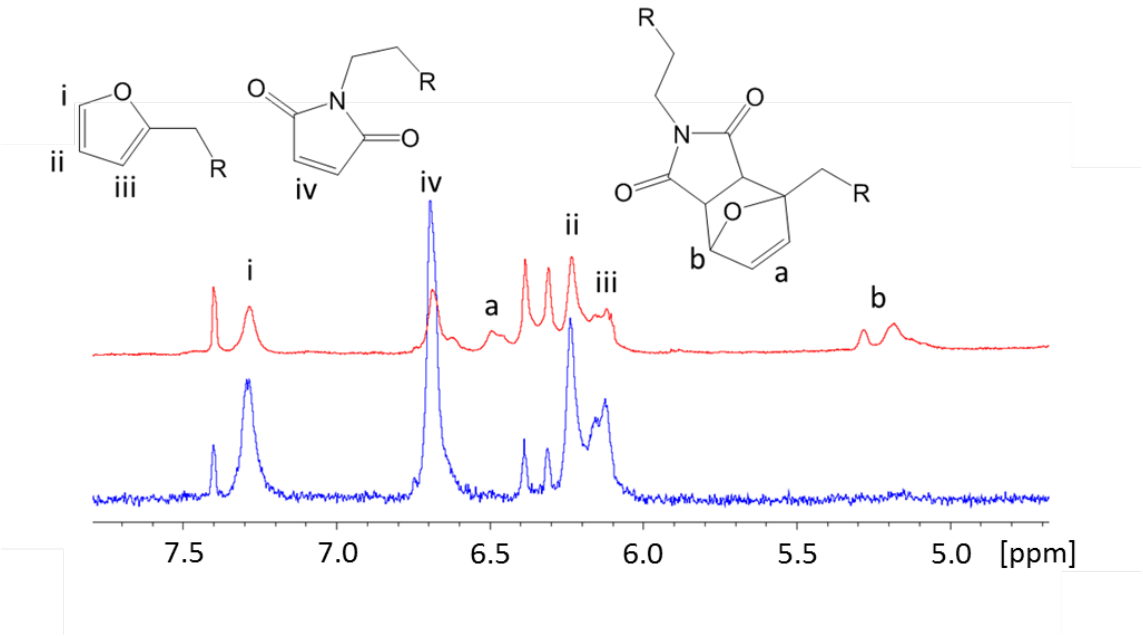

Figure A2.5. ^{1}H-NMR HR MAS spectrum of mixture containing 5% PMM-MAL24 and 5% PMM-FFA25 at pH 5.2 after 36 mins (bottom spectrum) and 18h (top spectrum) at 37°C. The polymer-polymer Diels-Alder adduct peaks appear between 6.4 and 6.5 ppm (vinyl protons) and at 5.1-5.3 ppm (bridgehead proton). The bridge head proton of the Diels-Alder adduct at 5.1 – 5.3 ppm becomes visible in the bottom spectrum, after 36 min of reaction. The sharp signals at 7.4 and 6.3-6.4 ppm correspond to free furfurylamine, while the signal at 5.3ppm is attributed to the Diels-Alder adduct formed between PMM-MAL and free FFA. MAS rate ~3500 Hz.

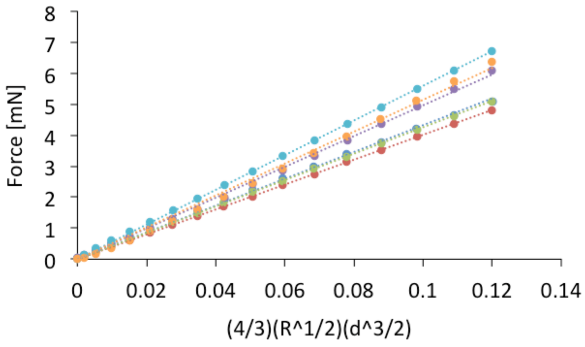

Figure A2.6. Force strain curve for PMM-FFA18/MAL24 hydrogel (10 w/v% total polymer concentration). The measured forces are plotted as a function of strain ($d^{3/2}$) and fitted to the equation: $F = \frac{4ER^{1/2}}{3(1-\nu^2)}d^{3/2}$. The slope of the above strain curves are given as E^*. The elastic modulus can then be found from the average E^* as

$\frac{1}{E*} = \frac{1-\upsilon}{E}\frac{1}{E^*} = \frac{1-\upsilon}{E}$, where ν is the Poisson's ratio (assumed to be 0.5) and E is the Young's modulus.

2.8 Appendix References

(1) Choi, W.; Kang, S.; Mok, Y.; Park, E.; Song, Y.; Choi, S.J.; Lee, Y. *Chem. Eur. J.* **2014**, *20*, 15715-15718.
(2) Sànchez, A.; Pedroso, E., Grandas, A. *Eur. J. Org. Chem.* **2010**, *13,* 2600-2606.

Chapter 3

Crosslinked hydrogel beads formed through Diels-Alder coupling of Furan- and Maleimide-modified Poly(methyl vinyl ether-*alt*-maleic acid) within a calcium alginate template

S. Alison Stewart, Mitchell A. Johnson, Nicholas A. D. Burke, Harald D. H. Stöver. To be submitted.

Alison Stewart primarily planned this study. Alison Stewart synthesized all polymers and beads and carried out physical characterization tests. Mitchell Johnson assisted with cell encapsulation studies. Nicholas Burke and Harald Stöver provided experimental guidance and editing feedback of the manuscript.

3.1. Abstract

The formation of covalently crosslinked hydrogel beads by Diels-Alder coupling between polyanions modified with furan and maleimide groups is described. Poly(methyl vinyl ether-*alt*-maleic anhydride) was reacted with 15 – 30 mol% furfurylamine (FFA), or 2-aminoethylmaleimide (MAL), respectively, followed by hydrolysis of residual anhydride groups. Aqueous solutions containing 0.5 - 1.5% w/v of each of the two resulting mutually reactive polyanions, PMM-FFA and PMM-MAL together with 1% w/v sodium alginate were extruded as droplets into a calcium chloride gelling bath. The resulting beads retained 88-97% of the functionalized PMM polymers, demonstrating efficient entrapment of these two network formers within the calcium alginate hydrogel. Confocal fluorescence microscopy of PMM-FFA and PMM-MAL labelled with TAMRA-cadaverine and aminofluorescein, respectively, showed both polymers co-located with each other and with the calcium alginate, all showing a trough-shaped density profile across the beads. In-diffusion tests using 10 kDa to 500 kDa fluorescently labelled dextran showed approximate MW cut-offs between 70 k and 250 k. Citrate-extraction of calcium from these composite beads led to swelling, but preserved the integrity of the Diels-Alder crosslinked networks. Significantly, covalent networks

within the calcium alginate beads could be formed at much lower polymer concentrations than required in absence of calcium alginate, and at physiological pH, suggesting that the crosslinking reaction is strongly promoted within the calcium alginate beads. Encapsulated NIH 3T3 cells showed good viability after encapsulation, confirming cyto-compatibility of these reactive polymers and their hydrogels.

3.2. Introduction

The transplantation of stem-cell-derived therapeutic cells encapsulated in semi-permeable polymer hydrogel beads is a promising approach for the treatment of enzyme- and hormone-deficiency disorders such as insulin-dependent diabetes,[1] Parkinson's,[2] dwarfism[3] and hemophilia,[4] as well as certain types of liver[5] and kidney[6] failure. Such hydrogel beads must protect the encapsulated cells from the host immune system,[7] and protect the host from the tumorigenic potential of encapsulated stem cells,[8] while serving as synthetic extracellular matrix (ECM) for the encapsulated cells.[9]

Solutions of sodium alginate, a naturally occurring, linear polysaccharide composed of (1-4)-linked β-D-mannuronate (M) and α-L-guluronate (G) units,[10] are commonly used to form such beads by gelation with divalent cations such as calcium, strontium and barium.[11,12] The resulting beads are typically coated with poly-L-lysine (PLL) or other polycations to improve capsule strength and control permeability,[13] and then with alginate to reduce the cationic charge density at the bead surface.[14] While generally compatible with both the host and encapsulated cells, such capsules can weaken though cation loss,[15] and can evoke immune responses through exposure of PLL[15] leading to fibrotic overgrowth of the beads.[16]

Covalently crosslinkable synthetic polymers incorporated into such alginate beads can mitigate gel weakening[17,18] and enable longer-term immuno-protection.[19] Crosslinking occurs in the presence of cells and thus cannot include cytotoxic reagents, monomers, catalysts or by-products, and must occur readily under physiological conditions. While layer-by-layer deposition of oppositely charged and mutually reactive polyelectrolytes on the surface of preformed calcium alginate beads has been well demonstrated,[20,21] another approach is to include one or both of the polymeric gel formers

within the calcium alginate bead, and avoid the use of polycations altogether.[22,23,24] These reactive polymers should not interfere with the ionic gelation of alginate and show minimal out-diffusion from the hydrogel beads.

Poly(methyl vinyl ether-*alt*-maleic anhydride) (PMMAn) is a commercially available polymer produced in a variety of molecular weights and easily functionalized via reaction of the anhydride groups with a nucleophile. Subsequent hydrolysis of residual anhydrides yields functional poly(methyl vinyl ether-*alt*-maleic acid) (PMM), a water-soluble polymer that is polyanionic under physiological conditions. Various PMM-based polymers are used as pharmaceutical thickening and suspending agents, denture adhesives, and adjuvants for drug delivery systems.[25,26,27,28] PMM is known to interact with calcium ions[29] and will precipitate or gel at calcium chloride concentrations above 1 M.[30,31] Functionalized PMM has been previously reported[31,32] and our group has shown that calcium alginate beads coated successively with PLL and partially hydrolyzed PMM showed good immune-protection of C2C12 cells in immuno-competent mice.[30]

Diels-Alder coupling reactions between furan and maleimide-modified polymers are becoming increasingly popular for functionalizing or crosslinking biomaterials. The reaction does not require small-molecule catalysts or additives, and occurs readily under aqueous conditions.[33] While the Diels-Alder reaction between furan- and maleimide-modified polymers has been used to form bulk hydrogels, typically it must be carried out at pH 5.5 - 6.0 in order to limit competing hydrolysis of maleimide moieties.[32] The present work demonstrates the first use of the Diels-Alder click reaction to reinforce alginate beads. Described is a matched pair of furan- and maleimide-functionalized poly(methyl vinyl ether – *alt* – maleic acid)s, PMM-FFA and PMM-MAL, as reactive polyanions that undergo covalent crosslinking at low loading percentages at physiological pH 7.4 when entrapped within a calcium alginate bead. PMM provides a common polyanionic backbone for both partners, while the moderate rate of Diels-Alder coupling, compared to alternate crosslinking approaches using nucleophile-electrophile pairs,[34,35] ensures adequate time for mixing and bead formation. The lack of enzymatic degradability of PMM offers the potential for long-term encapsulation, which is desirable for treatment of chronic endocrine disorders. Upon formation of a covalently crosslinked

network, the temporary calcium alginate scaffold may be extracted from the core, resulting in a completely synthetic matrix bead. The combination of PMM-FFA/MAL within calcium alginate beads was found to dramatically accelerate the Diels-Alder reaction, withstanding liquefaction of the alginate template in as little as 15 minutes and reaching equilibrium after 4 - 6 h, compared to 24 h in bulk gels, and allowing for the reaction to occur at physiologically relevant pH 7.4, making it suitable for use in cell encapsulation. Additionally, it allowed for significantly lower polymer-loading percentages of 0.5 - 1.5% w/v compared to 5 - 10% w/v needed for the bulk gel systems previously reported.[32]

3.3. Experimental Section

3.3.1. Materials

Poly(methyl vinyl ether-*alt*-maleic anhydride) (PMMAn, M_n = 80kDa, Sigma-Aldrich, Oakville, ON) was heated in a vacuum oven at 140°C for 5 days to ensure that it was completely in the anhydride form.[30] 5-Aminofluorescein, triethylamine, 2-(*N*-morpholino)-ethanesulfonate hemisodium salt (MES), *N*-hydroxysuccinimide (NHS), 1-Ethyl-3-(3-dimethylaminopropyl)carbodiimide (EDC), fluorescein isothiocyanate-conjugated dextran (dextran-*f*; 10, 70, 250, 500 kDa), 4-(2-hydroxyethyl)-1-piperazineethanesulfonic acid (HEPES) sodium salt, *N,N*-dimethylformamide, and furfurylamine (FFA) were purchased from Sigma Aldrich (Oakville, ON) and used as received. Sodium alginate (Pronova UP MVG, batch no. FP-610-03) was purchased from NovaMatrix (Sandvika, Norway) and used as received. Sodium chloride, sodium bicarbonate, acetonitrile and calcium chloride dihydrate (Reagent, Caledon Laboratories, Caledon, ON) and were used as received. 5(6)-((*N*-aminopentyl)amino) carbonyl) tetramethyl rhodamine (TAMRA-cadaverine or TAMRA-c) was purchased from Life Technologies Inc. Deuterium oxide (99.99 atom% D, Cambridge Isotope Laboratories, Andover, MA) was used as received. Tri-sodium citrate dehydrate was purchased from EMD Chemicals. *N*-(2-aminoethyl)maleimide trifluoroacetic acid was purchased from Santa Cruz Biotechnology Inc. (CA, USA).

3.3.2. Synthesis of PMM-FFA and PMM-MAL with 10 – 25 mol% FFA

PMM-FFA and PMM-MAL, both unlabelled and with TAMRA-cadaverine and fluoresceinamine labelling, respectively, were prepared as previously described.[32] Briefly, 0.500 g (3.2 mmol anhydride) PMMAn was dissolved in 10 mL acetonitrile to form a 5% w/v solution. Triethylamine (150 μL, 1.1 mmol) and TAMRA-cadaverine (3.3 mg, 0.0065 mmol, 0.2 mol% relative to anhydride groups in PMMAn) were dissolved in 0.33 mL DMF, added to the PMMAn solution and allowed to stir at room temperature overnight. FFA diluted in 2 mL acetonitrile was then added dropwise over a few minutes, at different molar ratios to achieve different degrees of furan substitution. After 24 h at room temperature, the mixture was diluted with 40 mL distilled water, 1.0 N NaOH was added slowly until the polymer became soluble, and the resulting solution was dialyzed against distilled water (adjusted to pH 7 and changed daily) for four days using cellulose dialysis tubing (molecular weight (MW) cut-off 3500 Da, Spectrapor). The dialyzed solution was freeze-dried to give PMM-FFA$_x$*r* as a pink powder. The degree of substitution (DS) was determined by ^{1}H-NMR in D_2O on a Bruker AV-600 NMR spectrometer, comparing the signals for furan protons at 6.25, 6.35 and 7.40 ppm to the signal for two PMM methylene backbone protons at 1.85 ppm. The degree of TAMRA-cadaverine labelling was determined by UV-Vis absorbance.

Similarly, PMM-MAL was prepared by dissolving 0.500 g PMMAn in 10 mL acetonitrile, followed by addition of triethylamine (150 μL, 1.1 mmol) and aminofluorescein (0.5 mol% relative to anhydride groups) in 0.33 mL DMF. The reaction was allowed to stir in the dark overnight. *N*-(2-aminoethyl)maleimide trifluoroacetate was dissolved in 1 mL of a 10:1 mixture of acetonitrile and DMF and added dropwise to the stirring PMMAn solution. The molar ratios of *N*-(2-aminoethyl)maleimide trifluoroacetate were varied to achieve different degrees of maleimide substitution. After 24 h of mixing at room temperature, in the dark, the mixture was diluted with distilled water, and dialysed against distilled water adjusted to a pH of 5.5 and changed daily for four days. The solution was freeze-dried to give PMM-MAL$_y$*f* as a yellow powder. The DS was determined by ^{1}H-NMR in D_2O on a Bruker AV-600 NMR spectrometer, comparing the signals for the two maleimide vinyl protons

at 6.75 ppm with those for the methylene backbone protons at 1.85 ppm. The degree of fluorescein labelling was determined using UV-vis absorbance. Other PMM-FFA_x and PMM-MAL_y derivatives, both labelled and unlabelled, were prepared analogously, as reported in Table 3.1.

3.3.3. Fluorescent Labelling of Alginate

Fluoresceinamine was used to label alginate via EDC coupling at the carboxylic acid groups. The procedure used was modified from that described by Donati *et al*.[36] Briefly, to a 0.3% w/v alginate solution (300 mg) in MES buffer (100 mL, 0.1 M, pH 4.5), fluoresceinamine dissolved in MeOH (1 mol%, 4.7 mg, 0.1% w/v) was added dropwise, followed by NHS (267 mg, 170 mol%, 1% w/v) and EDC (360 mg, 170 mol%, 1% w/v) in water. The solution was allowed to react in the dark overnight at room temperature and was then dialyzed against $NaHCO_3$ (0.1 M) for two days, followed by distilled water for three days. Before freeze drying, the pH was adjusted to 7.4. The freeze-dried material, alginate-*f*, was a yellow powder with 0.27% fluorescein labelling, determined using UV-vis absorbance.

3.3.4. Preparation of Alginate PMM-FFA_x/PMM-MAL_y Matrix Beads

A solution of sodium alginate (1.25% w/v) in HEPES buffer (800 µL, 50 mM, pH 7.4) was added to a 200 µL solution of PMM-MAL_y*f* (10 mg) and PMM-FFA_x*r* (10 mg) in water, to give final concentrations of 1% w/v alginate, and 1% w/v each PMM-MAL_y*f* and PMM-FFA_x*r*. The solution was briefly vortexed to ensure complete mixing, then air-sheared through a 27 gauge needle into 50 mL of gelling bath containing 0.45% w/v (77 mM) NaCl and 1.1% w/v (100 mM) $CaCl_2$ using a syringe pump set to a flow rate of 0.5 mL/min. A dense suspension of the resulting beads (ca. 1 mL) were collected and stored at 37 °C. Bead diameter was measured using an optical microscope set to transmission mode and a 5x magnification lens. At least 100 beads were measured to calculate the average bead diameter and standard deviation. An analogous procedure was used to prepare beads composed of 1.0% w/v alginate and 0.5% w/v, 1.0% w/v and 1.5% w/v of each of PMM-MAL_y and PMM-FFA_x, with both labelled and unlabelled polymers.

Bead stability over time was measured by rinsing 250 µL of beads from each of the nine sets prepared (0.5, 1.0, 1.5% w/v each of PMM-FFA11*r*/MAL11, PMM-FFA18*r*/MAL15, PMM-FFA25*r*/MAL25) with two 2.5 mL washes of sodium citrate. Beads were incubated in sodium citrate for 24 h at 37 °C to allow for complete liquefaction of the alginate template. Beads were then rinsed twice with 2 mL of saline and stored at 37 °C. A small aliquot was removed and bead diameters were measured at set time points using the microscope on transmitted light mode.

The effect of varying concentrations of sodium alginate was investigated by preparing beads composed of 1.5, 1.2, 1.0, 0.8 and 0.5% w/v alginate and 1.0% w/v each PMM-FFA18*r*/MAL15. The pH of the solutions was adjusted to 7.1 ± 0.2. Beads were incubated at 37 °C for 48 h, followed by treatment with sodium citrate (70 mM). Bead diameters were measured using the microscope on transmitted light mode.

3.3.5. Polymer Trapping Efficiency

A small amount of gelling bath supernatant from the gelled matrix beads was removed immediately after bead formation and measured using a UV-vis spectrometer. The concentration of fluorescent material in the supernatant was then used to determine the percentage of polymer trapped within the alginate matrix bead. To test for potential polymer leaching from the formed matrix beads, a small amount of supernatant was removed from a solution of beads that had been incubated in sodium citrate for one week and measured using a UV-Vis spectrometer.

3.3.6. Covalent Crosslinking vs. Bead Formation Time

Matrix beads were tested for covalent crosslinking by placing approximately 20 beads into a well on a glass microscope slide. The supernatant was removed with a Kimwipe and replaced with 200 µL of sodium citrate (70 mM). The beads were observed for one hour using epifluorescence mode on the microscope. Beads were challenged with sodium citrate 10 - 15 minutes after initial formation, and at subsequent time points, until covalent crosslinking was observed. To ensure that the beads remained intact due to covalent crosslinking, control beads composed of alginate (1% w/v) and

FFA12-25*r* (2% w/v) and alginate (1% w/v) and MAL9-24*f* (2% w/v) were incubated at 37 °C for 24 h and then placed in 70 mM sodium citrate.

3.3.7. Bead Swellability

Matrix beads were allowed to incubate at 37 °C for at least 24 h to ensure completion of the Diels-Alder crosslinking reaction. Approximately 300 beads were placed into a glass vial, and the supernatant was removed. The beads were rinsed with 1 mL of sodium citrate, which was then removed and replaced with 3 mL of fresh sodium citrate. The beads were gently agitated for 6 - 7 h and then observed and measured using the epifluorescence setting on the microscope. At least 100 beads were measured to determine the average bead diameter and standard deviation.

3.3.8. Measurement of Capsule Permeability using Fluorescently-Labelled Dextran

Alg-PMM-FFA$_x$/PMM-MAL$_y$ bead permeability was evaluated using fluorescently labelled dextran (dextran-*f*) with MWs of 10, 70, 250 and 500 kDa. For each measurement, approximately 50 beads were placed in a 2 mL conical vial. The beads were covered with 1.5 mL of 0.1% w/v dextran-*f* in HEPES buffer and gently agitated for 24 h to ensure complete and even indiffusion of dextran-*f*. Similarly, beads were treated with 70 mM sodium citrate for 24 h to liquefy the alginate and induce swelling. The beads were then removed from the citrate and placed into dextran-*f* solutions as described above. All beads were examined by confocal fluorescence microscopy and the fluorescent intensities from the central ca. 25% area of the beads as well as from the surrounding solution were obtained using NIS-Elements (Nikon) software (n = 4). The ratio of intensities of the bead centre and surrounding solution were reported, in order to compensate for any possible photobleaching. The measurement was conducted in quadruplicate for each dextran-*f* MW.

3.3.9. Cell Encapsulation Procedure

A sterile filtered (0.2 μm) solution of PMM-FFA17/MAL14 in HEPES-buffered saline was added to sterile filtered (0.2 μm) alginate (2% w/v) along with a NIH 3T3 *Mus musculus* fibroblasts cell suspension in HEPES-buffered saline to give a final

concentration of 2 million cells/mL, 1% w/v alginate and 1% w/v each PMM-FFA17 and PMM-MAL14. This solution was kept on ice and beads were prepared as described above by shearing the alginate solution through a 27 gauge flat tipped needle into three separate HEPES-buffered $CaCl_2$ gelling baths on ice. 0.3 mL of dense bead suspension from each gelling bath was transferred to conical vials and washed once with media before being transferred to a 24-well plate and diluted with 2 mL of media. Cells were incubated at 37 °C with 5% CO_2 for 7 days with a media change on day 4. Control beads containing 1% w/v alginate and 2 million cells/mL 3T3 cells were prepared in an analogous fashion.

3.3.10. Cell Viability

The cytotoxicity of the beads to NIH 3T3 fibroblasts was explored using a live/dead calcein AM/ethidium homodimer-1 (EthD-1) assay. The fibroblasts were cultured in tissue culture flasks in Dulbecco's Modified Eagle Medium (DMEM) supplemented with 10% v/v Bovine Calf Serum (BCS) and 1% v/v Penicillin/Streptomycin (PS) in a 5% CO_2 environment at 37 ^{o}C with 100% humidity in a water-jacketed incubator. When 75-80% confluency was reached, cells were washed with PBS (pH 7.4, Invitrogen) and detached using 0.25% Trypsin-EDTA (1X) phenol red. After encaspulsation and subsequent incubation, the live/dead assay was used to determine cell viability and examine the cytotoxicity on the encapsulated cells. Calcein AM/EthD-1 solution (50 μL of 2 μM calcein AM and 4 μM EthD-1 in sterile HEPES-buffered saline) was added to each well and incubated at room temperature for 20 minutes. Fluorescence images were obtained using a Nikon Eclipse Ti confocal microscope. Cell viability was calculated by counting the number of live and dead cells. Live/dead assays were conducted on days 0, 1, 3 and 7 and z-stacks of 3 beads per replicate were obtained.

3.4. Results and Discussion

3.4.1. Preparation of CaAlg - PMM-FFA/PMM-MAL Matrix Beads

PMMAn can serve as a useful scaffold for the preparation of reactive polymers and hydrogels. Functionalization was achieved by reaction of PMMAn with either furfurylamine or *N*-(2-aminoethyl)maleimide. Amine nucleophiles were selected due to the hydrolytically stable (at physiological pH) amide linkages between the PMM backbone and reactive moieties.

PMM-FFA$_x$ derivatives were prepared in a single step by reacting furfurylamine with PMMAn in acetonitrile in presence of tertiary amine. Varying the molar ratios of furfurylamine to anhydride gave access to PMM-FFA$_x$ with different DS, defined as the number of furans per anhydride repeat unit. Reaction with a small amount of TAMRA-c prior to furfurylamine addition resulted in analogous, rhodamine-labelled PMM-FFA$_x$*r* (Table 3.1). Due to steric hindrance, TAMRA-c reacts more slowly than furfurylamine with PMMAn and thus is added first. PMM-MAL$_y$ derivatives were prepared in a similar one-step fashion by reacting *N*-(2-aminoethyl)maleimide with PMMAn in acetonitrile in various molar ratios. Fluorescent labelling was achieved via reaction with a small amount of fluorescein amine.

Table 3.1. DS of PMM-FFA*r* and PMM-MAL*f*[a]

	DS	DS fluorophore
modified PMM	actual (target)	actual (target)
FFA11*r*	11 (15)	0.13 (0.2)
FFA18*r*	18 (25)	0.14 (0.2)
FFA23*r*	23 (30)	0.15 (0.2)
FFA12	12 (15)	N/A
FFA16	16 (25)	N/A
FFA25	25 (30)	N/A
MAL9*f*	9 (15)	0.39 (0.5)
MAL17*f*	17 (25)	0.18 (0.5)
MAL24*f*	24 (30)	0.59 (0.5)
MAL11	11 (15)	N/A
MAL15	15 (25)	N/A
MAL25	25 (30)	N/A

[a] "*r*": rhodamine-cadaverine labelled; "*f*": fluorescein labelled.

To evaluate the ability of PMM-FFA_x and PMM-MAL_y to form crosslinked hydrogels within the calcium alginate matrix, matrix beads were prepared by extruding a 1% w/v alginate solution containing between 0.5 – 1.5% w/v each PMM-FFA_x*r* and PMM-MAL_y*f* into a calcium chloride gelling bath. In all cases, the beads were of similar size and shape as those formed using alginate alone, indicating that the presence of PMM-FFA/MAL does not inhibit alginate gelation. For example, the beads formed from 1% w/v alginate and 1% w/v PMM-FFA11*r* and 1% w/v PMM-MAL9*f* were spherical with smooth surfaces and an average diameter of 522μm ± 22μm. While the average diameter showed minor batch-to-batch variations, they fell between 471 – 525 μm with standard deviations ≤ 36 μm (table A3.1).

Table 3.2. Percentage of polymer entrapped within matrix beads

Bead Composition	% Polymer Entrapped	
	FFA_x*r*	MAL_y*f*
Alg (1%)/FFA11*r* (1%)/MAL9*f* (1%)	88%	96%
Alg (1%)/FFA18*r* (1%)/MAL17*f* (1%)	88%	93%
Alg (1%)/FFA23*r* (1%)/MAL24*f* (1%)	89%	97%

Fluorescent labelling of both PMM-FFA and PMM-MAL was possible due to a higher number of functional groups per chain compared with commonly used bi- or tetra-functional polymers. UV-vis analysis of the calcium chloride gelling bath post-bead gelation indicated loss of 3 to 12% of each of the labelled polymers during gelation. This relatively low polymer loss indicates that the polymers are effectively trapped within the forming calcium alginate gel. This is a substantial improvement over previous work that showed up to 60% loss of reactive polymer during alginate bead gelation.[22] Alginate droplets typically shrink to about 50% of their original volume upon calcium gelation[37,38] during which solvent and other components that are not readily entrapped are lost to the bath. It was of further interest to determine whether there was subsequent leaching of PMM-FFA_x*r* or PMM-MAL_y*f* after initial bead formation. Beads were stored in a fresh solution of gelling bath for one week, after which a small sample of the supernatant was

removed and measured for fluorescence using UV-vis spectroscopy. No detectable amount of fluorescence was found, indicating that PMM-FFA$_x$*r* and PMM-MAL$_y$*f* remain effectively entrapped within the beads following initial gelation.

Developing materials that are suitable for long-term cell encapsulations is one of the motivations behind this project, making long-term stability of the beads a critical feature. Bead stability was monitored over a six-week period. Matrix beads were initially treated with sodium citrate to liquefy the alginate scaffold, leaving the Diels-Alder crosslinked matrix intact. Beads were then rinsed and stored in saline at 37 °C and at set time points were removed and bead diameter was measured using a microscope on transmitted light mode. It was found that 0.5% w/v beads of all functionalization percentages withstood the initial citrate challenge but were very weak and broke apart before the second time point at two weeks. Other bead compositions seemed to reach a swelling equilibrium after 4 weeks, and all remained intact after 6 weeks of incubation. Figure 3.1 shows the resulting swell ratios (diameter after and before calcium extraction) for 1 and 1.5 % w/v polymer loading. The slow swelling of the beads following calcium extraction is thought to reflect slow partial disentanglement of the crosslinked PMM network.

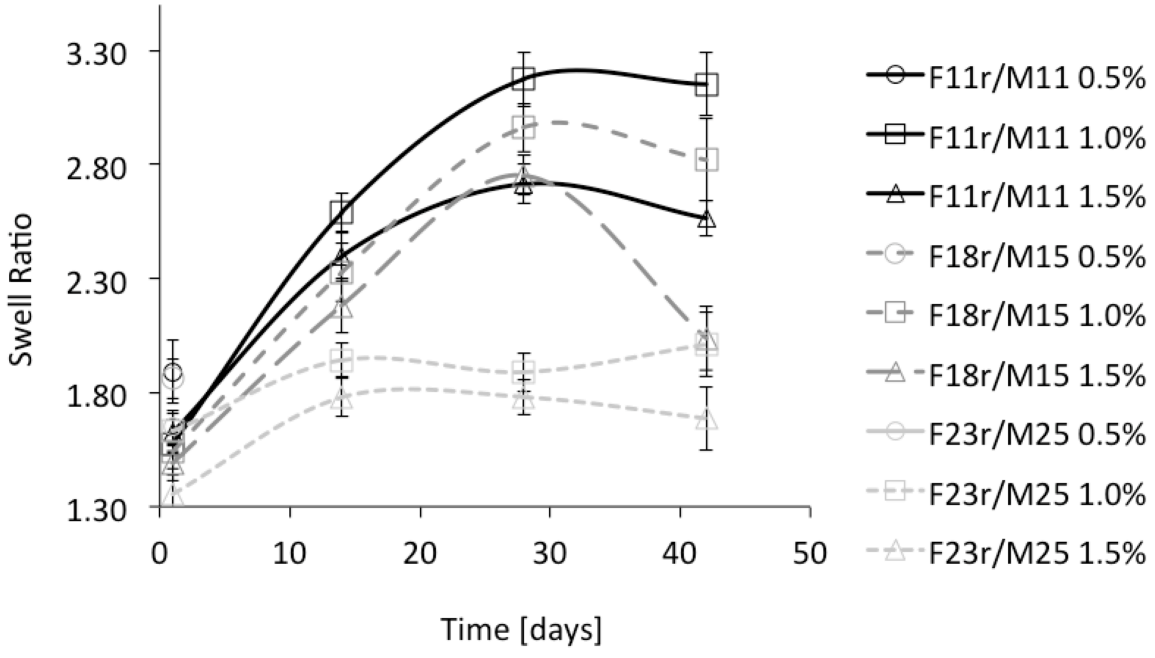

Figure 3.1. Matrix bead stability over time, following alginate scaffold liquefaction.

The effect of alginate concentration on bead swelling was investigated. Alginate concentrations ranging from 0.5 – 1.5% w/v were used to prepare matrix beads with 1% w/v each PMM-FFA18*r*/MAL14. After covalent crosslinking was complete, beads were treated with sodium citrate and diameters were measured and swell ratios were calculated. It was found that swell ratios decreased from 0.5 to 1.0% w/v sodium alginate loading, and then increased from 1.0 to 1.5% w/v. This demonstrates the synergistic effect between alginate and PMM-FFA_x/MAL_y in facilitating the Diels-Alder crosslinking reaction. At lower alginate concentrations, the effect is less pronounced and crosslinking is less effective. However, when alginate concentration becomes too high, the crosslinking is inhibited and beads show higher post-citrate swelling as a result.

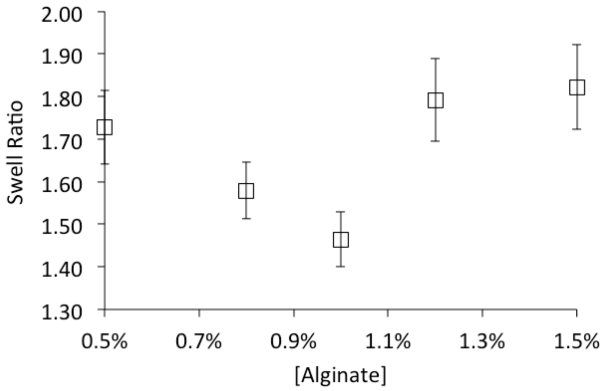

Figure 3.2. Swellability of 1% w/v PMM-FFA18*r*/MAL14 beads as a function of alginate concentration.

3.4.2. Fluorescently Labelled Alginate

Calcium alginate serves as a temporary scaffold in these matrix beads. Over time, as calcium ions are exchanged with sodium, the scaffold will dissolve. It was of interest to map out the distribution of alginate within the matrix beads, relative to PMM-FFA/MAL, and to explore the fate of alginate upon calcium chelation with sodium citrate and subsequent liquefaction of the scaffold. Alginate was fluorescently labelled using EDC coupling between fluoresceinamine and the carboxylic acid groups on sodium alginate. Beads containing alginate-*f* were prepared as described above. It was found that alginate and the functionalized PMMs had very similar radial distributions throughout the beads (figure 3.3), with a higher concentration at the surface of the beads.

This confirmed that calcium alginate behaves as a template, facilitating the Diels-Alder crosslinking of PMM-FFA/MAL, and resulting in a covalently crosslinked network that mimics the initial distribution of alginate. After the beads were treated with sodium citrate, alginate distribution became homogenous as the alginate was liquefied and began to diffuse into the supernatant.

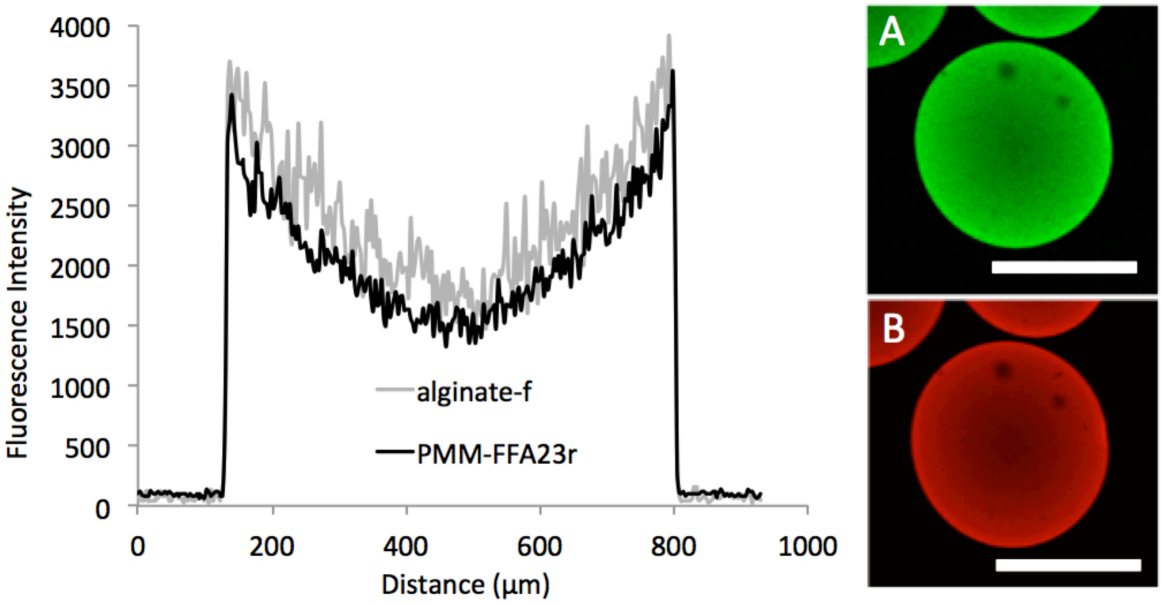

Figure 3.3. Line profile showing the distribution of fluorescent intensities of A) 1% w/v alginate-*f* and B) 1% w/v PMM-FFA23*r* throughout a matrix bead composed of 1% w/v alginate-*f*, 1% w/v each PMM-FFA23*r*/MAL25. Scale bars are 500 µm.

3.4.3. Covalent Crosslinking vs. Bead Formation Time

It was important to determine whether the reactive polymers were able to covalently crosslink inside the matrix beads, as well as how long it took for the crosslinking reaction to complete. PMM-FFA$_x$*r*/MAL$_y$*f* beads were exposed to sodium citrate, a calcium chelator that results in liquefaction of the alginate scaffold. Similar tests have been reported,[30] and upon dissolution of the ionically gelled alginate, only covalent crosslinks remain to preserve the structure of the matrix beads. After the initial ionic gelation in calcium chloride, matrix beads that contained alginate and both PMM-FFA$_x$*r* and PMM-MAL$_y$*f* were placed in a well on a glass microscope slide and exposed

to sodium citrate. For all compositions, beads that were allowed to gel for 10 - 15 minutes either did not remain intact upon exposure to citrate, or swelled and became deformed, indicating insufficient covalent crosslinking had occurred (figure 3.4).

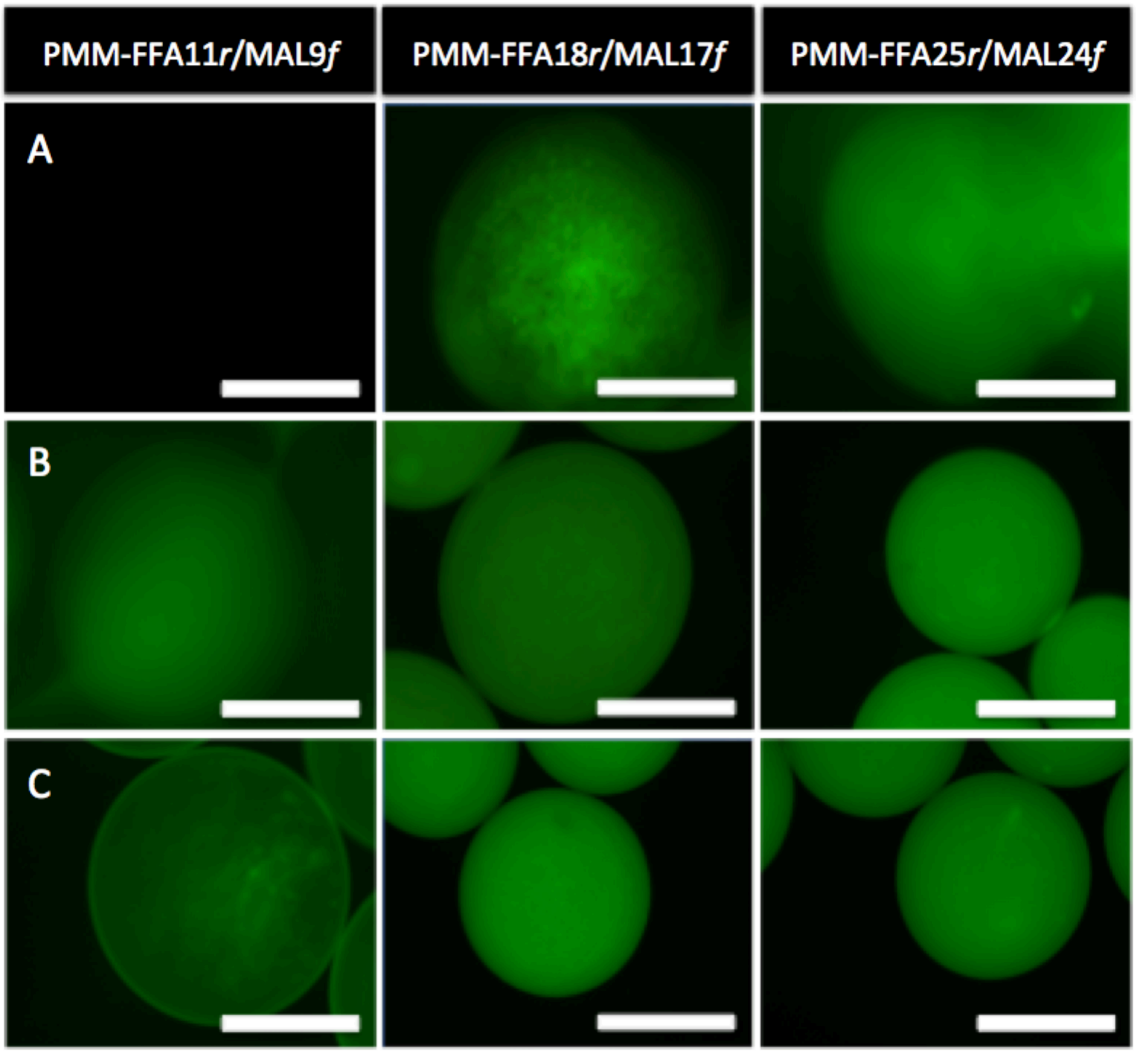

Figure 3.4. Swelling of PMM-FFA$_x$*r*/MAL$_y$*f* beads exposed to sodium citrate for 1 h at A: 15 minutes, B: 1.5 – 2.5 h, and C: 6 – 7 h post-bead formation. Scale bars are 500 μm.

With increasing incubation time after bead formation, the degree of swelling after citrate exposure decreased, indicating further Diels-Alder crosslinking. Matrix beads composed of PMM-FFA11*r*/MAL9*f* required up to 6.5 h incubation to remain intact, though still showed a high degree of swelling, and a heterogeneous distribution of

labelled polymer. This heterogeneity likely reflects areas of different crosslink density. Matrix beads composed of PMM-FFA18*r*/MAL17*f* remain intact after 1.25 h of crosslinking time. The post-citrate swelling of these beads decreased substantially between 1.25 h and 3 h, indicating further crosslinking can take place during the extended time. Beads composed of PMM-FFA23*r*/MAL24*f* remained intact and did not deform at 2.5 h. There appeared to be little difference in bead swelling between 2.5 h and 6 h, which suggests that the beads are fully crosslinked after 2.5 h. The time required for the Diels-Alder crosslinking reaction to reach completion is significantly shorter than that reported for bulk gel systems, and occurs under physiological pH 7.4, rather than pH 5.5 - 6.0 as is required for the analogous bulk (alginate-free) Diels-Alder gelling reactions. These factors indicate that the calcium alginate scaffold aids in accelerating the reaction within alginate beads, rendering the competing maleimide hydrolysis much less significant.[32]

Control beads were prepared using 1% w/v sodium alginate solutions containing 2% w/v of either PMM-FFA$_x$*r* or PMM-MAL$_y$*f*. These beads were expected to dissolve upon exposure to sodium citrate, due to the lack of covalent crosslinking. As expected, all control samples dissolved after a 1 h exposure to 70 mM sodium citrate, using the method described above. To further confirm that the control beads were not covalently crosslinked and the polymer chains were mobile within the beads, small regions within the beads were photobleached prior to citrate treatment using a confocal microscope. The beads exhibited between 38 – 57% fluorescent recovery within 1 h after FRAP, indicating significant mobility of the fluorescently labelled polymer chains. In comparison, beads composed of PMM-FFA$_x$*r*/MAL$_y$*f* exhibited between 6 – 12% fluorescent recovery within 1 h, confirming that the majority of polymer chains were fixed in place due to covalent crosslinking (figures A3.3 and A3.4).

3.4.4. Bead Swellability

In order to examine the degree of swelling upon citrate extraction of calcium as a function of bead composition, crosslinked beads were exposed to citrate and the bead diameter was measured. The matrix beads had been allowed to crosslink in gelling bath at 37 °C for at least 24 h to ensure that covalent crosslinking was complete. Beads were

treated with a large excess of sodium citrate and gently agitated for 6 - 7 h to ensure complete chelation of calcium from the beads. All nine compositions of matrix beads remained intact after the citrate extraction, which indicates that they were sufficiently crosslinked via the Diels-Alder reaction between PMM-FFA$_x$*r* and PMM-MAL$_y$*f*. The beads composed of PMM-FFA11*r*/MAL11 exhibited the highest degree of swelling (table A3.1) with a swell ratio of 1.9. This was expected as PMM-FFA11*r*/MAL11 has the lowest number of functional groups and therefore lower degrees of crosslinking. Beads composed of PMM-FFA18*r*/MAL15 and PMM-FFA23*r*/MAL25 both had comparable swell ratios. It is possible that once a certain number of crosslink points are achieved, chain mobility is sufficiently decreased that no more crosslinks are able to form. Additional functional groups would remain unreacted and therefore would not affect the degree of swelling of the beads.

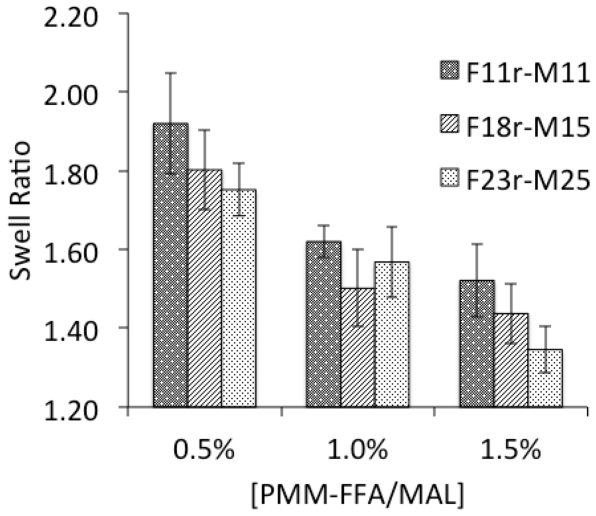

Figure 3.5. The swell ratio of matrix beads were calculated by measuring bead diameters before and after sodium citrate treatment and taking the ratio of the two values.

The citrate supernatant was removed and measured using UV-vis spectroscopy to determine whether any uncrosslinked, liquid polymer was released during citrate extraction. No fluorescence was detected, suggesting that all the polymer chains are covalently bound via the Diels-Alder crosslinking reaction.

3.4.5. Measurement of Capsule Permeability

Hydrogel beads are meant to provide immune protection for encapsulated cells or islets. They serve as a semi-permeable membrane and must allow for the in-diffusion of oxygen and nutrients to the encapsulated cells, while simultaneously permitting the out-diffusion of therapeutic agents such as insulin to the surrounding environment. The beads should also limit the access of the immune system to encapsulated cells by excluding antibodies and cytokines. In-diffusion studies of fluorescently labeled dextran showed that 10 and 70 kDa dextrans were able to readily diffuse into most beads. The 250 and 500 kDa dextrans were partially excluded from the beads, indicating that the matrix beads show differential permeability for lower and higher-MW species. As expected, citrate treated beads show higher permeability compared with untreated beads of analogous polymer loading percentages, attributed to the swelling of the polymer network. For all matrix bead compositions, 10 and 70 kDa dextran readily diffused into the beads. However, 250 and 500 kDa dextran could be partially excluded from the beads by increasing the polymer loading percentage to 1.0 or 1.5% w/v. Polymer loading percentage was found to have a greater effect on bead porosity than functionalization percentage. This fits with the swell ratio data that indicate that swelling is a function of loading percentage and not functionalization percentage which makes sense as porosity is a function of swelling. This trend is similar to previously reported results for core-crosslinked alginate beads where 10 and 70 kDa dextrans freely diffused into the beads, while 250 and 500 kDa dextrans were almost completely excluded.[22]

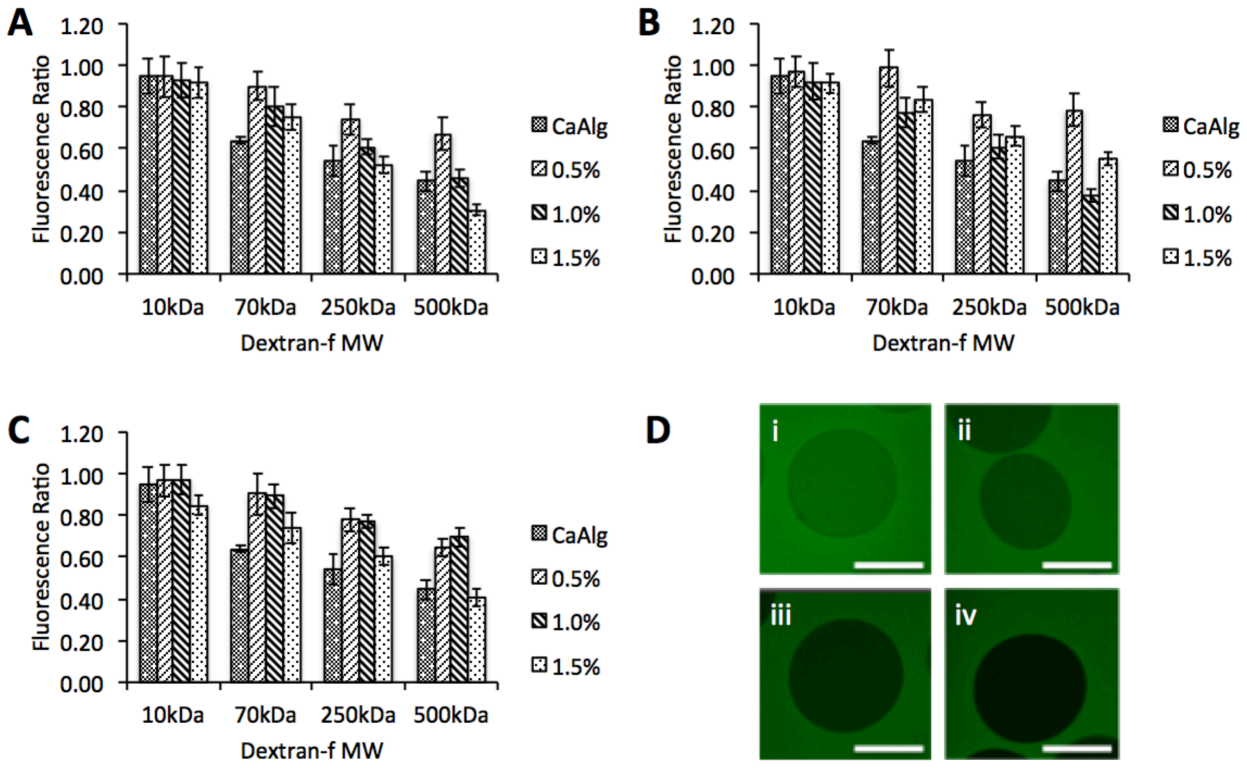

Figure 3.6. In-diffusion of dextran-*f* into citrate-treated matrix beads composed of A) PMM-FFA11*r*/MAL11, B) PMM-FFA18*r*/MAL15, C) PMM-FFA23*r*/MAL25. Image D shows the indiffusion of i) 10 kDa, ii) 70 kDa, iii) 250 kDa, and iv) 500 kDa dextran-*f* into citrate-treated matrix beads composed of 1.5% w/v each PMM-FFA11*r*/MAL11.

3.4.6. Cell Encapsulation and Cytotoxicity Study

The viability of encapsulated NIH 3T3 cells was assessed over a one-week period using calcein AM/ethydium homodimer live/dead assay to determine the percentage of live cells to dead cells in each bead. Initial (days 0 and 1) analysis showed that a similar percentage (~90%) of the cells were alive in both the alginate control and the PMM-FFA18/MAL14 matrix beads, indicating that the encapsulated cells were not negatively affected by the Diels-Alder crosslinking or the presence of PMM-FFA/MAL and readily survive the encapsulation process. Cell viability in both control and matrix beads decreased slightly to 76% and 67% respectively on day 3, likely due to the fact that NIH 3T3 cells are attachment dependant and no attachment sites were provided in either the alginate or matrix beads. Cell viability on day 7 was significantly lower for cells

encapsulated in the matrix beads (49% compared with 72%). This highlights the need to incorporate cell adhesion proteins such as RGD in the matrix beads to ensure long-term cell viability in attachment-dependent cells.

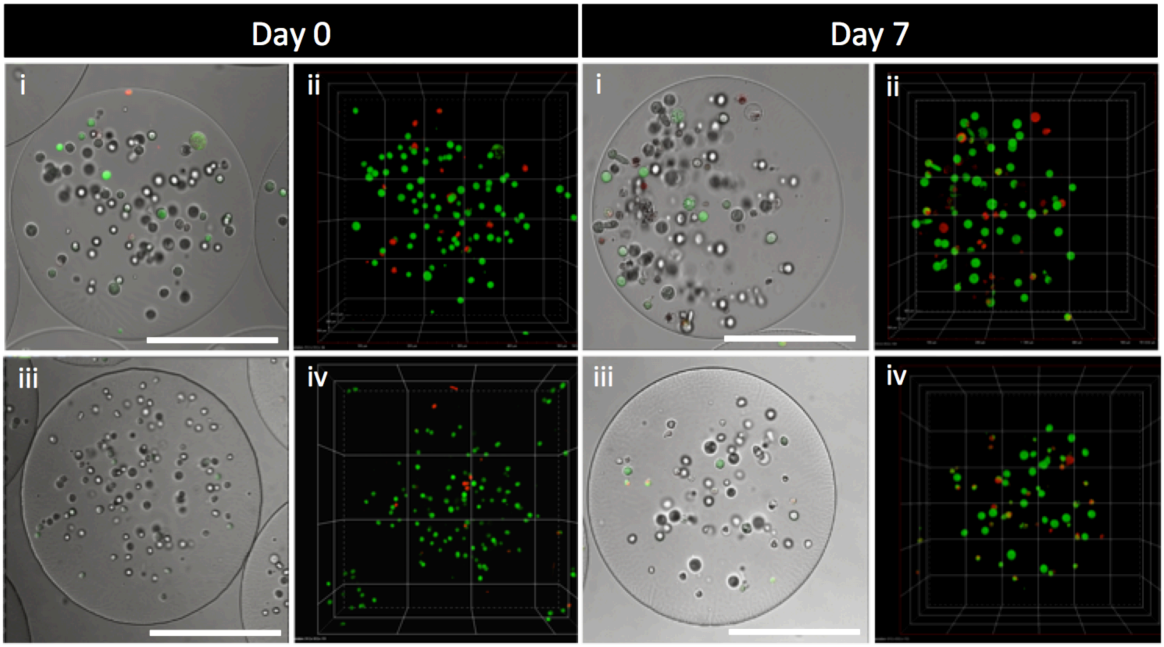

Figure 3.7. Calcein AM/Ethydium homodimer Live/Dead assay of encapsulated NIH 3T3 cells on days 0 and 7 for i) calcium alginate control (confocal slice, with brightfield), ii) calcium alginate control (3D confocal z-stack), iii) 1% w/v PMM-FFA16/MAL15 (confocal slice, with brightfield) and iv) 1% w/v PMM-FFA16/MAL15 (3D confocal z-stack). Scale bars are 250 μm.

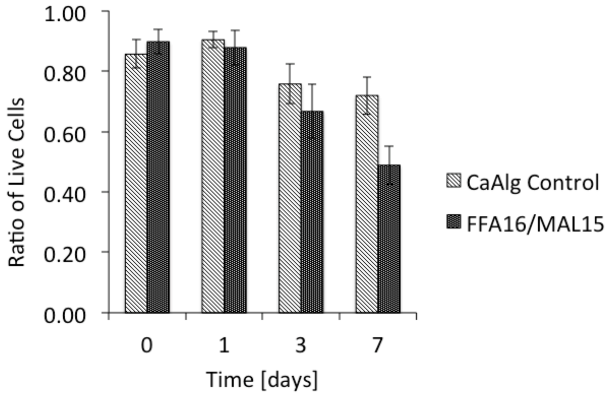

Figure 3.8. Ratio of live cells in both alginate control and 1% w/v each PMM-FFA16/MAL15 beads.

3.5. Conclusions

Calcium alginate beads were used to template the covalent Diels-Alder reaction between diene- and dienophile-modified PMM. The properties of the resulting crosslinked matrix beads may be tuned by varying the loading percentage, and to some extent the degree of functionalization, of these reactive gel forming polymers in the alginate beads. The Diels-Alder reaction between PMM-FFA/MAL is significantly accelerated within the calcium alginate matrix, allowing for rapid gelation at physiological pH. Encapsulated NIH 3T3 cells exhibited high viabilities after the encapsulation process and during Diels-Alder crosslinking, indicating that modified PMM-FFA/MAL matrix beads may be a promising approach for use in cell encapsulation applications.

3.6. Acknowledgements

We would like to thank the Natural Sciences and Engineering Research Council (NSERC) of Canada for supporting this work through Discovery and CREATE grants.

3.7. References

(1) Lim, F.; Sun, A.M. Microencapsulated islets as bioartificial endocrine pancreas. *Science* **1980**, *210*, 908-910.

(2) Shoichet, M.S.; Winn, S.R. Cell delivery to the central nervous system. *Adv Drug Deliv Rev* **2000**, *42*, 81.

(3) Hendy, A.; Hortelano, G.; Tannenbaum, G.; Chang, P. L. Correction of the growth defect in dwarf mice with nonautologous microencapsulated myoblasts – an alternate approach to somatic gene therapy. *Hum. Gene Ther*. **1995**, *6*, 165–175.

(4) Van Raamsdonk, J. M.; Ross, C.J.D.; Potter, M.A.; Kurachi, S.; Kurachi, K.; Stafford, D.W.; Chang, P. L. Treatment of Hemophilia B in mice with nonautologous somatic gene therapeutics. *J. Lab. Clin. Med.* **2000**, *139*, 35–42.

(5) Dixit, V.; Gitnick, G. Transplantation of microencapsulated hepatocytes for liver function replacement. *J. Biomater. Sci., Polym. Ed*. **1995**, *7*, 343–357.

(6) Prakash, S.; Chang, T. M. S. Microencapsulated genetically engineered live E. coli DH5 cells administered orally to maintain normal plasma urea level in uremic rats. *Nat. Med*. **1996***, 2*, 883–887.

(7) Desai, T.; Shea, L. D. Advances in islet encapsulation technologies. *Nat. Rev. Drug Discov.* **2017**, *16*, 338-350.

(8) Chhabra, P.; Brayman, K. L. Stem Cell Therapy to Cure Type 1 Diabetes: From Hype to Hope. *Stem Cells Transl. Med.* **2013**, *2*, 328-336.

(9) Erikson, A. G.; Laughlin, T. D.; Romereim, S. M.; Sargus-Patino, C. N.; Pannier, A. K.; Dudley, A. T. A Tunable, Three-Dimensional *In Vitro* Culture Model of Growth Plate Cartilage Using Alginate Hydrogel Scaffolds. *Tissue Eng. Part A*. **2018**, *24*, 94-105.

(10) Haug, A.; Larsen, B.; SmidsrØd, O. Uronic acid sequence in alginate from different sources. *Carbohydrate Res.* **1974**, *32*, 217-225.

(11) Orive, G.; Carcaboso, A. M.; Hernández, R. M.; Gascón, A. R.; Pedraz, J. L. Biocompatibility Evaluation of Different Alginates and Alginate-Based Microcapsules. *Biomacromolecules* **2005**, *6*, 927–931.

(12) Smidsrød, O.; Skjåk-Bræk, G. Alginate as immobilization matrix for cells. *Trends Biotechnol.* **1990**, *8*, 71–78.

(13) De Castro, M.; Orive, G.; Hernandez, R. M.; Gascon, A. R.; Pedraz, J. L. Comparative study of microcapsules elaborated with three polycations (PLL, PDL, PLO) for cell immobilization. *J. Microencapsul.*, **2005**, *22*, 303-315.

(14) Gravastrand, C.; Hamad, S.; Fure, H.; Steinkjer, B.; Ryan, L.; Oberholzer, J.; Lambris, J. D.; Lacík, I.; Mollnes, T. E.; Espevik, T.; Brekke, O.-L.; Rokstad, A. M. Alginate microbeads are coagulation compatible, while alginate microcapsules activate coagulation secondary to complement or directly through FXII. *Acta Biomater.* **2017**, *58*, 158-167.

(15) Thu, B.; Bruheim, P.; Espevik, T.; Smidsrød, O.; Soon-Shiong, P.; Skjåk-Bræk, G. Alginate polycation microcapsules. II. Some functional properties. *Biomaterials* **1996**, *17*, 1069–1079.

(16) Juste, S.; Lessard, M.; Henley, N.; Ménard, M.; Hallé, J. P. Effect of poly-L-lysine coating on macrophage activation by alginate-based microcapsules: Assessment using a new *in vitro* method. *J. Biomed. Mater. Res., Part A* **2005**, *72*, 389–398.

(17) Breguet, V.; Gugerli, R.; Pernetti, M.; von Stockar, U.; Marison, I.W. Formation of microcapsules from polyelectrolyte and covalent interactions. *Langmuir*, **2005**, *21*, 9764-9772.

(18) Ros, S.; Burke, N. A. D.; Stöver, H. D. H. Synthesis and Properties of Charge-Shifting Polycations: Poly[3-aminopropylmethacrylamide-*co*-2-(dimethylamino-ethyl acrylate]. *Macromolecules*, **2015**, *48*, 8958-8970.

(19) Rokstad, A. M.; Donati, I.; Borgogna, M.; Oberholzer, J.; Strand, B. L.; Espevik, T.; Skjak-Bræk, G. Cell-compatible covalently reinforced beads obtained from a chemoenzymatically engineered alginate. *Biomaterials*, **2006**, *27*, 4726–4737.

(20) Gardner, C.M.; Stöver, H.D.H. Reactive Polyanions Based on Poly(4,4-dimethyl-2-vinyl-2-oxazoline-5-one-*co*-methacrylic acid). *Macromolecules*, **2011**, *44*, 7115-7123.

(21) Gardner, C.M.; Potter, M.A.; Stöver, H.D.H. Improving covalent cell encapsulation with temporarily reactive polyelectrolytes. *J. Mater Sci: Mater Med* **2012**, *23*, 181-193.

(22) Mazumder, M.A.J.; Burke, N.A.D.; Shen, F.; Potter, M.A.; Stöver, H.D.H. Core-cross-linked alginate microcapsules for cell encapsulation. *Biomacromolecules*, **2009**, *10*, 1365-1373.

(23) Mahou, R.; Wandrey, C. Alginate- poly (ethylene glycol) hybrid microspheres with adjustable physical properties. *Macromolecules*, **2010**, *43*, 1371-1378.

(24) Gattás-Asfura, K.M.; Stabler, C.L. Chemoselective cross-linking and functionalization of alginate via Staudinger ligation. *Biomacromolecules*, **2009**, *10*, 3122-3129.

(25) Vandamme, K.; Melkebeek, V.; Cox, E.; Deforce, D.; Lenoir, J.; Adriaens, E.; Vervaet, C.; Remon, J.P. Influence of reaction medium during synthesis of Gantrez® AN 119 nanoparticles for oral vaccination. *Eur. J. Pharm. Biopharm*. **2010**, *74*, 202-208.

(26) Wong, T.W.; Wahab, S.; Anthony, Y. Effects of microwave on drug release property of poly (methyl vinyl ether-co-maleic acid) matrix. *Drug Dev. Ind. Pharm.* **2007**, *33*, 737-746.

(27) Arbós, P.; Wirth, M.; Arangoa, M.; Gabor, F.; Irache, J.M. Gantrez® AN as a new polymer for the preparation of ligand-nanoparticle conjugates. *J. Control. Rel.* **2002**, *83*, 321-330.

(28) Li, Y.; Lee, P.I. A new bioerodible system for sustained local drug delivery based on hydrolytically activated in situ macromolecular association. *Int. J. Pharm.* **2010**, *383*, 45-52.

(29) Shimizu, T.; Minakata, A. Effect of divalent cations on the volume of a maleic acid copolymer gel examined by incorporating lysozyme. *Eur. Polym. J.* **2002**, *38*, 1113-1120.

(30) Gardner, C.M.; Burke, N.A.D.; Stöver, H.D.H. Cross-linked microcapsules formed from self-deactivating reactive polyelectrolytes. *Langmuir*, **2010**, *26*, 4916-4924.

(31) Gardner, C.M; Burke, N.A.D.; Chu, T.; Shen, F.; Potter, M.A.; Stöver, H.D.H. Cross-Linked Microcapsules Formed From Self-Deactivating Reactive Polyelectrolytes. *J. Biomater. Sci., Polym. Ed.* **2011**, *22*, 2127-2145.

(32) Stewart, S. A.; Backholm, M.; Burke, N. A. D.; Stöver, H. D. H. Cross-Linked Hydrogels Formed through Diels-Alder Coupling of Furan- and Maleimide-Modified Poly(methyl vinyl ether-*alt*-maleic acid). *Langmuir*, **2016**, *32*, 1863-1870.

(33) Otto, S.; Engberts, J. B. Hydrophobic interaction and chemical reactivity. *Org. Biomol. Chem.* **2003**, *1*, 2809-2820.

(34) Li, S.; Xia, Y.; Qiu, Y.; Chen, X.; Shi, S. Preparation and property of starch nanoparticles reinforced aldehyde-hydrazide covalently crosslinked PNIPAM hydrogels. *J. Appl. Polym. Sci.*, **2018**, *135*, 45761.

(35) Kleinberger, R.M.; Burke, N.A.D.; Zhou, C.; Stöver, H.D.H. Synthetic polycations with controlled charge density and molecular weight as building blocks for biomaterials. *J. Biomater. Sci. Polym. Ed.*, **2016**, *27*, 351-369.

(36) Donati, I.; Borgogna, M.; Turello, E.; Cesàro, A.; Paoletti, S. Tuning Supramolecular Structuring at the Nanoscale Level: Nonstoichiometric Soluble Complexes in Diluted Mixed Solutions of Alginate and Lactose-Modified Chitosan (Chitlac). *Biomacromolecules*, **2007**, *8*, 1471-1479.

(37) Thu, B.; Gåserød, O.; Paus, D.; Mikkelson, A.; Skjåk-Bræk, G.; Toffanin, R.; Vittur, F.; Rizzo, R. Inhomogeneous alginate gel spheres: An assessment of the polymer gradients by synchrotron radiation-induced x-ray emission, magnetic resonance microimaging, and mathematical modeling. *Biopolymers* **2000**, *53*, 60–71.

(38) Velings, N. M.; Mestdagh, M. M. Physico-chemical properties of alginate beads. *Polym. Gels Networks* **1995**, *3*, 311–330.

3.8. Appendix

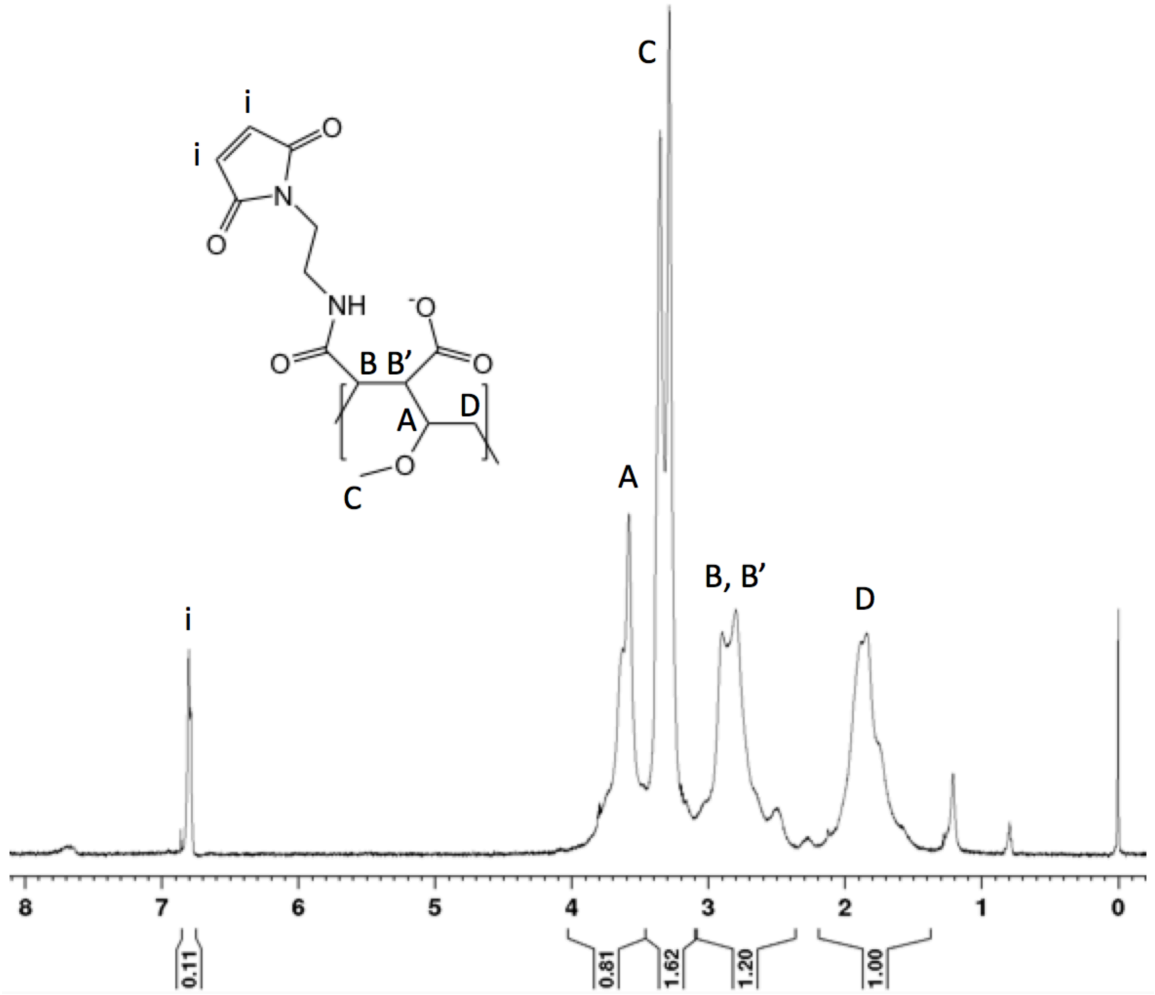

Figure A3.1. ^{1}H-NMR of PMM-MAL11 in D_2O using water suppression. The ratio of the maleimide vinyl signal at 6.81ppm (i) to the backbone methylene signal (D) was used to determine the percent functionalization with MAL.

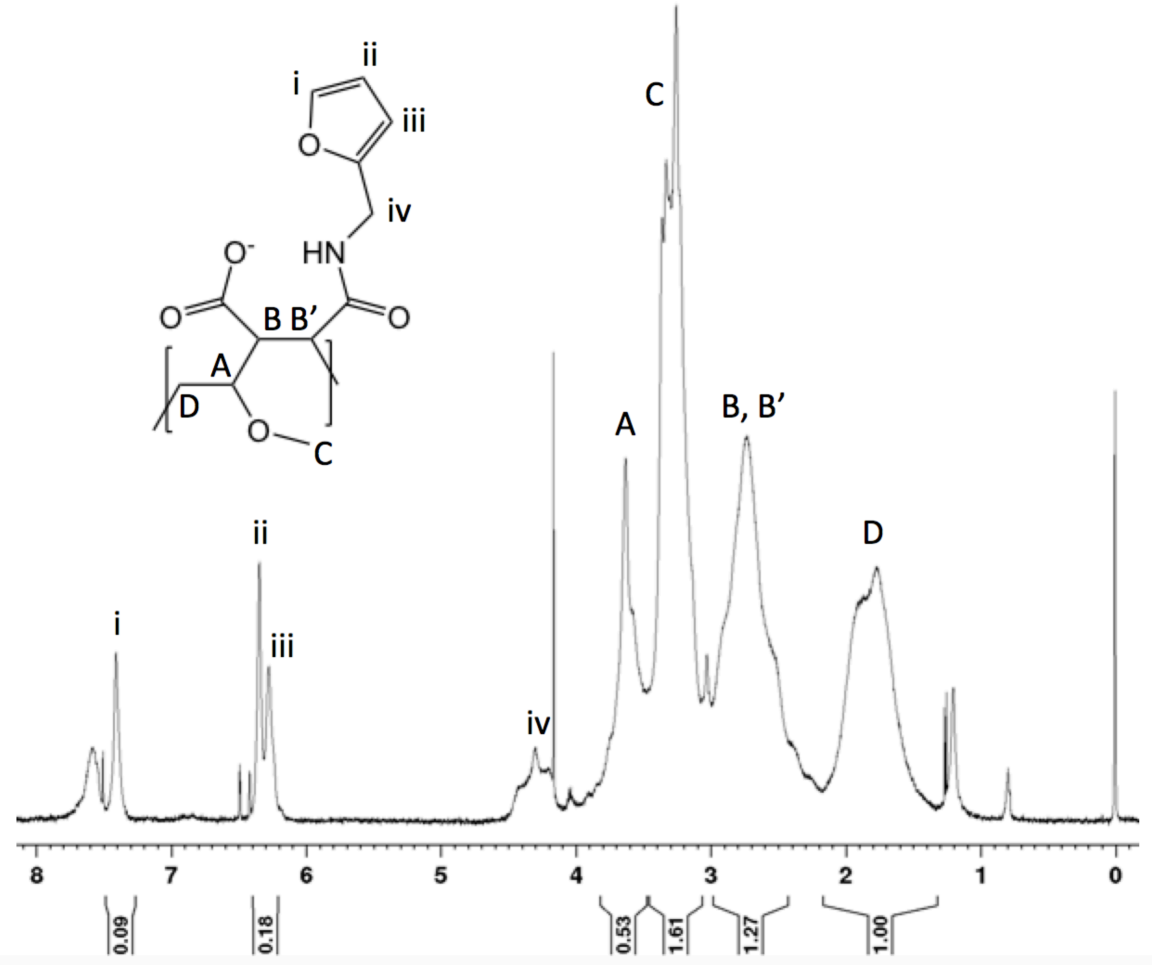

Figure A3.2. ^{1}H-NMR of PMM-FFA18*r* in D_2O. The ratio of the furan vinyl signals (at 6.25 (iii), 6.35 (ii), and 7.40 (i) ppm) to the backbone methylene signal (D), was used to determine the percent functionalization with FFA.

Table A3.1. Swell ratio of beads, measured before and after citrate treatment using Nikon microscope set to transmitted light mode. All bead diameters are listed in μm.

Polymer	Loading %	Post Citrate	Stdev	Pre Citrate	Stdev	Swell Ratio	Stdev
F11r-M11	0.5%	981.24	104.95	511.21	35.56	1.92	0.24
F11r-M11	1.0%	763.12	22.86	471.09	13.22	1.62	0.07
F11r-M11	1.5%	727.36	58.9	478.16	21.08	1.52	0.14
F18r-M15	0.5%	866.28	72.23	480.76	28.27	1.80	0.18
F18r-M15	1.0%	793.66	59.66	528.63	32.91	1.50	0.15
F18r-M15	1.5%	759.84	51.47	528.67	19.42	1.44	0.11
F23r-M25	0.5%	875.65	50.5	499.95	16.25	1.75	0.12
F23r-M25	1.0%	802.77	59.78	511.97	26.33	1.57	0.14
F23r-M25	1.5%	706.94	30.89	525.31	20.65	1.35	0.08

Bead swell ratio was seen to decrease, both as loading percentage of PMM-FFA/MAL was increased from 0.5% to 1.5% w/v each, and as the functionalization percentages of PMM-FFA and PMM-MAL increased from 11% to 23 and 25% respectively.

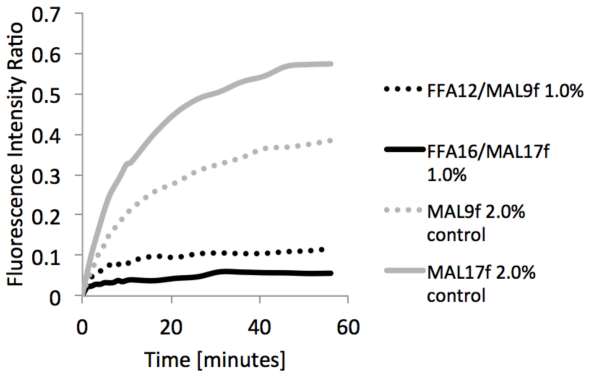

Figure A3.3. Fluorescence recovery after photobleaching for alginate-templated 1.0% w/v PMM-FFA12/MAL9*f* and PMM-FFA16/MAL17*f* beads as well as alginate-templated 2.0% w/v PMM-MAL9*f* and PMM-MAL17*f* control beads that have no covalent crosslinks.

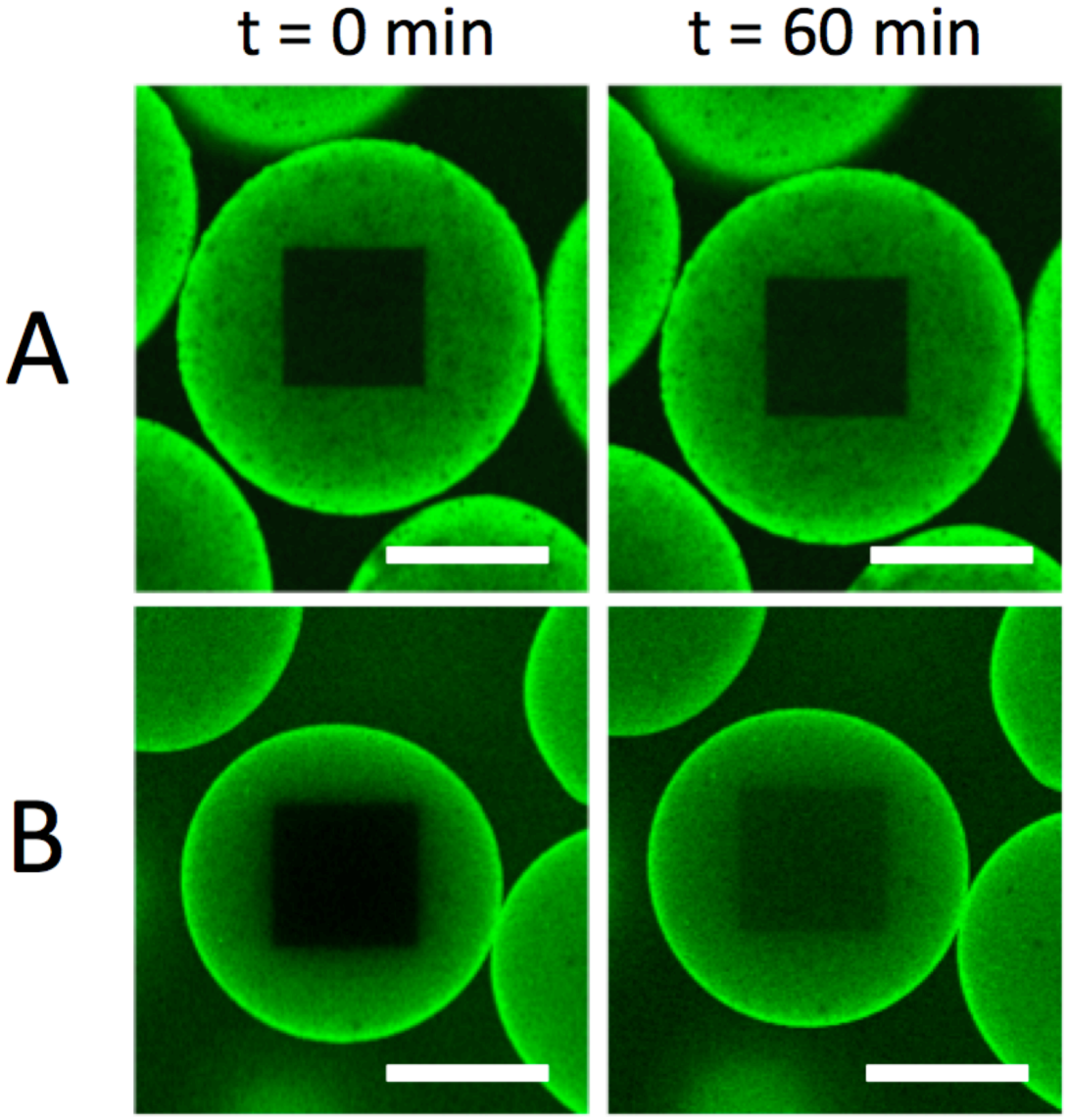

Figure A3.4. Confocal microscope images showing fluorescence recovery after photobleaching for A) alginate-templated 1.0% w/v PMM-FFA12/MAL9*f* beads and B) 2.0% w/v PMM-MAL17*f* control beads that have no covalent crosslinks at at t = 0 min and t = 60 mins post-photobleaching. Scale bars are 250 μm.

Minimal amounts of fluorescence recovery were observed for covalently crosslinked beads, while control beads of homopolymer exhibited a much higher degree of recovery after photobleaching, as expected due to the lack of covalent crosslinking.

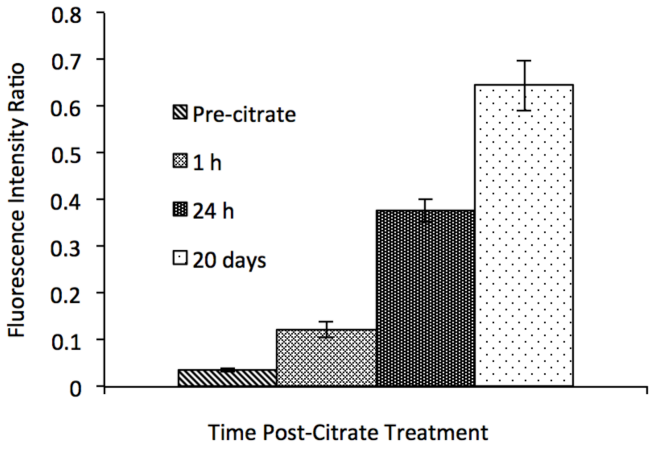

Figure A3.5. Graph showing the ratio of fluorescent intensity inside and outside alginate-*f* templated beads at set timepoints before and after citrate treatment.

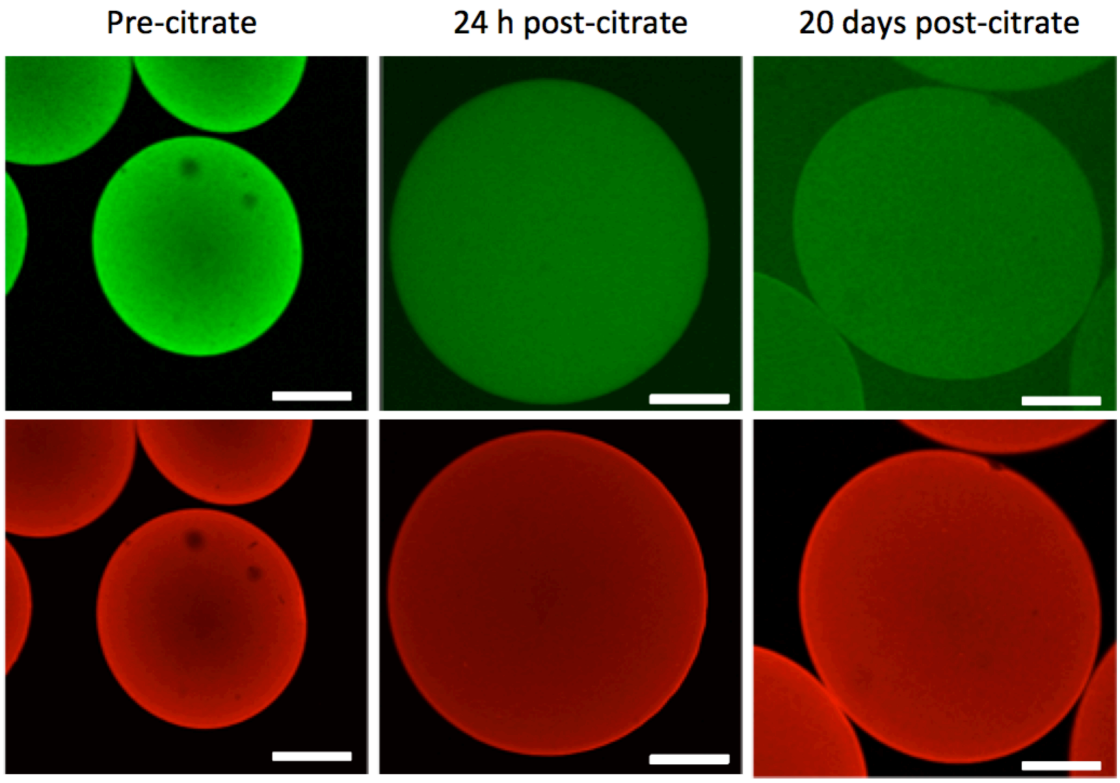

Figure A3.6. Confocal fluorescence images showing PMM-FFA11*r*/MAL11 alginate-*f* template beads prior to citrate treatment, and 24 h and 20 days post-citrate treatment. Scale bars are 250 μm.

After citrate treatment and subsequent liquefaction of the alginate-*f* template, beads swelled and alginate-*f* was observed in the supernatant. The ratio of fluorescence intensity inside the beads and in the supernatant was measured over time and was found to increase as more alginate escaped the beads, leading to increased fluorescence in the supernatant and decreased fluorescence within the beads themselves.

Chapter 4

Synthetic Hydrogels formed by Thiol-Ene Crosslinking of Vinyl Sulfone-functional Poly(Methyl Vinyl Ether-*alt*-Maleic Acid) with α,ω-Dithio-Polyethyleneglycol

S. Alison Stewart, Michael B. Coulson, Christal Zhou, Nicholas A. D. Burke and Harald D. H. Stöver. Accepted by Soft Matter on 31 August 2018, ID: SM-ART-05-2018-001066.R1.

Alison Stewart primarily developed and supervised the project and experimental methods and contributed to writing the manuscript. Michael Coulson synthesized all polymers and hydrogels and carried out physical characterization tests and contributed to writing the manuscript. Christal Zhou assisted with cell viability studies and contributed to writing the cell viability section. Nicholas Burke and Harald Stöver provided experimental guidance and editing feedback of the manuscript.

4.1. Abstract

Polymer hydrogels formed by rapid thiol-ene coupling of macromolecular gel formers can offer access to versatile new matrices. This paper describes the efficient synthesis of cysteamine vinyl sulfone (CVS) trifluoroacetate, and its incorporation into poly(methyl vinyl ether-*alt*-maleic anhydride) (PMM) to form a series of CVS-functionalized poly(methyl vinyl ether-*alt*-maleic acid) polymers (PMM-CVS_x) containing 10 to 30 mol% pendant vinyl sulfone groups. Aqueous mixtures of these PMM-CVS and a dithiol crosslinker, α,ω-dithio-polyethyleneglycol (HS-PEG-SH, M_n = 1 kDa), gelled through crosslinking by Michael addition within seconds to minutes, depending on pH, degree of functionalization, and polymer loading. Gelation efficiency, Young's modulus, equilibrium swelling and hydrolytic stability are described, and step-wise hydrogel post-functionalization with a small molecule thiol, cysteamine, was demonstrated. Cytocompatibility of these crosslinked hydrogels towards entrapped 3T3 fibroblast was confirmed using a Live/Dead fluorescence assay.

4.2. Introduction

The extracellular matrix (ECM), composed of proteins and polysaccharides, is a critical component of all biological tissues, and key to cellular health. Macromolecular hydrogels show many features reminiscent of natural ECMs and are hence being explored for use as ECM mimics in regenerative medicine.[1,2,3,4] They can provide structural integrity to tissue constructs,[5,6] control drug delivery,[7,8] and serve as immuno-isolation barriers for transplantation of therapeutic cells.[9,10,11]

Both biological and synthetic macromolecules are being explored for hydrogel formation.[12, 13] While biologically derived materials tend to face fewer regulatory hurdles then their synthetic counterparts, issues such as batch-to-batch variation,[5] biological impurities,[14] and poor control over mechanical properties[15] have spurred a desire for fully synthetic hydrogels.[13]

Synthetic, covalently crosslinked gels offer long-term mechanical stability, and the ability to tune physical properties through, e.g., composition, crosslink density[10, 16], and polymer loading. They are chemically defined, scalable, and increasingly employ rapid click crosslinking chemistry,[17, 18, 19] including the thiol-ene Michael addition, a conjugate thiolate addition to electron poor olefins.[20] Thiol-ene pairs reported include thiol-maleimide,[21,22] thiol-(meth)acrylate,[23,24] thiol-norbornene,[25, 26] thiol-allylether,[27] and thiol-vinylsulfone.[28]

This work describes hydrogels formed by rapid[29] and irreversible[26, 30] dithiol-crosslinking of vinylsulfone-functional water-soluble polyanions. While poly(ethylene glycol) (PEG) has been widely used to prepare crosslinked hydrogels,[31, 32, 33] its functionalization is restricted to the chain ends. To increase versatility,[34, 35, 36] we focussed on poly(methyl vinyl ether–*alt*–maleic anhydride) (PMMAn), a commercially available polymer already used for biomedical applications.[37, 38] The anhydride groups enable functionalization,[39, 40] while its hydrolyzed form, poly(methyl vinyl ether-*alt*-maleic acid) (PMM), can electrostatically complex with polycations and multi-valent metal cations. Both PMMAn and PMM have been used to coat cell-containing capsules.[41,42,43] Mixtures of PMM functionalized with furan and maleimide, respectively, were found to gel within hours to form bulk Diels-Alder crosslinked hydrogels.[44]

Here, PMMAn functionalized with vinyl sulfone groups is shown to rapidly crosslink with PEG-dithiols to form new, hydrolytically stable hydrogels. Key aspects of this work are the efficient synthesis of cysteamine vinyl sulfone (CVS) as the trifluoroacetate salt, and its introduction into PMMAn. Gelation rate with PEG-dithiol, gel swellability, crosslinking efficiency and Young's modulus, as well as hydrolytic stability and post-functionalization of the crosslinked gels, are described as function of polymer composition, concentration, and pH. Preliminary cell viability studies showed excellent cytocompatibility of the hydrogel with entrapped 3T3 cells.

4.3. Experimental Section

4.3.1. Materials

Cysteamine hydrochloride, divinyl sulfone (DVS), poly(methyl vinyl ether-*alt*-maleic anhydride) (M_n = 80 kDa), 4-(2-hydroxyethyl)-1-piperazineethanesulfonic acid (HEPES) sodium salt, fluoresceinamine, DMSO-d_6, potassium hydrogen phthalate (PHT) and 2-(N-morpholino)ethanesulfonic acid (MES hemisodium salt) were purchased from Sigma-Aldrich and used as received. Poly(ethylene glycol)-dithiol (M_n = 1 kDa) (HS-PEG-SH) was purchased from Creative PEGWorks. Di-*tert*-butyl dicarbonate was purchased from Fluka Analytical. Triethylamine (TEA) was purchased from EMD Performance Chemicals. Arg-Gly-Asp-Cys was purchased from GenScript. Formic acid (≥98%) was purchased from EM Science. Anhydrous sodium sulfate, sodium chloride, calcium chloride dihydrate, acetonitrile, dichloromethane (DCM), Ethyl acetate, hexane, dimethyl sulfoxide (DMSO), and trifluoroacetic acid (TFA) were purchased from Caledon Laboratory Chemicals and used as received. Deuterium oxide (99.99 atom% D) was purchased from Cambridge Isotope Laboratories. Sodium hydroxide (1.0 N) was purchased from LabChem Inc. Dulbecco's modified Eagle's medium (DMEM, high glucose, pyruvate), fetal bovine serum (qualified, Canada origin), and 0.25% Trypsin-EDTA (1X) phenol red were obtained from Invitrogen (Burlington, ON). Calcein-AM/ethidium homodimer-1 (LIVE/DEAD Viability/Cytotoxicity Kit, for mammalian cells) was purchased from ThermoFisher Scientific. NIH/3T3 *Mus musculus* fibroblasts (CRL-1658) were obtained from ATCC.

4.3.2. Synthesis of N-BOC Protected Cysteamine Vinyl Sulfone (1)

Cysteamine hydrochloride (1.102 g, 9.6 mmol) in DMSO (50 mL) was added dropwise to a stirred solution of DVS (5.73 g, 48.5 mmol, 5.0 eq relative to cysteamine hydrochloride) in DMSO (10 mL) under stirring at room temperature. After vigorous stirring for 4 h, a solution of di-*tert*-butyl dicarbonate (3.175 g, 14.6 mmol) in DMSO (10 mL) and triethylamine (2.03 mL, 14.6 mmol, 1.5 eq relative to cysteamine hydrochloride) in DMSO (2 mL) was added dropwise at room temperature. After 24 h of stirring, distilled water (300 mL) was added to the flask, and the aqueous phase extracted in a separatory funnel with 4 x 150 mL DCM. The organic phases were combined, dried over anhydrous sodium sulphate, gravity filtered through filter paper, and concentrated by rotary evaporation. The resulting oil was loaded on a neutral silica gel column and eluted with 2 x 400 mL 1:3 ethyl acetate/hexanes, 2 x 300 mL 1:2 ethyl acetate/hexanes, followed by 1 x 400 mL ethyl acetate (scheme 4.1), monitored by silica TLC. *N*-BOC cysteamine vinyl sulfone (1) (2.47 g, 8.4 mmol) was obtained as a clear, colorless oil in 87.5% yield. ^{1}H NMR (600 MHz, DMSO-d_6): 6.99 (dd, J = 9.6 Hz, 16.8 Hz, CH_2=C*H*SO_2, 1H), 6.92 (bt, BOC-N*H*C), 6.29 (m, CH_2=C, 2H), 3.40 (m, NHC$H_2$$CH_2$, 2H), 3.09 (m, CH_2C$H_2$$SO_2$, 2H), 2.75 (m, NHC$H_2CH_2$S, 2H), 2.60 (m, SC$H_2$$CH_2$$SO_2$, 2H), 1.39 (s, (C$H_3$)$_3$C, 9H).

4.3.3. Synthesis of Cysteamine Vinyl Sulfone Trifluoroacetate (2)

N-BOC cysteamine vinyl sulfone (1) (1.01 g, 3.42 mmol) was dissolved in DCM (50 mL), and an excess of TFA (2 mL, 26 mmol) was added dropwise to the vigorously stirred solution (Scheme 4.1). The reaction mixture was stirred for 4 h, and then concentrated under a stream of nitrogen while the solution was warmed in a 40 °C water bath. Cysteamine vinyl sulfone trifluoroacetate (2) (0.83 g, 2.66 mmol) was obtained as a viscous yellow oil in 78% yield. ^{1}H NMR (600 MHz, DMSO-d_6): 7.91 (bs, $^{+}$N$H_3$$CH_2$), 7.01 (dd, CH_2=C*H*SO_2,1H), 6.30 (q, CH_2=CH, 2H), 3.45 (m, NH_3C$H_2$$CH_2$, 2H), 3.00 (m, CH_2C$H_2$$SO_2$, 2H), 2.80 (m, CH_2CH_2SC$H_2$$CH_2$, 4H).

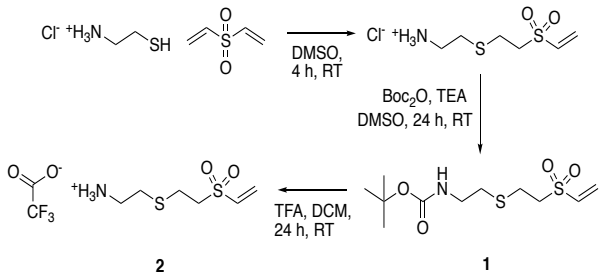

Scheme 4.1. A three-step synthesis for the formation of CVS TFA (2) through intermediate product *N*-BOC CVS

4.3.4. Synthesis of PMM-CVS*f* containing 10, 20, and 30 mol% CVS

PMMAn (0.250 g, 1.6 mmol anhydride) was dissolved in 10 mL acetonitrile. Fluoresceinamine (5 mg, 0.014 mmol, 0.9 mol%) was dissolved in 1 mL 1:1 DMF:acetonitrile and added dropwise to the vigorously stirring PMMAn solution. To this solution, triethylamine (TEA) (150 μL, 0.1088 g 1.1 mmol) was added and allowed to react overnight at room temperature. Cysteamine vinyl sulfone trifluoroacetate (2) (175.1 mg, 0.577 mmol, 35 mol% relative to anhydride groups in PMMAn) was dissolved in 5 mL 1:1 DMSO:acetonitrile and was added dropwise over a few minutes to the stirring solution. After 24 h at room temperature, the resulting solution was dialyzed (Spectrapor, MWCO = 3500 Da) against 4 L of 0.05 M NaCl for 1 day and then against 4 L distilled water for 3 days, changed daily. The dialyzed solution was then lyophilized, leading to the isolation of PMM-CVS_{30} as a yellow powder. Other PMM-CVS_x derivatives ranging from 10-30% functional loading were prepared, along with unlabelled analogs. ^{1}H NMR was used to determine the degree of functionalization, using the CVS vinyl signals (δ6.25-7.0 3H), referenced to the polymer backbone CH_2 signal (δ1.75 2H).

4.3.5. Preparation of PMM-CVS_x / HS-PEG-SH gels for Physical Characterization

Hydrogels were prepared by combining PMM-CVSx and HS-PEG-SH with a 1:1 CVS:thiol molar ratio in varying polymer concentrations and degrees of CVS functionalization. The following example describes the preparation of a gel with 2.5% w/v PMM-CVS_{10}. PMM-CVS_{10}, (10 mg; 5.3 μmol CVS) was dissolved in 300 μL HEPES buffer (50 mM) and the pH adjusted to 7.4 ± 0.2 using 5 M NaOH. HS-PEG-SH

(2.7 mg; 5.4 μmol thiol) was placed in a separate vial and dissolved in 100 μL of distilled water. The two solutions were mixed and pipetted into 4 silicone rubber mould wells, on a glass slide (diameter = 7 mm, depth = 5 mm, volume = 100 μL, n = 4). The moulds were then sealed using a sheet of silicone rubber, wrapped in a damp paper towel to avoid water evaporation and allowed to gel for 24 h at 37 ^{o}C. Gels were prepared in a similar fashion from PMM-CVS with 10, 20 and 30% degrees of functionalization and PMM-CVS loadings of 2.5, 5 and 7.5% w/v.

4.3.6. Gelation Profiling and Efficiency

Gelation of a PMM-CVS HS-PEG-SH hydrogel was monitored over a 24 h period by ^{1}H NMR, using a 600 MHz Bruker spectrometer (ns = 64, d1 = 1 sec). 30 mg PMM-CVS_{30} (42.8 μmol CVS) was dissolved in 500 μL D_2O HEPES buffer (25 mM) with an external PHT standard (0.5 mg, 2.45 μmol), fixed to pD 7.5 using 5 M D_2O/NaOH, loaded into an NMR sample tube, and a preliminary spectrum was obtained. 21.4 mg HS-PEG-SH (42.8 μmol thiol) was dissolved in 100 μL D_2O, and mixed thoroughly with the vinyl sulfone-containing solution. ^{1}H spectra were obtained at set time points throughout the 24 h period.

4.3.7. Mechanical Properties of Gels

Gel disks prepared in silicone moulds as described above, were uncovered, coated with one drop (~0.05 mL) of silicone oil to reduce water evaporation, and placed on a microscope stage. A glass melting point tube (VWR, diameter = 0.85 mm) was attached to a force transducer (Transducer Techniques GSO, 10 g full scale) and positioned with the closed rounded end just above a gel disk. The indenter was programmed to move downward at a constant speed of 0.2 mm/s for as-formed gels, and 0.4 mm/s for swollen gels, while measuring the force relative to time and vertical position. Each gel was measured at three points on its surface.

4.3.8. Swelling Studies

Gel disks prepared in silicone moulds as described above were weighed, placed in 24-well plates, covered with 3 mL PBS buffer (10 mM phosphate, 154 mM NaCl, pH 7.4), and incubated at 37 ^{o}C for 7 days. Wells not containing gels were filled with

distilled water and the lidded plates wrapped in a damp paper towel in order to limit water loss. Buffer was replaced five times during this time. After one week, gels were removed from their wells, wiped gently with a Kimwipe to remove excess water, and weighed. Swelling ratios were calculated as the ratio of final to initial mass.

4.3.9. Hydrolytic Stability of PMM-CVS

10 mg of PMM-CVS_{30} was dissolved in 1 mL HEPES buffer (50 mM) with an internal formic acid standard (50 mM), prepared in D_2O, fixed to either pD 7.7. or 8.7 with 5M NaOH/D_2O. The samples were maintained at 37 ^oC and the disappearance of CVS vinyl signals (δ6.25 to δ7.0) were monitored by ^1H NMR for three weeks.

4.3.10. Post Modification of Residual Vinyl Sulfone Units

50 mg of PMM-CVS_{30} (71.2 μmol CVS) was dissolved in 0.8 mL HEPES buffer (25 mM, pH 7.8) with an external PHT standard (2.7 mg, 13.1 μmol), prepared in D_2O, fixed to pD 7.4 with 5M NaOH/D_2O. 18 mg HS-PEG-SH (36 μmol thiol, 0.5:1 Thiol:CVS) was dissolved in 200 μL D_2O. The two solutions were mixed briefly and pipetted into 6 silicone rubber mould wells, on a glass slide (diameter = 7 mm, depth = 5 mm, volume = 150 μL, n = 6). The moulds were then sealed using a sheet of silicone rubber, wrapped in a damp paper towel to avoid water evaporation and allowed to gel for 24 h at 37 ^oC. The resulting gels were removed from moulds, ground to particles 50-150 nm in size using a mortar and pestle, suspended in 4 mL D_2O and fixed to pD 7.4. The resulting suspension was collected and centrifuged (3500 RPM, 5 min), and the supernatant removed. Two NMR samples were prepared containing 1.1 mL of dense gel packing. Sample 1 was used as a control, and nothing further was added. To sample 2 (0.733 mg, 3.6 μmol PHT, 4.71 μmol CVS), 3 stepwise additions of cysteamine HCl were added. Cysteamine HCl was dissolved in 1 mL D_2O and 100 μL of this solution was added into Sample 2 (A: 0.175 mg, 1.5 μmol B: 0.35 mg, 3.1 μmol C: 0.175 mg, 3.1 μmol) and mixed thoroughly. ^1H spectra were acquired using a 600 MHz NMR spectrometer (ns = 64, d1 = 1 second).

4.3.11. pH Dependent Gel Time Investigation

The gelation times of 5% w/v PMM-CVS solutions of different functional percentages (10, 20, 30%), crosslinked with HS-PEG-SH, were measured in triplicate at four different pH values (6.5, 7, 7.5, and 8.5) using a horizontal tilt test. 40 mg PMM-CVS_x was dissolved in HEPES buffer (300 μL, 100 mM) and the pH adjusted to the target value using sodium hydroxide (5 M) or hydrochloric acid (1 M). Deionized water was added to bring the solution to 400 μL in volume, resulting in HEPES buffered (75 mM) solution of 10% w/v PMM-CVS_x. An analogous stock solution of equimolar HS-PEG-SH was prepared in 1 mL deionized water, and 100 μL aliquots of each PMM-CVS_x stock solution was mixed with 100 μL of HS-PEG-SH stock solution.

The mixtures were maintained at 37 ^oC, tested every ~30 sec for the first 5 min, every ~60 s until 20 min, and every ~5 min until 45 min. If the mixture did not flow when the vial was tilted 90°, the sample was considered to have gelled. Hydrogels that did not gel during this time were maintained at 37 ^oC and tested at 24 and 48 h time points. These tests were carried out in triplicate.

4.3.12. In Vitro Cytotoxicity

The cytotoxicity of the PMM-CVS hydrogels, and PMM-CVS hydrogels modified with Arg-Gly-Asp-Cys, to NIH 3T3 *Mus musculus* fibroblasts was explored using a live/dead calcein AM/ethidium homodimer-1 (EthD-1) assay. The fibroblasts were cultured in tissue culture flasks in Dulbecco's Modified Eagle Medium (DMEM) supplemented with 10% v/v Bovine Calf Serum (BCS) in a 5% CO_2 environment at 37 ^oC with 100% humidity in a water-jacketed incubator. When 75-80% confluency was reached, cells were washed with PBS (pH 7.4, Invitrogen) and detached using 0.25% Trypsin-EDTA (1X) phenol red before subculturing into renewed DMEM. Solutions of PMM-CVS_{20}, PMM-CVS_{20} functionalized with Arg-Gly-Asp-Cys (1.0 mg, 2.2 μmol, 0.5 mol %) and HS-PEG-SH were syringe filtered prior to the cytotoxicity assays and measurements were taken in quadruplicate for the PMM-CVS_{20} gels, and triplicate for the control. NIH 3T3 fibroblasts were suspended in DMEM media supplemented with 10% FBS, and containing 5% w/v PMM-CVS_{20} or PMM-CVS_{20} and Arg-Gly-Asp-Cys, plus an equimolar amount of HS-PEG-SH. The fibroblast/polymer solutions (1.0×10^6

cells/mL) were mixed by pipette aspiration for several minutes until solution viscosity began to increase, to ensure homogeneous cell distribution throughout the gels, and then transferred into the wells of a glass-bottom 96-well plate, and incubated for 24 h. After incubation, a fluorescence live/dead assay was used to determine cell viability and examine the cytotoxicity of the resulting hydrogels on the encapsulated cells. Calcein AM/EthD-1 solution (100 μL of 10 μM calcein AM and 4 μM EthD-1 in sterile PBS) was added to each well and incubated at room temperature for 20 minutes. Fluorescence images were obtained using a Nikon Eclipse Ti confocal microscope. Cell viability was calculated by counting the number of live and dead cells (Equation 4.1).

Equation 4.1:

$$\% \text{ cell viability} = \frac{(\#\text{ live cells})}{(\#\text{ live cells}) + (\#\text{ dead cells})} \times 100\%$$

4.4. Results and Discussion

4.4.1. Synthesis of Cysteamine Vinyl Sulfone Trifluoroacetate

Vinyl sulfone-functional polymers are typically prepared by reaction of excess DVS with hydroxy-containing polymers such as PEG, polyvinyl alcohol or polysaccharides (e.g., alginate, dextran).[45] Kong et al. described the functionalization of hyaluronic acid with the non-purified hydrochloride salt of cysteamine vinyl sulfone (CVS), by amidation.[46] In the current work, CVS was isolated and purified as the TFA salt (scheme 4.1): cysteamine HCl was reacted with an excess of DVS (figure A4.1) and the resulting CVS was converted to N-BOC CVS, purified by column chromatography (figures A4.2 and A4.3), deprotected and isolated in pure form in 68% yield (figure A4.4).

4.4.2. PMM-CVS by Polymer Modification

PMMAn was readily modified using CVS TFA in presence of TEA in acetonitrile (scheme 4.2). An excess of TEA was used to ensure deprotonation of CVS and of the maleamic acid formed by ring opening of the anhydride. A series of PMM-CVS with 10,

20 and 30 mol% CVS was studied. PMM-CVS with >30% CVS was formed but showed limited water solubility, while PMM-CVS with <10% CVS did not gel efficiently. Aliquots of each PMM-CVS_x were further functionalized with aminofluorescein to allow characterization of the gels by fluorescence microscopy.

The CVS-modified PMMAn in acetonitrile were then dialyzed against 1% w/v NaCl (aq.), followed by deionized water, in order to hydrolyze residual anhydrides, remove small molecule reactants, and exchange triethylammonium cations for sodium cations. The degree of functionalization was determined using ^{1}H NMR (figure S-5), by comparing CVS vinyl signals (δ6.25-6.5, 2H; δ6.75-7.0, 1H) to the backbone methylene signal (δ1.85, 2H). Incorporation of CVS was 65 to 85% efficient (table S-1).

4.4.3. Bulk Gels

Gels were formed by mixing aqueous solutions of PMM-CVS and HS-PEG-SH, maintaining a 1:1 vinyl sulfone/thiol ratio. Nine compositions, containing 2.5, 5 and 7.5% w/v of each of the PMM-CVS polymers with 10, 20 and 30% CVS, were prepared in triplicate, and swelling and Young's moduli of the resulting gels determined. PMM-CVS_{10} only formed gels at loadings of 7.5% w/v or higher, while PMM-CVS_{20} and PMM-CVS_{30} formed gels at all three loading percentages.

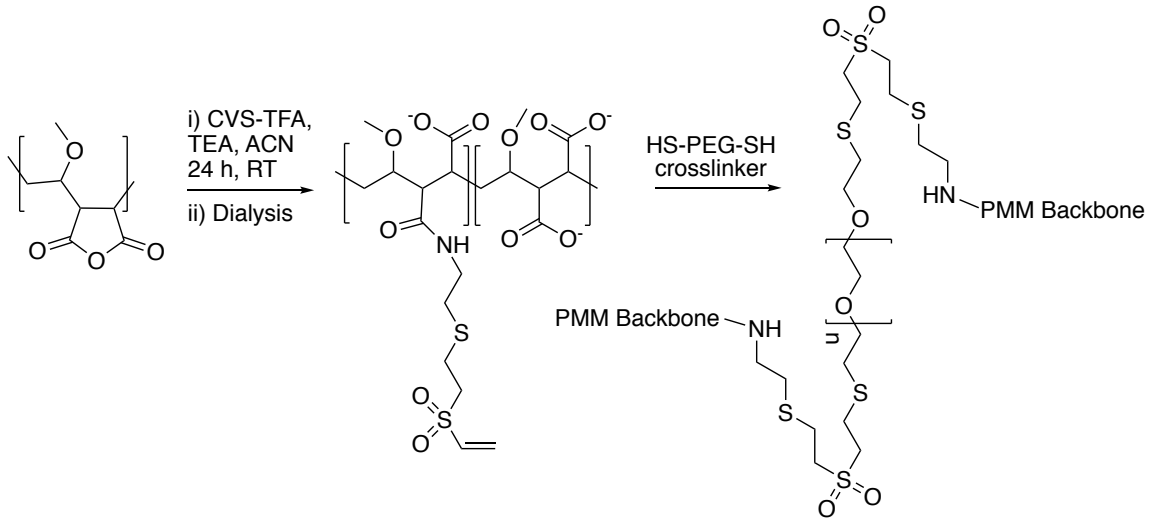

Scheme 4.2. PMM functionalization with CVS TFA and crosslinking of resulting PMM-CVS polymer with HS-PEG-SH.

Gelation times, defined as time needed to achieve zero flow upon sample inversion, were measured at pH 6.5, 7.5 and 8.5 for PMM-CVS_x gels prepared at 5% w/v. The time required for gelation strongly depended on the degree of CVS functionalization, and, as reported previously for PEG-based gels,[34] on the pH of the polymer solutions. Figure 4.1 shows gelation time decreasing with increasing pH, and with CVS functionalization. For example, PMM-CVS_{20} gelled in 5.6 ± 0.5 min at pH 7.5, and in 44 ± 5 min at pH 6.5. In contrast, PMM-CVS_{30} gelled within a minute at pH 7.5, and within a few seconds at pH 8.5.

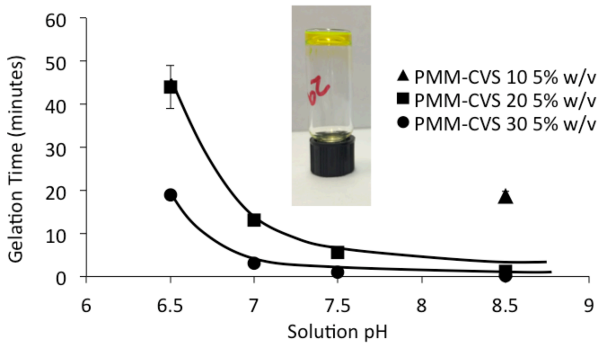

Figure 4.1. Gelation time for 5% w/v PMM-CVS/HS-PEG-SH system, measured by horizontal tilt test, as a function of CVS content and pH.

Cysteamine has a pKa value of 8.32[47] so the fraction of thiolate anions, and hence the thiol-ene coupling rate, are highly sensitive to small changes in pH in this range. No gelation was observed at pH 6.0 and below for PMM-CVS_{20} and PMM-CVS_{30}, and at pH 8.0 and below for PMM-CVS_{10}.

^{1}H-NMR was used to measure the rate of thiol-ene reaction during gelation of 5% w/v PMM-CVS_{30} / HS-PEG-SH (figure 4.2), by monitoring the disappearance of PMM-CVS vinyl signals at δ6.4 and δ6.75. This composition gels at about one minute and as little as 1-5% vinyl consumption, and levels off after 12 hrs with 18% vinyl groups remaining. Reactions between polymers are known to rarely reach completion, due to spatial isolation of reactive groups, and possibly electrostatic repulsion of the anionic backbones as well as disulfide formation of some of the thiols.[36] These residual vinyl

groups provide an opportunity to post-functionalize the hydrogel, as described further below.

The rapid gelation rates, as well as concentration and pH dependencies observed here, are comparable to those for a PEG/peptide-based vinyl sulfone-thiol crosslinking system described by Lutolf and Hubbell.[36]

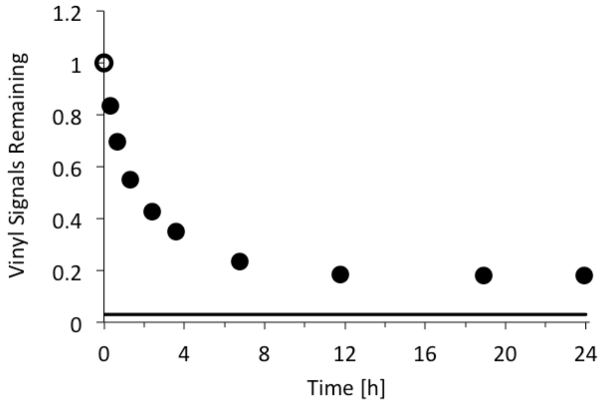

Figure 4.2. Profile of remaining vinyl signals during gellation of 5% w/v PMM-CVS_{30} HS-PEG-SH system at pH 7.1 determined by NMR integration. The reaction levels off at ca. 20% remaining vinyl signals, due to immobilization of the polymer-bound reactants.

4.4.4. Swelling Studies

Equilibrium hydrogel swelling reflects the balance between the free energy of mixing between network and solvent plus the net osmotic pressure of mobile counter ions, and the swelling pressure of expansion.[48, 49] Figure 4.3 shows the swelling ratios for as-formed PMM-CVS gel disks incubated in PBS buffer at 37 ^{o}C for 7 days. Swelling ratio is defined here as the volume ratios of a PBS-incubated sample to the as-formed gel, not the ratio of swollen versus dry material.

Gels prepared with 7.5% w/v PMM-CVS_{10} exhibit more PBS-induced swelling than PMM-CVS_{30} 2.5% w/v (Figure 4.3), despite their equivalent molar amounts of CVS. This is attributed to the lower crosslink efficiency and higher swelling pressure, due to higher electrostatic repulsion for PMM-CVS_{10}.

The horizontal dashed line in Figure 4.3 represents an equilibrium swelling ratio of 1, *i.e.* no additional swelling of the as-formed gels. PMM-CVS_{30} gels at all three

weight percentages have swelling ratios close to 1, attributed to their high crosslink density and the hydrophobic contributions from the CVS side groups.

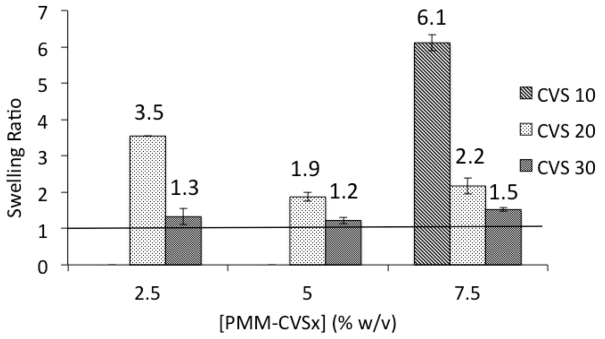

Figure 4.3. Equilibrium swelling ratios of PMM-CVS/HS-PEG-SH crosslinked hydrogels. Horizontal line indicates swelling ratio of 1.

4.4.5. Mechanical Properties of Hydrogels

The stiffness of hydrogel substrates can affect proliferation and differentiation potential of anchorage-dependent cells.[50] Figure 4.4a and 4.4b show the Young's moduli of the PMM-CVS_x / HS-PEG-SH hydrogels obtained by indentation, before and after swelling in 10 mM PBS. These Young's moduli are estimated according to Hertzian theory for contact between a sphere and an elastically deformed incompressible material, Equation 2, where F is the force in mN, d is the depth of deformation, R is the radius of the indenter (R = 0.85 mm), ν is Poisson's ratio (assumed to be 0.5 for elastomeric hydrogels), and E is Young's Modulus.

Equation 4.2: Hertzian Theory: $$F = \frac{E\,(4/3)R^{1/2}d^{3/2}}{1 - \upsilon^2}$$

Young's moduli, E, were obtained from the initial slopes ($d \leq 0.3$ mm) of the force versus strain plots, where the linear Hertzian theory is considered reliable.[51] Moduli increased from 1 to 141 kPa with increasing degree of functionalization and increasing polymer loading. Specifically, the moduli of the as-formed gels made with 7.5% w/v polymer increased with increasing CVS content: PMM-CVS_{10} (4.8 kPa), PMM-CVS_{20}

(86 kPa) and PMM-CVS_{30} (141 kPa). Similarly, the moduli for PMM-CVS_{30} increased from 4.1 kPa (2.5% w/v) to 141 kPa (7.5% w/v) with polymer loading. The gels swollen to equilibrium in PBS showed moduli covering a slightly lower range, from 1 to 96 kPa, with PMM-CVS_{20} 2.5% w/v and PMM-CVS_{10} 7.5% w/v becoming too soft to test with the indenter. These trends allow the mechanical properties of the PMM-CVS_x HS-PEG-SH system to be tuned within a large range, covering much of the stiffnesses observed in human soft tissues,[52] by altering either the degree of functionalization or the polymer loading.

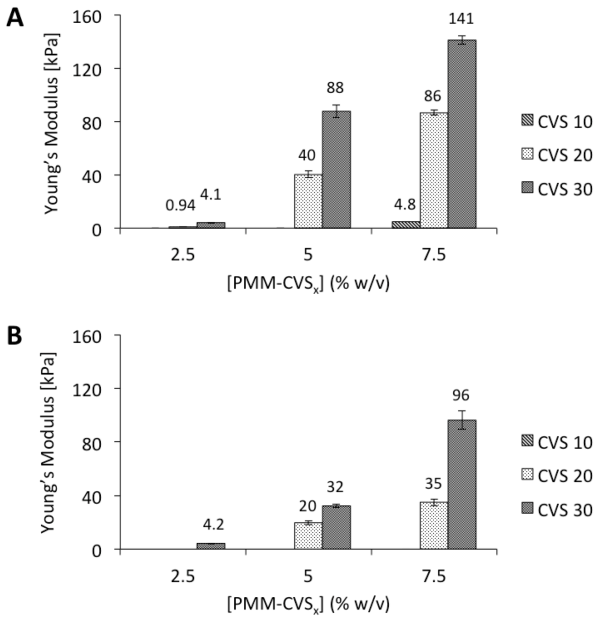

Figure 4.4. Young's moduli for as-formed gels (A), and swollen gels (B), as a function of PMM-CVS functionalization, and loading percentage. All gels made with 1:1 vinyl sulfone:thiol.

4.4.6. Hydrolytic Stability of Thioether, Amide and Vinyl Sulfone Groups in PMM-CVS

Many reactive polymers are prone to sometimes unexpected hydrolytic side reactions in aqueous environments.[36, 53] While thioether linkages[54] and most polymeric amides are stable under physiological pH and temperature,[55] the presence of a neighboring carboxylic acid group in maleamic or succinamic acids[56] is known to promote amide hydrolysis, especially at pH < 7 where at least some of the carboxylic acid is in the acid form. A recent study showed good hydrolytic stability of such amide-

linkages on PMM-based polymers at pH > 7.[49] Several literature reports describe the stability of vinyl sulfone in water as one of the benefits of using this group for, e.g., protein modification.[57,58] To assess the current polymers, PMM-CVS_{30} solutions in D_2O at pD 7.7 and 8.7 were stored for 3 weeks at 37 °C, and monitored at intervals by ^1H NMR. The only spectral changes observed were attributed to the hydration of the pendant vinyl groups. This reaction has a half-life of about 10 days, suggesting it would not interfere with gelation and post-modification, even at higher pH.

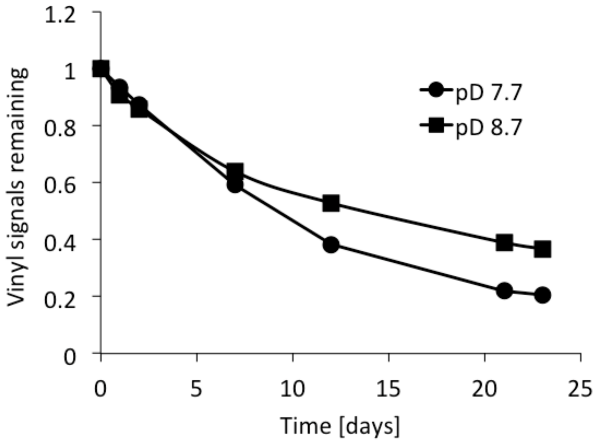

Figure 4.5. Disappearance of distal proton signals (6.0 ppm) in HEPES buffer (pD 7.7 and 8.7) over time. Hydration of the vinyl sulfone moiety occurs orders of magnitude more slowly than the thiol-ene crosslinking reaction.

4.4.7. Post Modification of Residual Vinyl Sulfone Units

Controlled post-modification of reactive polymers and hydrogels is important to cap reactive groups and incorporate functional biomolecules.[59] Thiol-ene Michael additions have already been used to incorporate VEGF[60] and RGD[61] into PEG-based vinyl sulfone- and maleimide- containing hydrogels.

Cysteamine, a small thiol containing molecule, was used to test step-wise post-functionalization of as-formed PMM-CVS_{30} HS-PEG-SH hydrogels (figure 4.6). The gel was crosslinked using a 0.5:1 ratio of thiol:CVS, in order to offer a higher concentration of residual CVS for post-functionalization. A first 36 mol% aliquot (figure 4.6, A) of capping agent added led to 28% deactivation of gel-bound vinyl as assessed by ^1H NMR. A subsequent addition of a 66% cysteamine aliquot (figure 4.6, B) led to another 52%

deactivation, followed by capping the residual 20% of vinyl groups with a final aliquot of cysteamine (figure 4.6, C). This stepwise post-functionalization suggests the possibility of immobilizing different thiol-functional groups including, e.g., cell adhesion motifs, before or after gelation.

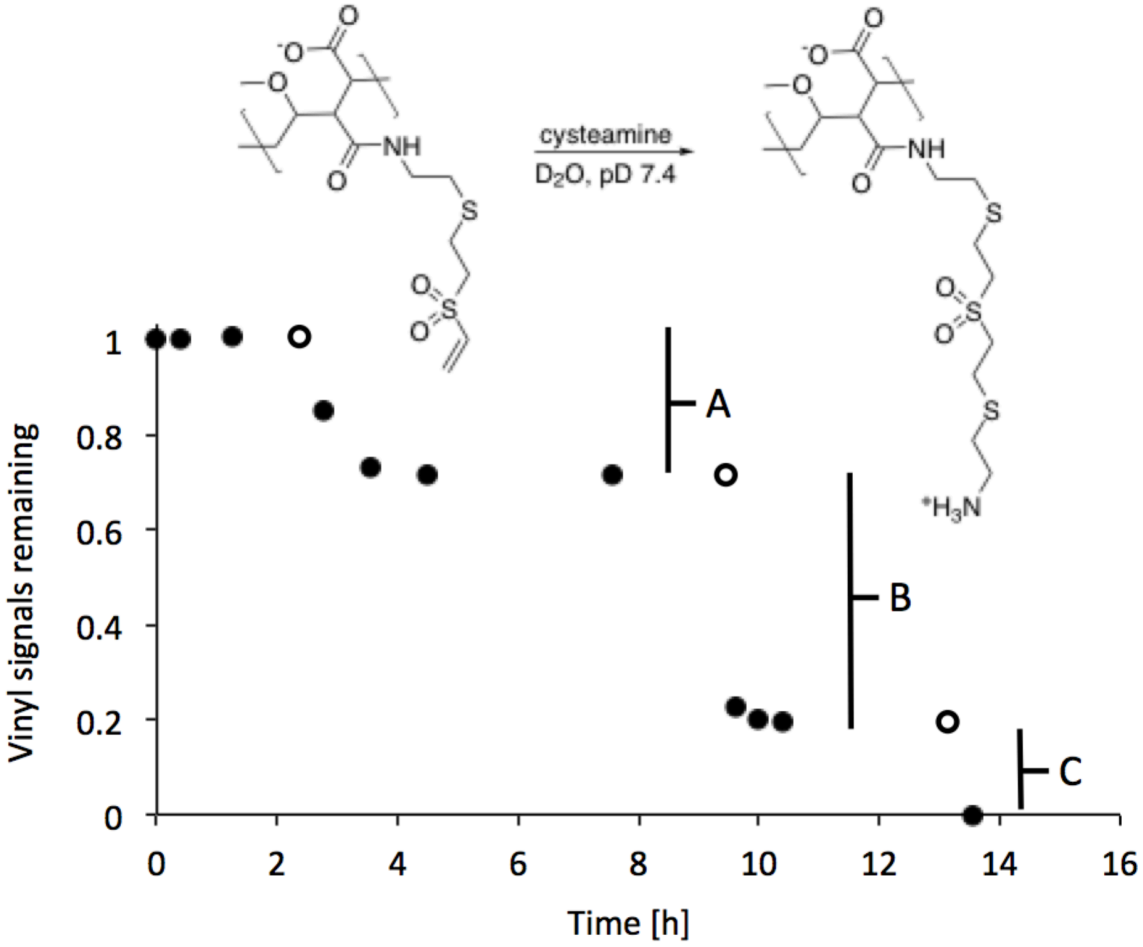

Figure 4.6. Stepwise post-functionalization of residual functional units in PMM-CVS_{30} HS-PEG-SH gel. Hollow circle indicates injection time of cysteamine capping agent.

4.4.8. In Vitro Cytotoxicity Screening

In vitro cytotoxicity of 5% w/v PMM-CVS_{20} / HS-PEG-SH and PMM-CVS_{20} Arg-Gly-Asp-Cys / HS-PEG-SH hydrogels towards embedded 3T3 fibroblasts was evaluated using a live/dead assay. Hubbell *et. al.* previously reported excellent cell viability and proliferation in vinyl sulfone-terminated PEG hydrogels,[62] so minimal cell toxicity was expected. Gels were found to be 2500 μm thick via confocal microscopy and

the central 1000 μm (z-direction) substack, a representative volume, were imaged for cell viability. Cell viability after incubation for 24 h was found to be statistically identical for all samples, at 96 ± 1% for control, 93 ± 2% for PMM-CVS_{20} hydrogels, and 95 ± 3% for PMM-CVS_{20} Arg-Gly-Asp-Cys hydrogels. This is based on assessing 8 to 12 sample areas with about 30 cells each, selected from each physical sample, for cells in the control wells and in the PMM-CVS_{20} and PMM-CVS_{20} Arg-Gly-Asp-Cys hydrogels, respectively (Figure 4.7). These results indicate that PMM-CVSx / HS-PEG-SH hydrogels have potential for biomedical applications. Pre-functionalization of PMM-CVS_{20} with Arg-Gly-Asp-Cys did not interfere with gelation or cell viability and offers attachment motifs for embedded cells. Testing of different cell lines is currently being explored in more detail.

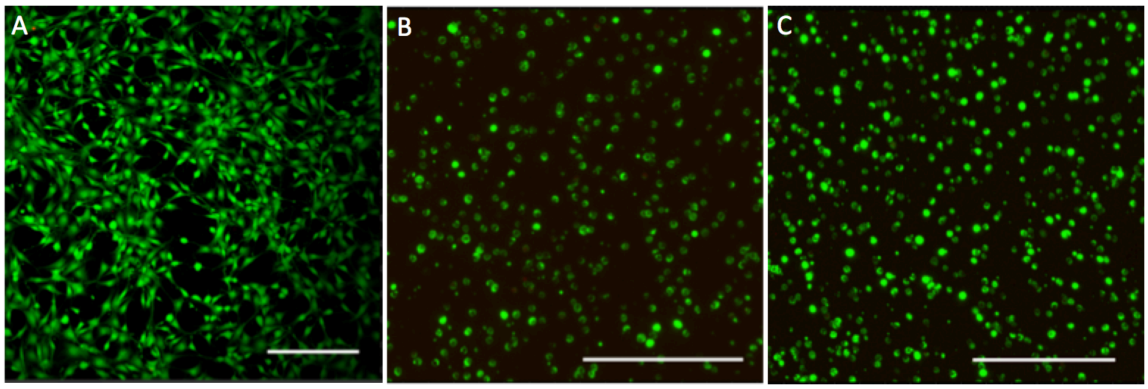

Figure 4.7. NIH 3T3 fibroblast cells after 24 h on A: tissue-culture treated glass with DMEM (control) and encapsulated within 5% w/v B: PMM-CVS_{20} HS-PEG-SH and C: PMM-CVS_{20} Arg-Gly-Asp-Cys HS-PEG-SH hydrogels. Green fluorescent cells indicate live cells, while red fluorescent cell indicate dead cells. Scale bars = 250 μm)

4.5. Conclusions

Cysteamine vinyl sulfone (CVS) trifluoroacetate was synthesized and used to functionalize poly(methyl vinyl ether-alt-maleic anhydride) (PMMAn) by amine-anhydride coupling. The remaining anhydride groups were hydrolyzed to succinic acid units, forming a series of PMM-CVSx with 10, 20 and 30 mol% CVS. Thiol-ene click reactions with HS-PEG-SH led to a series of hydrolytically stable, covalently crosslinked

hydrogels. Gel properties including Young's moduli, gel time, and equilibrium swelling could be tuned through the degree of CVS functionalization, the percent polymer loading, and pH. The resulting hydrogels have elastic moduli matching those of fat, muscle and cartilage, and display negligible cytotoxicity towards 3T3 cells. The pendant vinyl sulfone groups not used for crosslinking may be used for modification or capped. Due to their facile preparation, efficient crosslinking, stable reactive groups, and high tunability, these hydrogels show promise for future applications as synthetic ECMs.

4.6. Acknowledgements

We would like to thank the Natural Sciences and Engineering Research Council (NSERC) of Canada for supporting this work through Discovery and CREATE grants.

4.7. References

1 M. P. Lutolf, G. P. Raeber, A. H. Zisch, N. Tirelli, J. A. Hubbell, *Adv. Mat.,* 2003, **15**, 888-892.

2 J. J. Rice, M. M. Martino, L. De Laporte, F. Tortelli, P. S. Briquez, J. A. Hubbell, *Adv. Health. Mater.,* 2013, **2**, 57-71.

3 M. Arslan, T. N. Gevrek, R. Sanyal, A. Sanyal, *Eur. Polym. J.,* 2015, **62**, 426-434.

4 L. Yu, J. Ding, *Chem. Soc. Rev.,* 2008, **37**, 1473-1481.

5 K. Y. Lee, D. H. Mooney, *Chem. Rev.,* 2001, **101**, 1869 – 1879.

6 S. Varghese, J. H. Elisseeff, *Adv. Polym. Sci.,* 2006, **203**, 95-144.

7 B. V. Slaughter, S. S. Khurshid, O. Z. Fisher, A. Khademhossini, N. A. Peppas, *Adv. Mat*., 2009, **21**, 3307-3329.

8 J. Li, L. Ma, G. Chen, Z. Zhou, Q. Li, *J. Mater. Chem. B*, 2015, **3**, 8401-8409.

9 E. H. Nafea, A. Marson, L. A. Poole-Warren, P. J. Martens, *J. Control. Release.* 2011, **154,** 110-122.

10 S. C. Lee, I. K. Kwon, K. Park, *Adv. Drug. Del. Rev*., 2013, **65,** 17-20.

11 K. Y. Lee, J. A. Rowley, P. Eiselt, E. M. Moy, K. H. Bouhadir, D. J. Mooney, *Macromolecules*, 2000, **33**, 97-101.

12 X. Hu, L. Lu, C. Xu, X. Li, *Int. J. Biol. Macromolec*., 2015, **72**, 403-409.

13 E. M. Ahmed, *J. Adv. Res*., 2015, **6**, 105-121.

14 M. P. Lutolf, J. A. Hubbell, *Nat. Biotechnol*., 2005, **23**, 47-55.

15 X. Liu, P. X. Ma, *Ann. Biomed. Eng*., 2004, **32**, 477-486.

16 T. R. Hoare, D. S. Kohane, *Polymer*, 2008, **49**, 1993-2007.

17 C. A. DeForest, B. D. Polizzotti, K. S. Anseth, *Nat. Mater*., 2009, **8**, 659-664.

18 M. Malkoch, R. Vestber, N. Gupta, L. Mespouille, P. Dubois, A. F. Mason, J. L. Hedrick, Q. Liao, C. W. Frank, K. Kingsbury, C. J. Hawker, *Chem. Commun. (Camb)*., 2006, **14**, 2774-2776.

19 V. Crescenzi, L. Cornelio, C. Di Meo, S. Nardecchia, R. Lamanna, *Biomacromolecules*, 2007, **8**, 1844-1850.

20 D. P. Nair, M. Podgórski, S. Chatani, T. Gong, W. Xi, C. R. Fenoli, C. N. Bowman, *Chem. Mater*., 2014, **26**, 724-744.

21 R. J. Pounder, M. J. Stanford, P. Brooks, S. P. Richards, A. P. Dove, *Chem. Commun*. *(Camb).,* 2008, 5158-5160.

22 P. M. Kharkar, A. M. Kloxin, K. L. Kiick, *J. Mater. Chem. B,* 2014, **2**, 5511-5521.

23 G.-Z. Li, R. K. Randev, A. H. Soeriyadi, G. Rees, C. Boyer, Z. Tong, T. P. Davis, C. R. Becer, D. M. Haddleton, *Polym. Chem*., 2010, **1**, 1196-1204.

24 J. Chang, Y. Tao, B. Wang, B.-h. Guo, H. Xu, Y.-r. Jiang, Y. Huang, *J. Mater. Chem. B*, 2015, **3**, 1097-1105.

25 H. Shih, C. C. Lin, *Biomacromolecules*, 2012, **13**, 2003-2012.

26 M. S. Rehmann, A. C. Garibian, A. M. Kloxin, *Macromol. Symp*., 2013, **329**, 58-65.

27 H. Shih, C.-C Lin, *Biomacromolecules*, 2015, **16**, 1915-1923.

28 R. Mahou, C. Wandrey, *Macromolecules*, 2010, **43**, 1371-1378.

29 S. Chatani, D. P. Nair, C. N. Bowman, *Polym. Chem*., 2013, **4**, 1048-1055.

30 R. Ettari, C. Bonaccorso, N. Micale, C. Heindl, T. Schirmeister, M. L. Calabro, S. Grasso, M. Zappala, *ChemMedChem.,* 2011, **6**, 1228-1237.

31 M. P. Lutolf, J. A. Hubbell, *Biomacromolecules*, 2003, **4**, 713-722.

32 A. M. Jonker, A. Borrmann, E. R. H. Van Eck, F. L. Van Delft, D. W. P. M. Lowik, J. C. M. Van Hest, *Advanced Material*s, 2015, **27**, 1235-1240.

33 S. Allazetta, T. C. Hausherr, M. P. Lutolf, *Biomacromolecules*, 2013, **14**, 1122-1131.

34 F. S. Palumbo, C. Fiorica, M. Di Stefano, G. Pitarresi, A. Gulino, S. Agnello, G. Giammona, *Carbohydr. Polym*. 2015, **122**, 408-416.

35 K. Chawla, T.-B. Yu, S. W. Liao, Z. Guan, *Biomacromolecules*, 2011, **12**, 560-567.

36 A. Dubbini, R. Censi, M. E. Butini, M. G. Sabbieti, D. Agas, T. Vermonden, P. Di Martino, *Eur. Polym. J*., 2015, **72**, 423-437.

37 K. Vandamme, V. Melkebeek, E. Cox, D. Deforce, J. Lenoir, E. Adriaens, C. Vervaet, J. P. Remon, *Eur. J. Pharm. Biopharm.,* 2010, **74**, 202-208.

38 T. W. Wong, S. Wahab, Y. Anthony, *Drug Dev. Ind. Pharm.,* 2007, **33**, 737-746.

39 K. Yoncheva, E. Lizarraga, J. M. Irache, *Eur. J. Pharm. Sci.,* 2005, **24**, 411-419.

40 L. J. Goujon, S. Hariharan, B. Sayyar, N. A. D. Burke, E. D. Cranston, D. W. Andrews, H. D. H. Stöver, *Langmuir*. 2015, **31**, 5623-5632.

41 C. M. Gardner, N. A. D. Burke, T. Chu, F. Shen, M. A. Potter, H. D. H. Stöver, *J. Biomater. Sci. Polym. Ed.,* 2011, **22**, 2127-2145.

42 C. M. Gardner, N. A. D. Burke, H. D. H. Stöver, *Langmuir,* 2010, **26**, 4916-4924.

43 C. M. Gardner, M. A. Potter, H. D. H. Stöver, *J. Mater. Sci: Mater. Med.,* 2012, **23**, 181-193.

44 S. A. Stewart, M. Backholm, N. A. D. Burke, H.D.H Stöver,. *Langmuir*, 2016, **32**, 1863-1870.

45 Y. Yu, Y. Chau, *Biomacromolecules*, 2012, **13**, 937-942.

46 J.-H. Kong, E. J. Oh, S. Y. Chae, K. C. Lee, S. K. Hahn, *Biomaterials,* 2010, **31**, 4121-4128.

47 L. Riauba, G. Niaura, O. Eicher-Lorka, E. Butkus, *J. Phys. Chem. A.,* 2006, **110**, 13394-13404.

48 R. A. Siegel, B. A. Firestone, *Macromolecules,* 1988, **21**, 3254-3259.

49 T. Tanaka, D. Fillmore, S.-T. Sun, I. Nishio, G. Swislow, A. Shah, *Phys. Rev. Lett.,* 1980, **45**, 1636-1638.

50 N. D. Leipzig, M. S. Shoichet, *Biomaterials*, 2009, **30**, 6867-6878.

51 R. Long, M. S. Hall, C.-Y. Hui, *Biophys. J.,* 2011, **101**, 643-650.

52 A. Buxboim, I. L. Ivanovska, D. E. Discher, *J. Cell Sci*., 2010, **123**, 297-308.

53 S. Mohajeri, N. A. D. Burke, H. D. H. Stöver, *Polym. Degrad. Stab*., 2015, **114**, 94-104.

54 P. A. Trail, D. Willner, J. Knipe, A. J. Henderson, S. J. Lasch, M. E. Zoeckler, M. D. TrailSmith, T. W. Doyle, H. D. King, A. M. Casazza, G. R. Braslawsky, J. Brown, S. J. Hofstead, R. S. Greenfield, R. A. Firestone, K. Mosure, K. F. Kadow, M. B. Yang, K. E. Hellström, I. Hellström, *Cancer Res.,* 1997, **57**, 100-105.

55 T. Higuchi, L. Eberson, A. K. Herd, *J. Am. Chem. Soc*. 1966, **88**, 3805−3808.

56 M. L. Bender, Y.-L. Chow, F. Chloupek, *J. Am. Chem. Soc*. 1958, **80**, 5380−5384.

57 M. Bogyo, S. Verhelst, V. Bellingard-Dubouchaud, S. Toba, D. Greenbaum, *Chem. Biol.,* 2000, **7**, 27-38.

58 E.-W. Lin, N. Boehnke, H. D. Maynard, *Bioconjugate Chem.* 2014, **25**, 1902-1909.

59 J. Zhu, *Biomaterials*, 2010, **31**, 4639-4656.

60 D. Seliktar, A. H. Zisch, M. P. Lutolf, J. L. Wrana, J. A> Hubbell, *J. Biomed. Mater. Res. A*., 2004, **68**, 704-716.

61 T. Nie, R. E. Jr. Akins, K. L. Kiick, *Acta Biomater*., 2009, **5**, 865-875.

62 J. Patterson, J. A. Hubbell, *Biomaterials*, 2010, **31**, 7836-7845.

4.8. Appendix

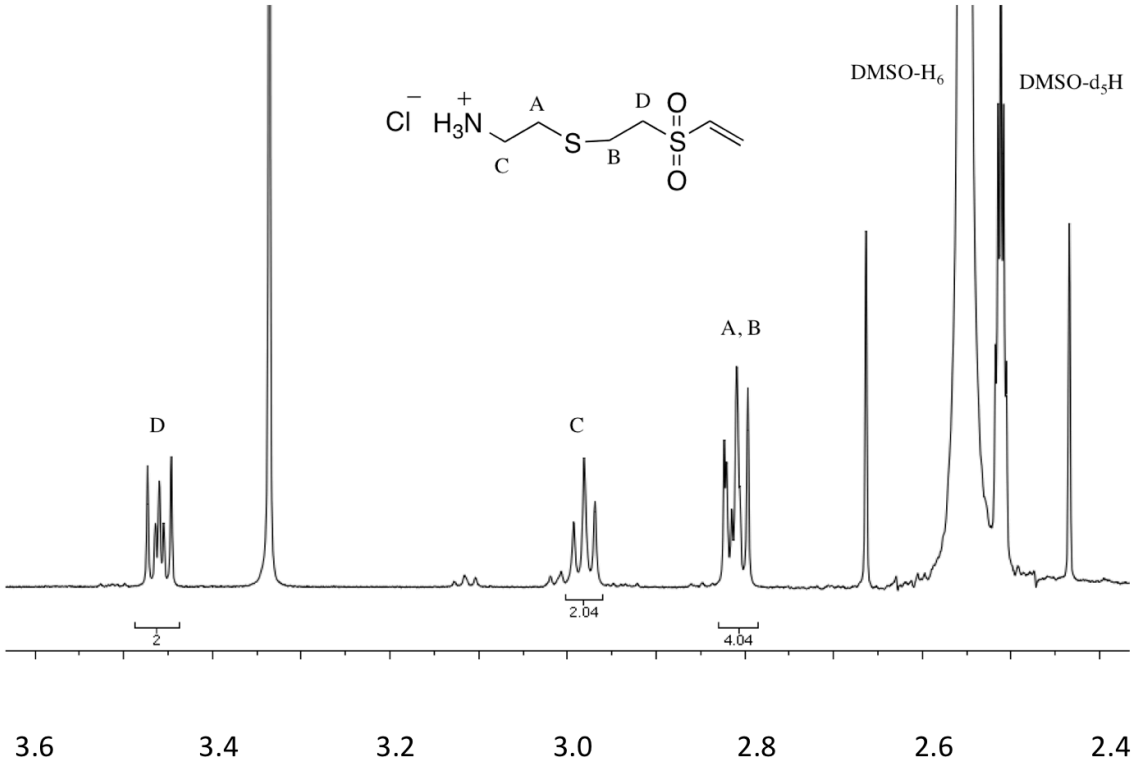

Figure A4.1. ^{1}H NMR spectrum of crude CVS·HCl in DMSO/DMSO-d_6, focused on the aliphatic region (∂3.6 to δ2.4).

To assess the progress of the cysteamine divinyl sulfone Michael addition (figure A4.1), a drop of the crude mixture in DMSO was diluted in DMSO-d_6 giving rise to the dual peaks at δ2.5 from both DMSO-H_6 and DMSO-d_5H. Near-quantitative conversion of cysteamine to cysteamine vinyl sulfone HCl was determined by the ethylene integrations 4:2:2 (A+B:D:C), and the near disappearance of cysteamine ethylene signals at δ3.1 and δ3.0.

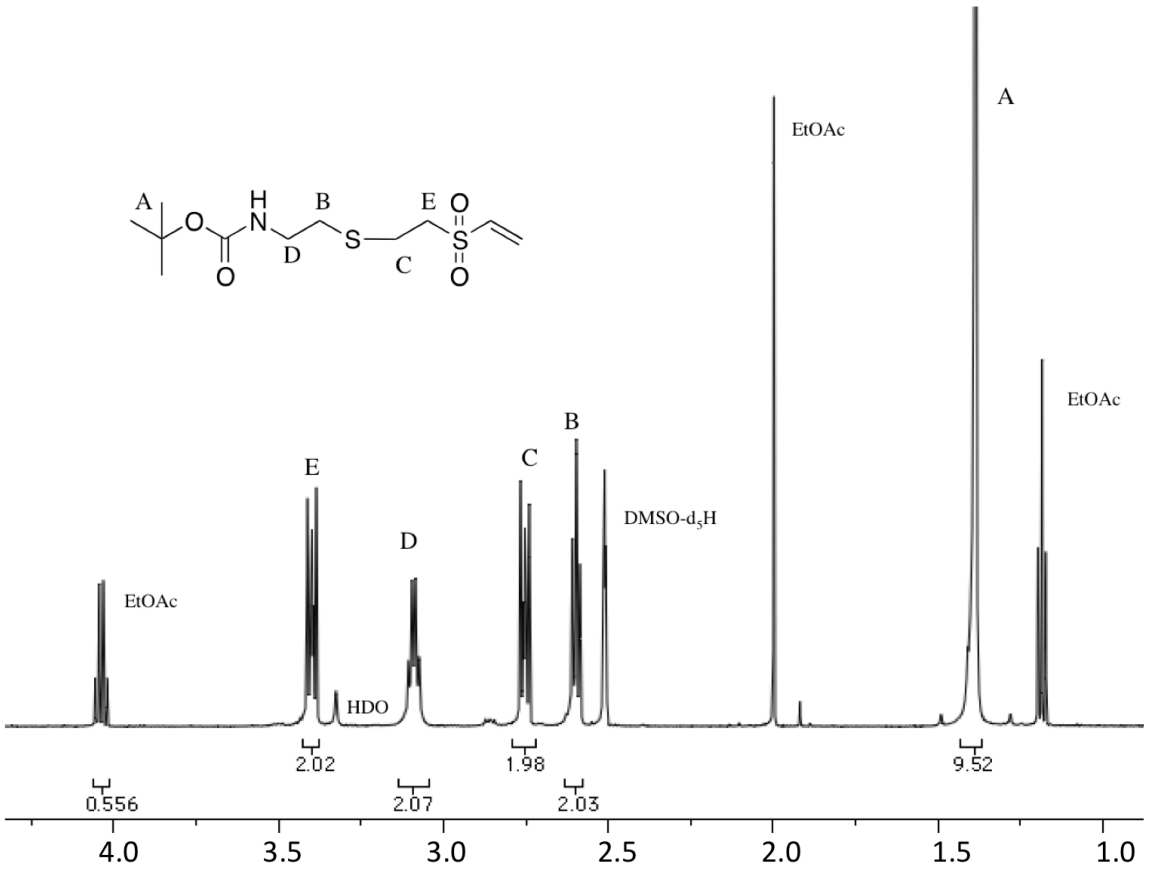

Figure A4.2. ^{1}H NMR spectrum of isolated N-BOC CVS in DMSO-d_6, focused on the aliphatic region (δ4.25 to δ1.0).

^{1}H NMR confirmed the presence of the tert-butyl signal of the BOC protecting group (δ1.4, 9H, s), as well as a downfield shift of the cysteamine methylenes adjacent to the thioether (δ2.75 2H, δ2.6 2H).

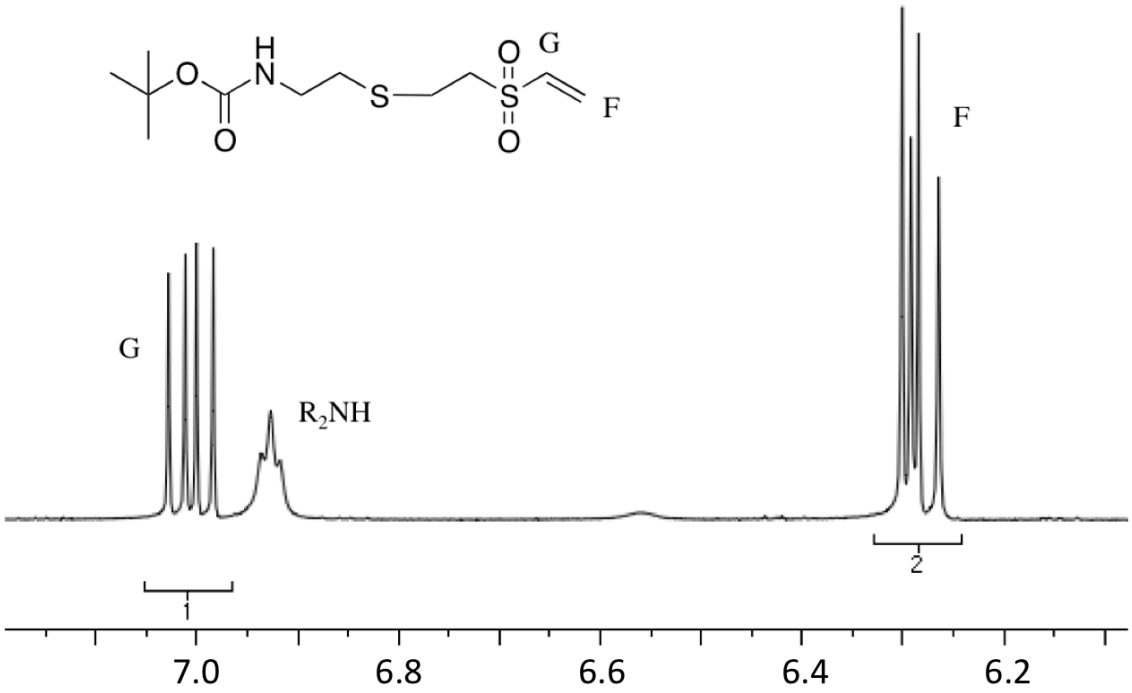

Figure A4.3. ^{1}H NMR spectrum of N-BOC CVS in DMSO-d_6, focused on the vinyl region (∂7.2 to δ6.1).

Ethyl acetate, used as column eluent, was present in the N-BOC CVS sample (figure A4.2), however it was removed in subsequent steps and therefore was deemed insignificant. The four main ethylene peaks (δ3.4, δ3.09, δ2.75 and δ2.6) provided assurance of amine protection, with the divergence of the peak from protons adjacent to the thioether. The presence of the triplet at δ6.9 also affirms presence of the N-BOC linkage, as the aprotic solvent allows for the retention of the NH proton (figure A4.3). No peaks were seen between δ6.1 - 4.25.

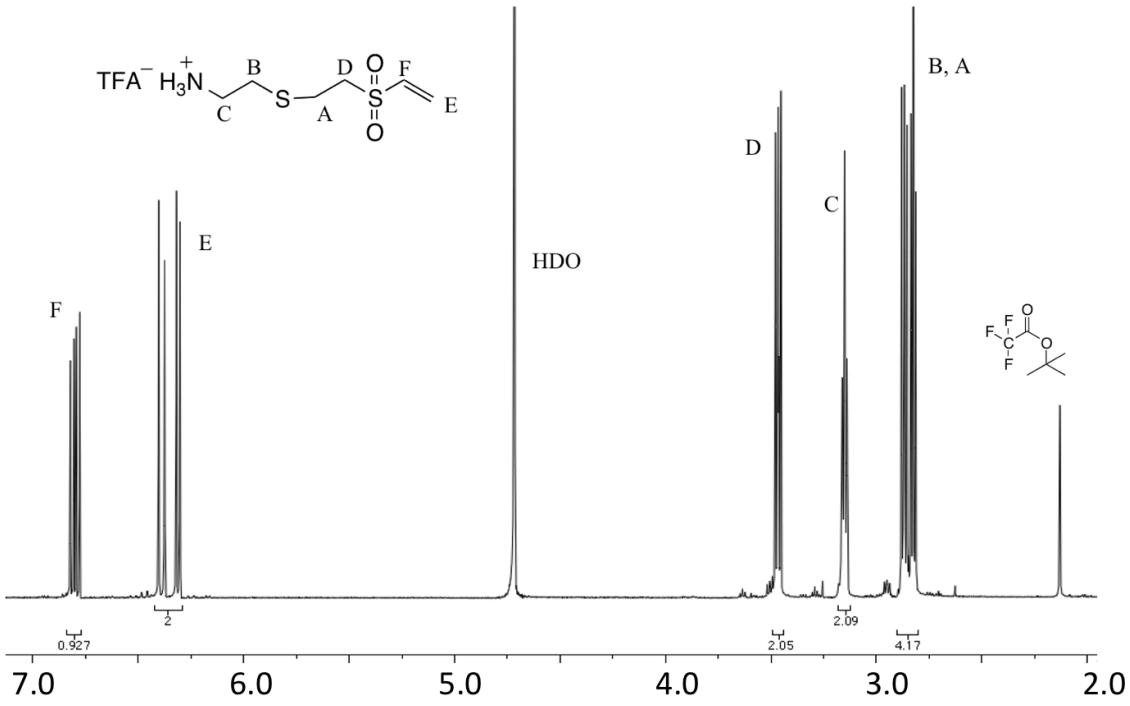

Figure A4.4. ^{1}H NMR spectrum of CVS TFA in D_2O.

Deprotection of N-BOC CVS to form the final CVS TFA product was confirmed by the disappearance of the t-butyl signal (δ1.4, 9H, s), as well as the convergence of the proton environments A and B (figure A4.4), leading to a similar spectrum as CVS·HCl. Side product *tert*-butyl trifluoracetate was present in this sample (δ2.2) which was a side product from the preceeding TFA deprotection.

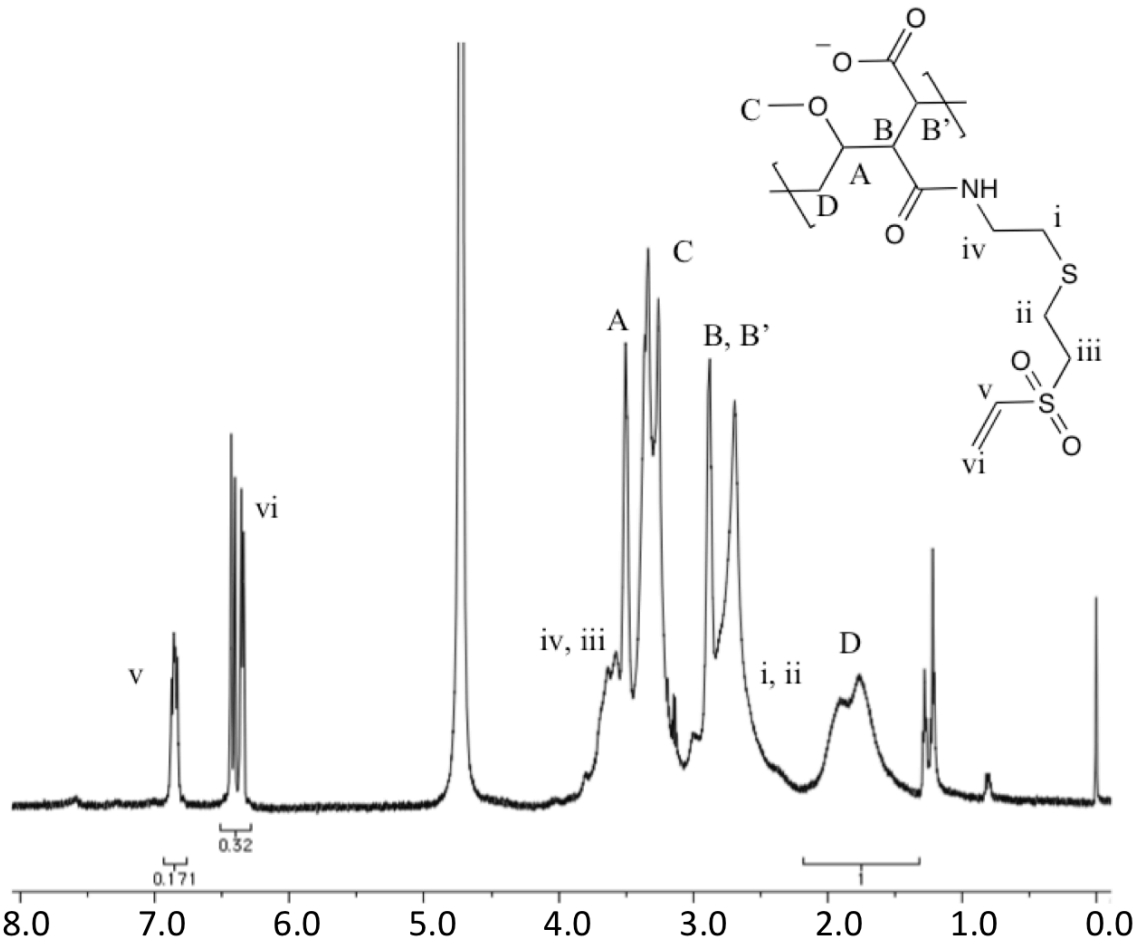

Figure A4.5. ^{1}H NMR spectrum of PMM-CVS$_{30}$ in D_2O. The ratio of grafted CVS groups was determined by vinyl signal integration (v, 1H, δ6.8; vi, 2H, δ6.4) compared to a backbone methylene peak (D, 2H, δ1.5-2).

Table A4.1. Degree of substitution of PMM-CVS$_x$ polymers comparing target to outcome percentage, and the shorthand used to denote polymer functionalization.

PMM-CVS$_{10}$		PMM-CVS$_{20}$		PMM-CVS$_{30}$	
Target	Actual	Target	Actual	Target	Actual
15	11	25	19	35	32

Small variations in integration can be seen due to line broadening of the polymeric methylene internal standard, as well as variations in vinylic peaks, due to

impurities that are present in the purchased poly (methyl vinyl ether-*alt*-maleic anhydride). Due to these integration variations, ratios were rounded to the nearest ten, and denoted as such (Table A4.1). Sodium chloride (0.05 M) was added to the first two dialysis baths, successfully displacing ionically bound cations, TEA and CVS.

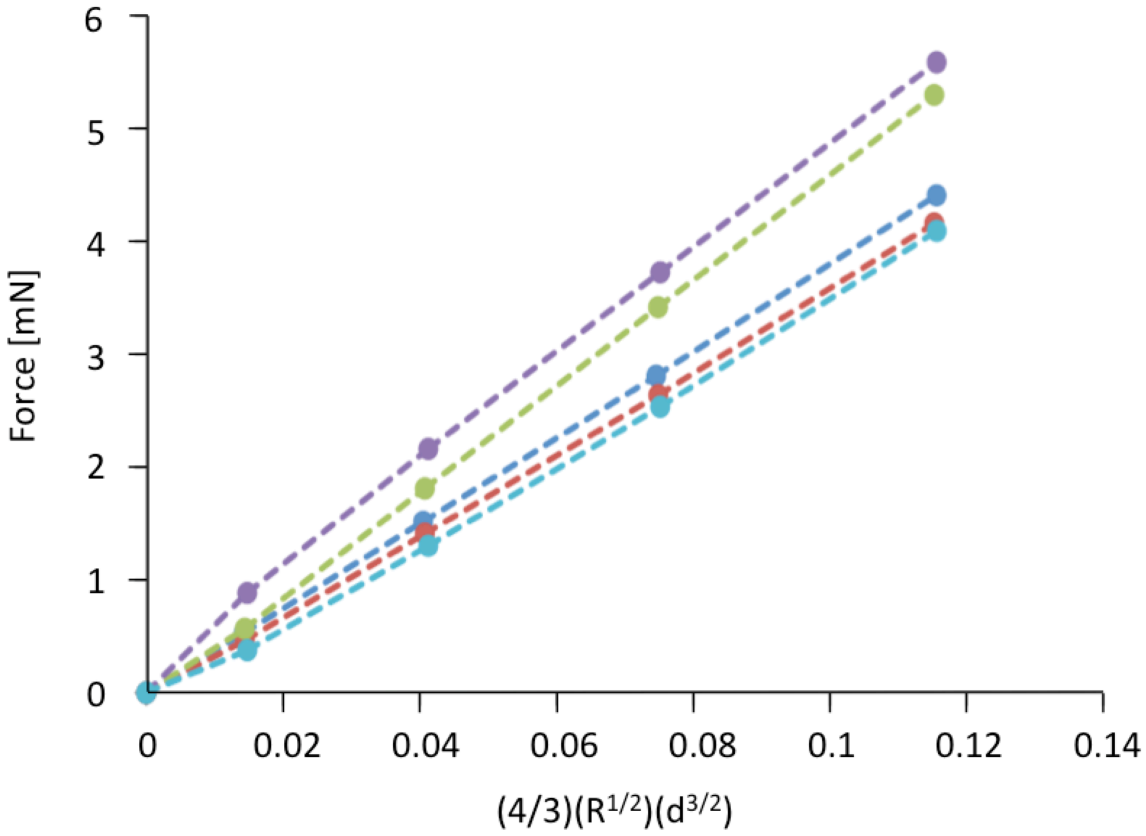

Figure A4.6. Force strain curve for PMM-CVS_{20} 7.5% w/v HS-PEG-SH hydrogel.

In order to calculate the Young's modulus from contact stress, the measured force from indentation was plotted against displacement ($d^{3/2}$) multiplied by a constant ($[4/3][R^{1/2}]$) and fitted to by Hertzian theory. The slope of the strain curve (E*) was multiplied by Poisson's ratio (ν) [$1/E^* = (1-\nu)/E$], assumed to be 0.5 for elastically deformed materials, where E is the Young's modulus (E).

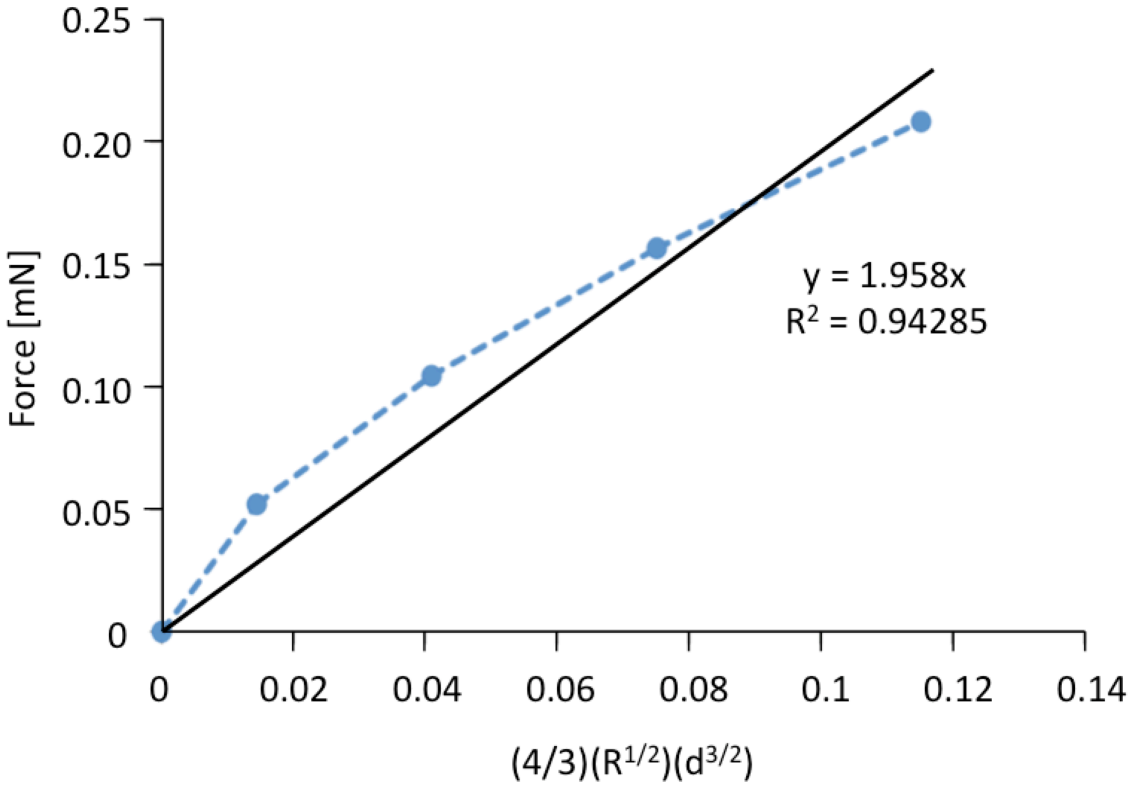

Figure A4.7. Force strain curve for PMM-CVS_{10} 7.5% w/v HS-PEG-SH hydrogel, swollen in PBS buffer for 7 days, demonstrating fast relaxation after contact stress.

Highly swollen gels exhibited creep compliance under contact stress, even at high deformation speeds, shown by the concave nature of the force-strain curve. Curves with R^2 values lower than 0.98 were not used in calculation of Young's modulus average.

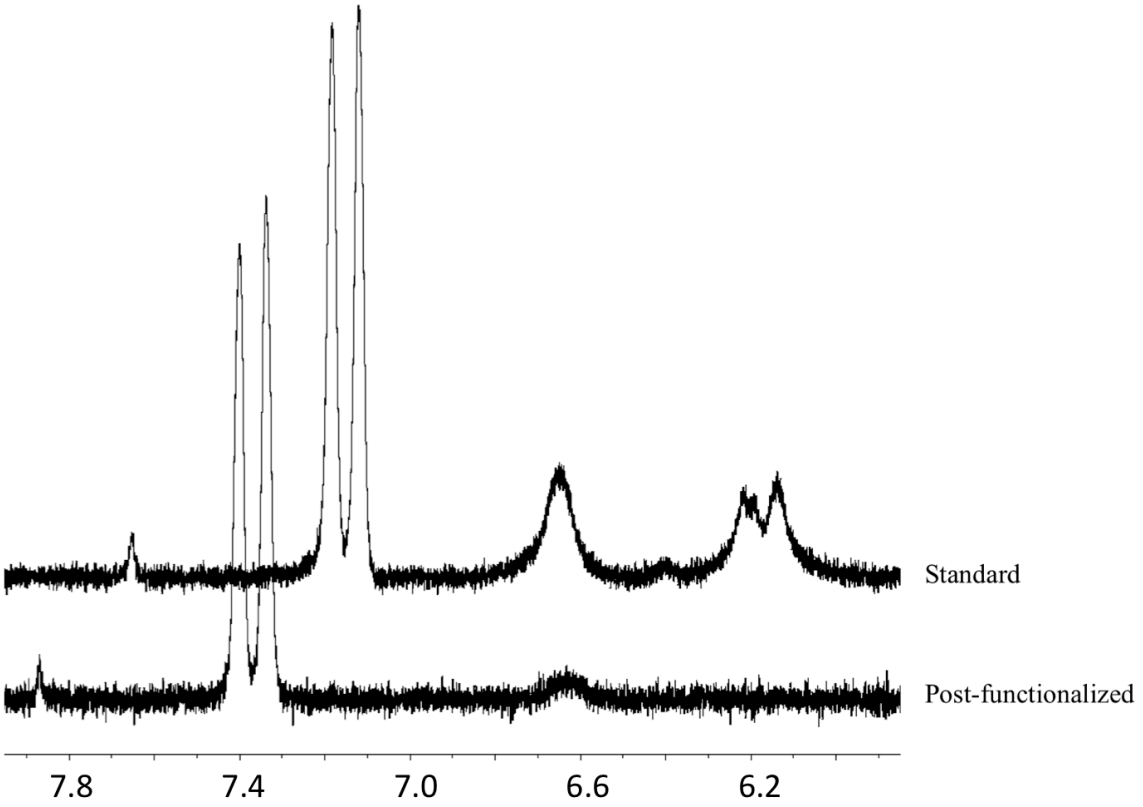

Figure A4.8. Post-functionalization using cysteamine of 50% crosslinked PMM-CVS_{30} 5% w/v HS-PEG-SH. Displayed is a vinyl region horizontal offset of the resulting ^{1}H NMR spectrum, with (standard), and without (post-functionalized) cysteamine addition.

In order to determine the degree of post functionalization via the addition of small molecules, a standard was monitored and no change in integration was seen over the period of post-functionalization (figure A4.8). To integrate the vinyl region of the post functionalized spectrum, both peaks (δ6.8 and δ6.4) were analyzed separately, leaving out the vinylic impurity (δ6.65). The external standard, PHT, can be seen at δ7.4.

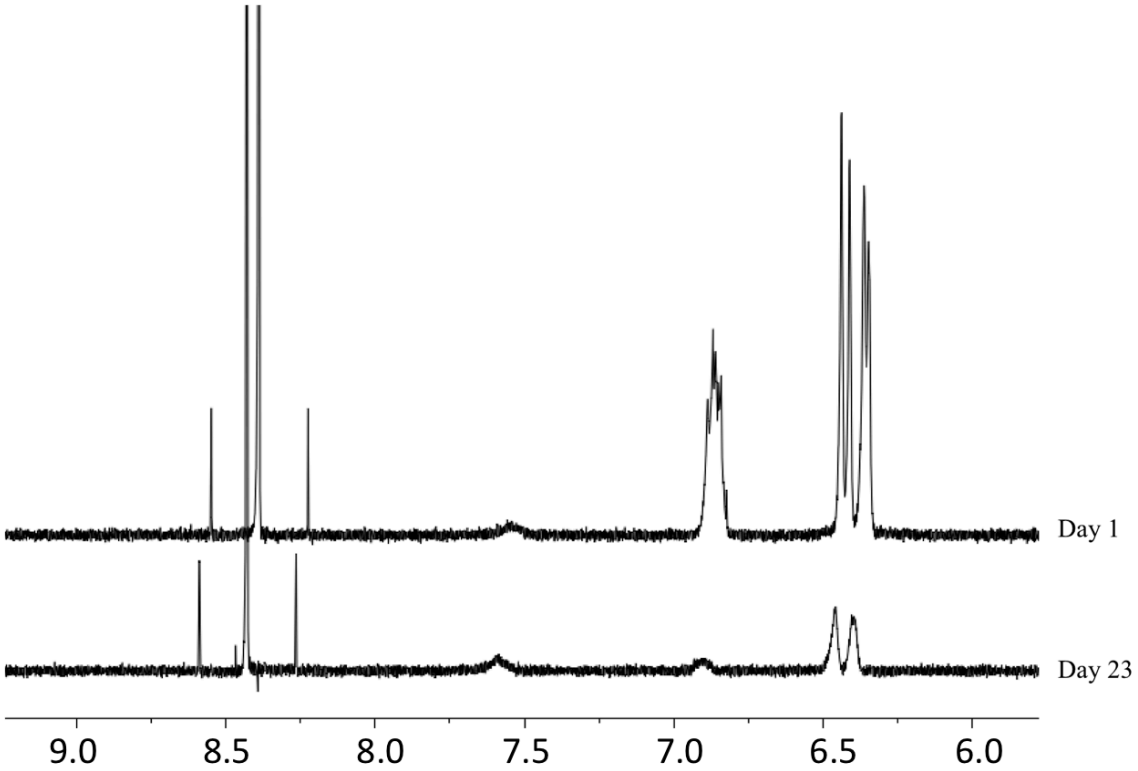

Figure A4.9. Hydration of PMM-CVS_{30} fixed at pD 7.7, with a formic acid standard. Displayed is a vinyl region horizontal offset of the resulting ^{1}H NMR spectrum, at day 1 and day 23.

The hydration of polymer bound vinyl groups was monitored by 1H NMR, over a period of 23 days. Displayed in figure A4.9 are the first and final spectra of the profile, including vinyl signals (δ6.8 and δ6.4), formic acid internal standard (δ8.4) and vinylic impurity (δ7.6).

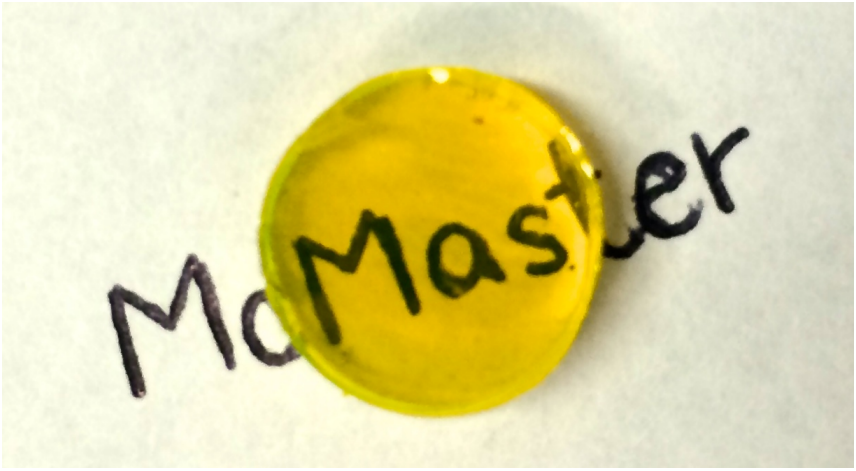

Figure A4.10. Image of as formed PMM-CVS_{30}*f* 5% w/v HS-PEG-SH hydrogel, demonstrating high transparency.

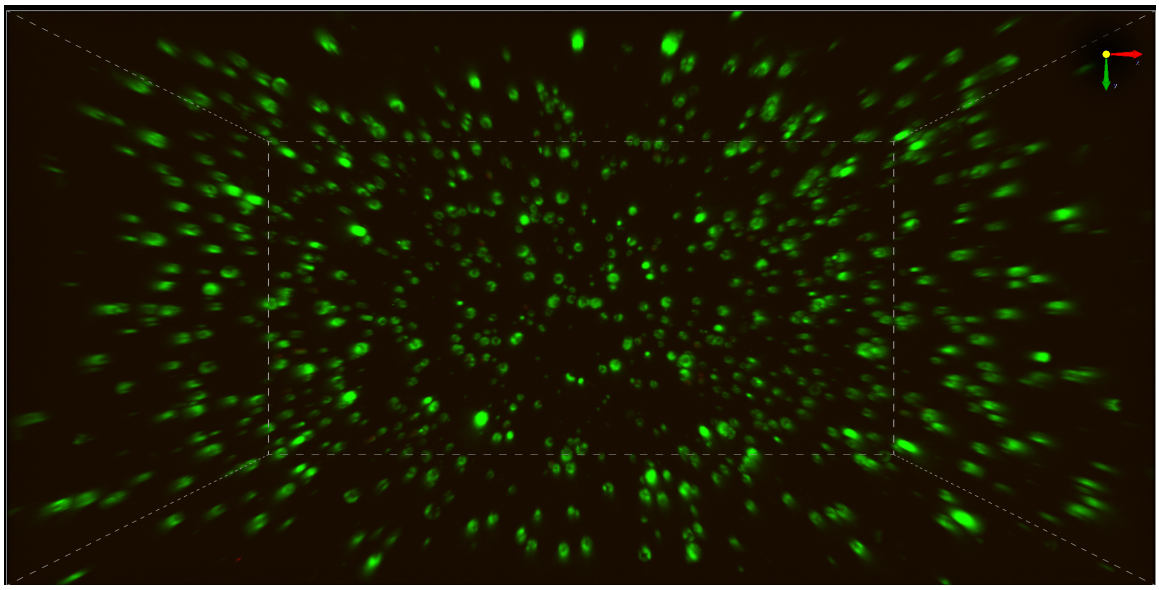

Figure A4.11. 1000 μm thick z-stack obtained using Nikon confocal Ti microscope of the central portion of a 5% w/v PMM-CVS_{20} HS-PEG-SH hydrogel, demonstrating homogeneous distribution of cells throughout the gel.

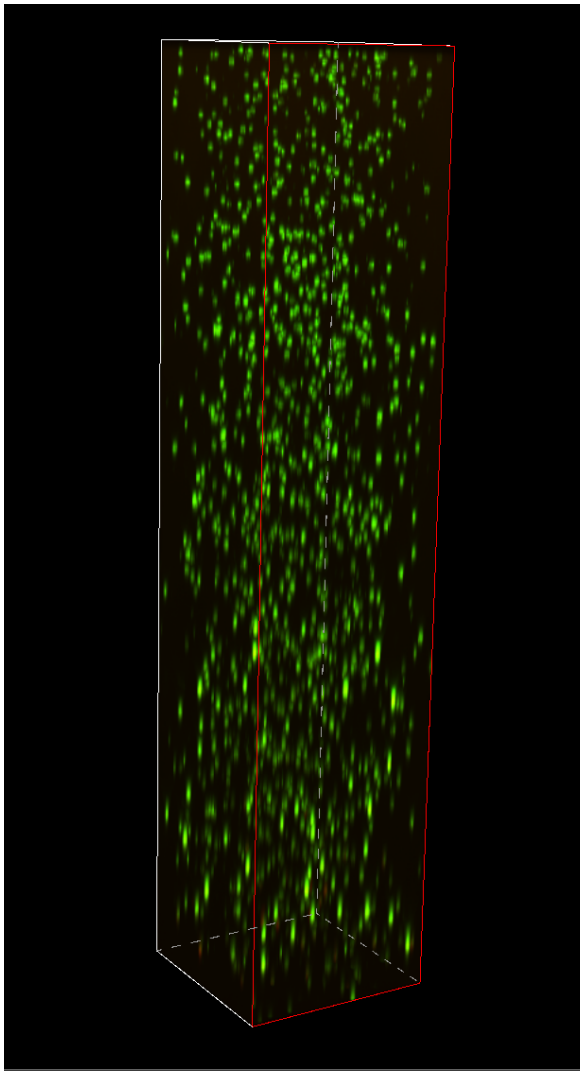

Figure A4.12. 2500 μm thick z-stack obtained using Nikon confocal Ti microscope of the full depth of a 5% w/v PMM-CVS_{20} HS-PEG-SH hydrogel, demonstrating homogeneous distribution of cells throughout the gel.

Chapter 5

Controlled "click" crosslinked hydrogel beads formed through the Michael reaction of polyanions modified with vinyl sulfones and protected thiols, within a calcium alginate template

S. Alison Stewart, Rachelle Lassaline, Nicholas A. D. Burke, Harald D. H. Stöver.

Alison Stewart primarily developed the project and experimental methods, carried out most of the experimental work and contributed to writing the manuscript. Rachelle Lassaline carried out preliminary syntheses, and physical characterization tests on the PMM-CVS/HS-PEG-SH beads. Nicholas Burke and Harald Stöver provided experimental guidance and editing feedback of the manuscript.

5.1. Abstract

This chapter focuses on the preparation, formation and characterization of covalently crosslinked hydrogel beads by thiol-ene coupling between poly(methyl vinyl ether-*alt*-maleic acid) (PMM)-based polyanions with three different thiol-containing polymers. The crosslinking efficiency of calcium alginate-templated PMM-based polymers bearing pendant cysteamine vinyl sulfone moieties (PMM-CVS) with oligomeric PEG-dithiols and with a PMM-based polymer with pendant-protected thiols was compared and the resulting hydrogel beads were studied. An improved synthesis and isolation of cysteamine vinyl sulfone (CVS), used for the preparation of PMM-CVS, is also described. Poly(methyl vinyl ether-*alt*-maleic anhydride) (PMMAn) was reacted with CVS, or 2-pyridylthio cysteamine (SPy), followed by hydrolysis of residual anhydride groups to form vinyl sulfone- or protected thiol-pendant polymers, respectively. Sodium alginate solutions containing PMM-CVS were extruded in droplet form into a calcium chloride gelling bath, and the PMM-CVS was crosslinked with α,ω-dithio-polyethylene glycol (HS-PEG-SH, Mn = 1 kDa and 8 kDa) in varying CVS:thiol ratios. Solutions of sodium alginate containing both PMM-CVS and PMM-SPy were extruded into calcium chloride gelling bath, followed by subsequent exposure to tris(2-carboxyethyl)phosphine (TCEP). TCEP deprotection of the thiols allowed rapid and controllable covalent crosslinking of the beads via a thiol-ene Michael addition. Bead

properties such as swellability in sodium citrate, pore-size and in-diffusion kinetics, and preliminary cell encapsulation experiments are described. While PMM-CVS/HS-PEG-SH beads were found to successfully undergo covalent crosslinking, PMM-CVS/SPy beads demonstrated increased tunability and control, as well as more efficient crosslinking.

5.2. Introduction

Calcium alginate hydrogel beads have served as a platform for many different approaches to cell-based hormone- and enzyme-replacement therapies.[1,2,3,4] Alginate immobilizes the encapsulated cells while preserving their metabolic activities and providing immune protection from the host. The alginate beads allow for in-diffusion of oxygen and nutrients, while allowing out-diffusion of therapeutic agents. However, there are several disadvantages associated with alginate beads. Chelating agents, such as citrate, and anti-gelling cations, such as Na^+, present in biological systems can cause liquefaction of the alginate bead.[5] To circumvent this issue, alginate beads are often coated with poly-L-lysine (PLL) or other polycations to improve capsule strength and control permeability.[6] Polycation coating is typically followed by a final coating of alginate to mask the positive charge on the capsule surface.[7] In spite of their generally good compatibility with both the host and encapsulated cells, capsules based entirely on alginate-PLL-alginate (APA) have drawbacks, including gel weakening by cation loss,[8] and failure of the surface polyelectrolyte complex, leading to exposure of PLL to the immune system[8] and fibrotic overgrowth.[9]

One approach to avoiding the use of polycation coating of alginate beads is incorporation of at least one reactive polymer inside the forming calcium alginate bead.[10,11,12] Introducing covalent crosslinking to the alginate beads can circumvent some of the issues with alginate, such as capsule weakening and degradation due to calcium exchange, resulting in mechanically reinforced capsules,[13,14] and enable longer-term immuno-protection.[15] Covalent crosslinking that occurs in the presence of cells cannot include cytotoxic reagents, monomers, catalysts or by-products, and must occur readily under physiological conditions.

"Click" chemistry is a term for fast and efficient coupling reactions that was introduced by the group of Sharpless in 2001,[16] and that has drawn increased attention in recent years.[17,18,19,20,21] Characteristics of click reactions include simple reaction conditions, commonly use of water as a solvent, absence of toxic byproducts, and high yields without use of a catalyst. Examples include Diels-Alder,[22] copper-free azide-alkyne,[23] and Michael additions.[24] The thiol-ene Michael addition was selected for this work. Thiol-ene Michael additions are typically very rapid, due to the activation of the vinyl group by the adjacent electron withdrawing group.[25,26] Such reactions can be mediated by weak bases, with the resulting thiolate nucleophile reacting with the activated C=C bond.[27] Previous work found that while the Michael addition of a thiol to an activated alkene can occur at weakly acidic pH (6.5) it is greatly accelerated at pHs above 7.0.[28,29,30,31] While maleimide is a very reactive activated alkene in thiol-ene Michael additions, it has been shown to hydrolyse in water under physiological conditions.[32,33,34] To avoid competition between crosslinking and hydrolysis, vinyl sulfone was selected as activated vinyl group due to its good reactivity with thiols, low reactivity with water, and hydrolytically stable thioether sulfone bonds formed.[35,36,37]

Incorporation of two mutually reactive polymers within a calcium alginate bead requires that the crosslinking reaction occur at a slow enough rate for adequate mixing and bead formation, prior to increase in solution viscosity or gelation. The rapid rate of the thiol-ene Michael addition presented a challenge in this regard. Two different approaches were explored in this chapter to circumvent this issue. In the first, one reactive polymer, PMM-CVS, was entrapped in the calcium alginate matrix and crosslinked by subsequent in-diffusion of HS-PEG-SH. Second, PMM functionalized with pendant 2-pyridylthio-protected thiols was co-entrapped in the calcium alginate matrix along with PMM-CVS, with crosslinking between these two polymers within the calcium alginate matrix triggered by subsequent reductive deprotection of the polymeric thiols using TCEP (scheme 5.1).

Bead physical properties were found to be highly dependent on both loading percentage of PMM-CVS and PMM-SPy, as well as functionalization percentage of the polymers. The use of protected thiols enabled mixing of both reactive polymers with no

reaction until the disulphide bonds are cleaved, allowing for excellent control over the crosslinking reaction.

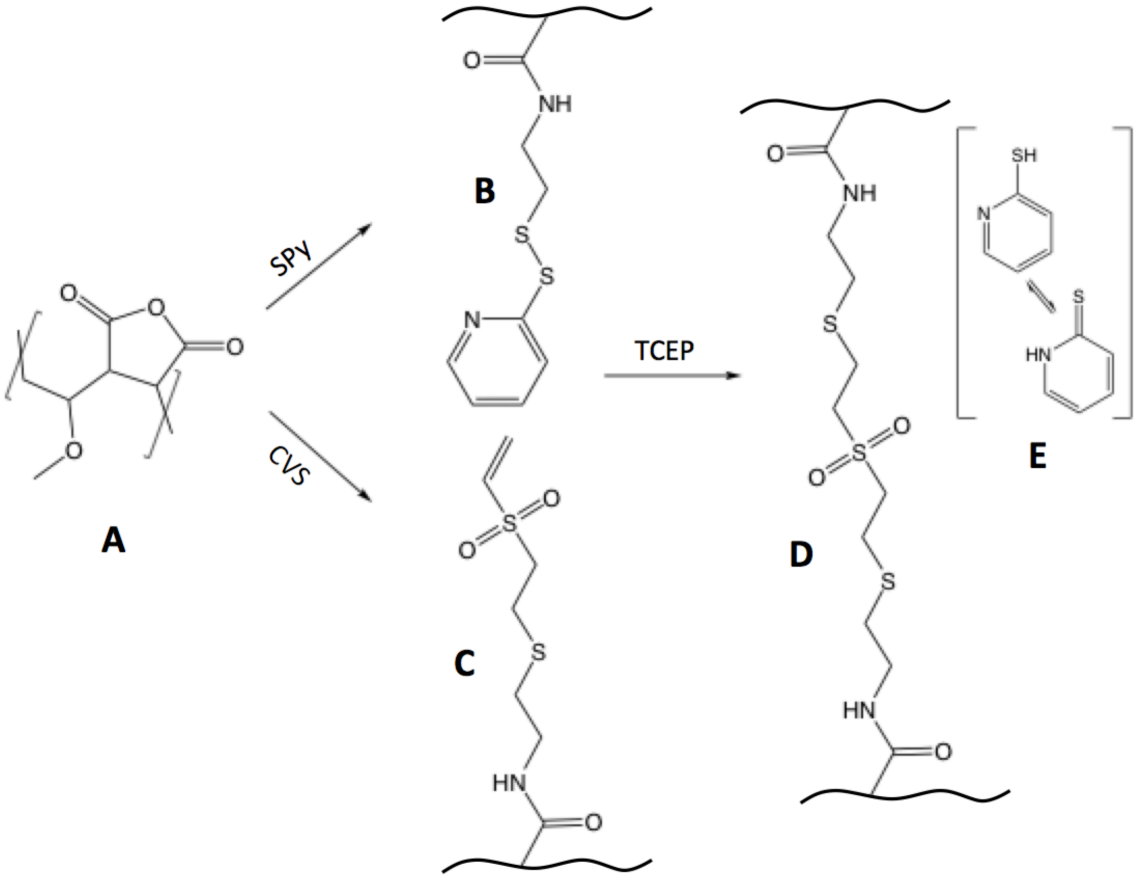

Scheme 5.1. Synthesis of PMM-CVS (C) and PMM-SPy (B) from PMMAn (A). Treatment of PMM-SPy with TCEP results in reduction of the disulphide linkage and Michael addition covalent crosslinking between the free thiols on PMM-SPy and the vinyl sulfones on PMM-CVS (D). 2-mercaptopyridine tautomerizes (E), preventing its participation in the Michael addition with PMM-SPy during crosslinking.

The focus of this chapter is on the development of a rapidly crosslinkable hydrogel network based on the thiol-ene Michael addition reaction. An improved synthesis of CVS, preparation of the reactive polymers, characterization of key physical and chemical properties of the resulting matrix beads, and proof-of-concept of cell encapsulation are described.

5.3. Experimental Section

5.3.1. Materials

Poly(methyl vinyl ether-*alt*-maleic anhydride) (PMMAn, M_n = 80kDa, Sigma-Aldrich, Oakville, ON) was heated in a vacuum oven at 140 °C for 5 days to ensure that it was completely in the anhydride form.[38] Divinyl sulfone (97%), fluoresceinamine, triethylamine, 4-(2-hydroxyethyl)-1-piperazineethanesulfonic acid (HEPES) sodium salt (≥ 99.5%), tris(2-carboxyethyl)phosphine hydrochloride (TCEP) (≥ 98%), silica gel (technical grade, pore size 60 Å, 230 – 400 mesh particle size, 40 – 63 μm particle size) and fluorescein isothiocyanate-conjugated dextran (dextran-*f*; 10, 70, 250, 500 kDa) were purchased from Sigma Aldrich (Oakville, ON) and used as received. Polyethylene glycol dithiol (M_n = 1 kDa) and polyethylene glycol dithiol (M_n = 8 kDa) were purchased from Creative PEGWorks. 2-pyridylthio cysteamine (SPy) (98%), cysteamine hydrochloride (98+%) and di-*tert*-butyl dicarbonate (97+%) were purchased from Alfa Aesar and used as received. Sodium chloride, acetonitrile, chloroform, dichloromethane, dimethylsulfoxide, methanol and calcium chloride dihydrate were used as received (Reagent, Caledon Laboratories, Caledon, ON). Sodium alginate (Pronova UP MVG, batch no. FP-610-03) was purchased from NovaMatrix (Sandvika, Norway) and used as received. Tri-sodium citrate dihydrate was purchased from EMD Chemicals. Deuterium oxide (99.99 atom% D) was purchased from Cambridge Isotope Laboratories. Tetramethylrhodamine 5- (and 6-) carboxamide cadaverine (TAMRA-cadaverine) was purchased from AnaSpec Inc.

5.3.2. Synthesis of cysteamine vinylsulfone HCl

1.0 g cysteamine HCl (8.8 mmol) was dissolved in 10 mL water and added dropwise through an addition funnel to a stirring solution of divinyl sulfone (5.0 mL, 50.0 mmol, 5.6x molar excess). The biphasic mixture was allowed to react at room temperature for 6 h, and was then extracted once with 40 mL $CHCl_3$, followed by 5x 20 mL $CHCl_3$. The aqueous phase was dried with sodium sulphate and then lyophilized to give a viscous oil. The oil was dissolved in 10 mL of MeOH to give a saturated solution, followed by addition of 90 mL of dry DCM. The precipitate was filtered out and discarded. The MeOH/DCM mixture containing the product was passed through a 1 cm

silica plug using 800 mL of 10% MeOH in DCM. The collected fraction was taken to dryness on a rotary evaporator to give the product, CVS HCl, as a waxy white solid with 77% yield. The product was characterized via ^{1}H NMR: δ 6.85 (1H), δ 6.43 (1H), 6.36 (1H), δ 3.52 (2H), δ 3.19 (2H), δ 2.92 (2H) and δ 2.87 (2H).

5.3.3. Synthesis of PMM-CVS and PMM-SPy with 10-30 mol% CVS and SPy

PMM-CVS12 was prepared by dissolving PMMAn (0.250 g, 1.6 mmol anhydride) in 10 mL of acetonitrile, followed by addition of triethylamine (TEA) (150 μL, 0.1088 g 1.1 mmol). CVS (45 mg, 0.24 mmol, 15 mol% relative to anhydride groups on PMMAn) dissolved in 5 mL 1:1 (v/v) DMSO:acetonitrile and was added dropwise over a few minutes to the stirring solution. The reaction was left mixing for 24 h at room temperature, followed by dialysis (Spectrapor, MWCO = 3500 Da) against 4 L of 0.05 M NaCl for 1 day and then against 4 L distilled water for 3 days, changed daily. The dialyzed solution was then lyophilized, leading to the isolation of PMM-CVS10 as a white powder, with yields >90%. ^{1}H NMR in D_2O on a Bruker AV600 NMR Spectrometer was used to determine the degrees of functionalization, using the CVS vinyl signals (δ 6.25 - 7.0 3H), referenced to the methylene signal on the polymer backbone (δ 1.8, 2H). PMM-CVS20 and PMM-CVS30 were prepared in an analogous manner. PMM-CVS14 and PMM-CVS22 was labelled with fluorescein amine and TAMRA-cadaverine as previously described.[31]

PMM-SPy12 was prepared by dissolving PMMAn (0.250 g, 1.6 mmol anhydride) in 10 mL of acetonitrile, followed by addition of triethylamine (TEA) (150 μL, 0.1088 g 1.1 mmol). SPy (53.6 mg, 0.24 mmol, 15 mol% relative to anhydride groups on PMMAn) dissolved in 5 mL 1:1 DMSO:acetonitrile and was added dropwise over a few minutes to the stirring solution. The reaction was left mixing for 24 h at room temperature, followed by dialysis (Spectrapor, MWCO = 3500 Da) against 4 L of 0.05 M NaCl for 1 day and then against 4 L distilled water for 3 days, changed daily. The dialyzed solution was then lyophilized, leading to the isolation of PMM-SPy10 as a white powder with yields >90%. ^{1}H NMR in D_2O on a Bruker AV600 NMR Spectrometer was used to determine the degrees of functionalization, using the SPy vinyl signals (δ 7.0 – 8.4, 4H), referenced to

the methylene signal on the polymer backbone (δ 1.8, 2H). PMM-SPy19 and PMM-SPy30 were prepared in an analogous manner.

5.3.4. Preparation of PMM-CVSx/HS-PEG-SH Alginate-Templated Beads

Beads were prepared at various functional group loadings and polymer concentrations. The following is the procedure for preparation of 1% w/v PMM-CVS21 beads with a 4:1 thiol:CVS ratio. Sodium alginate (75 mg, 1.5% w/v) was dissolved in 5 mL of 100 mM HEPES buffer solution and filtered through a 0.45 μm, followed by a 0.20 μm, syringe filter. PMM-CVS21 (10 mg) was dissolved in 250 μL of 100 mM HEPES buffer solution. 750 μL of the alginate solution was added to the PMM-CVS_{20} solution. The resulting 1 mL solution, containing 1% w/v PMM-CVS21 and 1.125% w/v alginate, was extruded through a 27-gauge needle at a flow rate of 0.5 mL/min into 50 mL of a 100 mM $CaCl_2$/77 mM NaCl gelling bath. The beads were allowed to settle in the gelling bath for approximately 10 minutes before being removed by a plastic pipette and placed in a conical vial with 3 mL gelling bath. Approximately 50% of the beads were placed in a glass vial and the supernatant removed. A 1 mL solution of HS-PEG-SH (1 kDa) (38.2 mg, 4 x molar excess relative to CVS) was added to the vial. After 24 hours the beads were washed five times with 5 mL gelling bath. This was repeated with 4 different concentrations of 1 kDa HS-PEG-SH solution, resulting in 4:1, 3:1, 2:1 and 1:1 ratios of thiol:vinyl sulfone.

Additional sets of beads were prepared using 8 kDa HS-PEG-SH at 1% w/v PMM-CVS as well as 1 kDa HS-PEG-SH at 2% w/v PMM-CVS, according to the above procedure.

5.3.5. Determination of PMM-CVS/HS-PEG-SH Alginate-Templated Bead Swelling Ratio

Approximately 50 beads were divided between five wells in a 48-well plate. Bead diameter was measured using a Nikon eclipse Ti inverted fluorescent microscope. Supernatant was removed from the wells using a glass pipette, and replaced with 0.3 mL 75 mM sodium citrate solution. Bead diameter was again measured at 1, 2, 10, 20, 40 and 60 minutes after citrate addition. Citrate swelling ratios were calculated by dividing the

average bead diameter at 60 minutes by the average bead diameter before citrate addition (t=0 min). This was repeated for all sets of PMM-CVS/HS-PEG-SH beads.

5.3.6. Preparation of Calcium Alginate-templated PMM-CVS$_x$/SPy$_y$ Beads

A solution of sodium alginate (1.2% w/v) in HEPES buffered saline (800 μL, 50 mM HEPES, pH 7.4) was added to a 200 μL solution of PMM-CVS (5 - 15 mg, 0.5 – 1.5% w/v) and PMM-SPy (5 – 15 mg, 0.5 – 1.5% w/v) in HEPES buffered saline, to give final concentrations of 1% w/v sodium alginate, and 0.5 - 1.5% w/v each of PMM-CVS and PMM-SPy. The solution was briefly vortexed to ensure complete mixing, then air-sheared through a 27 gauge needle into 50 mL of HEPES buffered gelling bath containing 50mM HEPES, 0.45% w/v (77 mM) NaCl and 1.1% w/v (100 mM) $CaCl_2$ (pH 7.4) using a syringe pump set to a flow rate of 0.5 mL/min. A dense suspension of the resulting beads (ca. 1 mL) were collected, the gelling bath was removed and replaced with gelling bath containing TCEP (20 x molar excess compared to SPy, 50mM HEPES, 0.45% w/v (77 mM) NaCl, 1.1% w/v (100 mM) $CaCl_2$, pH 7.4). After 10 minutes in the TCEP solution, the supernatant was removed and the beads were rinsed 1 x with 5 mL of HEPES buffered gelling bath, followed by 2 x 5 mL saline and stored at 37 °C in 50 mL of saline solution. Bead diameter was measured (n = 20) using an upright optical microscope in brightfield mode and a 5 x objective lens.

Table 5.1. Moles of disulphide bonds (S-S) and TCEP used

Polymer	Loading% (each)	mol S-S	mol TCEP	mass TCEP (mg)
CVS12/SPy12	0.5%	2.65×10^{-6}	5.3×10^{-5}	15.2
CVS12/SPy12	1.0%	5.30×10^{-6}	1.06×10^{-4}	30.3
CVS12/SPy12	1.5%	7.95×10^{-6}	1.59×10^{-4}	45.6
CVS21/SPy19	0.5%	4.86×10^{-6}	9.5×10^{-5}	27.9
CVS21/SPy19	1.0%	9.73×10^{-6}	1.90×10^{-4}	55.8
CVS21/SPy19	1.5%	14.6×10^{-6}	2.85×10^{-4}	83.7
CVS32/SPy30	0.5%	6.5×10^{-6}	1.35×10^{-4}	38.7
CVS32/SPy30	1.0%	1.30×10^{-5}	2.70×10^{-4}	77.3

CVS32/SPy30	1.5%	1.95×10^{-5}	4.05×10^{-4}	116

5.3.7. Effect of TCEP Concentration and Exposure Time on Bead Crosslinking

Beads composed of 1.0% w/v alginate and 1.0% w/v each PMM-CVS21 and PMM-SPy19 were prepared using the standard procedure, detailed above. The gelling bath was removed 10 minutes after extrusion was complete, and replaced with TCEP in HEPES-buffered gelling bath in 10, 20, 30, 40 and 50 x molar excess TCEP (compared to SPy units) in 50 mL of gelling bath. At set time-points, 0.1 mL of beads were removed from the TCEP gelling bath and rinsed once with 1 mL HEPES-buffered gelling bath and twice with 1 mL saline (0.9% NaCl). Bead diameters were measured on a microscope set to brightfield (n = 20). The supernatant was then removed and replaced with 1 mL of sodium citrate (70 mM) and incubated at 37 °C for 1 h. The bead diameters were measured post-citrate extraction (n = 20) and the ratio was used to determine the degree of swelling. Control beads that were not exposed to TCEP were also rinsed once with 1 mL HEPES-buffered gelling bath and 2 x 1 mL saline, incubated, and then treated with sodium citrate.

Table 5.2. TCEP concentrations

xs TCEP	**Amount TCEP (mmol)**	**Mass TCEP (mg)**	**Volume (mL)**	**Concentration (mM)**
10 x	0.0972	27.9	50	1.94
20 x	0.194	55.8	50	3.88
30 x	0.292	83.7	50	5.84
40 x	0.389	111.6	50	7.78
50 x	0.486	140.0	50	9.72

5.3.8. Measurement of Covalent Crosslinking Efficiency using Sodium Citrate

Beads composed of 1.0% alginate and varying loading percentages of PMM-CVS/SPy were prepared as described above, and treated with a 20 x excess of TCEP for

10 minutes. TCEP supernatant was then removed and beads were rinsed 1 x with 5 mL HEPES-buffered gelling bath, followed by 2 x 10 mL saline. Bead diameters were measured using a microscope on transmitted light mode (n = 20). Approximately 300 beads were then placed into a glass vial, and the supernatant was removed. The beads were rinsed with 1 mL of sodium citrate, which was then removed and replaced with 3 mL of fresh sodium citrate. The beads were gently agitated for 4 h and then observed and measured using the transmitted light setting on the microscope, or a confocal microscope (n = 20).

5.3.9. Study of Bead Permeability Using Fluorescently Labelled Dextrans

The permeability of PMM-CVS/SPy beads was investigated using fluorescently labelled dextrans of varying molecular weights (10 kDa, 70 kDa, 250 kDa, 500 kDa). The beads were prepared as described above and allowed to incubate at 37 °C for 24 h to ensure complete covalent crosslinking of the beads. Approximately 150 μL of concentrated bead suspension was removed and placed into a 2 mL conical vial. 1 mL of sodium citrate (70 mM) was added to the suspension and the vial was gently agitated then stored at 37 °C for 24 h to ensure complete liquefaction of the calcium alginate template. Approximately 50 beads were then removed from the vial and placed into a well in a 96-well plate and 100 μL of fluorescently labelled dextran (0.05% w/v) in HEPES buffered saline was added. Beads were allowed to incubate at 37 °C for 24 h.

Beads were imaged using a Nikon confocal microscope and the fluorescent intensity from approximately the central 25% of the beads (n = 4), as well as from the surrounding fluorescent solutions (n = 4), were obtained using NIS-Elements (Nikon) software and the ratio was determined.

5.3.10. Kinetic Permeability Study

Matrix bead permeability was evaluated using dextran-*f* of varying molecular weights (10 kDa, 70 kDa, 250 kDa, 500 kDa). Beads composed of 1.0% w/v alginate and 1.0% w/v PMM-CVS21/SPy19 were treated with sodium citrate as described above to liquefy the alginate scaffold. Approximately 50 beads were then removed from the citrate solution and placed into a well in a 96-well plate and 100 μL of fluorescently

labelled dextran (0.05% w/v) in HEPES buffered saline was added. Beads were imaged at set time-points using a Nikon confocal microscope and the fluorescent intensity from approximately the central 25% of the beads (n = 4), as well as from the surrounding fluorescent solutions (n = 4), were obtained using NIS-Elements (Nikon) software and the ratio was determined.

5.3.11. Photobleaching of PMM-CVS/PMM-SPy Alginate-Templated Beads

PMM-CVS22*r*/SPy19 alginate-templated beads were prepared as described above, at a 1.0% w/v polymer loading. Approximately 10 beads were placed in one well of a 48-well plate. 0.3 mL of 70 mM sodium citrate solution was added to the well, and the beads were allowed to sit for 1 h. The beads were imaged on a Nikon Eclipse Ti confocal microscope and a small region of the bead interior was photobleached by focusing the microscope on one region and increasing the laser intensity. The laser intensity was returned to normal settings and the bead was imaged at 1, 10, 20, 30, 40, 50 and 60 minutes after photobleaching.

5.3.12. NIH 3T3 Cell Encapsulations

NIH-3T3 fibroblasts were cultured in tissue culture flasks in Dulbecco's Modified Eagle Medium (DMEM) supplemented with 10% v/v Bovine Calf Serum (BCS) and 1% v/v Penicillin/Streptomycin (PS) in a 5% CO_2 environment at 37 ^{o}C with 100% humidity in a water-jacketed incubator. When 75-80% confluency was reached, cells were washed with PBS (pH 7.4, Invitrogen) and detached using 0.25% Trypsin-EDTA (1X) phenol red.

Preliminary cell encapsulations were carried out under non-sterile conditions. A solution of PMM-CVS/SPy in HEPES-buffered saline was added to sterile filtered (0.2 μm) alginate (2% w/v) along with a NIH 3T3 *Mus musculus* fibroblasts cell suspension in HEPES-buffered saline to give a final concentration of approximately 2 million cells/mL, 1% w/v alginate and 1% w/v each PMM-CVS and PMM-SPy. This solution was kept on ice and beads were prepared as described above by shearing the alginate solution through a 27 gauge flat tipped needle into a HEPES-buffered $CaCl_2$ gelling bath. Beads were then exposed to 50 mL of sterile filtered (0.2 μm) TCEP in gelling bath (20 x molar excess), as described above. After 10 minutes in the TCEP solution, the supernatant was

removed and the beads were rinsed 1 x with 5 mL of sterile filtered (0.2 μm) HEPES buffered gelling bath, followed by 2 x 5 mL sterile filtered (0.2 μm) saline. Approximately 0.3 mL of dense bead suspension from each gelling bath was transferred to conical vials and washed once with media before being transferred to a 24-well plate and diluted with 2 mL of media. Cells were incubated at 37 °C with 5% CO_2 for 24 h. Control beads containing 1% w/v alginate and 2 million cells/mL 3T3 cells were prepared in an analogous fashion.

After encapsulation and subsequent incubation, fluorescent Live/Dead cell staining was used to determine positioning of the encapsulated cells. Calcein AM/EthD-1 solution (50 μL of 2 μM calcein AM and 4 μM EthD-1 in sterile HEPES-buffered saline) was added to each well and incubated at room temperature for 20 minutes. 2 drops of NucBlue Live Reagent (ThermoFisher Scientific) were added for every 1 mL of bead solution, and then incubated for 20 minutes at room temperature in the dark. A 5 mg/mL 4',6-diamidino-2-phenylindole dihydrochloride (DAPI, ThermoFisher Scientific) solution was prepared by addition of 2 mL of distilled water to a vial of DAPI (10 mg), followed by sonication until all DAPI was dissolved. The stock solution was diluted with HEPES buffered saline to 300 nM, and 50 μL was added to encapsulated beads in one well of a 96-well plate. The solution was allowed to incubate at room temperature for 5 minutes, in the dark, followed by removal of the staining solution and rinsing with HEPES-buffered gelling bath. Fluorescence images were obtained using a Nikon Eclipse Ti confocal microscope.

5.4. Results and Discussion

5.4.1. Synthesis of CVS HCl

We recently reported the first synthesis and isolation of pure CVS, using a time consuming process with two 24 h reactions followed by workup using a silica column.[31] In the present work, the synthesis of CVS was simplified by conducting a biphasic reaction between aqueous cysteamine HCl and neat DVS. Here, protonation protects the amine on cysteamine from undergoing a competing Michael addition with DVS, while the biphasic reaction and excess DVS limits the formation of disubstituted vinyl sulfone.

Chloroform was used to extract unreacted DVS, and byproduct, which is attributed to disubstituted vinyl sulfone, is removed as a precipitate followed by a simple passage through a silica plug. CVS HCl was isolated as a waxy solid, containing 12% water by ^{1}H NMR, in 77% yield. The synthesis can be completed within 24 h and does not involve a silica column for purification.

5.4.2. PMM-CVS/HS-PEG-SH Alginate-Templated Matrix Beads

A solution of 1.125% w/v sodium alginate and variable concentrations of PMM-CVS were extruded through a needle. Droplets were sheared off using concentric airflow, and then collected in a buffered calcium ion gelling bath. The ionic crosslinking of alginate in the presence of Ca^{2+} formed a gel-scaffold for the subsequent thiol-ene Michael crosslinking between PMM-CVS and a HS-PEG-SH crosslinker. The polyanionic nature of PMM-CVS allowed for entrapment of the polymer within the alginate bead before covalent crosslinking, as the anionic PMM backbone interacts with Ca^{2+} cations, as previously reported.[32,39]

After 24 h incubation in a 1000 Da HS-PEG-SH solution, at ratios between 1:1 to 4:1 of thiol:CVS, chelation of Ca^{2+} with 70 mM sodium citrate did not result in bead dissolution. PMM-CVS/HS-PEG-SH beads formed using all but two compositions remained intact after calcium chelation and subsequent alginate liquefaction. Bead diameter was measured both before and 1 h after an excess of citrate was added, to calculate the citrate swelling ratios shown in figure 5.1.

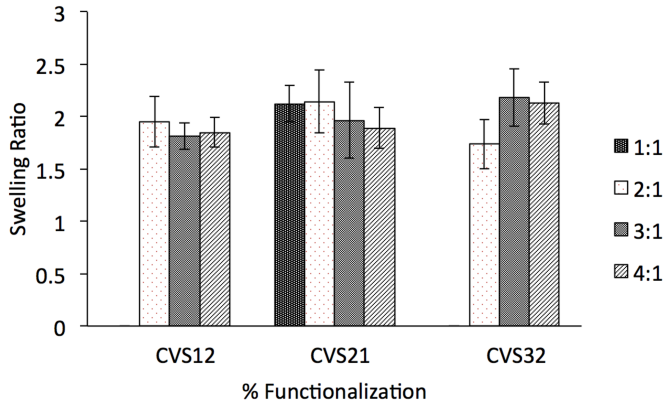

Figure 5.1. Swelling ratios of 1.125% w/v alginate 1000 Da HS-PEG-SH/PMM-CVS$_x$ beads over a series of CVS functional percentages and crosslinker concentrations (1:1, 2:1, 3:1 and 4:1 thiol:CVS).

It was expected that increased degree of CVS functionalization and crosslinker concentration would lead to increased crosslink density, and hence lower citrate swelling ratios. As seen in figure 5.1, citrate swelling ratios for intact beads did not vary significantly with degree of functionalization or crosslinker amount. Two samples, PMM-CVS12 with 1:1 HS-PEG-SH and PMM-CVS32 with 1:1 HS-PEG-SH, were insufficiently crosslinked to maintain a cohesive bead after the alginate scaffold was removed.

The swelling ratio of beads containing 1% w/v PMM-CVS with an 8000 Da HS-PEG-SH crosslinker were also determined. The capsules remained intact after Ca^{2+} removal by citrate at all CVS functionalization percentages and thiol:CVS ratios and again did not display a significant difference in swelling ratio (figure A5.6). Beads were also made at 2% w/v PMM-CVS with a 1000 Da HS-PEG-SH crosslinker. Again, beads maintained their capsule integrity at all CVS percent functionalization and thiol:CVS concentration ratios (figure A5.7). The CVS percent functionalization had an impact on swelling ratio in this case, as a significant decrease in swelling ratio was seen when comparing the PMM-CVS12 beads to PMM-CVS21 beads. It was again seen that the ratio of thiol:CVS concentration had no effect on swelling ratio.

While the PMM-CVS/HS-PEG-SH beads demonstrated successful covalent crosslinking via the Michael addition reaction, there were a number of considerations.

The beads were required to incubate in a solution of HS-PEG-SH while the crosslinker diffused into the beads, necessitating longer crosslinking times (up to 24 h). There was also a lack of effect of PMM-CVS composition and HS-PEG-SH crosslinker ratio on the citrate swelling ratios. It is hypothesized that this may be due to i) the hydrophilic nature of PEG and ii) low PMM-CVS concentration (1% w/v relative to 2.5 – 7.5% w/v for bulk hydrogels) resulting in inefficient crosslinking between polymer chains due to the bifunctional nature of the PEG-crosslinker.

Designing a thiol-ene click crosslinked bead to circumvent these issues provided a unique challenge. A thiol-containing polymer cannot be directly incorporated into a sodium alginate solution with PMM-CVS due to a rapid reaction rate that would interfere with extrusion and bead formation. To circumvent this issue, a protected thiol, SPy, was incorporated into PMM to form a polymer with pendant thiols that are unreactive in the presence of PMM-CVS, until exposed to a reducing agent such as TCEP.

5.4.3. Preparation of alginate-templated PMM-CVS and PMM-SPy matrix beads

PMMAn was functionalized with either CVS or SPy to form PMM-CVS and PMM-SPy respectively. The use of PMM as a common polymeric backbone for both thiol– and –ene–bearing polymers allowed for exploitation of the affinity of PMM for divalent cations, ensuring immobilization within the alginate scaffold.

Table 5.3. DS of PMM-CVS_x and PMM-SPy_y[a]

	DS	DS fluorophore
modified PMM	actual (target)	actual (target)
CVS12	12 (15)	N/A
CVS21	21 (30)	N/A
CVS32	32 (45)	N/A
CVS14*f*	14 (15)	0.31 (0.5)
CVS22*r*	22 (25)	0.14 (0.2)
SPy12	12 (15)	N/A
SPy19	19 (25)	N/A
SPy30	30 (35)	N/A

[a] "*r*": rhodamine-cadaverine labelled; "*f*": fluorescein labelled.

Matrix beads were prepared by extruding a solution of 1% w/v sodium alginate and 0.5 – 1.5% w/v PMM-CVS/SPy into a HEPES-buffered saline $CaCl_2$ gelling bath. Alginate ionically gels in the presence of divalent cations such as Ca^{2+}, providing a temporary template for the reactive polymers. The supernatant was removed and beads were then exposed to a solution of TCEP, a reducing agent that cleaves the disulphide bond in SPy, resulting in a free thiol that rapidly participates in the thiol-ene Michael addition with CVS.

Matrix beads were found to be of similar size and shape to those formed with alginate alone, indicating that PMM-CVS / PMM-SPy do not interfere with alginate gelation. It was noted that as the functionalization percentage and the loading percentage of reactive polymers increased, the opacity of the beads decreased. This is likely due to some phase separation or salting out of the reactive polymers. PMM is known to interact with Ca^{2+} [39] and this, coupled with charge shielding, may increase the hydrophobicity of the reactive polymers. Previous bulk experiments showed phase separation upon mixing of alginate and PMM-CVS32 solutions on a microscope slide (figure A5.9),[40] supporting the increased opacity observed as functionalization percentage and polymer loading percentage increases.

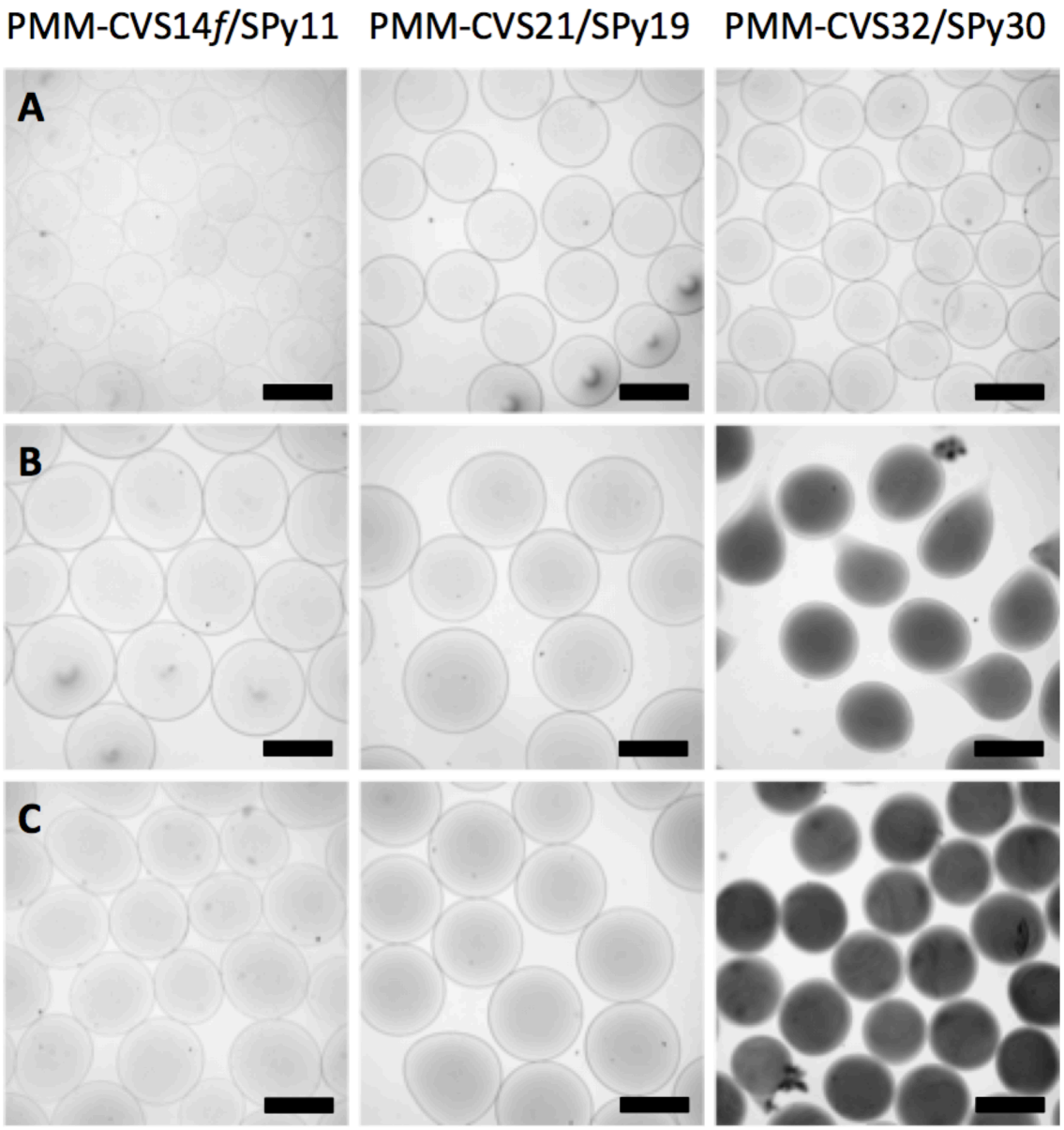

Figure 5.2. Matrix beads composed of 1% w/v alginate and PMM-CVS/SPy at 0.5% w/v (A), 1.0% w/v (B) and 1.5% w/v (C) loading percentages. Note the increased opacity for 1.0% w/v and 1.5% w/v PMM-CVS32/SPy30. Scale bars are 500 μm. Images were obtained using a Nikon upright microscope on transmitted light mode 5 x lens.

5.4.4. Effect of TCEP concentration and exposure time on covalent crosslinking of matrix beads

While the thiol-ene Michael addition occurs rapidly, it cannot occur until TCEP has cleaved the disulphide linkages on PMM-SPy. It was of interest to characterize the effect of TCEP concentration and exposure times to determine the optimal conditions for deprotection of SPy. To evaluate the effects of TCEP concentration and exposure time on crosslinking, beads composed of 1.0% w/v alginate and 1.0% w/v each PMM-CVS21/SPy19 were exposed to 5 different concentrations of TCEP (10, 20, 30, 40 and 50x molar excess, with respect to disulphide bonds in PMM-SPy) for 10, 20, 30, 40 and 60 minutes. After exposure, beads were rinsed with gelling bath and saline, and bead diameters were measured before and after citrate exposure. It was found that for a 10 x excess of TCEP, the exposure time made a significant difference in the swell ratio, with swelling decreasing as the beads were exposed to TCEP for longer times. A 20 x excess was found to have a similar impact on swelling regardless of the amount of time beads spent exposed to the TCEP solution, indicating that at this concentration, TCEP rapidly reduced the disulphide linkages and allowed for covalent crosslinking. As the TCEP concentrations increased to 30 – 50 x excess, the beads exhibited a greater degree of swelling that increased with TCEP exposure time. Based on these findings, a molar excess of 20 x TCEP was selected for crosslinking beads due to disulphide cleavage being complete within 10 minutes, allowing for short exposure time of beads to TCEP solutions.

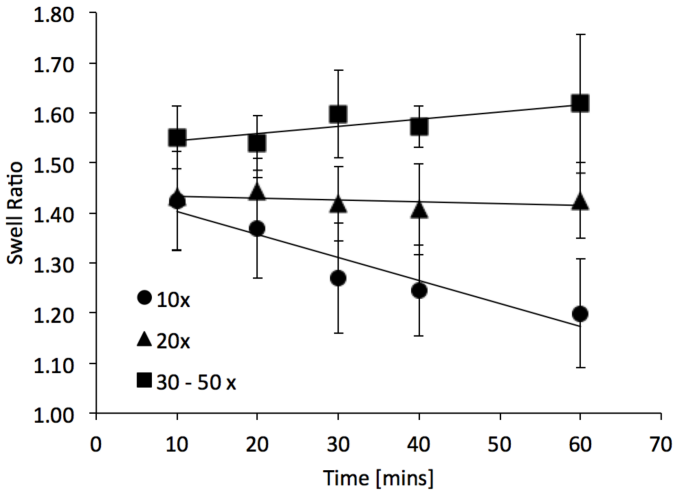

Figure 5.3. Bead swell ratios as function of exposure time to TCEP, for 10x, 20x, and 30 - 50x excess TCEP.

5.5.5. Bead swellability

In order to examine the degree of swelling upon citrate extraction of calcium as a function of bead composition, beads were exposed to citrate and the bead diameter was measured both before and after exposure. The matrix beads were then exposed to a 20 x molar excess solution of TCEP for 10 minutes, followed by rinsing with gelling bath and saline. Beads were then treated with a large excess of sodium citrate and gently agitated for several hours to ensure complete chelation of calcium from the beads. Beads composed of 0.5% PMM-CVS14*f*/SPy12 did not withstand calcium chelation, indicating that there were not enough functional groups present to provide adequate amounts of covalent crosslinking. While beads composed of 1.0% and 1.5% w/v PMM-CVS14*f*/SPy12 did not experience complete dissolution, they did swell significantly, and many beads broke. The refractive index of the swollen beads was almost identical to water, making it necessary to image the beads using fluorescence microscopy. Beads composed of 0.5, 1.0 and 1.5% w/v PMM-CVS21/SPy19 all remained intact after citrate treatment, although the 0.5% w/v beads became weak and easily deformable. All three compositions remained intact for PMM-CVS32/SPy30, and the opacity apparent in the 1.0% and 1.5% w/v beads decreased after citrate treatment, perhaps due to decreased charge shielding and increased swelling.

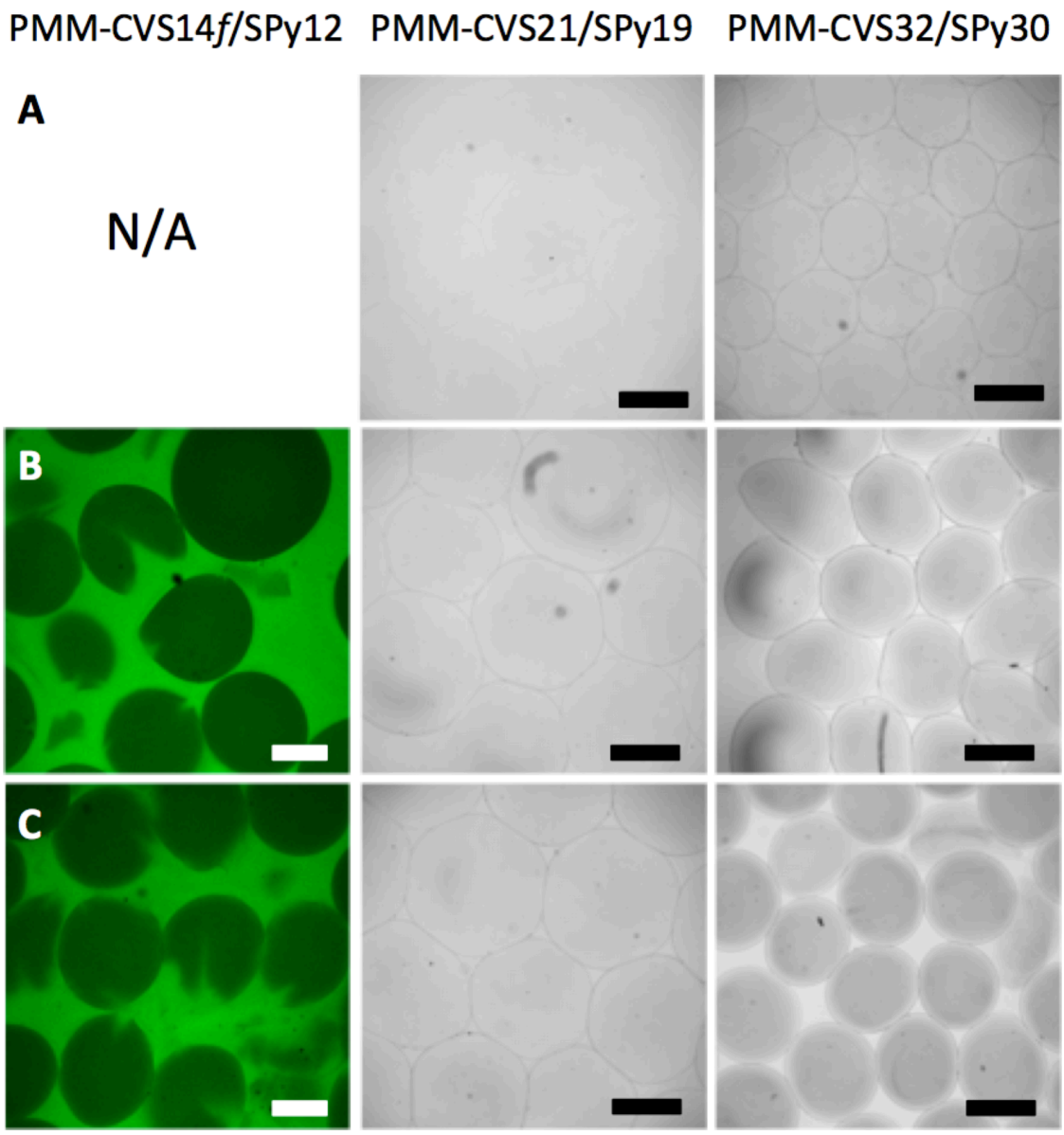

Figure 5.4. Matrix beads composed of PMM-CVS/SPy at 0.5% w/v (A), 1.0% w/v (B) and 1.5% w/v (C) after citrate treatment, resulting in liquefaction of the alginate scaffold and swelling of the matrix beads. Beads composed of 0.5% w/v PMM-CVS14*f*/SPy12 did not withstand citrate treatment, while beads at 1.0% w/v and 1.5% w/v polymer loading were weak and had a high degree of bead breakage. Scale bars are 500 μm. Images of PMM-CVS14*f*/SPy12 were obtained using a Nikon Eclipse Ti confocal microscope 4 x objective lens. Images of PMM-CVS21/SPy19 and PMM-CVS32/SPy30

were obtained using a Nikon upright microscope on transmitted light mode 5 x objective lens.

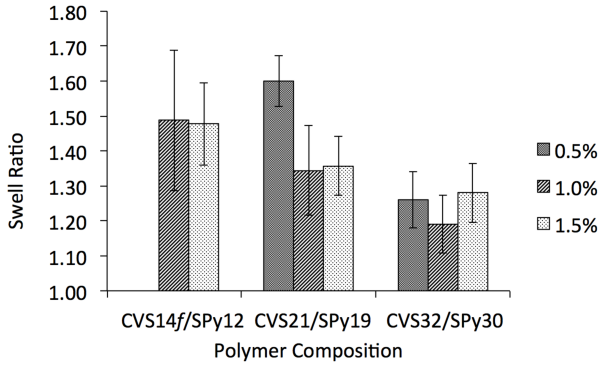

Figure 5.5. The swelling of matrix beads was calculated by measuring bead diameters before and after sodium citrate treatment and taking the ratio of the two values.

5.5.6. Indiffusion of fluorescently-labelled dextrans to determine bead permeability

Hydrogel beads serve as a semi-permeable membrane, providing protection for encapsulated cells. It is important to have control over the pore size of the beads. The beads must allow for in-diffusion of oxygen and nutrients, and out-diffusion of therapeutic agents such as insulin to the surrounding environment. The beads should also provide immune-protection to encapsulated cells by excluding antibodies and cytokines. Beads composed of 0.5% w/v PMM-CVS12/SPy12 were insufficiently crosslinked to withstand the citrate challenge. Beads composed of 1.0% and 1.5% w/v PMM-CVS12/SPy12 were weak and experienced some breakage. Broken beads were not used to measure permeability. Polymer loading percentage was found to have a greater effect on bead porosity than functionalization percentage. This fits with the swell ratio data that indicates that swelling is a function of loading percentage and not functionalization percentage which makes sense as porosity is a function of swelling. Beads composed of PMM-CVS12/SPy12 and PMM-CVS21/SPy19 showed similar permeabilities to that of standard alginate beads, indicating that the reactive polymers retain similar porosity upon liquefaction of the alginate scaffold. There was seen to be considerable indiffusion of 10 kDa dextran-*f*, and an increase in partial exclusion as dextran-*f* MW increased. Beads composed of 0.5% and 1.0% PMM-CVS32/SPy30 also had similar porosities to alginate beads. However, at 1.5% polymer loading, beads demonstrated partial exclusion of

dextran-*f*, perhaps due to the somewhat hydrophobic nature of the polymer scaffold.

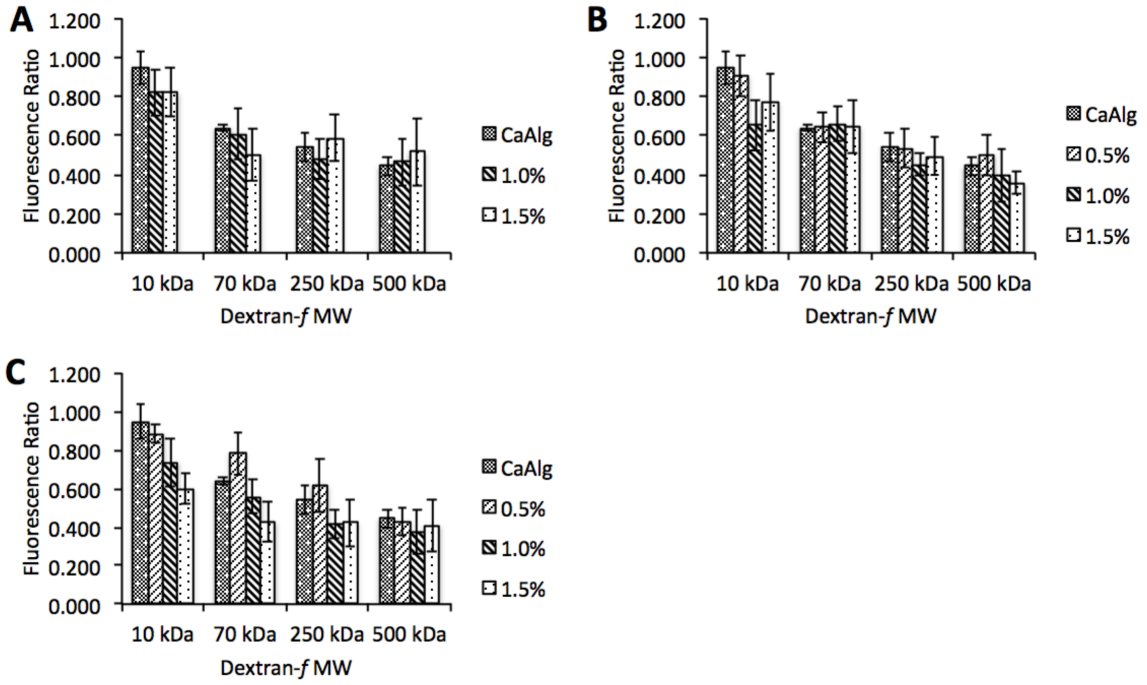

Figure 5.6. In-diffusion of dextran-*f* into citrate-treated matrix beads composed of A) PMM-CVS12/SPy12, B) PMM-CVS21/SPy19, C) PMM-CVS32/SPy30.

5.5.7. Kinetic Permeability Study

A kinetic permeability test was used to measure the rate of indiffusion of fluorescently labeled dextrans of varying molecular weights. It was seen that 10 kDa dextran-*f* is able to rapidly diffuse into the beads, reaching equilibrium within 20 minutes. This suggests that oxygen and other small metabolites would also rapidly diffuse in and out of the matrix beads. 70 kDa and 250 kDa dextran-*f* diffuse into the beads more slowly, and reach equilibrium around 1 h, while 500 kDa dextran-*f* exhibits even slower indiffusion.

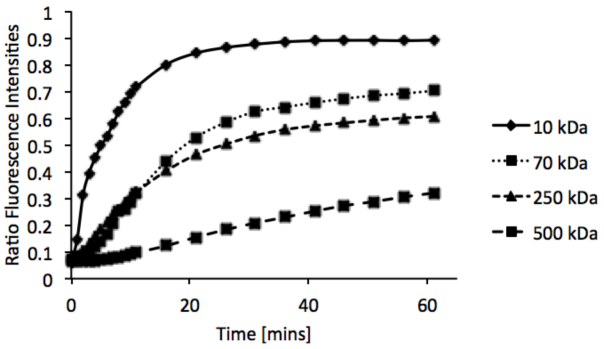

Figure 5.7. Rate of indiffusion of dextran-*f* (10, 70, 250 and 500 kDa) into citrate-treated 1.0% w/v PMM-CVS21/SPy19 beads.

5.5.8. Photobleaching of PMM-CVS22*r*/PMM-SPy19 Alginate-Templated Beads

A small section of the interior of a 1.0% w/v PMM-CVS22*r*/SPy19 bead was photobleached after citrate treatment, and then the bead was imaged over an hour to determine the level of fluorescence recovery (figure 5.8).

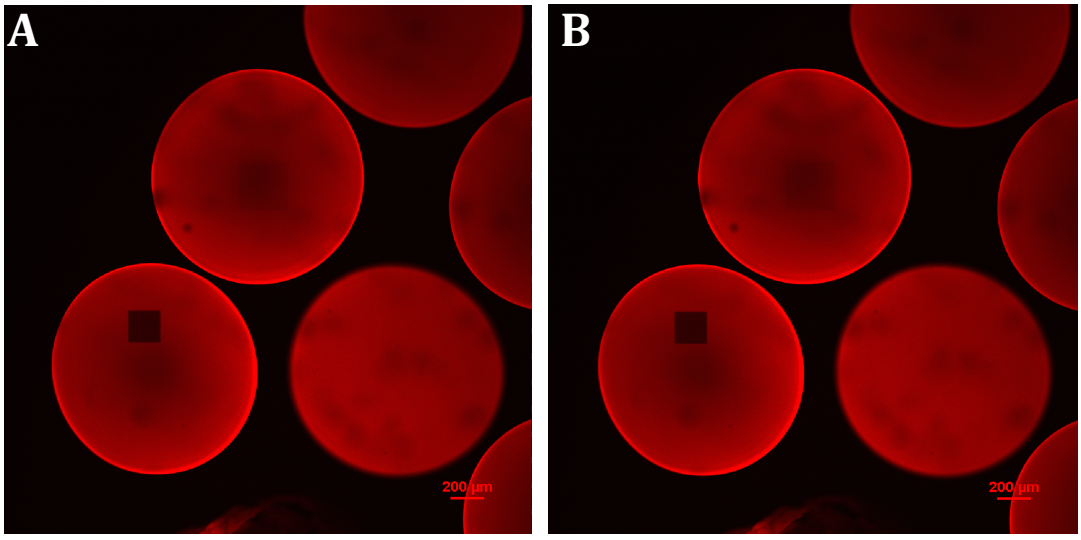

Figure 5.8. Confocal microscope images of PMM-CVS22*r*/SPy19 beads A) 1 minute after photobleaching and B) 60 minutes after photobleaching.

Noticeable fluorescence recovery would indicate that covalent crosslinking only occurred at the bead surface, and mobile polymer existed in the bead core. No visible

fluorescence recovery occurred in the photobleached region, indicating that PMM-CVS22*r* was covalently immobilized in the bead core.

5.5.9. Preliminary Cell Encapsulations

Preliminary cell encapsulation experiments were carried out as proof-of-concept as well as a way to test different cell stains and examine cell positioning within the beads. This preliminary work was conducted under aseptic conditions, although measures were taken to limit contamination during preparation and encapsulation. Encapsulations were carried out for 1.0 and 1.5% PMM-CVS21/SPy19, and 0.5 and 1.0% PMM-CVS32/SPy30. Calcein AM, NucBlue and DAPI were all explored as potential stains for live/all cells. However, they were all found to preferentially stain the polymer matrix, making them unsuitable as cell stain choices for this work. Ethidium homodimer, however, was found to selectively stain dead cells. A possible alternative live/all cell stain is 3,3'-dioctadecyl-5,5'-di(4-sulfophenyl)oxacarbocyanine (SP-DiOC$_{18}$(3)), a lipophilic carbocyanine analog that is weakly fluorescent in water but highly fluorescent under the fluorescein channel and photostable when incorporated into cellular membranes.

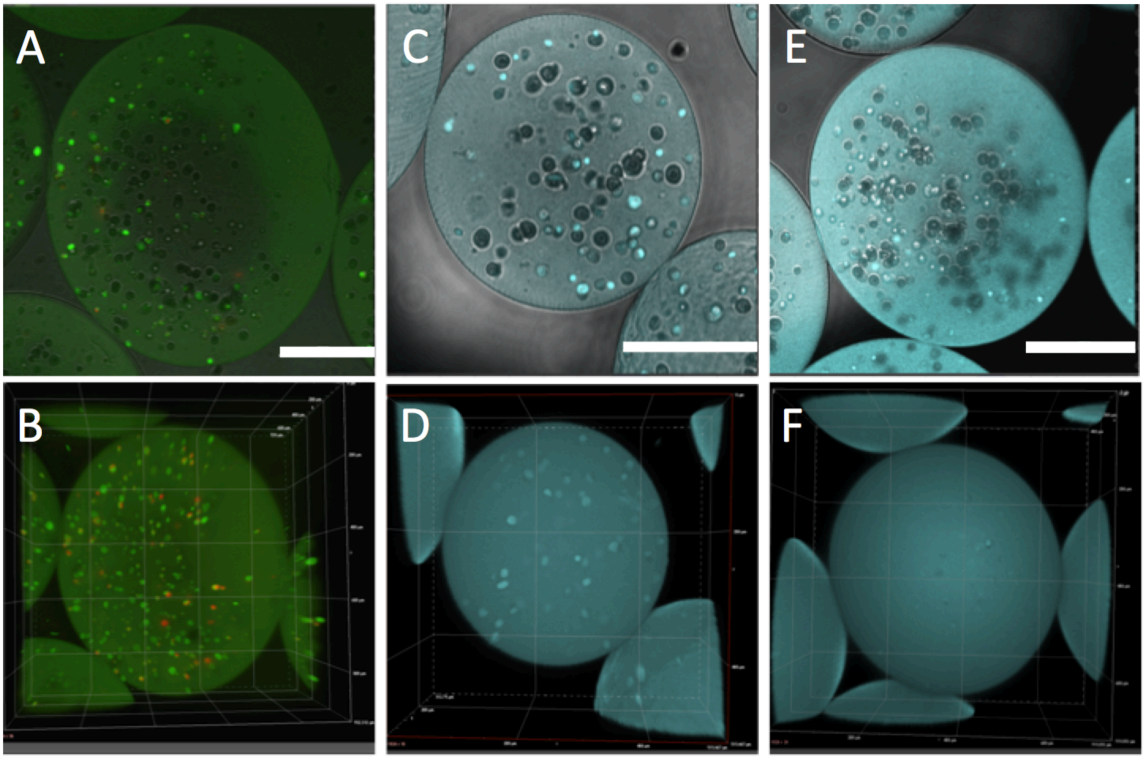

Figure 5.9. Confocal fluorescence images of beads composed of: A and B) 1.0% w/v PMM-CVS32/SPy30 24 h after initial encapsulation of 3T3 cells and stained with calcein AM (green, live)/ethidium homodimer (red, dead); C and D) 1.0% w/v PMM-CVS21/SPy19 1 h after initial encapsulation and stained with NucBlue; and E and F) 1.5% w/v PMM-CVS21/SPy19 1 h after initial encapsulation and stained with NucBlue. Scale bars are 250 μm. Images A, C and E show an equatorial confocal cross-section and images B, D and F show a 3D volume profile, generated from z-stacks.

It is hypothesized that the phase separation observed for beads composed of 1.5% w/v PMM-CVS21/SPy19 and 1.0 and 1.5% PMM-CVS32/SPy30 will result in hydrophobic regions in the interior of the beads. This may facilitate cell attachment, and a follow up project is planned to examine cell attachment through confocal microscopy fluorescent analysis of cell morphology and viability. Figure 5.2 appears to show a core-shell morphology with higher opacity in the core of the beads. This morphology may make it possible to isolate the hydrophobic core from immune proteins of the host upon implantation. Further studies are also planned to incorporate RGD into the matrix beads as a control study for cellular attachment. Cell viabilities for varied exposure times and

concentrations of TCEP and other reducing agents such as tris(hydroxypropyl)phosphine (THPP) will also be explored in detail.

5.6. Conclusions

Covalently crosslinked alginate-templated beads were achieved using PMM-CVS and HS-PEG-SH (1 kDa and 8 kDa). However, tunability of the beads was low, and crosslink density was not affected by polymer loading percentage, varying the thiol ratio, or increasing the functionalization percentage of CVS. To improve tunability and control over the hydrogel networks, a disulphide-protected thiol, PMM-SPy, was introduced. Aqueous mixtures of PMM-CVS and PMM-SPy were used to prepare alginate-templated matrix beads which were then exposed to TCEP, a disulphide-reducing agent. These beads showed excellent tunability that was dependent on polymer concentration, loading percentage, and TCEP exposure time and concentration.

5.7. Acknowledgements

We would like to thank the Natural Sciences and Engineering Research Council (NSERC) of Canada for supporting this work through Discovery and CREATE grants.

5.8. References

(1) Pareta, R. A.; Farney, A. C.; Opara, E. C. Design of a bioartificial pancreas. *Pathobiology*, **2013**, *80*, 194-202.

(2) Lim, F.; Sun, A. M. Microencapsulated islets as bioartificial endocrine pancreas. *Science,* **1980,** *210*, 908-910.

(3) Liu, H. W.; Ofosu, F. A.; Chang, P. L. Expression of human factor IX by microencapsulated recombinant fibroblasts. *Hum. Gene Ther.*, **1993**, *4*, 291-301.

(4) Colton, C. K. Implantable biohybrid artificial organs. *Cell Transplant.,* **1995**, *4*, 415-436.

(5) Ching, S. H.; Bansal, N.; Bhandari, B. Alginate gel particles-a review of production techniques and physical properties. *Critical Reviews in Food Science and Nutrition*, **2015**, *57*, 1133-1152.

(6) De Castro, M.; Orive, G.; Hernandez, R. M.; Gascon, A. R.; Pedraz, J. L. Comparative study of microcapsules elaborated with three polycations (PLL, PDL, PLO) for cell immobilization. *J. Microencapsul.*, **2005**, *22*, 303-315.

(7) Gravastrand, C.; Hamad, S.; Fure, H.; Steinkjer, B.; Ryan, L.; Oberholzer, J.; Lambris, J. D.; Lacík, I.; Mollnes, T. E.; Espevik, T.; Brekke, O.-L.; Rokstad, A. M. Alginate microbeads are coagulation compatible, while alginate microcapsules activate coagulation secondary to complement or directly through FXII. *Acta Biomater.* **2017**, *58*, 158-167.

(8) Thu, B.; Bruheim, P.; Espevik, T.; Smidsrød, O.; Soon-Shiong, P.; Skjåk-Bræk, G. Alginate polycation microcapsules. II. Some functional properties. *Biomaterials* **1996**, *17*, 1069–1079.

(9) Juste, S.; Lessard, M.; Henley, N.; Ménard, M.; Hallé, J. P. Effect of poly-L-lysine coating on macrophage activation by alginate-based microcapsules: Assessment using a new *in vitro* method. *J. Biomed. Mater. Res., A*, **2005**, *72*, 389–398.

(10) Mazumder, M.A.J.; Burke, N.A.D.; Shen, F.; Potter, M.A.; Stöver, H.D.H. Core-cross-linked alginate microcapsules for cell encapsulation. *Biomacromolecules*, **2009**, *10*, 1365-1373.

(11) Mahou, R.; Wandrey, C. Alginate- poly (ethylene glycol) hybrid microspheres with adjustable physical properties. *Macromolecules*, **2010**, *43*, 1371-1378.

(12) Gattás-Asfura, K.M.; Stabler, C.L. Chemoselective cross-linking and functionalization of alginate via Staudinger ligation. *Biomacromolecules*, **2009**, *10*, 3122-3129.

(13) Breguet, V.; Gugerli, R.; Pernetti, M.; von Stockar, U.; Marison, I.W. Formation of microcapsules from polyelectrolyte and covalent interactions. *Langmuir*, **2005**, *21*, 9764-9772.

(14) Ros, S.; Burke, N. A. D.; Stöver, H. D. H. Synthesis and Properties of Charge-Shifting Polycations: Poly[3-aminopropylmethacrylamide-*co*-2-(dimethylamino-ethyl acrylate]. *Macromolecules*, **2015**, *48*, 8958-8970.

(15) Rokstad, A. M.; Donati, I.; Borgogna, M.; Oberholzer, J.; Strand, B. L.; Espevik, T.; Skjak-Bræk, G. Cell-compatible covalently reinforced beads obtained from a chemoenzymatically engineered alginate. *Biomaterials*, **2006**, *27*, 4726–4737.

(16) Kolb, H. C.; Finn, M. G.; Sharpless, K. B. Click Chemistry: Diverse Chemical Function from a Few Good Reactions. *Angew. Chem., Int. Ed.*, **2001**, *40*, 2004-2021.

(17) Binder, W. H.; Sachsenhofer, R. 'Click' chemistry in polymer and material science: an update. *Macromol. Rapid Commun.,* **2008**, *29*, 952-981.

(18) Evans, R. A. The rise of azide-alkyne 1, 3-dipolar 'click' cycloaddition and its application to polymer science and surface modification. *Aust. J. Chem.*, **2007**, *60*, 384-395.

(19) Smith, L. J.; Taimoory, S. M.; Tam, R. Y.; Baker, A. E. G.; Mohammad, N. B.; Trant, J. F.; Shoichet, M. S. Diels-Alder Click-Cross-Linked Hydrogels with Increased Reactivity Enable 3D Cell Encapsulation. *Biomacromolecules*, **2018**, *19*, 926-935.

(20) Anseth, K. S.; Klok, H.-A. Click Chemistry in Biomaterials, Nanomedicine, and Drug Delivery. *Biomacromolecules*, **2016**, *17*, 1-3.

(21) Brown, T. E.; Carberry, B. J.; Worrell, B. T.; Dudaryeva, O. Y.; McBride, M. K.; Bowman, C. N.; Anseth, K. S. Photopolymerized dynamic hydrogels with tunable viscoelastic properties through thioester exchange. *Biomaterials*, **2018**, in press.

(22) Munkhbat, O.; Gok, O.; Sanyal, R.; Sanyal, A. Multiarm star polymers with a thermally cleavable core: A "grafting-from" approach paves the way. *J. Polym. Sci. A.*, **2017**, *55*, 885-893.

(23) Hodgson, S. M.; Bakaic, E.; Stewart, S. A.; Hoare, T.; Adronov, A. Properties of Poly(ethylene glycol) Hydrogels Cross-Linked via Strain-Promoted Alkyne-Azide Cycoladdition (SPAAC). *Biomacromolecules*, **2016**, *17*, 1093-1100.

(24) Mather, B. D.; Viswanathan, K.; Miller, K. M.; Long, T. E. Michael addition reactions in macromolecular design for emerging technologies. *Prog. Polym. Sci.*, **2006**, *31*, 487-531.

(25) Lowe, A. B. Thiol-ene "click" reactions and recent applications in polymer and materials synthesis. *Polym. Chem.* **2010**, *1*, 17-36.

(26) Chan, J. W.; Yu, B.; Hoyle, C. E.; Lowe, A. B. The nucleophilic, phosphine-catalyzed thiol-ene click reaction and convergent star synthesis with RAFT-prepared homopolymers. *Polymer*, **2009**, *50*, 3158-3168.

(27) Nair, D.P.; Podgórski, M.; Chatani, S.; Gong, T.; Xi, W.; Fenoli, C.R.; Bowman, C.N. The Thiol-Michael Addition Click Reaction: A Powerful and Widely Used Tool in Materials Chemistry. *Chem. Mater.*, **2014**, *26*, 724-744.

(28) Lutolf, M.P.; Hubbell, J.A. Synthesis and Physicochemical Characterization of End-Linked Poly(ethylene glycol)-*co*-peptide Hydrogels Formed by Michael-Type Addition. *Biomacromolecules*, **2003**, *4*, 713-722.

(29) Bednar, R.A. Reactivity and pH dependence of thiol conjugation to N-ethylmaleimide: detection of a conformational change in chalcone isomerase. *Biochemistry*, **1990**, *29*, 3684-3690.

(30) Wang, H.; Cheng, F.; Li, M.; Peng, W.; Qu, J. Reactivity and Kinetics of Vinyl Sulfone-Functionalized Self-Assembled Monolayers for Bioactive Ligand Immobilization. *Langmuir*, **2015**, *31*, 3413-3421.

(31) Stewart, S. A.; Coulson, M. B.; Zhou, C.; Burke, N. A. D.; Stöver, H. D. H. *Submitted.*

(32) Stewart, S.A.; Backholm, M.; Burke, N. A. D.; Stöver, H. D. H. Cross-Linked Hydrogels Formed Through Diels-Alder Coupling of Furan- and Maleimide-Modified Poly(methyl vinyl ether-*alt*-maleic acid). *Langmuir*, **2016**, *32*, 1863-1870.

(33) Khan, M. N. Kinetics and Mechanism of the Alkaline Hydrolysis of Maleimide. *J. Pharm. Sci.,* **1984**, *73*, 1767−1771.

(34) Matsui, S.; Aida, H. Hydrolysis of some N-alkylmaleimides. *J. Chem. Soc., Perkin Trans. 2,* **1978**, 1277−1280.

(35) Morpurgo, M.; Veronese, F.M.; Kachensky, D.; Harris, J.M. Preparation and Characterization of Poly(ethylene glycol) Vinyl Sulfone. *Bioconjugate Chem.*, **1996**, *7*, 363-368.

(36) Chatani, S.; Nair, D.P.; Bowman, C.N. Relative reactivity and selectivity of vinyl sulfones and acrylates towards the thiol-Michael addition reaction and polymerization. *Polym. Chem.*, **2013**, *4*, 1048-1055.

(37) Masri, M.S.; Friedman, M. Protein reactions with methyl and ethyl vinyl sulfones. *J. Protein Chem.*, **1988**, *7*, 49-54.

(38) Gardner, C.M.; Burke, N.A.D.; Stöver, H.D.H. Cross-Linked Microcapsules Formed From Self-Deactivating Reactive Polyelectrolytes. *Langmuir*, **2010**, *26*, 4916-4924.

(39) Shimizu, T.; Minakata, A. Effect of Divalent Cations on the Volume of a Maleic Acid Copolymer Gel Examined by Incorporating Lysozome. *Eur. Polym. J.*, **2002**, *38*, 1113-1120.

(40) Coulson, M.B.; Stewart, S.A.; Burke, N.A.D.; Stöver, H.D.H. Crosslinkable Hydrogel Matrices via Thiol-Vinyl Sulfone Michael Addition. B.Sc. Dissertation, McMaster University, Hamilton, ON, 2014.

5.9. Appendix

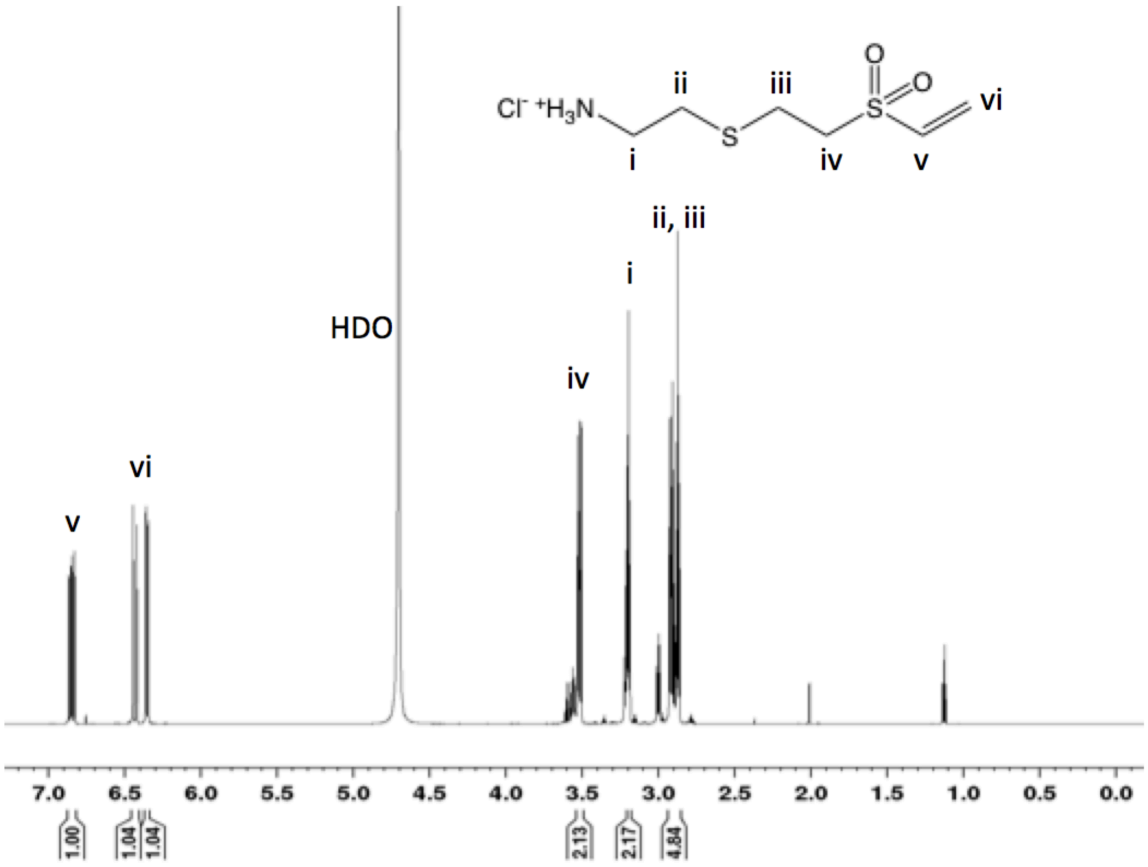

Figure A5.1. ^{1}H NMR of CVS-HCl in D_2O.

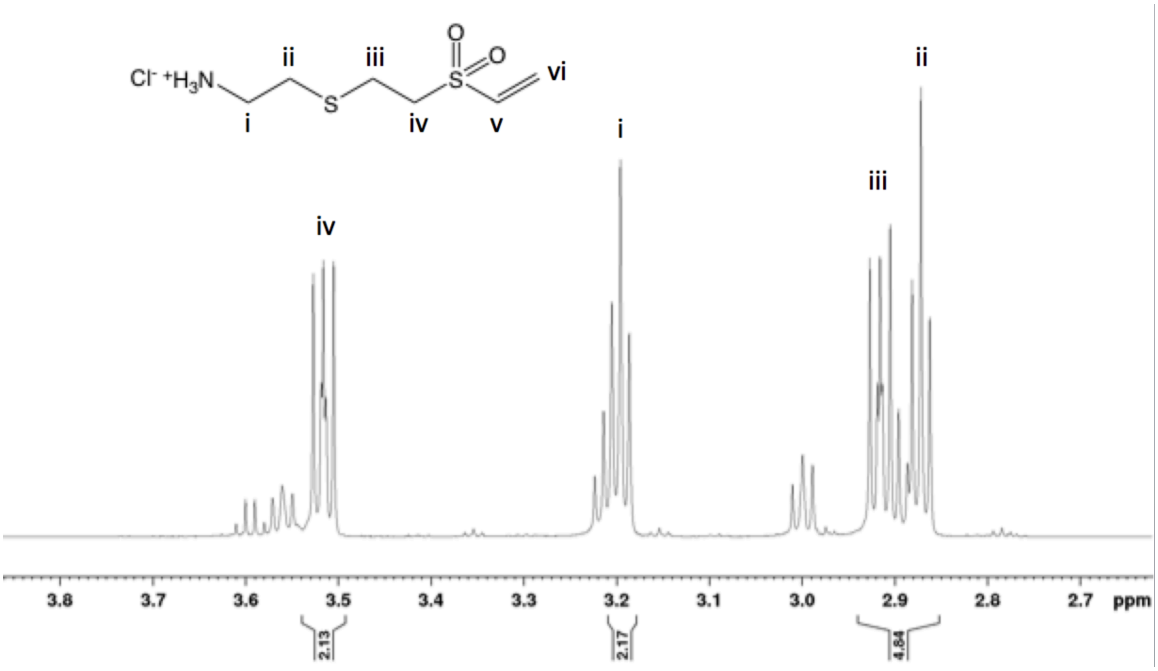

Figure A5.2. ^{1}H NMR of CVS-HCl in D_2O, focused on the aliphatic region. The signals at δ 3.55 - 3.61, δ 3.20, and δ 3.00 are due to a small amount of hydrolysis of the vinyl sulfone that occurs during reaction with cysteamine in H_2O, and later upon dissolution in D_2O.

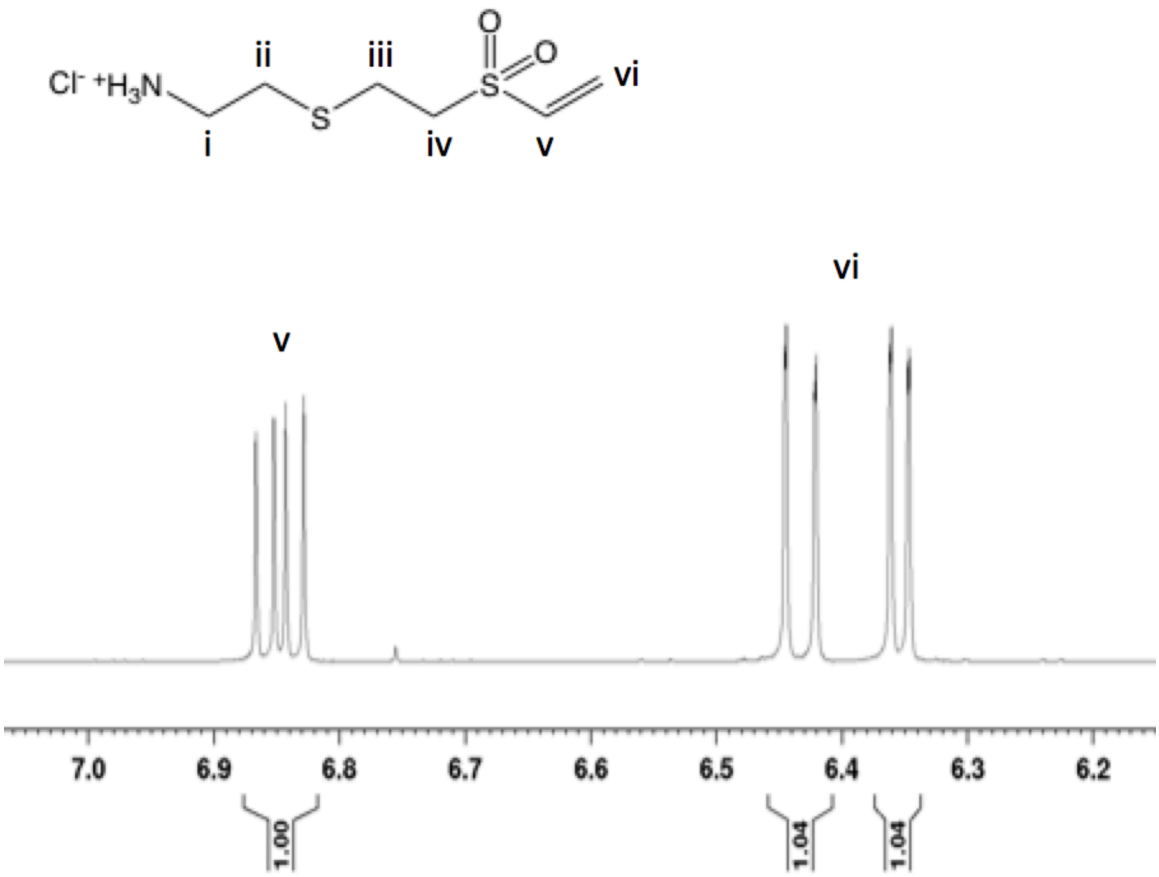

Figure A5.3. ^{1}H NMR of CVS-HCl in D_2O, focused on the vinyl region.

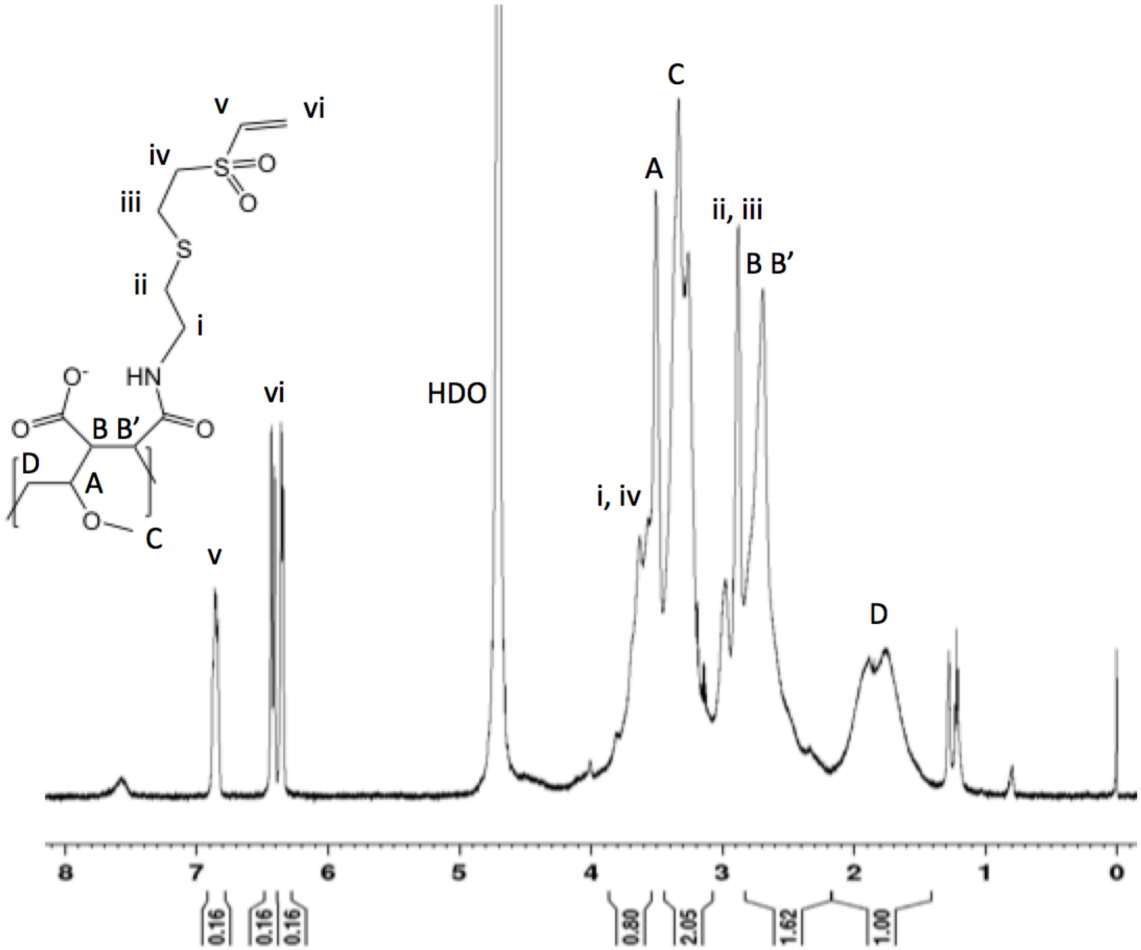

Figure A5.4. ^{1}H NMR of PMM-CVS32 in D_2O. The ratio of grafted CVS groups was determined by vinyl signal integration (v, 1H, δ6.8; vi, 2H, δ6.4) compared to a backbone methylene peak (D, 2H, δ1.4 – 2.0).

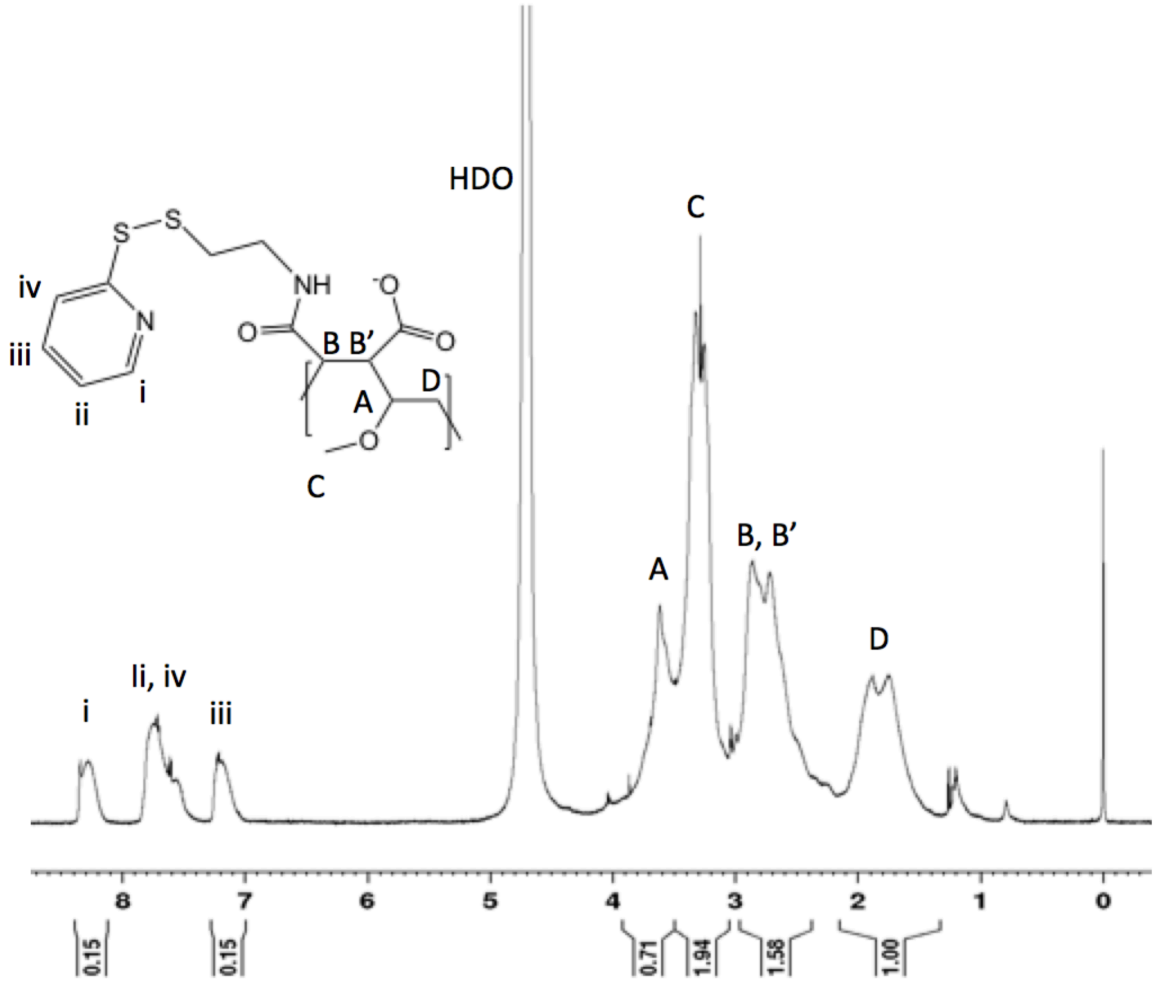

Figure A5.5. ^{1}H NMR of PMM-SPy30 in D_2O. The ratio of grafted SPy groups was determined by vinyl signal integration (i, 1H, δ8.3; iii, 1H, δ7.2) compared to a backbone methylene peak (D, 2H, δ1.4 – 2).

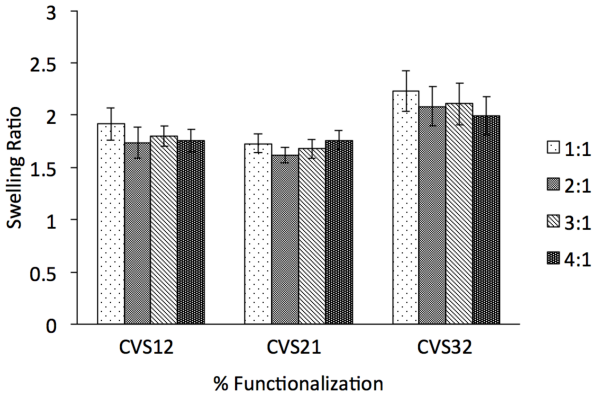

Figure A5.6. Citrate swelling ratios of 1% w/v PMM-CVS$_x$ beads with varying 8000 Da HS-PEG-SH crosslinker molar ratios.

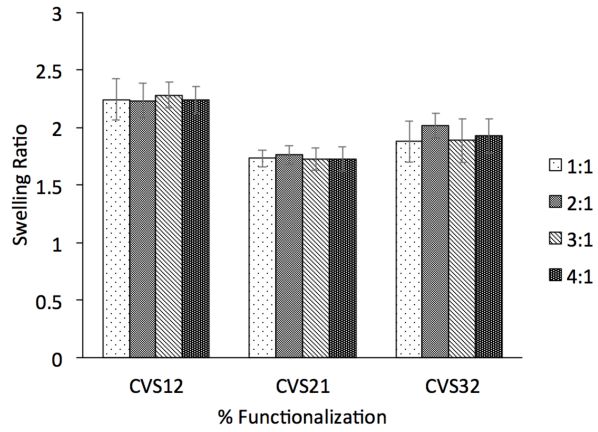

Figure A5.7. Citrate swelling ratios of 2% w/v PMM-CVS$_x$ beads with varying 1000 Da HS-PEG-SH crosslinker molar ratios.

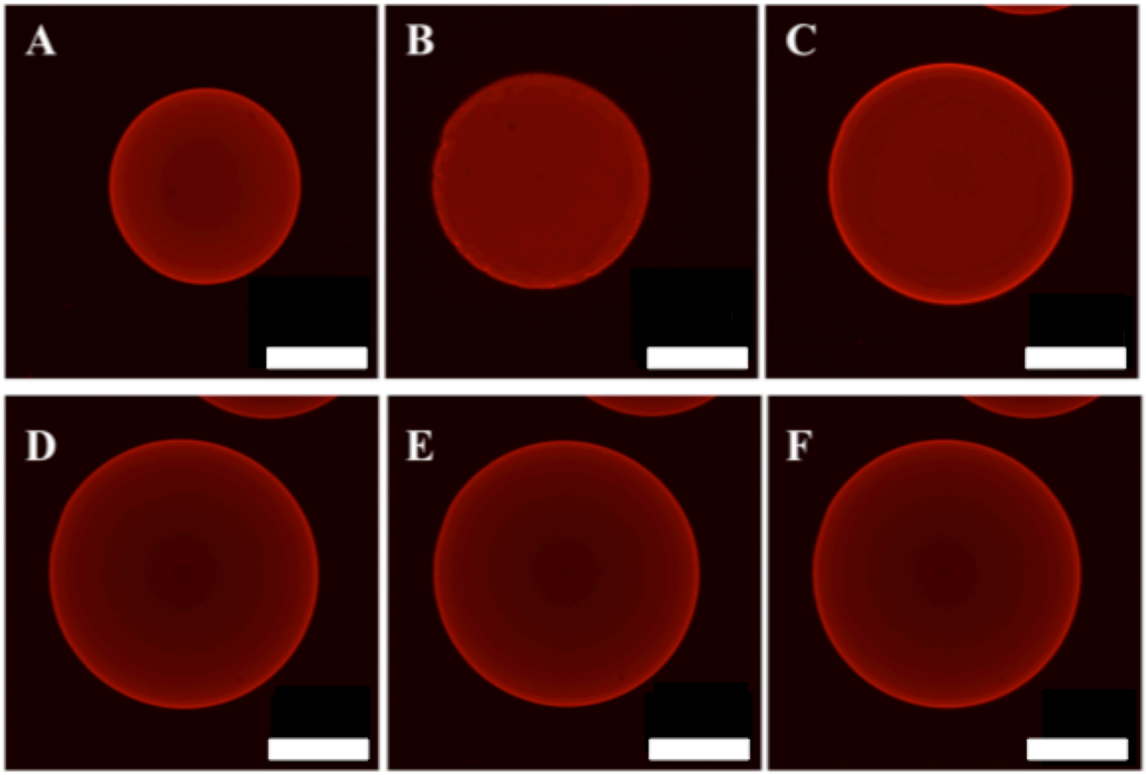

Figure A5.8. Confocal microscope images of 1% PMM-CVS22*r*/SPy19 alginate-templated beads at time points A) before citrate addition, B) 1 minute after citrate addition, C) 2 minutes after citrate addition, D) 20 minutes after citrate addition, E) 40 minutes after citrate addition and, F) 60 minutes after citrate addition. Scale bars are 250 μm.

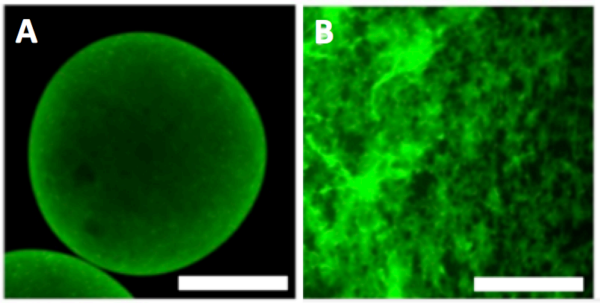

Figure A5.9 A) Confocal microscope images of fluorescently labelled PMM-CVS32 (1% w/v) in an alginate templated bead (1.125% w/v) and B) An image of a solution of fluorescently labelled PMM-CVS32 mixing with sodium alginate at the interface on a glass slide. Scale bars are 250 μm.

Chapter 6

Thesis Summary and Recommendations for Future Work

6.1. Summary

6.1.1. Chapter 2

PMMAn in the anhydride form was reacted with 10 - 30 mol% furfurylamine or *N*-(2-aminoethyl)maleimide followed by hydrolysis of residual anhydride groups to form PMM-FFA and PMM-MAL respectively. Aqueous solutions of these mutually reactive polymers were combined and spontaneously formed bulk hydrogels within 15 minutes to 18 h, depending on degree of functionalization and concentration. Both solution-state and high-resolution magic angle spinning ^{1}H NMR were used to assess the extent of Diels Alder reaction and competing hydrolyses, and polymer handling was adjusted accordingly to minimize side reactions. The ability to post-functionalize the gels using residual furan moieties was demonstrated via the addition of *N*-ethyl maleimide to swollen hydrogels.

Swelling of the hydrogels was found to depend on the degree of functionalization, with higher swelling being observed for gels formed from less functionalized polymers. Similarly, the Young's Modulus of the gels was found to be inversely proportional to the swelling ratios, with higher moduli measured for more highly functionalized hydrogels. The elastic moduli for the gels were found to cover a wide range, matching stiffnesses measured for tissues ranging from muscle to collagenous bone.

The porosity of the crosslinked gels was investigated using fluorescently labelled dextrans, and pore sizes were found to range from 2.3 to 10.9 nm, demonstrating that porosity may be controlled via functional group loading. It was also found that incorporation of Ca^{2+} resulted in decreased swelling of the hydrogels and increased modulus, attributed to electrostatic shielding as well as calcium ion bridging between PMM chains. A controlled release experiment using entrapped 10 kDa fluorescently labelled dextran found that hydrogels treated with Ca^{2+} showed a persistent release of the dextran over the course of several days, indicating the potential for these hydrogels as controlled release devices.

6.1.2. Chapter 3

Aqueous solutions containing 0.5 to 1.5% w/v each of PMM-FFA/MAL were mixed with a solution of sodium alginate and extruded in droplet form into a calcium chloride gelling bath to form calcium alginate-templated crosslinked matrix beads of about 500 micrometer diameter. These beads were found to retain 88-97% of the reactive polymers, demonstrating excellent entrapment, likely due to a combination of their high molecular weight and participation in calcium bridging of the PMM backbone. Confocal fluorescence microscopy showed co-localization of the reactive polymers with calcium alginate along identical trough-shaped density profiles across the beads, and allowed tracking of alginate during calcium removal with sodium citrate.

Beads were stable for over six weeks even after liquefaction of the alginate scaffold apart from the 0.5% w/v beads. Alginate concentration was also found to have an effect on crosslinking efficiency, with less crosslinking observed at both high and low alginate concentrations, attributed to less facilitation of the Diels-Alder reaction at low concentration, and inhibition of polymer chain mobility at higher concentrations.

Beads were found to be fully crosslinked after 1.5 – 6 hours, depending on composition, which was significantly faster than the equilibrium achieved for bulk gels. Some bead compositions did remain intact upon alginate liquefaction after as little as 15 minutes. Bead swelling after alginate liquefaction was found to be composition dependent, with no PMM-FFA/MAL detected in the supernatants. Fluorescently labelled dextrans were used to determine capsule permeability, with 10 and 70 kDa dextrans diffusing into the beads while 250 and 500 kDa dextrans were partially excluded.

Encapsulation of 3T3 fibroblasts demonstrated excellent initial viability after encapsulation. However, viabilities showed a decrease after 3 days, possibly due to the lack of attachment sites available in the capsules.

6.1.3. Chapter 4

Cysteamine vinyl sulfone trifluoroacetate (CVS TFA) was synthesized and isolated in a three- step reaction and used to functionalize PMMAn to form PMM-CVS with 10 – 30% pendant vinyl sulfone moieties. Aqueous solutions of PMM-CVS and a

PEG-dithiol crosslinker were combined in equimolar amounts, resulting in thiol-ene crosslinked hydrogels within seconds to 45 minutes, depending on concentration and degree of functionalization. The reaction was found to be strongly pH dependent, as expected, with faster reaction observed at higher pH.

The as-formed gels were found to swell further in buffer, depending on polymer concentration and degree of functionalization, with lower degrees of swelling observed at higher concentration and degree of functionalization. Young's modulus was found to be very sensitive to gel composition, with ranges from 0.94 to 141 kPa measured. In contrast to the Diels-Alder system, hydrolysis of pendant reactive moieties was found to be negligible compared with the crosslinking reaction. Post-modification of the gels with cysteamine demonstrated the ability to functionalize the hydrogels in a step-wise fashion.

Cytotoxicity of the polymers was investigated by mixing aqueous solutions of PMM-CVS and PEG-dithiol with 3T3 cells and evaluating the cell viability in the formed gel after 24 hours by fluorescent live/dead assay. Cells exhibited viabilities of 98%, indicating gel formation is not toxic to cells. Cell morphology showed that the cells did not adhere to the gels, potentially necessitating the incorporation of RGD or other attachment moieties for future applications in cell encapsulation.

6.1.4. Chapter 5

Synthesis of cysteamine vinyl sulfone was further optimized to a single-pot reaction with a more rapid purification using extraction and a silica plug, without the need for a boc-protecting group. PMMAn was functionalized with CVS and SPy, a protected thiol, to form PMM-CVS and PMM-SPy respectively. Aqueous mixtures of PMM-CVS/SPy were mixed with sodium alginate and extruded into a HEPES-buffered saline $CaCl_2$ gelling bath, followed by exposure to tris(2-carboxyethyl)phosphine (TCEP) to deprotect the thiol component and initiate crosslinking. Some opacity was observed for beads with higher functionalization percentages and concentrations, suggesting onset of phase-separation of the synthetic polymers from the calcium alginate.

TCEP concentration and exposure times were investigated for effect on crosslinking efficiency, with intermediate TCEP concentrations resulting in maximal crosslink density. Swellability of as-formed beads in excess buffer was found to be

inversely proportional to gelformer concentration and functionalization. Similarly, permeability as determined with fluorescently labelled dextrans was inversely dependent on functional group loading and concentration, with in-diffusion of 10 kDa dextran-f reaching equilibrium within as little as 20 minutes.

6.2. Future Work

6.2.1. Cell Attachment

One significant challenge in biomaterials design is insufficient attachment of cells within capsules, which can lead to cell death and subsequent inflammatory response.[1] Attachment can be improved by immobilizing cell-recognition peptides within the hydrogels.[2,3,4] One such peptide, RGD, triggers cell adhesion and can also elicit specific cell responses.[5]

Biomaterials were originally coated with proteins such as fibronectin, collagen and laminin to improve cellular interactions.[6,7,8,9,10,11,12] However, the use of proteins is associated with several disadvantages, including higher cost, and potential for immune response to due incomplete purification.[13,14] RGD is the best characterized and most commonly used peptide for stimulated cell adhesion on synthetic surfaces.[15] First identified in 1984 by Pierschbacher, it is an essential cell adhesion peptide sequence in fibronectin.[16]

Contact of cells with neighbouring cells and the surrounding ECM is mediated by cell adhesion receptors, with the integrin family playing an important role.[17] Integrin is critical for anchoring molecules, as well functions such as embryogenesis,[18] cell differentiation,[19] and immune response.[20]

Results from chapter 3 showed that encapsulation of 3T3 cells within alginate-templated PMM-FFA/MAL beads retained excellent viabilities post-encapsulation. However, viabilities decreased with time, likely due to lack of cell-attachment sites in the matrix beads. Similar to 3T3 cells, mesenchymal stem cells are known to be attachment dependent and it has been demonstrated that MSC survival is enhanced when MSC spheroids are entrapped in alginate hydrogels that have been modified with integrin-binding RGD peptides.[21]

Functionalization of PMM with RGD prior to incorporation of FFA, MAL, SPy and CVS would encourage cell attachment to the scaffold and may help improve long-term cell viabilities. Incorporation of RGD into the polymers would also allow for precise control and characterization of degree of functionalization.

6.2.2. Varying the Molecular Weight of PMM

PMM is available in a wide range of molecular weights ranging from low molecular weight oligomers to 1000 kDa chains. In this work, functionalization of PMM was restricted to 80 kDa and 1000 kDa chains. It was found that 1000 kDa PMM became insoluble post-functionalization with FFA and MAL, likely due to physical chain entanglement. However, it would be useful to explore the functionalization of intermediate chain length PMMs between 80 and 500 kDa. The effect of chain length on rate of crosslinking, gel modulus, swellability and permeability would be explored. In the current system, PMM is entrapped within the alginate beads partially due to molecular weight, and partially due to the binding interaction between PMM chains and Ca^{2+} ions. Increasing the molecular weight may further reduce the amount of PMM that escapes the alginate beads during initial ionic gelation.

6.2.3. Cell Encapsulation

In the current work 3T3 fibroblasts were encapsulated in alginate-templated PMM-FFA/MAL beads and a similar encapsulation will be carried out for alginate-templated PMM-CVS/SPy beads. While 3T3 cells serve as a convenient option for early encapsulation studies, it is of interest to encapsulate more therapeutically relevant cells such as INS-1E (rat pancreatic β cells) and MSCs. An exploration of cell viability and longevity post-encapsulation as well as cellular response to glucose challenges will provide important information about the suitability of these alginate-templated matrix beads for therapeutic cell encapsulation.

6.2.4. Exploring Alternative Reactive Moieties

The Diels-Alder reaction involves the reaction between an electron-rich diene and an electron-poor dieneophile. Incorporation of electron-donating substituents on the

diene, such as alkyl chains, results in acceleration of the reaction.[22,23] It is of interest to explore a library of different dienes, dieneophiles, Michael acceptors and Michael donors and examine the effects of different reactive groups on reaction rate and gel properties.

6.3. References

(1) Paredes Juárez, G. A.; Spasojevic, M.; Faas, M.M.; de Vos, P. Immunological and Technical Considerations in Application of Alginate-Based Microencapsulation Systems. *Front. Bioeng. Biotechnol.*, **2014**, *2*, DOI: 10.3389/fbioe.2014.00026

(2) Comisar, W.A.; Mooney, D.J.; Linderman, J.J. Integrin organization: linking adhesion ligand nanopatterns with altered cell responses. *J. Theor. Biol*., **2011**, *274*, 120-130.

(3) Prowse, A.B.J.; Chong, F.; Gray, P.P.; Munro, T.P. Stem cell integrins: implications for ex-vivo culture and cellular therapies. *Stem. Cell Res.*, **2011**, *6*, 1-12.

(4) Cosgrove, B.D.; Mui, K.L.; Driscoll, T.P.; Caliari, S.R.; Mehta, K.D.; Assoian, R.K.; Burdick, J.A.; Mauck, R.L. N-cadherin adhesive interactions modulate matrix mechanosensing and fate commitment of mesenchymal stem cells. *Nat. Mater.*, **2016**, *15*, 1297-1306.

(5) Garate, A.; Santos, E.; Pedraz, J.L.; Hernández, R.M.; Orive, G. Evaluation of different RGD ligand densities in the development of cell-based drug delivery systems. *J. Drug Target*., **2015**, *23*, 806-812.

(6) Li, J.M.; Menconi, M.J.; Wheeler, H.B.; Rohrer, M.J.; Klassen, V.A.; Ansell, J.E.; Appel, M.C. Precoating expanded polytetrafluoroethylene grafts alters production of endothelial cell-derived thrombomodulators. *J. Vasc. Surg.*, **1992**, *15*, 1010-1017.

(7) Miyata, T.; Conte, M.S.; Trudell, L.A.; Mason, D.; Whittemore, A.D.; Birinyi, L.K. Delayed exposure to pulsatile shear stress improves retention of human saphenous vein endothelial cells on seeded ePTFE grafts. *J. Surg. Res.*, **1991**, *50*, 485-493.

(8) Vohra, R.; Thomson, G.J.; Carr, H.M.; Sharma, H.; Walker, M.G. Comparison of different vascular prostheses and matrices in relation to endothelial seeding. *Br. J. Surg*, **1991**, *78*, 417-420.

(9) Thomson, G.J.; Vohra, R.K.; Carr, M.H.; Walker, M.G.; Adult human endothelial cell seeding using expanded polytetrafluoroethylene vascular grafts: a comparison of four substrates. *Surgery*, **1991**, *109*, 20-27.

(10) Kaehler, J.; Zilla, P.; Fasol, R.; Deutsch, M.; Kadletz, M. Precoating substrate and surface configuration determine adherence and spreading of seeded endothelial cells on polytetrafluoroethylene grafts. *J. Vasc. Surg.*, **1989**, *9*, 535-541.

(11) Sentissi, J.M.; Ramberg, K.; O'Donnell Jr, T.F.; Connolly, R.J.; Callow, A.D. The effect of flow on vascular endothelial cells grown in tissue culture on polytetrafluoroethylene grafts. *Surgery*, **1986**, *99*, 337-343.

(12) Seeger, J.M.; Klingman, N. Improved endothelial cell seeding with cultured cells and fibronectin-coated grafts. *J. Surg. Res.*, **1985**, *38*, 641-647.

(13) Collier, J.H.; Segura, T. Evolving the use of peptides as components of biomaterials. *Biomaterials*, **2011**, *32*, 4198-4204.

(14) Williams, D.F. The role of short synthetic adhesion peptides in regenerative medicine: the debate. *Biomaterials*, **2011**, *32*, 4195-4197.

(15) Sobers, C.J.; Wood, S.E.; Mrksich, M. A gene expression-based comparison of cell adhesion to extracellular matrix and RGD-terminated monolayers. *Biomaterials*, **2015**, *52*, 385-394.

(16) Pierschbacher, M.D.; Ruoslahti, E. Cell attachment activity of fibronectin can be duplicated by small synthetic fragments of the molecule. *Nature*, **1984**, *309*, 30-33.

(17) Gauthier, N.C.; Roca-Cusachs, P. Mechanosensing at integrin-mediated cell-matrix adhesions: from molecular to integrated mechanisms. *Curr. Opin. Cell Biol.*, **2018**, *50*, 20-26.

(18) Peng, Z.-W.; Ikenaga, N.; Liu, S.B.; Sverdlov, D.Y.; Vaid, K.A.; Dixit, R.; Weinreb, P.H.; Violette, S.; Sheppard, D.; Schuppan, D.; Popov, Y. Integrin αvβ6

critically regulates hepatic progenitor cell function and promotes ductular reaction, fibrosis, and tumorigenesis. *Hepatology*, **2016**, *63*, 217-232.

(19) Lee, J.; Abdeen, A.A.; Tang, X.; Saif, T.A.; Kilian, K.A. Geometric guidance of integrin mediated traction stress during stem cell differentiation. *Biomaterials*, **2015**, *69*, 174-183.

(20) Tian, Y.F.; Ahn, H.; Schneider, R.S.; Yang, S.N.; Roman-Gonzalez, L.; Melnick, A.M.; Cerchietti, L.; Singh, A. Integrin-specific hydrogels as adaptable tumor organoids for malignant B and T cells. *Biomaterials*, **2015**, *73*, 110-119.

(21) Ho, S. S.; Murphy, K. C.; Binder, B. Y. K.; Vissers, C. B.; Leach, J. K. Increased survival and function of mesenchymal stem cell spheroids entrapped in instructive alginate hydrogels. *Stem Cells Transl. Med*. 2016, *5*, 773−81.

(22) Froidevaux, V.; Borne, M.; Laborbe, E.; Auvergne, R.; Gandini, A.; Boutevin, B. Study of the Diels-Alder and retro-Diels-Alder reaction between furan derivatives and maleimide for the creation of new materials. *RSC Adv.*, **2015**, *5*, 37742-37754.

(23) Smith, L.J.; Taimoory, S.M.; Tam, R.Y.; Baker, A.E.G.; Mohammad, N.B.; Trant, J.F.; Shoichet, M.S. Diels-Alder Click-Cross-Linked Hydrogels with Increased Reactivity Encable 3D Cell Encapsulation. *Biomacromolecules*, **2018**, *19*, 926-935.